GREEN SYNTHESIS, CHARECTERIZATION AND FUNCTIONALIZATION OF GOLD NANOPARTICLES USING SOME MEDICINAL PLANTS OF NORTH EAST INDIA

by

PUNURI JAYASEKHAR BABU

In Partial Fulfillment of the

Requirements for the Degree of

DOCTOR OF PHILOSOPHY

DEPARTMENT OF BIOTECHNOLOGY

INDIAN INSTITUTE OF TECHNOLOGY GUWAHATI

GUWAHATI 781039, ASSAM, INDIA

JANUARY 2013

INDIAN INSTITUTE OF TECHNOLOGY GUWAHATI
भारतीय प्रौद्योगिकी संस्थान गुवाहाटी
Department of Biotechnology, Guwahati 781039, Assam, India
जैवप्रौद्योगिकी विभाग, गुवाहाटी 781039, असम, भारत

DECLARATION

It is to declare that the matter embodied in this thesis entitled "***Green synthesis, characterization and functionalization of gold nanoparticles using some medicinal plants of North East India***" is the result of investigations carried out by me under the supervision of **Dr. Utpal Bora and Dr. Ranjan Tamuli**, and is submitted to the Indian Institute of Technology Guwahati, Guwahati-781039, Assam, India for the award of degree of *Doctor of Philosophy in Biotechnology*. This work has not been submitted elsewhere for any degree or diploma of any institute or university to the best of my knowledge and belief.

In keeping with the general practice of reporting scientific observations, due acknowledgements have been made wherever the work of other investigators are referred, and copyright licenses have been taken from respective publishers.

Guwahati **PUNURI JAYASEKHAR BABU**

_____January 2013 Roll No: 08610602

INDIAN INSTITUTE OF TECHNOLOGY GUWAHATI
भारतीय प्रौद्योगिकी संस्थान गुवाहाटी
Department of Biotechnology, Guwahati 781039, Assam, India
जैवप्रौद्योगिकी विभाग, गुवाहाटी 781039, असम, भारत

CERTIFICATE

It is to certify that the matter embodied in this thesis entitled "***Green synthesis, characterization and functionalization of gold nanoparticles using some medicinal plants of North East India***" is the result of investigations carried out by **Mr. Punuri Jayasekhar Babu** (Roll No: 08610602) under my supervision, and is submitted to the Indian Institute of Technology Guwahati, Guwahati-781039, Assam, India for the award of degree of *Doctor of Philosophy in Biotechnology*. This work has not been submitted elsewhere for a degree.

Guwahati
_____January 2013

UTPAL BORA
Associate Professor
Dept. of Biotechnology
IIT Guwahati

RANJAN TAMULI
Assistant Professor
Dept. of Biotechnology
IIT Guwahati

DEDICATION

मातृ देवो भाव:

Honor thy mother as God

पितृ देवो भाव:

Honor thy father as God

आचार्य देवो भाव:

Honor thy teacher as God

Dedicated to

my father Sri. Punuri Mohan Rao

my mother Smt. Punuri Sarala Kumari

my wife Smt. Punuri Saranya

all my teachers

Punuri Jayasekhar Babu

ACKNOWLEDGEMENT

At the outset, I would like to express my deep sense of gratitude to my thesis supervisors **Dr. Utpal Bora** and **Dr. R. Tamuli** for their guidance, support and direction. He has been the leading light in my endeavor for meaningful and fruitful research in the fast growing field of Biotechnology. I must acknowledge the freedom that I was given in every step of my research work. I am grateful to the chairman *Dr. Lingaraj Sahoo* and members of the Doctoral Committee *Dr. K. Pakshirajan* and *Dr. S. Bandopadhyay* and for their valuable suggestions and advices which enabled me to improve my work.

I would take this opportunity to thank *Prof. Gautam Barua*, Director, IITG, for providing all the necessary facilities and a conductive academic environment. I sincerely acknowledge the financial support from *Ministry of Human Resource Development* (MHRD) for providing me fellowship, and *Dept. of Biotechnology* (DBT), *Department of Science and Technology* (DST), *Govt. of India* for research grants to my supervisor.

I owe my gratitude to the *Department of Biotechnology*, *Central Instruments Facility* and *Central Library* for providing me all the support and necessary facilities. Also, thanks to the *Dept. of Chemistry* (for TGA, FTIR), *Physics* (for XRD), *Chemical Engineering* (for TGA), *Center for Nanotechnology* (for XRD); thanks to all the scientific staff. My special thanks to the *technical staff of the Dept. of Biotechnology* for their kind co-operation. I extend my gratitude to NCCS, Pune for providing necessary cell lines.

My great thanks to my research group previous members *Dr. Abhishek, Dr. Naresh Kosaju, Mr. Ratul* and *Mr. Debajeet* current members *Mr. Anil, Mr. Suradip, Mr. Arghya, Mr. Shamim, Mr. Y. Disco Singh, Mr. Anuj, Mr. Nayanmoni Gogoi, Mrs. Deepika*, for providing a healthy and enjoyable environment in the lab. I am immensely pleased to express my heartiest thanks to my departmental seniors *Dr. Kiran, Dr. Shiva, Dr. Sanjay, Dr. Mahanty, Dr. Priyanka, Dr. Ramesh,* and friends *Dr. Achlesh, Mr. Kaushik, Dr. Seema, Dr. Nandini, Dr. Kasturi,* and others from all departments, centers and hostel, for the moral support. Their presence made my five years stay at IITG memorable.

Last but not the least, I would like to thank my father *Punuri Mohan Rao*, my mother – *Punuri Sarala Kumari*, my wife *Mrs. Punuri Saranya* my elders sister *Punuri Sudha*, younger sisters *Punuri Sasikala, Punuri Surekha and my brother-in-laws Mr. Johan Babu and Mr. Steven and my friends Mr. M. Venkataswamy, Mr. Rajsekhar, Mr.Sanjeev and Auta Sivasnakar,* and *their family members, other relatives, well-wishers* and *my teachers* for their endless love, unlimited support and motivation.

January, 2013 *Punuri Jayasekhar Babu*

SYNOPSIS

Synthesis of gold nanoparticles (AuNPs) has gained importance as they possess unique chemical, physical, biological and optoelectronic properties which depend on shape and size of nanoparticles and are exploited in a wide range of applications such as in biology, chemical sensing of single molecule, controlled release, catalysis, and immunoassays, medical, electronics, materials science, alternative energy generation, environmental restoration. To cater the demand of AuNPs, various conventional synthesis methods such as seed growth, laser/photo irradiation, chemical vapour deposition, solvolysis, thermolytic reduction, solvothermal, sonochemical, electrochemical, chemical and microwave reduction, etc., have been employed for the synthesis of AuNPs.

Conventional physical and chemical methods of AuNPs synthesis mostly rely on the use of synthetic chemicals and prolonged heating. These methods of AuNPs synthesis involve application of harsh chemicals as reducing and stabilizing agents. Studies have shown that even the purest forms of such synthesized AuNPs carry unreacted traces of the reducing or stabilizing agents, which are potential hazards to human health. Owing to the increased awareness for potential toxicity of AuNPs associated with biological applications, alternative methodologies for biocompatible AuNPs synthesis are gaining importance. Currently, nano fabrication is laying emphasis on the principle of 'green' nanotechnology which advocates the application of environmentally sound and non-polluting methods for synthesis of nanoparticles and their derivatives. There are numerous reports about the synthesis of AuNPs using 'green' method (microbes) in literature. However, microbial mediated synthesis of AuNPs is not ideal as it is having some substantial limitations such as uncontrollability over shape, size and importantly, crystallinity of AuNPs. Therefore, synthesis of AuNPs using plant extracts has gained importance as they can address all the limitation associated with microbial synthesis. To

accomplish the same, we fixed the following as the objectives of the present research work:

1. Screening of indigenous plant and fruit extracts for gold nanoparticles synthesis.
2. Synthesis of gold nanoparticles using screened plant and fruit extracts.
3. Characterization and functionalization of the gold nanoparticles.

We have tried to screen out the reducing, capping and dispersing capabilities of plant and fruit extracts for the synthesis of AuNPs in this present investigation. We have successfully synthesized AuNPs using some indigenous medicinal plant and fruit extracts such as *Mentha arvensis* leaf extract (MLE), *Fagopyrum esculentum* leaf extract (FLE), *Andrographis paniculata* (ALE), *Piper betle* leaf extract (PLE), *Cocos nucifera* (coconut water; CW), *Solanum indicum* fruit extract (SFE) and *Sapindus mukorossi* fruit extracts (SmFE) and *Calotropis procera* Aqueous fraction of latex. We have employed various methods to mediate the synthesis of AuNPs includes heat, UV irradiation, microwave irradiation and sonocatalysis. The synthesized AuNPs were extensively characterized with biophysical tools.

Overall the thesis is divided into six chapters as described below.

Chapter One: Introduction & Review of Literature.

Chapter Two: Heat Mediated Synthesis of Gold Nanoparticles Using *Mentha arvensis.*

Chapter Three: Sonocatalytic UV Light Mediated Synthesis of Gold Nanoparticles Using *Bacopa monnieri* Leaf Extract.

Chapter Four: Microwave Mediated Synthesis of Gold Nanoparticles using Plant and Fruit extracts.

Chapter Five: Sonocatalytic Synthesis of Gold Nanoparticles and Functionalized with PCL, GL and PCL-GL composites.

Chapter Six: Summary and future prospects.

Chapter One deals with brief introduction on the concept of nanotechnology and comparison of 'nano' with the macroscopic matter which is visible with the naked eye. This chapter opens with a short description of different types of nanomaterials and its properties. It also confronts about the gold history, discovery and first synthesis and usage of gold nanoparticles. It mainly describes the fundamental understanding of gold nanoparticles and their synthesis method with an emphasis of analytical and non analytical applications in various fields. At the end this chapter presents the brief overview of nanotechnology and gold nanoparticles.

Chapter Two describes heat mediated synthesis of AuNPs using ethanolic extract of *Mentha arvensis* leaves, an edible plant used as a condiment and traditional medicine in India. UV-Vis spectroscopy analysis confirmed the formation of gold nanoparticles. The different reaction parameters such as plant extract, gold solution, temperature and time were optimized for the synthesis of AuNPs. Typical bright-field TEM image of AuNPs with optimum reaction conditions, which reveals that nanoparticles are of hexagonal and nearly circular shape. The synthesized AuNPs were stable even after 6 weeks of storage at room temperature. The crystalline nature of AuNPs was confirmed with X-ray diffraction analysis. The crystallinity of AuNPs also confirmed from the typical selected area electron diffraction (SAED) and XRD pattern with bright circular rings corresponding to the (1 1 1), (2 0 0), and (2 2 0) planes corresponding to gold lattice fringes. In addition to gold, energy-dispersive X-ray analysis (EDX) showed the presence of carbon and oxygen elements. The evidence from Fourier transform infrared (FTIR) spectroscopy and energy-dispersive X-ray analysis (EDX) suggested that flavonoids and phenol compounds were involved in reduction and stability of AuNPs synthesized using

Mentha arvensis leaf extract. The UV-Vis spectroscopic analysis displayed an intense peak at 530±10 nm indicating the formation of AuNPs that can be used for biomedical applications.

Chapter Three demonstrates the green synthesis field for AuNPs synthesis using *Bacopa monnieri* leaf extract (BLE) and UV irradiation. The reducing and capping functions provided by BLE can replace synthetic reducing and stabilizing agents required for nanoparticles synthesis. UV irradiation in aqueous reaction mixtures generates hydroxyl radicals from aqueous solution and free electrons from bioactive molecules which can reduce the gold salt (Au^{3+}) to corresponding gold nanoparticles (Au^{o}). The bioactive molecules present in BLE are known to act as potential reducing agents and we speculated that they are involved in the reduction of the $HAuCl_4$ (Au^{3+}) to AuNPs (Au^{o}) by donating the free electrons or •-electrons. We observed the solution containing gold ions (Au^{3+}) and BLE turned into ruby red after 15 min of UV irradiation (~254 nm). We investigated the parameters (BLE, chlor auric acid, time) for the AuNPs synthesis. The synthesized AuNPs were extensively characterized by biophysical tools to reveal their properties. TGA spectrum of AuNPs occurs over a wide temperature range (225–580 ^{o}C) which revealed the significant weight loss (5%) of AuNPs. This clearly indicated that bioactive molecules were capped on the AuNPs and were completely degraded due to high temperature. These capped AuNPs were tested on the human cancer cell lines (HeLa, MCF-7) and were found to be biocompatible opportunities for use in drug delivery, molecular imaging and therapy.

Chapter Four confronts the 'green' opportunity for the production of gold nanoparticles with a very less time. This chapter deals with investigations of reducing and stabilizing capabilities of *Fagopyrum esculentum* leaf extract (FLE), *Piper betle* leaf extract (PLE), *Cocos nucifera* (CW), *Solanum indicum* fruit extract (SFE) and *Sapindus*

mukorossi fruit extracts (SmFE) and Aqueous fraction (AF) of *Calotropis procera* latex for the synthesis of the AuNPs. We have used the microwave irradiation for the AuNPs synthesis. Microwave (MW) dielectric heating is a fast emerging and widely accepted new processing technology for a variety of inorganic synthesis and biomedical applications. Compared to the conventional heating, MW irradiation shortens reaction times and improve yield without causing any appreciable alteration in the composition of products of a chemical reaction. In contrast to general heating treatment, MW synthesis favors homogeneous heating through the entire bulk of the reaction mixture in a container, leading to a more homogeneous and easy nucleation of noble metal nanoparticles. UV-visible spectroscopy analysis indicated the successful formation of gold nanoparticles. We have optimized the parameters for the synthesis of AuNPs using FLE (0.4% FLE, 1 mmol/L $HAuCl_4$ and 16 s MW irradiation time), PLE (2% PLE, 0.5 mM $HAuCl_4$, and 18 s MW irradiation time), CW (0.250 mM HAuCl4 for 17 s), SFE (0.03% FLE, 0.5 mM $HAuCl_4$ and 20 sec MW irradiation time), SmFE (8% PFE, 1 mM $HAuCl_4$ and 25 sec of MW irradiation time) and *C. procera* (AF) (3% procera latex, 1mM $HAuCl_4$ and 40 sec MW irradiation).

We have employed the TEM technique to visualize the size and shape of formed AuNPs and showed shapes of triangular, hexagonal, rod shaped and spherical. XRD pattern suggested that the AuNPs synthesized by plant materials were crystalline in nature. Intense diffraction peaks were clearly observed at (111), (200) and (220) corresponding to the Bragg's angles at 38.1°, 44.4° and 64.5°, respectively. FT-IR, NMR and EDX analyses demonstrated the presence of biomolecules on the surface of AuNPs arising from the strong reducing molecules such as phenolic compounds, flavonoids and antioxidants which are involved in the reduction of gold salts to AuNPs. Cytotoxicity studies revealed that there is no significant toxicity of AuNPs on the proliferation of cells.

The small size of AuNPs synthesized with these plant leaf extracts provides an opportunity for safe delivery to sub cellular organelles and applications in molecular imaging and therapy.

Chapter Five confronts the sonocatalytic mediated synthesis of AuNPs. In this study, we determined the optimum conditions for synthesis of AuNPs by using ethanolic extract of *A. paniculata* as ALE, $HAuCl_4$, amplitude, ultrasonication and pH time for the spherical synthesis of the AuNPs. Biomolecules such as flavonoids and phenolic compounds found in *A. paniculata* are involved in the reduction of gold ions to AuNPs. The properties of synthesized AuNPs were extensively characterized with biophysical tools. The crystalline nature of the synthesized AuNPs was confirmed from the selected area electron diffraction (SAED) pattern with bright circular rings corresponding to the (1 1 1), (2 0 0), and (2 2 0) planes. We observed the different coloured colloidal solutions for AuNP–PCL, AuNP–GL, and AuNP–PCL–GL composites. The successful functionalization of PCL, GL, and PCL–GL onto the AuNPs was confirmed from XRD and FT-IR analyses. The cytotoxic studies revealed that the maximum dose (100 µmol/L) of synthesized AuNPs showed insignificant toxicity on HeLa and MCF-7 cells. The rapidness and eco-friendly method mentioned here for the synthesis of AuNPs provides an opportunity for application in drug delivery and molecular imaging.

Chapter Six presents the overall summary of the investigations, and the scope for further studies. This chapter present the outline of synthesis of AuNPs using some indigenous medicinal plant and fruit extracts from North East India, includes *Fagopyrum esculentum* leaf extract (FLE), *Piper betle* leaf extract (PLE), *Cocos nucifera* (coconut water; CW), *Solanum indicum* fruit extract (SFE) and *Sapindus mukorossi* fruit extracts (SmFE) and *Calotropis procera* Aqueous fraction of latex. This chapter also confronts various methods to mediate the synthesis of AuNPs such as heat, UV irradiation,

microwave irradiation and sonocatalysis. The work presented in the thesis has been peer reviewed and resulted in the following international journal publications and reprints are included under section of list of publication:

1. **Babu PJ**, Sharma P, Saranya S, Bora U. UV Light mediated synthesis of gold nanoparticles using ethonolic leaf extract of *Bacopa monnieri*. Materials Letters. 2012; 93: 431–434.
2. **Babu PJ,** Sharma P, Bora U. *Sapindus mukorossi* aqueous fruit extract as reducing, capping and dispersing agents in synthesis of gold nanoparticles. (Accepted for publication in Micro and Nano Letters, 2012).
3. **Babu PJ,** Saranya S, Sharma P, Tamuli R, Bora U. Sonocatalytic Synthesis of Gold Nanoparticles Using Ethnolic Extract of *Andrographis paniculata* and Functionalization with Gelatin-Polycaprolactone Composites. Front Mater Sci. 2012**;** 6(3): 236–249.
4. **Babu PJ**, Das RK, Gogoi N, Sharma P, Bora U. Microwave mediated rapid synthesis of gold nanoparticles using *Calotropis procera* latex and study of optical properties. ISRN Nanomaterials. 2012: 1–6.
5. **Babu PJ**, Sharma P, Saranya S, Tamuli R, Bora U. *Piper betle* Mediated Green Synthesis of Biocompatible Gold Nanoparticles. International Nano Letters. 2012; 2:18–28.
6. **Babu PJ,** Sharma P, Kalita MC, Bora U. Green Synthesis of Biocompatible Gold Nanoparticles Using *Fagopyrum esculentum* Leaf Extract. Front Mater Sci. 2011**;** 5(4): 379–387**.**

7. **Babu PJ,** Das RK, Kumar A, Bora U. Microwave Mediated Synthesis of Gold Nanoparticles Using Coconut Water. Int J Green Nanotechnol Biomed. 2011; 3:13–21.
8. **Babu PJ,** Sharma P, Borthakur BB, Das RK, Nahar P, Bora U. Synthesis of Gold Nanoparticles Using *Mentha arvensis* Leaf Extract. Int J Green Nanotechnol Phys and chem. **2010;** 2(2): 62–68.

Manuscripts in Communication

9. **Babu PJ,** Saranya S, Sharma P, Tamuli R, Bora U. Green Synthesis and Characterization of Biocompatible Gold Nanoparticles Using *Solanum indicum* Fruits (Minor Review under progress in Nanomaterials and Nanotechnology, 2012).

AuNPs	:	Gold nanoparticles
TEM	:	Transmission Electron Microscope
HRTEM	:	High Resolution Transmission Electron Microscope
SAED	:	Selected Area Electron Diffraction
SEM	:	Scanning Electron Microscope
FTIR	:	Fourier Transform Infrared Spectroscopy
XRD	:	X-Ray Diffraction Spectroscopy
EDX	:	Energy-dispersive X-ray spectroscopy
TGA	:	Thermo gravimetric Analysis
MTT	:	3-(4,5-Dimethylthiazol-2-Yl)-2,5-Diphenyltetrazolium Bromide
MLE		*Mentha arvensis* Leaf Extract
ALE		*Andrographis paniculata* Leaf Extract
BLE		*Bacopa monnieri* Leaf Extract
FLE		*Fagopyrum esculentum* Leaf Extract
PLE		*Piper betle* Leaf Extract
CW		Coconut Water
SFE		*Solanum indicum* Fruit Extract
SmFE		*Sapindus mukorossi* Fruit Extract
AF		Aqueous Fraction
MW		Microwave Irradiation
PCL		Poly Caprolactone
GL		Gelatin
PCL–GL		Poly Caprolactone- Gelatin
AuNP–PCL		Gold nanoparticles - Poly Caprolactone

AuNP–GL	Gold nanoparticles- Gelatin
AuNP–PCL-GL	Gold nanoparticles - Poly Caprolactone- Gelatin
NPs	Nanoparticles

-- * --

LIST OF TABLES

-- * --

LIST OF FIGURES

LIST OF SCHEMES

TABLE OF CONTENTS

TABLE OF CONTENTS

TABLE OF CONTENTS

1.1 Nanotechnology

Nanotechnology is the engineering of functional systems at the molecular scale. Generally, nanotechnology works with materials, devices, and other structures with at least one dimension sized from 1 to 100 nanometers. Nanotechnology, nanoscience, nanostructure, nanoparticles are now of the most widely used words in scientific literature. Nanoscale materials are very attractive for possible machine, which will be able to travel through the human body and repair damaged tissues or supercomputers which small enough to fit in shirt pocket. Although the term nanotechnology is new, it has been widely used for the development of more efficient technology in diverse fields. Its diversity, range from extensions of conventional devices to completely new approaches for developing new materials with dimensions on the nanoscale to direct control of matter on the atomic scale. In recent years, nanotechnology has been embraced by industrial sectors due to its applications in the field of electronic storage systems (Kang et al., 1996) biotechnology (Pankhurst et al., 2003), targeted drug delivery (Dobson et al., 2006; Rudge et al., 2001) and vehicles for gene and drug delivery (Pankhurst et al., 2003; Dobson et al., 2006; Rudge et al., 2001). Consequently, with wide range of applications available, nanotechnology has potential to make a significant impact to the society. The difference in the physiochemical properties of nanomaterials in contrast to macromolecules can be attributed to their high surface-to-volume ratio. Due to this unique property, nanomaterials make excellent candidate for biomedical applications as variety of biological processes occur at nanometer scales.

Metal nanoparticles were used a long time ago. For e.g. The famous Glass Lycurgus Cup from the Romans times (4th century AD) contains silver and gold nanoparticles in approximate ratio 7:3 which have size diameter about 70 nm. Even though, nanoparticle use

is quite ancient, its earlier practitioners never realized that they have fabricated items at the nano scale. After the development of modern devices to analyze materials in nanoscale, scientists become empowered to prove their scale of fabrication more convincingly and this provided an opportunity for nanotechnology to become an interesting subject for science and mankind.

Figure 1.1 *Lycurgus Cup (a) green color, if light source comes from outside of the cup (b) red color, if the light source comes from inside of the cup*

1.1.1 Richard Feynman's idea of nanotechnology

The idea of nanotechnology was first introduced in 1959, by noble laureate Richard Feynman, through his revolutionary lecture "There's Plenty of Room at the Bottom" (Feynman et al., 1960). Though he never explicitly mentioned "nanotechnology," Feynman suggested that it will eventually be possible to precisely manipulate atoms and molecules. He said it was possible to create "nano-scale" machines, through a cascade of billions of

factories. According to the physicist, these factories would be progressively smaller scaled versions of machine hands and tools. He proposed that these tiny "machine shops" would then eventually be able to create billions of tinier factories. In these speculations, he also suggested that there are various factors, which uniquely affect the nano-scale level. Specifically, he suggested that as the scale got smaller and smaller, gravity would become more negligible, while both Van Der Waals attraction and surface tension would become very important. In the end, Feynman's talk has been viewed as the first academic talk that dealt with a main tenet of nanotechnology, the direct manipulation of individual atoms (molecular manufacturing) (Appenzeller et al., 1991).

1.1.2 Concept of 'nano' and comparison

Matter can be placed into broad categories according to size. Macroscopic matter is visible with the naked eye. Atoms and (most) molecules are microscopic with dimensions < 1nm. Mesoscopic particles, such as bacteria and cells that have dimensions on the order of micron(s), can be observed with optical microscopes. Falling into the gap between the microscopic and the mesoscopic is another class of matter, the nanoscopic particles. The size of nanoparticles is compared to that of other "small" particles as shown in **Figure 1.2**

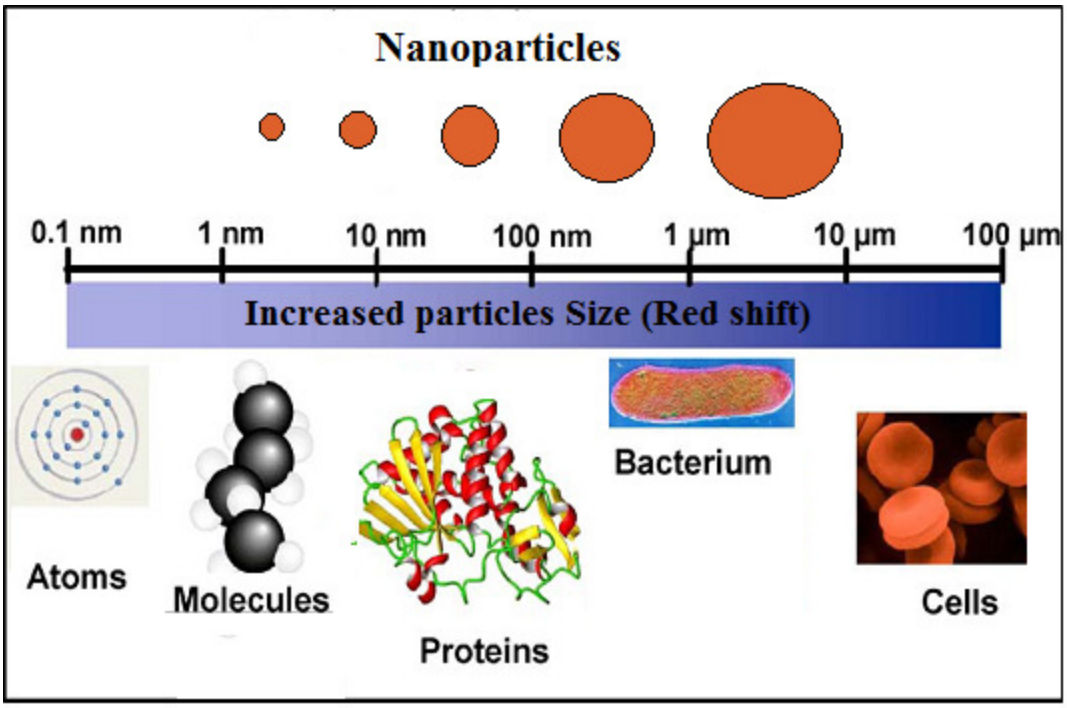

Figure 1.2 *Comparison of nanoparticles with the biological molecules*

One nanometer (nm) is one billionth, or 10^{-9}, of a meter. By comparison, typical carbon-carbon bond lengths, or the spacing between these atoms in a molecule is in the range 0.12–0.15 nm, and a DNA double-helix has a diameter around 2 nm. On the other hand, the smallest cellular life-forms, the bacteria of the genus Mycoplasma, are around 200 nm in length. By convention, nanotechnology is taken as the scale range 1 to 100 nm, the lower limit is set by the size of atoms (hydrogen has the smallest atoms, which are approximately a quarter of a nm diameter) since nanotechnology must build its devices from atoms and molecules. The upper limit is more or less arbitrary but is around the size not observed in larger structures (Salata et al., 2004). These new phenomena make nanotechnology distinct from devices which are merely miniaturized versions of an equivalent macroscopic device; such devices are on a larger scale and come under the description of micro technology.

1.1.3 General purpose of nanotechnology

Nanotechnology is referred to as a general purpose technology because of its advanced form. It has significant impact on almost all industries and all areas of society. Nanotechnology applications are widely distributed in communication, medicine, transportation, agriculture, and industry sector as it offers significant advantages such as better built, longer lasting, safer, smarter products.

1.1.4 Nanotechnology– a revolution technology

Throughout history, revolutionary technical advances have emerged and changed the world businesses. Nanotechnology emerged as the latest entrant in the list of all revolutionary technical advances. "Nanotechnology has the potential to be the most revolutionary development in this century," said Jack W. Plunkett, the chief executive officer of Plunkett Research and is supported by many scientists. It has the potential to revolutionize how materials are constructed and enable suppliers to deliver items that cost less, are environmentally safe, and are stronger and lighter than steel. By keeping the following criteria listed in **Table 1.1.** We can undoubtedly say nanotechnology is the revolution technology.

Table 1.1 *Outlines some of the salient features of a nano revolution.*

Criterion	Comments
Basis	Nanotechnology is firmly grounded in reality—the physical properties and phenomena associated with nanotechnology are real and significant—they are the drivers behind the "revolution."
Speed	Although speed is not the only major component of a revolution, the faster it happens, the more revolutionary is its impact and the more profound its legacy. Nanotech has hit the mainstream since the mid-1990s—not that long ago. Changes nowadays are expected to occur quickly.
Track record	Outside of computers, pharmaceuticals, and nanoparticles, the glamorous and highly touted quantum-dots, carbon nanotubes, and drug delivery nanomaterials have not yet made a
Research papers, conferences	The scientifi c community has fully embraced nanoscience and nanotechnology. There is no single scientifi c conference in physics, chemistry, engineering, biology or medicine that does not have presentations, posters, sessions or the whole conference dedicated to nano.
Nanocompanies	There are more and more nanocompanies every year. Small Times Magazine lists 3500 nanocompanies just in the United States [4]. Nearly all Fortune 500 companies have some involvement in nanotechnology
Patents	The number of patents (and the trend) is burgeoning—if anything, this trend indicates revolutionary proportions.
Stock market	Not big yet.
Institutions	About 500 institutions ranging from nonprofi ts, industry associations, research labs, economic development organizations, and university and educational institutions are registered with Small Times Magazine as nano groups [4].
% Workforce	Technology workforce contributes less than 10% of the total U.S. workforce in general. Nanotechnology, in its broadest sense (computers, pharmaceuticals, etc.), is already involved in many sectors. By 2015, 2 million more "nanotech" jobs are expected to emerge.
Education	Concerted efforts are underway to promote nanotechnology in K-12 and higher. Although a great proportion of the U.S. population knows about nanotechnology through movies, it is not considered to be a signifi cant part of curricula at this time, but this too is changing.
Products	Nanosized transistors are already part of computer chips—although developed rather quietly without much fanfare via the natural evolutionary process of miniaturization. There is no doubt that more products will undergo enabling/ enhancement from nanotechnology.
Evolutionary	Evolutionary components are not considered to be revolutionary. In

component	this case, nano is very evolutionary—emerging from micro- and biotech industries—a natural, nonrevolutionary process of miniaturization, ever since the first timepiece was developed.
Hype	Since the days of the "turbo," nothing has been hyped more than nanotechnology.
Upside	The reality-based upside and promise of nanotechnology is tremendous.

1.1.5 Nanotechnology time line

Nanotechnology is the unknowingly used from ancient period and many remarkable incidents and milestone were took place in the history of mankind. The following **Table 1.2** describes the timeline features of premodern as well as modern Era discoveries and milestones in the field of nanotechnology.

Table 1.2 *Milestone of the nanotechnology*

Time Period	Milestones
4th Century	The Lycurgus Cup (Rome) is an example of dichroic glass; colloidal gold and silver in the glass allow it to look opaque green when lit from outside but translucent red when light shines through the inside.
9th-17th Centuries	Glowing, glittering "luster" ceramic glazes used in the Islamic world, and later in Europe, contained silver or copper or other metallic nanoparticles.
6th-15th Centuries	Vibrant stained glass windows in European cathedrals owed their rich colors to nanoparticles of gold chloride and other metal oxides and chlorides; gold nanoparticles also acted as photocatalytic air purifiers.
13th-18th Centurties	"Damascus" saber blades contained carbon nanotubes and cementite nanowires—an ultrahigh-carbon steel formulation that gave them strength, resilience, the ability to hold a keen edge, and a visible moiré pattern in the steel that give the blades their name.
1936	Erwin Müller, working at Siemens Research Laboratory, invented the field emission microscope, allowing near-atomic-resolution images of materials.
1947	John Bardeen, William Shockley, and Walter Brattain at Bell Labs discovered the semiconductor transistor and greatly expanded scientific knowledge of semiconductor interfaces, laying the foundation for electronic devices and the Information Age.
1950	Victor La Mer and Robert Dinegar developed the theory and a process for growing monodisperse colloidal materials. Controlled ability to fabricate colloids enables myriad industrial uses such as specialized papers, paints, and thin films, even dialysis treatments
1951	Erwin Müller pioneered the field ion microscope, a means to image the

	arrangement of atoms at the surface of a sharp metal tip; he first imaged tungsten atoms.
1956	Arthur von Hippel at MIT introduced many concepts of—and coined the term—"molecular engineering" as applied to dielectrics, ferroelectrics, and piezoelectrics.
1958	Jack Kilby of Texas Instruments originated the concept of, designed, and built the first integrated circuit, for which he received the Nobel Prize in 2000.
1959	Richard Feynman of the California Institute of Technology gave what is considered to be the first lecture on technology and engineering at the atomic scale, "There's Plenty of Room at the Bottom" at an American Physical Society meeting at Caltech.
1965	Intel co-founder Gordon Moore described in Electronics magazine several trends he foresaw in the field of electronics. One trend now known as "Moore's Law," described the density of transistors on an integrated chip (IC) doubling every 12 months (later amended to every 2 years).
1974	Tokyo Science University Professor Norio Taniguchi coined the term nanotechnology to describe precision machining of materials to within atomic-scale dimensional tolerances.
1981	Gerd Binnig and Heinrich Rohrer at IBM's Zurich lab invented the scanning tunneling microscope, allowing scientists to "see" (create direct spatial images of) individual atoms for the first time. Binnig and Rohrer won the Nobel Prize for this discovery in 1986.
1981	Russia's Alexei Ekimov discovered nanocrystalline, semiconducting quantum dots in a glass matrix and conducted pioneering studies of their electronic and optical properties.
1985:	Bell Labs's Louis Brus discovered colloidal semiconductor nanocrystals (quantum dots), for which he shared the 2008 Kavli Prize in Nanotechnology.
1986:	Gerd Binnig, Calvin Quate, and Christoph Gerber invented the atomic force microscope, which has the capability to view, measure, and manipulate materials down to fractions of a nanometer in size, including measurement of various forces intrinsic to nanomaterials.
1986:	Gerd Binnig, Calvin Quate, and Christoph Gerber invented the atomic force microscope, which has the capability to view, measure, and manipulate materials down to fractions of a nanometer in size, including measurement of various forces intrinsic to nanomaterials.
1999:	Chad Mirkin at Northwestern University invented dip-pen nanolithography® (DPN®), leading to manufacturable, reproducible "writing" of electronic circuits as well as patterning of biomaterials for cell biology research, nanoencryption, and other applications.

2004:	Britain's Royal Society and the Royal Academy of Engineering published Nanoscience and Nanotechnologies: Opportunities and Uncertainties advocating the need to address potential health, environmental, social, ethical, and regulatory issues associated with nanotechnology. SUNY Albany launched the first college-level education program in nanotechnology in the United States, the College of Nanoscale Science and Engineering.
2005	Erik Winfree and Paul Rothemund from the California Institute of Technology developed theories for DNA-based computation and "algorithmic self-assembly" in which computations are embedded in the process of nanocrystal growth.
2006:	James Tour and colleagues at Rice University built a nanoscale car made of oligo(phenylene ethynylene) with alkynyl axles and four spherical C60 fullerene (buckyball) wheels. In response to increases in temperature, the nanocar moved about on a gold surface as a result of the buckyball wheels turning, as in a conventional car. At temperatures above 300°C it moved around too fast for the chemists to keep track of it!
2007	Angela Belcher and colleagues at MIT built a lithium-ion battery with a common type of virus that is nonharmful to humans, using a low-cost and environmentally benign process. The batteries have the same energy capacity and power performance as state-of-the-art rechargeable batteries being considered to power plug-in hybrid cars, and they could also be used to power personal electronic devices
2008	The first official NNI Strategy for Nanotechnology-Related Environmental, Health, and Safety (EHS) Research was published, based on a two-year process of NNI-sponsored investigations and public dialogs. This strategy document was updated in 2011, following a series of workshops and public review.
2009–2010	Nadrian Seeman and colleagues at New York University created several DNA-like robotic nanoscale assembly devices.
2010	IBM used a silicon tip measuring only a few nanometers at its apex (similar to the tips used in atomic force microscopes) to chisel away material from a substrate to create a complete nanoscale 3D relief map of the world one-one-thousandth the size of a grain of salt—in 2 minutes and 23 seconds.
2011	The NSET Subcommittee updated the NNI Strategic Plan and the NNI Environmental, Health, and Safety Research Strategy, drawing on extensive input from public workshops and online dialog with stakeholders from Government, academia, NGOs, and the public, and others.

1.2 Nanotechnology and its applications

Nanotechnology made it possible to manufacture lighter, stronger and programmable materials that require less energy to produce than conventional methods that produce less waste than with conventional manufacturing, and that promise greater fuel efficiency in land transportation, ships, aircraft, and space vehicles. Nanocoatings for both opaque and translucent surfaces may render them resistant to corrosion, scratches, and radiation. Nanoscale electronic, magnetic, mechanical devices and systems with unprecedented levels of information processing can be fabricated which can be acts as biological sensors for protection, health care, manufacturing and the environment. The potential for improvements in health, safety, quality of life, and conservation of the environment are vast. Nanotechnology is helping to considerably improve even revolutionize many technology and industry sectors such as information technology, energy, environmental science, medicine, homeland security, food safety, and transportation, among many others. Described below is a sampling of the rapidly growing list of benefits and applications of nanotechnology (**Figure 1.3**). The following information was draw from the site of national nanotechnology initiative (NNI) which is an official website for the nanotechnology.

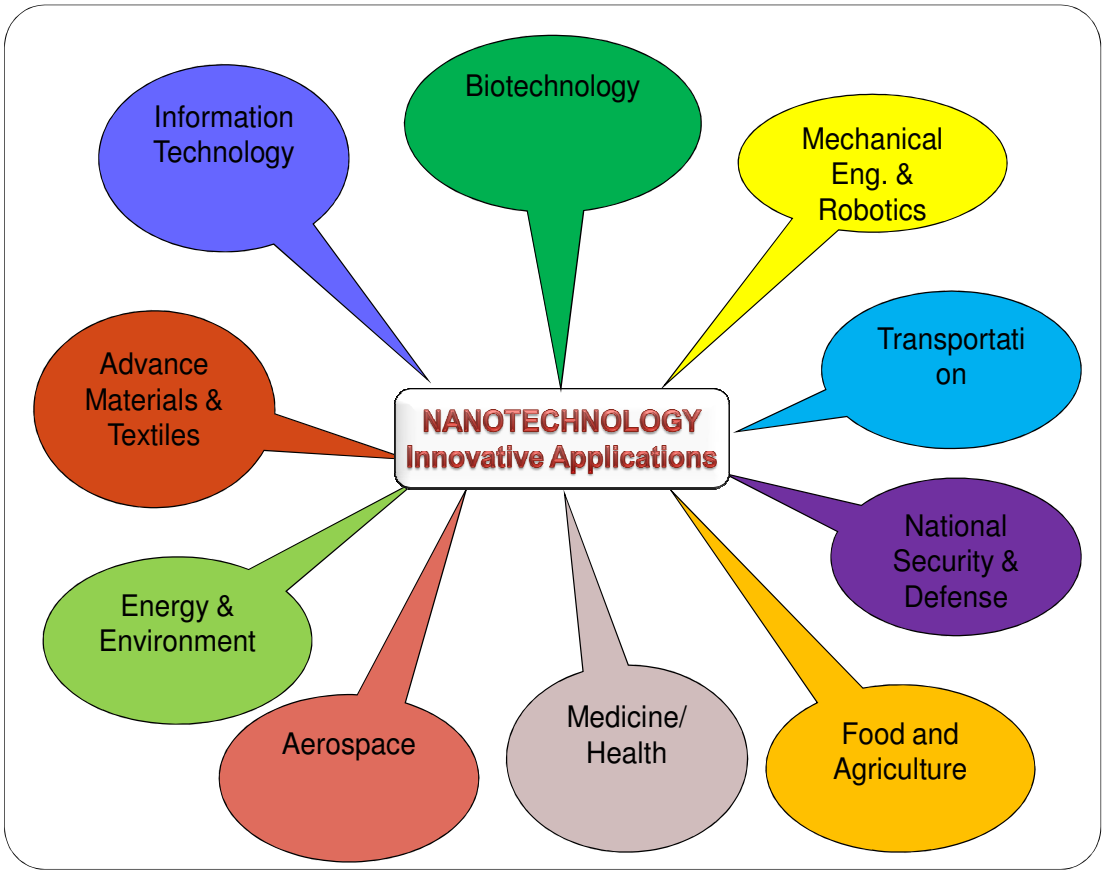

Figure 1.3 *Diverse applications of nanotechnology in today's life*

1.2.1 Electronics and information technology

Nanotechnology is already in use in many computing, communications, and other electronics applications to provide faster, smaller, and more portable systems that can manage and store larger and larger amounts of information. These continuously evolving applications include:

- Nanoscale transistors that are faster, more powerful and energy-efficient; computer's entire memory may be stored on a single tiny chip.

- Magnetic random access memory (MRAM) enabled by nanometer-scale magnetic tunnel junctions that can quickly and effectively save even encrypted data during a system shutdown or crash, enable resume-play features, and gather vehicle accident data.

- Displays for many new TVs, laptop computers, cell phones, digital cameras, and other devices incorporate nanostructured polymer films known as organic light-emitting diodes, or OLEDs. OLED screens offer brighter images in a flat format, as well as wider viewing angles, lighter weight, better picture density, lower power consumption, and longer lifetimes.

- Other computing and electronic products include flash memory chips for iPod nanos; ultraresponsive hearing aids; antimicrobial/antibacterial coatings on mouse/keyboard/cell phone casings; conductive inks for printed electronics for RFID/smart cards/smart packaging; more life-like video games; and flexible displays for e-book readers.

1.2.2 Sustainable energy

Nanotechnology is expected to have a major impact on the energy industry. Once manufacturing techniques have matured, utilities will have new ways to capture, store and transfer energy. For example, the nanotechnology may be used to conduct energy more efficiently. In addition, it has the potential to enable energy producers to address the storage challenges that hydrogen and solar energy now present. The difficulty of meeting the world's

energy demand is compounded by the growing need to protect our environment. Many scientists are looking into ways to develop clean, affordable, and renewable energy sources along with means to reduce energy consumption and lessen toxicity burdens on the environment. Some of the applications in energy sector as followed.

- Nanotechnology is already being used in numerous new kinds of batteries that are less flammable, quicker-charging, more efficient, lighter weight, and that has a higher power density and hold electrical charge longer. One new lithium-ion battery type uses a common, nontoxic virus in an environmentally benign production process.
- Nanostructured materials are being pursued to greatly improve hydrogen membrane and storage materials and the catalysts needed to realize fuel cells for alternative transportation technologies at reduced cost. Researchers are also working to develop a safe, lightweight hydrogen fuel tank.
- Various nanoscience-based options are being pursued to convert waste heat in computers, automobiles, homes, power plants, etc., to usable electrical power.
- An epoxy containing carbon nanotubes is being used to make windmill blades that are longer, stronger, and lighter-weight than other blades to increase the amount of electricity that windmills can generate.
- Researchers are developing wires containing carbon nanotubes to have much lower resistance than the high-tension wires currently used in the electric grid and thus reduce transmission power loss.
- To power mobile electronic devices, researchers are developing thin-film solar electric panels that can be fitted onto computer cases and flexible piezoelectric

nanowires woven into clothing to generate usable energy on-the-go from light, friction, and/or body heat.

1.2.3 Environmental remediation

There are many eco-friendly applications for nanotechnology such as materials that provide clean water from polluted water sources in both large-scale and portable applications and ones that detect and clean up environmental contaminants.

- Researchers have developed a nanofabric "paper towel," woven from tiny wires of potassium manganese oxide that can absorb 20 times its weight in oil for cleanup applications.
- Many airplane cabin and other types of air filters are nanotechnology-based filters that allow “mechanical filtration,” in which the fiber material creates nanoscale pores that trap particles larger than the size of the pores. They also may contain charcoal layers that remove odors. Almost 80% of the cars sold in the U.S. include built-in nanotechnology-based filters.
- Nanoparticles will someday be used to clean industrial water pollutants in ground water through chemical reactions that render them harmless, at much lower cost than methods that require pumping the water out of the ground for treatment.

1.2.4 Future transportation

In addition to contributing to building and maintaining lighter, smarter, more efficient, and “greener” vehicles, aircraft, and ships, nanotechnology offers various means to improve the transportation infrastructure:

- Nano-engineering of steel, concrete, asphalt, and other cementitious materials, and their recycled forms, offers great promise in terms of improving the performance and longevity of highway and transportation infrastructure components while reducing their cost. New systems may incorporate innovative capabilities into traditional infrastructure materials, such as the ability to generate or transmit energy.

- Nanoscale sensors and devices may provide cost-effective continuous structural monitoring of the condition and performance of bridges, tunnels, rails, parking structures and pavements over time. Nanoscale sensors and devices may also support an enhanced transportation infrastructure that can communicate with vehicle-based systems to help drivers maintain lane position, avoid collisions, adjust travel routes to circumnavigate congestion, and other such activities.

1.2.5 Nanobiosystems, medical, and health

Nanotechnology has the real potential to revolutionize a wide array of medical and biotechnology tools and procedures so that they are more personalized, portable, cheaper, safer, and easier to administer. Below are some examples of important advances in these areas.

- Quantum dots are semiconducting nanocrystals that can enhance biological imaging for medical diagnostics. When illuminated with ultraviolet light, they emit a wide spectrum of bright colors that can be used to locate and identify specific kinds of cells and biological activities. These crystals offer optical detection up to 1,000 times

better than conventional dyes used in many biological tests, such as MRIs, and render significantly more information.

- Gold nanoparticles can be used to detect early-stage Alzheimer's disease.
- Molecular imaging for the early detection where sensitive biosensors constructed of nanoscale components (e.g., nanocantilevers, nanowires, and nanochannels) can recognize genetic and molecular events and have reporting capabilities, thereby offering the potential to detect rare molecular signals associated with malignancy.
- Multifunctional therapeutics where a nanoparticle serves as a platform to facilitate its specific targeting to cancer cells and delivery of a potent treatment, minimizing the risk to normal tissues.
- Research enablers such as microfluidic chip-based nanolabs capable of monitoring and manipulating individual cells and nanoscale probes to track the movements of cells and individual molecules as they move about in their environments.

1.3 Nanomaterials and its types

The field of nanocomposite materials has the attention, imagination and close scrutiny of scientists and engineers in recent years. This scrutiny results from the simple premise that using building blocks with dimensions in the nano size range makes it possible to design and create new materials with unprecedented flexibility and improvements in their properties and used in the various applications. These nanomaterials can be broadly divided into four categories include metallic, ceramic, polymeric and nanocomposites. In the broad sense, nanocomposites are the combination of the metallic, ceramic, and polymeric nanomaterials to form composites. Nanocomposites include porous media, colloids, gels and copolymers.

1.3.1 Metallic nanomaterials

Owing to their unique electric, magnetic, optical, and catalytic properties, metal nanoparticles (NPs) have emerged as a new class of compounds that are interesting in several areas from chemistry to physics, to material sciences, to biology and medicine (Georgakilas et al., 2007; Cozzoli et al., 2006). Importantly, these properties differ from those of the bulk materials and mainly depend on the particle size and morphology (Hamley et al., 2003; Schlögl et al., 2004; Hodes et al., 2007). The hot research points in metal NPs focus on the synthesis of noble metal NPs such as Au, Ag, Pt, Pd, Ru and their alloys (Wang et al ., 2008; Choi et al ., 2009; Wang et al .,2009; Zhang er al ., 2009; Guo et al ., 2010).

Metal nanoparticles with nanometer-scale dimensions are of great interest due to their unusual properties. Fundamentally, the mean free path of an electron in a metal at room temperature is ~10-100 nm, and one would predict that as the metallic particle shrinks to this dimension, unusual effects should be observed (El-Sayed et al., 2001; Feldheim et al., 2002; Daniel et al., 2004). Indeed, gold nanospheres of diameter ~100 nm or smaller appear red (not gold) when suspended in transparent media (El-Sayed et al., 2001; Feldheim et al., 2002; Daniel et al., 2004), and gold nanoparticles of diameter less than ~3 nm are no longer "noble" and un reactive, but can catalyze chemical reactions (Valden et al., 1998; Chen et al., 2004). In addition to favorable functional properties, nanometer scale metallic wires show extraordinarily high combinations of strength, stiffness, and ductility relative to bulk materials. Nanorods and nanowires have promising applications in electronics (Huang et al., 2001; Mallouk et al., 2002), photonics (Law et al., 2004: Maier et al., 2001; Maier et al. 2003), hierarchical biologically inspired nano composites (Fan et al., 2000; Gaoet al., 2003; Ji et al., 2004), (bio)chemical sensing and imaging (Katz et al., 2004; Schultz et al., 2003),

and drug delivery (Salem et al., 2003; Tkachenko et al., 2003). Gold colloids have been used for years as contrast agents in electron microscopy because gold is so electron-dense. More recently, gold and silver nanoparticles are used in biological optical imaging and sensing applications (Schultz et al., 2003; Elghanian et al., 1997).

1.3.2 Polymeric nanomaterials

As name itself suggest polymeric nanoparticles are nanoparticles which are prepared from polymers. Biodegradable polymers such as poly (D,L-lactic acid) (PLA), poly (D,L-lactic-*co*-glycolic acid) (PLGA), and poly (ε-caprolactone) (PCL) and their copolymers diblocked or multiblocked with poly(ethylene glycol) (PEG) have been commonly used to form polymeric nanoparticles to encapsulate a variety of therapeutic compounds (Lupold et al., 2002; Farokhzad et al., 2004; Farokhzad et al., 2006). These include polymeric micelles, capsules, colloids, dendrimers, etc.

In recent years, biodegradable polymeric nanoparticles have attracted considerable attention as potential drug delivery devices in view of their applications in drug targeting to particular organs/tissues, as carriers of DNA in gene therapy, and in their ability to deliver proteins, peptides and genes (Avgoustakis et al., 2004; Gref et al., 1995). One such polymeric NP is Genexol-PM^{TM}, a PLGA-*b*-methoxy PEG NP encapsulating paclitaxel, which has received regulatory approval in South Korea for clinical use and same is currently undergoing phase II clinical trials for a number of cancer indications in the United States.

Polymeric NPs can be formulated by self-assembly of block copolymers consisting of two or more polymer chains with different hydrophobicity (Grobmyer et al., 2010). These copolymers spontaneously assemble into a core-shell structure in an aqueous environment to

minimize the system's free energy. Specifically, the hydrophobic blocks form the core to minimize their exposure to aqueous surroundings, whereas the hydrophilic blocks form the coronalike shell to stabilize the core through direct contact with water. Drug release rates from the polymeric NPs can be controlled by modifying polymer chemical and physical properties (Avgoustakis et al., 2004; Gref et al., 1995; Grobmyer et al., 2010).

1.3.3 Ceramic nanomaterials

Over the past half century ceramics have received significant attention as candidate materials for use as structural materials under conditions of high loading rates, high temperature and chemical attack that are too severe for metals. However, inherent brittleness of the ceramics has prevented their wide use in different applications. The definition of nanocomposite material has broadened significantly to encompass a large variety of systems such as one-dimensional, two-dimensional, three-dimensional and amorphous materials, made of distinctly dissimilar components and mixed at the nanometer scale. The general class of nanocomposite organic/inorganic materials is a fast growing area of research. One of the most recent developments has been the distribution of multiple phases in a ceramic composite at the nanoscopic length scale with robustness. Owing to prevalence of nanoscopic features, they can be used in various applications.

We described some important applications of the ceramics in biomedical field. Ceramics and glasses can directly bound to living bone without the formation of surrounding fibrous tissue. In such cases a bone-like apatite layer is deposited in vivo between the implant and bone (Kokubo et al., 2003). This mineralization ability has been defined as bioactivity of biomaterial. Hydroxyapatite (HA), which constitutes the inorganic fraction of bone, has been

considered to be a bioactive material due to its osteoconductivity (Hench et al., 1996). However, recent investigation has revealed that bioactive glasses (BAGs) or bioactive glass ceramics (BGCs) have a much better performance in bone tissue engineering than HA (Xynos et al., 2000; Wheeler et al., 2001). BAG has been used as bone filler material, applied in clinical treatment of periodontal disease (Hench et al., 1998), and used to replace damaged middle ear bone (Hench et al., 1997). Porous BAG can facilitate vascularization and new bone in growth, so has became a potential useful material for orthopedic applications (Gauthier et al., 1998; Jiang et al., 1999; Shi et al., 2000). Meanwhile, the bioactive filler, comprising BAG and BGC particles, can serve as a reinforcing component to enhance the stiffness of polymer composites. Composites of polymers and bioactive ceramics have attracted increasing attention as promising biomaterials for bone tissue engineering (Maquet et a., 2004; Mano et al., 20047; Chouzouri et at., 2007). Three dimensional (3D) porous composite scaffolds can induce the growth of cell to the desired shape and may facilitate the vascularization of new generated tissue (Chouzouri et al., 2002; Griffith et al., 2007).

1.3.4 Composite nanomaterials

Nanocomposite is a multiphase solid material where one of the phases has one, two or three dimensions of less than 100 nanometers (nm), or structures having nano-scale repeat distances between the different phases that make up the material (Ajayan et al., 2003). In the broadest sense this definition can include porous media, colloids, gels and copolymers, but is more usually taken to mean the solid combination of a bulk matrix and nano-dimensional phase(s) differing in properties due to dissimilarities in structure and chemistry. The mechanical, electrical, thermal, optical, electrochemical, catalytic properties of the nanocomposite will differ markedly from that of the component materials. Size limits for

these effects have been proposed, <5 nm for catalytic activity, <20 nm for making a hard magnetic material soft, <50 nm for refractive index changes, and <100 nm for achieving superparamagnetism, mechanical strengthening or restricting matrix dislocation movement (Kamigaito et al., 1991). Nanocomposites can be broadly classified in to three types such as ceramic, metallic and polymeric nanocomposites.

1.3.4.1 Ceramic nanocomposites

In this group of composites the main part of the volume is occupied by a ceramic, i.e. a chemical compound from the group of oxides, nitrides, borides, silicides etc. In most cases, ceramic-matrix nanocomposites encompass a metal as the second component. Ideally both components, the metallic one and the ceramic one, are finely dispersed in each other in order to elicit the particular nanoscopic properties. Nanocomposite from these combinations were demonstrated in improving their optical, electrical and magnetic properties (Kruis et al., 1998) as well as tribological, corrosion-resistance and other protective properties

1.3.4.2 Metallic nanocomposites

Metal matrix nanocomposites can also define as reinforced metal matrix composites. This kind of composites can be classified as continuous and non continuous reinforced materials. One of the important nanocomposites is carbon nanotube metal matrix composites which is emerging new materials that are being developed to take advantage of the high tensile strength and electrical conductivity of carbon nanotube materials. Critical to the realization of CNT-MMC possessing optimal properties in these areas are the development of synthetic techniques that are (a) economically producible, (b) provide for a homogeneous dispersion of nanotubes in the metallic matrix, and (c) lead to strong interfacial adhesion between the

metallic matrix and the carbon nanotubes.In addition to carbon nanotube metal matrix composites, boron nitride reinforced metal matrix composites and carbon nitride metal matrix composites are the new research areas on metal matrix nanocomposites (Bakshi et al., 2010).

1.3.4.3 Polymeric nanocomposites

In the simplest case, appropriately adding nanoparticulates to a polymer matrix can enhance its performance, often in very dramatic degree, by simply capitalizing on the nature and properties of the nanoscale filler (Manias et al., 2007). This strategy is particularly effective in yielding high performance composites, when good dispersion of the filler is achieved and the properties of the nanoscale filler are substantially different or better than those of the matrix, for example, reinforcing a polymer matrix by much stiffer nanoparticles of ceramics, clays, or carbon nanotubes (Mai et al., 2006; Pinnavaia et al., 2001). It should be noted that the improvement in mechanical properties may not be limited to stiffness or strength. Time-dependent properties could be improved by addition of the nanofillers (Zandiatashbar et al., 2012). Alternatively, the enhanced crystallization behavior, and other physical properties of high performance nanocomposites may be mainly due to the high aspect ratio and/or the high surface area of the fillers, since nanoparticulates have extremely high surface area to volume ratios when good dispersion is achieved (Nilesh et al., 2010; Usuki et al., 1993a; Usuki et al., 1993b).

1.3.5 Properties of nanomaterials

Nanomaterials have the structural features in between of atoms and the bulk materials. While most microstructured materials have similar properties to the corresponding bulk materials, the properties of materials with nanometer dimensions are significantly

different from those of atoms and bulks materials. This is mainly due to the nanometer size of the materials which render them: (i) large fraction of surface atoms; (ii) high surface energy; (iii) spatial confinement; (iv) reduced imperfections which do not exist in the corresponding bulk materials. Due to their small dimensions, nanomaterials have extremely large surface area to volume ratio, which makes a large to be the surface or interfacial atoms, resulting in more "surface" dependent material properties. Especially when the sizes of nanomaterials are comparable to length, entire material will be affected by the surface properties of nanomaterials. This in turn may enhance or modify the properties of the bulk materials. For example, metallic nanoparticles can be used as very active catalysts. Chemical sensors from nanoparticles and nanowires enhanced the sensitivity and sensor selectivity. The nanometer feature sizes of nanomaterials also have spatial confinement effect on the materials which bring the quantum effects. The energy band structure and charge carrier density in the materials can be modified quite differently from their bulk and in turn will modify the electronic and optical properties of the materials. For example, lasers and light emitting diodes (LED) from both of the quantum dots and quantum wires are very promising in the future optoelections. High density information storage using quantum dot devices is also a fast developing area. Reduced imperfections are also an important factor in determination of the properties of the nanomaterials. Nanosturctures and Nanomaterials favors of a self purification process in that the impurities and intrinsic material defects will move to near the surface upon thermal annealing. This increased materials perfection affects the properties of nanomaterials. For example, the chemical stability for certain nanomaterials may be enhanced and the mechanical properties of nanomaterials will be better than the bulk materials. The superior mechanical properties of carbon nanotubes are well known. Due to

their nanometer size, nanomaterials are already known to have many novel properties. Many novel applications of the nanomaterials rose from these novel properties have also been proposed.

1.3.5.1 Optical properties

One of the most fascinating and useful aspects of nanomaterials is their optical properties. Applications based on optical properties of nanomaterials include optical detector, laser, sensor, imaging, phosphor, display, solar cell, photocatalysis, photoelectrochemistry and biomedicine (Susie et al., 2006). The optical properties of nanomaterials depend on parameters such as feature size, shape, surface characteristics, and other variables including doping and interaction with the surrounding environment or other nanostructures. Likewise, shape can have dramatic influence on optical properties of metal nanostructures. **Figure 1.4** exemplifies the difference in the optical properties of metal and semiconductor nanoparticles. With the CdSe semiconductor nanoparticles, simple change in size alters the optical properties of the nanoparticles. When metal nanoparticles are enlarged, their optical properties change only slightly as observed for the different samples of gold nanospheres in **Figure 1.4.** However, when an anisotropy is added to the nanoparticle, such as growth of nanorods, the optical properties of the nanoparticles change dramatically.

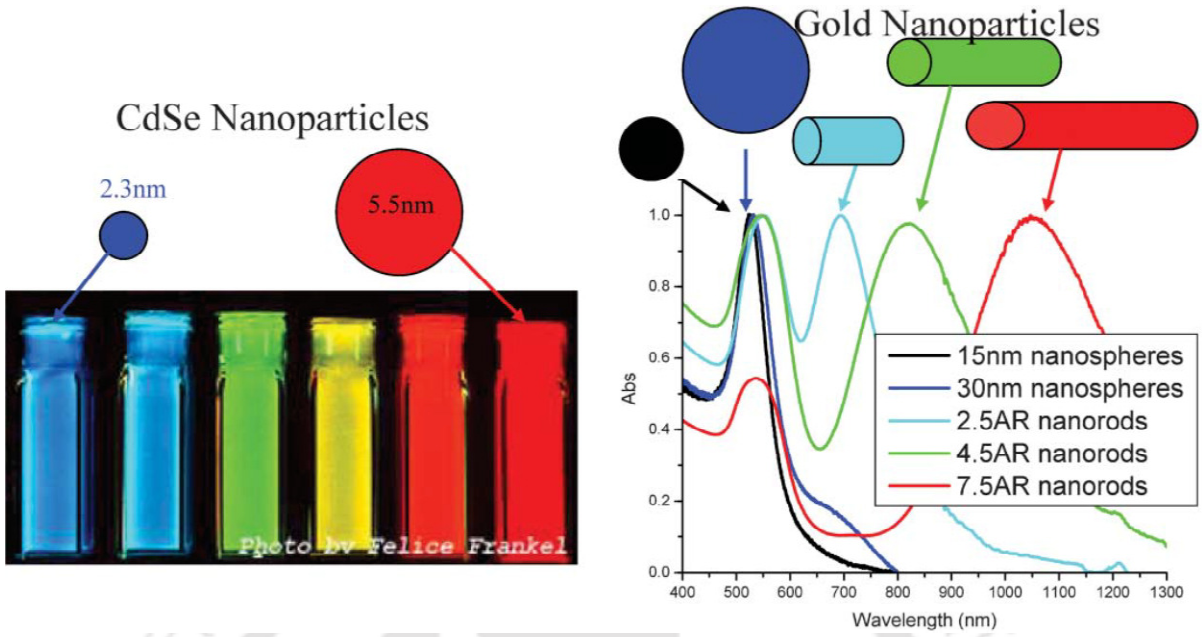

Figure 1.4. *Fluorescence emission of (CdSe) ZnS quantum dots of various sizes and absorption spectra of various sizes and shapes of gold nanoparticles (reproduced with the permission Royal society of chemistry).*

1.3.5.2 Electrical properties

Electrical properties of nanoparticles discuss about fundamentals of electrical conductivity in nanotubes and nanorods, carbon nanotubes, photoconductivity of nanorods, electrical conductivity of nanocomposites. One interesting method which can be used to demonstrate the steps in conductance is the mechanical thinning of a nanowire and measurement of the electrical current at a constant applied voltage (Collins et al., 2000). The important point here is that, with decreasing diameter of the wire, the number of electron wave modes contributing to the electrical conductivity is becoming increasingly smaller by well-defined quantized steps. In electrically conducting carbon nanotubes, only one electron wave mode is observed which transport the electrical current. As the lengths and orientations of the carbon nanotubes

are different, they touch the surface of the mercury at different times which provides two sets of information: (i) the influence of carbon nanotube length on the resistance; and (ii) the resistances of the different nanotubes (Collins et al., 2000). As the nanotubes have different lengths, then with increasing protrusion of the fiber bundle an increasing number of carbon nanotubes will touch the surface of the mercury droplet and contribute to the electrical current transport (**Figure 1.5**).

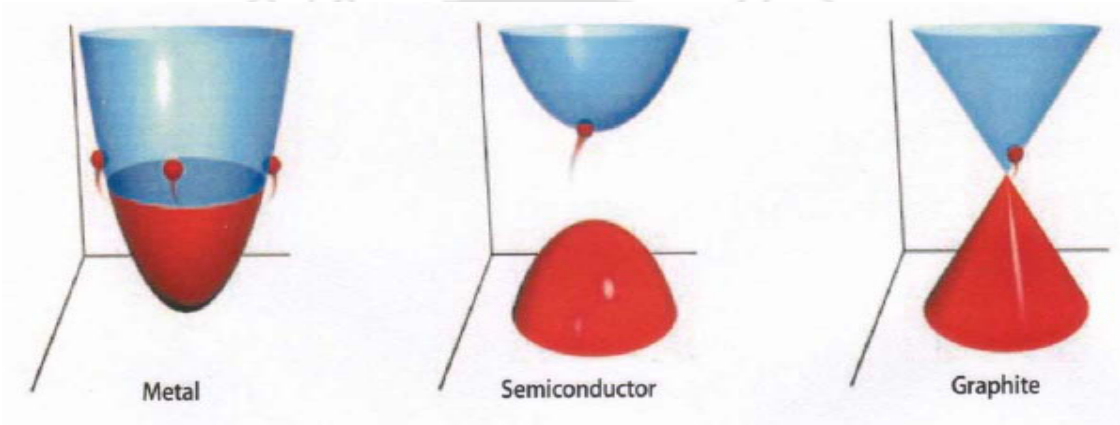

Figure 1.5. *Electrical behavior of naotubes (Reproduced with the permission from Collins PG, Avouris PH et al., Scientific American, 2000, 62, 283).*

1.3.5.3 Mechanical properties

It is problematic to produce macroscopic bodies with a high density and a grain size in the range of less than 100 nm (Dieter Vollath et al., 2008). However, two materials, neither of which is produced by pressing and sintering, have attracted much greater interest as they will undoubtedly achieve industrial importance. These materials are polymers which contain nanoparticles or nanotubes to improve their mechanical behaviors, and severely plastic-deformed metals, which exhibit astonishing properties (Dieter Vollath et al., 2008). However, because of their larger grain size, the latter are generally not accepted as

nanomaterials. Experimental studies on the mechanical properties of bulk nanomaterials are generally impaired by major experimental problems in producing specimens with exactly defined grain sizes and porosities (Dieter Vollath et al., 2008). Therefore, model calculations and molecular dynamic studies are of major importance for an understanding of the mechanical properties of these materials.

1.3.5.4 Magnetic properties

Magnetic nanoparticles show remarkable new phenomena such as superparamagnetism, high field irreversibility, high saturation field, extra anisotropy contributions or shifted loops after field cooling. These phenomena arise from finite size and surface effects that dominate the magnetic behaviour of individual nanoparticles (Batlle et al., 2002). Frenkel and Dorfman (Frenkel et al., 1930) were the first to predict that a particle of ferromagnetic material, below a critical particle size (<15 nmfor the common materials) would consist of a single magnetic domain, i.e. a particle that is a state of uniform magnetization at any field. The magnetization behaviour of these particles above a certain temperature, i.e. the blocking temperature, is identical to that of atomic paramagnets (superparamagnetism) except that an extremely large moment and thus, large susceptibilities are involved (Bean et al., 1959).

Industrial applications of magnetic nanoparticles cover a broad spectrum such as magnetic seals in motors, magnetic inks for bank cheques, magnetic recording media and biomedical applications such as magnetic resonance contrast media and therapeutic agents in cancer treatment (Berkovsky et al., 1993; Charles et al., 1986; Hilbert et al., 1997). Each potential application requires the magnetic nanoparticles to have different properties. For

example, in data storage applications, the particles need to have a stable, switchable magnetic state to represent bits of information, a state that is not affected by temperature fluctuations.

1.4 Gold nanoparticles

1.4.1 Gold: The Yellow Metal

No other element fascinates people as much as gold. It is easily recognizable colour and metallic lustre ensure that it is as eagerly sought after today as it was during the nineteenth century gold rushes in America and Australia and even as far back as the Pharaohs (Catherine et al., 2012). On daily news services the price of gold is regularly reported, providing an insight into the global economy. Inspite of the fact that, many bank vaults around the world are filled with gold bullion and ingots, still the search for undiscovered deposits continues and the cries of 'gold' can spark the imagination. The properties of the gold are as showed in **Table 1.3.**

Table 1.3 *Properties of gold*

Name	Gold
Symbol	Au
Atomic number	79
Mass number	196.96
Melting point	1063 ^{o}C
Boiling point	2807.8 ^{o}C
Density	19.32 g/cm
Malleability	High
Ductibility	High

1.4.2 Gold deposits

Gold is a naturally occurring metal found in low concentrations throughout the earth's crust. Many millions of years ago, gold was sweated out of rocks buried deep beneath the earth's surface. Hot solutions of salty water carried the dissolved gold towards the surface. Before reaching the surface the solutions cooled. This caused the gold to crystallise as particles ranging in size from small grains to large nuggets. These particles were often enclosed in quartz reefs (Catherine et al., 2012). After millions of years of erosion, the quartz and gold veins are eventually exposed to the atmosphere and carried into nearby streams and soil. Gold is not only prized because of its rareness but also due to its many unique properties and is represented as Carat (Catherine et al., 2012).

Carat

The gold content of jewellery is expressed as 'carats'. Pure gold is known as 24 carat gold. 18 carat gold contains 75 per cent pure gold. 18 or 9 carat gold is often used in jewellery as it is harder than 24 carat gold

1.4.3 The first usage of gold

The role played by gold in history relies on its outstanding qualities among metals, making it exceptionally valuable from the earliest civilizations until the present day. Gold is attractive due to 'its brilliance, its colour, its divine heaviness', and also due to its incorruptibility and scarcity (Catherine et al., 2012). Its great malleability makes gold one the easiest of the metals to work with. Moreover it often occurs naturally in a fairly pure state. The first uses of

gold were linked to deities and royalty in early civilizations. The word 'gold' exists in all old languages, often connected with the image of the Sun, with light and life giving warmth, growth and hence power. In cultures like ancient Egypt, which deified the Sun, gold represented its earthly form (Catherine et al., 2012). In fact, nothing has changed through history and the same thinking about gold keeps going (golden crown of the kings, gold medals, wedding rings, cult objects, gold ingots, etc.).

1.4.4 Quest for gold and gold production

The earliest signs of crude metallurgy occurred 9000–7000 BCE (before the Common Era). For instance, in Alikosh in Iran and Cayönü Tepesi close to Ergani in Anatoly, humans first began using native copper, gold, meteoric iron, silver and tin to create tools and possibly jewellery ornamentation. Gold was most probably discovered as shining, yellow nuggets. Although it can be easily worked because of its ductility, it is not clear whether it was worked before copper.

It is known that the Egyptians mined gold before 2000 BCE in Nubia. The *Turin Papyrus* drawn during the reign of Ramesses IV (1151–1145 BCE) is the earliest known topographic and geological map (Harrell et al., 1992) along with specifics of the geology and topography. It shows an ancient gold-working settlement, gold-bearing quartz veins in Wadi Hammamat, a dry river bed in Egypt's Eastern desert.

Occasional passages on mining and metallurgy of metals can be found in the works of Theophrastus (Greek, 372–288 BCE), Vitruvius (Roman, 90–20 BCE), Strabo (Greek, 63/64 BCE–c. 24 CE), Pliny the Elder (Roman, 23–79 CE) and Discorides (Greek, 40–90 CE) (Hunt et al., 1976). One important surviving document is the *Leyden Papyrus X* of the

Museum of Antiquities in the Netherlands: it is the working notebook of a goldsmith and jeweller, probably written in the early years of the fourth century. It gathers 111 recipes of refining, alloying and working of gold; some of them are reported in Hunt's paper (Hunt et al., 1976).

1.4.5 Gold for human well-being: food, drinks and medicine

Pure metallic gold is non-toxic and non-irritating when it is ingested. Metallic gold has been approved as a food additive in the EU (E175 in the *Codex Alimentarius*). As gold leaf, it is sometimes used as food decoration in China, Japan, India and also in Europe. Since the discovery of gold, people have thought of it as having an immortal nature and have associated it with longevity, probably because of its resistance to chemical corrosion. Many ancient cultures, such as those in India and Egypt, used gold in medicine but mainly for its magico-religious power. However, gold played almost no role in rational therapeutics. An exception is China, with the earliest application of gold as a therapeutic agent back in 2500 BCE. Pliny the elder, in the first century, reported gold for healing fistulas and haemorrhoids (Parish et al., 1987; Fricker et al., 1996; Tiekink et al., 2003; Knosp et al., 2003). The uses of gold were limited because at that time people did not know how to dissolve it and make it soluble. It was with the medieval period and the European chemists hypothesized that gold became a prominent medicinal element, with the idea that the elixir of life, *Aurum potabile*, can restore youth. *Aurum potabile* was closely related with the discovery of *aqua regia* (a mixture of hydrochloric and nitric acids), the 'royal' solvent of gold. Gold cordial was advocated in the seventeenth century for the treatment of ailments caused by a decrease in the vital spirits, such as melancholy, fainting, fevers and falling sickness. Later, in the nineteenth century, a mixture of gold chloride and sodium chloride was used to treat syphilis.

Gold therapy proved to be effective against rheumatoid arthritis. Since that time gold drugs have also been used to treat a variety of other rheumatic diseases such as juvenile arthritis, palindromic rheumatism and various inflammatory skin disorders such as pemphigus, urticaria and psoriasis (Brown et al., 2007; Pérez-Arantegui et al., 2001).

1.4.6 Gold Nanoparticles (AuNPs)

Metallic nanoparticles, especially gold nanoparticles have fascinated scientist for over a century and are now heavily utilized in many fields importantly in biomedical sciences. They are focus of interest because of their huge potential in nanotechnology. As of now, scientist can be synthesized and modified with various chemical functional groups which allow them to be conjugated with antibodies, ligands, and drugs of interest and thus opening a wide range of potential applications in biotechnology (Pankhurst et al., 2003), and preconcentration of target analytes, targeted drug delivery (Dobson et al., 2006; Rudge et al., 2001), vehicles for gene and drug delivery (Pankhurst et al., 2003; Dobson et al., 2006; Rudge et al., 2001) and more importantly diagnostic imaging. Moreover, various imaging modalities have been developed over the period of time such as MRI, CT, PET, ultrasound, SERS, and optical imaging as an aid to image various disease states (Christophe et al., 2008). These imaging modalities differ in both techniques and instrumentation and more importantly require a contrast agent with unique physiochemical properties. This led to the invention of various nanoparticulated contrast agent such as magnetic nanoparticles (Fe_3O_4), gold, and silver nanoparticles for their application in these imaging modalities. The unique physical chemical properties of the AuNPs are due to the fact that they possess the surface plasmon resonance.

Surface plasmon resonance (SPR) is the most outstanding feature of gold nanoparticles. The excitation of surface Plasmon's (SPs) in metallic nanoparticles induces optical properties hardly achievable in other optical materials, yielding a wide range of applications in many fields. It consists on a collective oscillation of the conduction electrons inside the nanoparticles. The resonant frequency of gold nanoparticles particles specifically, falls in the visible part of the spectrum. Therefore, when illuminating gold nanoparticles with visible light, surface plasmons (SP) can be excited leading to a great light absorption even with very small quantities of nanoparticles. The SPR in gold nanoparticles is so strong that it enhances locally the light electric field several orders of magnitude. Due to these effects, as well as the high biocompatibility and photonic properties render gold nanoparticles as attractive elements for applications such as electronic wiring, optics, photonics, optoelectronics, catalysis and biomedicine.

1.4.7 The first use of gold nanoparticles

The first use of gold nanoparticles is intimately related to the history of red-coloured glass. The production of red glass (opaque) starts with the very beginning of glassmaking in Egypt and Mesopotamia back in 1400–1300 BCE (Brill et al., 1988). The colour of this red glass was given by gold nanoparticles. According to most of the textbooks and technical encyclopedias on gold, glass and ceramics, the production of the so-called 'gold ruby glass' did not take place until the end of the seventeenth century. The discovery is attributed to Johann Kunckel (1637–1703, Brandenburg) and that of the gold preparation that is added to melted glass to give it the ruby red colour is attributed to Andreas Cassius of Leyden (Hunt et al., 1976). This is so-called *Purple of Cassius*, which is a precipitate obtained from the

dissolution of gold metal in *aqua regia* followed by the precipitation of metallic gold by a mixture of stannous and stannic chloride.

1.4.8 Synthesis of gold nanoparticles

Synthesis methods for the preparation of AuNPs have to be reproducible, yielding nanoparticles of a predetermined size, structure, shape and composition. A systematic study of synthesis and colours of gold colloids was ever first reported in 1857, through the work of Michael Faraday (Faraday et al., 1857). In a two-phase reaction, Faraday reported the formation of ruby-red colloidal gold solutions by reducing a gold salt with phosphorus in carbon disulfide. He further studied the interactions of light and the thin films of dried colloids, observing a reversible colour change upon compression. Since this pioneering work, many procedures have been reported for nanoparticles synthesis, reactions and functionalization. These gold nanoparticles synthesis was achieved with many methods and are broadly classified in to the chemical, physical and biological method. Initially, AuNPs more preferably synthesized with conventional synthesis so called such as chemical reduction where harsh chemical used as reducing and stabilizing agents. These chemical synthesis methods afford facile control over nanoparticles size, size-distribution, shape and surface-chemistry (Jin et al., 2001). However, such synthesized AuNPs carry unreacted traces of chemicals that are potential hazards to human health (Uboldi) et al., 2009. Therefore, there is growing need to develop a green method for synthesis the AuNPs. In an effort to develop a green method scientists have used biological materials such as bacteria, yeast and fungi for the synthesis of AuNPs. However, these methods also have their own drawbacks as it cannot provide the controllability over size and shape of AuNPs. All these miserable problems makes the scientists to replace the microbe with the plant and fruit

extracts as they can address the drawback associated with microbes. **Figure 1.6** shows the different method to synthesis the AuNPs.

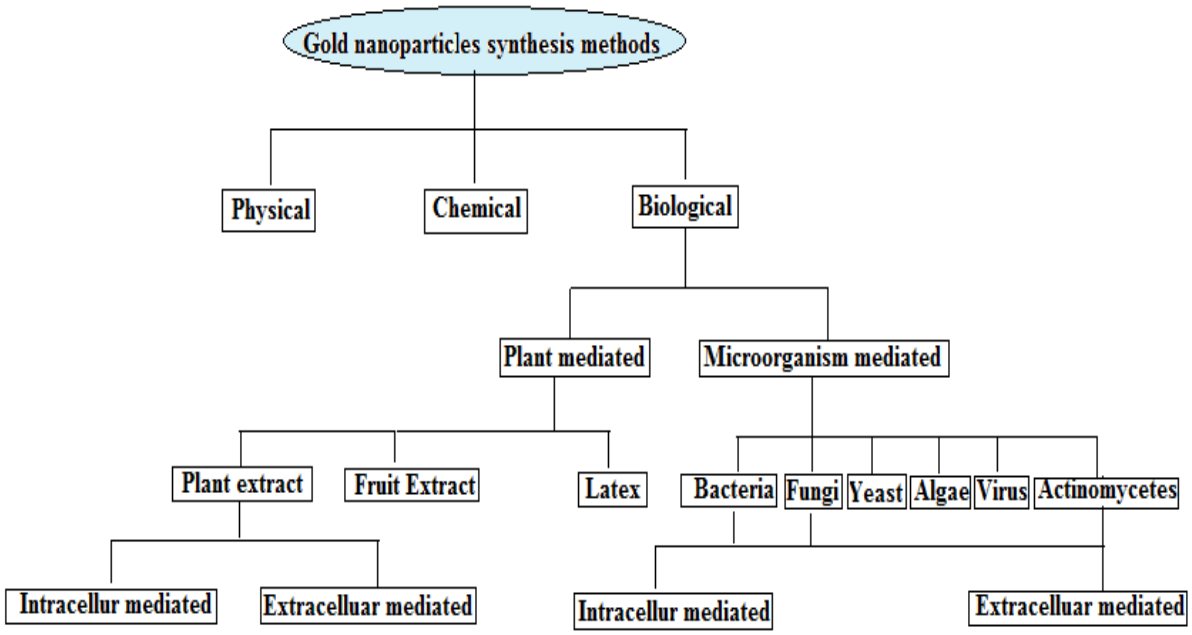

***Figure 1.6** Different methods of gold nanoparticles synthesis.*

1.4.9 Biological synthesis of gold nanoparticles

The green synthesis of nanoparticles requires the development of environmentally benign synthetic protocols, involving minimum number of steps, employing less toxic materials, involving as few reagents as possible under commonly prevalent laboratory conditions. This has led to a plethora of biomimmetic synthetic approaches for the synthesis of nanoparticles. Increasing awareness towards green chemistry and other biological processes has led to a desire to develop an eco-friendly approach for the synthesis of nanoparticles. The biosynthesis of nanoparticles can be plant mediated which includes from leaf, fruit and latex extracts. The AuNPs synthesis also can be accomplished by using microorganisms includes

bacteria, fungi, yeast, actinomycetes and viruses. However, a major limitation in using microorganisms is the intricacy of control over the shape, size and crystallinity of AuNPs (Narayanan et al., 2010). In this connection, researchers are more focused on plant and fruits (Shashi et al., 2010; Preeti et al., 2012; Nagaraj et al., 2012) extract as they not only acts as both reducing and stabilizing agents but also overcome problems associated with microorganisms.

1.4.10 Plant mediated synthesis of nanoparticles

The use of plants and plant products as sustainable and renewable resources in the synthesis of gold nanoparticles is more advantageous over prokaryotic microbes, which needs expensive methodologies for maintaining microbial cultures and downstream processing and also its simplicity and eco-friendliness. Thus this method is gaining importance in these days for the synthesis of AuNPs. We can synthesis the AuNPs using different parts of the plants such as leaves, fruits and latex. The synthesis may be extra cellular or intra cellular (Narayanan et al., 2011).

1.4.10.1 Intracellular synthesis of gold nanoparticles by plants

The use of plants in the recovery of noble metals from ore mines and runoffs is known as phytomining. It is the cost-effective environmentally compatible method compared to the conventional chemical methods. It can uptake even very low levels of metals and accumulate in tissues compared to the chemical methods, which is less effective in low levels of metals. The use of nontoxic chelators like thiourea and others such as iodide, bromide, cyanide, thiocyanate and thiosulfate can solubilize the metals from ores and facilitate the efficient uptake by plants. In phytomining, it can also scavenge metal ions from large volume of soil

and bioconcentrate into their biomass, which can be harvested and recovered from the contaminated site. In *Brassica juncea* and *Berkheya coddii*, hyper accumulation of gold was found with thiocyanate solution as solubilizer, whereas *B. juncea* and *C. linearis* hyper accumulated gold with iodide, bromide, cyanide, thiocyanate or thiosulfate solution (Terry et al., 1998). **Table 1.4** illustrates the intracellular synthesis of gold nanoparticles.

Table 1.4 *Intracellular bioaccumulation of gold nanoparticles by plants.*

Trivial name	Botanical name	Part	Particle	Morphology/ localization	Size (nm)	Reference
Indian mustard	Brassica juncea	Shoot	Au^0	Spherical, hexagonal	5–50	Marshall et al., 2007
Alfalfa	M. sativa	Shoot	Au^0	Icosahedron	6–10	Gardea-T JL et al., 2002
Desert willow	Chilopsis linearis	Stem, Leaf	Au^0	Spherical	1.1	Rodriguez E et al., 2007
Rattlebush	Sesbania drummondii	Shoot, Root	Au^0	Spherical/ cytoplasm	6–20	Sharma NC et al., 2007

1.4.10.2 Extracellular synthesis of gold nanoparticles

1.4.10.2.1 Synthesis of gold nanoparticles plant biomasses

Biomass can be normally used to generate electricity, biogas, biofuel, etc. Therefore, the utilization of biomass wastes in the synthesis of nanoparticles is intriguing. For the first time AuNPs were synthesized using Alfalfa biomass which can passively binds and reduces gold (III) ions in a pH-dependent manner to form gold nanoparticles of ~100 nm. The resultant particles were tetrahedral, hexagonal platelet, icosahedral multi-twinned, decahedral multiple-twinned and irregular shaped (Gardea-T JL et al., 2002). There are more instances in the literature where AuNPs were synthesized suing plant biomass and are listed in the **Table 1.5.**

Table 1.5 *Extracellular syntheses of gold nanoparticles by plant biomasses.*

Trivial name	Botanical name	Part	Particle	Morphology	Size	Reference
Alfalfa	Medicago sativa	Biomass	Au^0	Icosahedral multiple twinned, decahedral multiple twinned	100	Gardea-T JL et al., 1999
Wheat	Triticum aestivum	Biomass	Au^0	Tetrahedral, decahedral hexagonal, icosahedral	10–30	Armendariz et al., 2004
Cone hop	Humulus lupulus	Biomass	Au^0	hexagonal, icosahedral multiple twinned	–	Lopez et al., 2005

1.4.10.2.2 Synthesis of gold nanoparticles plant extracts

The presence of various secondary metabolites, enzymes, proteins and/or other reducing agents with electron-shuttling compounds is usually involved in the synthesis of gold nanoparticles by plant components. In bioaccumulation, the localization of nanoparticles is based on the presence of particular enzymes or proteins involved in it. The recovery of these nanoparticles from plant tissues is tedious and expensive and needs enzymes to degrade the cellulosic materials, which surrounds it (Marshall et al., 2007). Thus, the synthesis of various metal nanoparticles using plant extracts is easy in downstream processing and in scaling up of nanoparticles. For the first time, geranium plant extracts from leaf, stem and root have been documented for the extracellular production of gold nanoparticles. Shankar et al. reported the biological reduction of gold ions to gold nanoparticles using geranium leaf broth and UV–Vis spectroscopic analysis identified the SPR band centered at 551 nm (Shankar et al., 2003). There are many report which involved in the synthesis of AuNPs are listed in **Table 1.6**.

Table 1.6 *Extracellular synthesis of gold nanoparticles by plant extracts*

Trivial name	Botanical name	Part	Particle	Morphology	Size (nm)	Reference
Geranium	Pelargonium graveolens	Leaf	Au^0	Decahedral, icosahedral	20–40	Shankar et al., 2003
Geranium	P. graveolens	Stem	Au^0	Spherical	8.3–23.8	Shankar et al., 2004a
Geranium	P. graveolens	Root	Au^0	Spherical, triangle	11.4–34	Shankar et al., 2004a
Lemongrass	Cymbopogon flexuosus	Leaf	Au^0	Triangle, spherical	0.05–1.8 μm	Shankar et al., 2004b
Neem	Azadirachta indica	Leaf	Au^0	Spherical, triangle, hexagonal	50–35	Shankar et al., 2004c
Indian gooseberry	Emblica officinalis	Fruit	Au^0	–	15–25	Ankamwar et al., 2005a
Tamarind	Tamarindus indica Leaf		Au^0	Flat-triangle, hexagonal	20–40	Ankamwar et al., 2005b
Aloe vera	Aloe barbadensis	Leaf	Au^0	Spherical, triangle	50–350	Chandran et al., 2006
Camphor tree	Cinnamomum camphora	Leaf	Au^0	Flat, plate-like triangle	55–80	Huang et al., 2007
Coriander	Coriandrum sativum	Leaf	Au^0	Spherical, triangle, truncated triangle	20.6±7.0	Narayanan et al., 2008
Indian Borage	Coleus amboinicus	Leaf	Au^0	Spherical, truncated triangle, hexagonal	4.6–55.1	Narayanan et al., 2010
Red river gum	Eucalyptus camaldulensis	Leaf	Au^0	–	1.25–17.5	Ramezani et al., 2008
Rose geranium	P. roseum	Leaf	Au^0	–	2.5–27.5	Ramezani et al., 2008
Tea plant	Camellia sinensis	Leaf	Au^0	Nanotriangles	~40	Vilchis et al., 2008
Henna	Lawsonia inermis	Leaf	Au^0	Spherical, triangular	7.5–65	Kasthuri et al., 2009a
Phyllanthus	Phyllanthus amarus	Leaf	Au^0	Hexagonal, triangular, rod-shaped, spherical	18–38	Kasthuri et al., 2009b
Cape aloe	Aloe ferox	Leaf	Au^0	Spherical, triangular	6–35, 4–4550	Krpetic et al., 2009
Hibiscus	Hibiscus rosa sinensis	Leaf	Au^0	Spherical, triangular, hexagonal, dodecahedral	14	Philip et al., 2009

Guava	Psidium guajava	Leaf	Au^0	Spherical, triangular, hexagonal	27±3	Raghunanda n et al., 2009
Magnolia	Magnolia kobus	Leaf	Au^0	Triangles, pentagons, hexagons, spherical	5–300	Song et al., 2009
Persimmon	Diopyros kaki	Leaf	Au^0	Triangles, pentagons, hexagons, spherical	~300	Song et al., 2009
Barbated Skullcup	Scutellaria barbata	Plant	Au^0	Spherical, triangles	5–30	Wang et al., 2009
Common Tansy	Tanacetum vulgare	Fruit	Au^0	Spherical, triangular	11	Dubey et al., 2010
Clove	Szyygium aromaticum	Flower Bud	Au^0	Triangular, polygonal	100–300	Singh et al., 2010
Almond	Terminalia catappa	Leaf	Au^0	Spherical	21.9	Ankamwar et al., 2010
Velvet bean	Mucuna pruriens	Seed	Au^0	Spherical	6–17.7	Arulkumar et al., 2010
Banana	Musa paradisiaca	Peel	Au^0	Microcubes, microwire	300	Bankar et al., 2010
Sugar beet	Beta vulgaris	Pulp	Au^0	Nanorods, triangular, Spherical	25, 160 20	Castro et al., 2010
Sugar beet	Beta vulgaris	Pulp	Au^0	Nanowires	30	Castro et al,2011
Indian pennywort	Centella asiatica	Leaf	Au^0	Triangular, hexagonal	9.3–10.9	Das et al., 2010
European mountain ash	Sorbus aucuparia	Leaf	Au^0	Spherical, triangular, hexagonal	18	Dubey et al., 2010a
Japanese Rosa	Rosa rugosa	Leaf	Au^0	Triangular, hexagonal	11	Dubey et al., 2010b
Pig weed	Chenopodium album	Plant	Au^0	Quasi-spherical	10	Dwivedi et al., 2011
Green tea	Camellia sinensis	Leaf	Au^0	Spherical	~20	Gupta et al., 2010
Olive	Olea europaea	Leaf	Au^0	Triangle, hexagonal, spherical	50–100	Khalil et al., 2010

Weeping bottlebrush	Callistemon viminalis	Leaf	Au^0	Nanotriangles, Spherical	~90	Kumar et al., 2011
Korean red ginseng	Panax ginseng	Root	Au^0	Spherical	16.2±3	Leonard et al., 2011
Sweet leaf	Stevia rebaudiana	Leaf	Au^0	Octahedral	8–20	Mishra et al., 2010
Mango tree	Magnifera indica	Leaf	Au^0	Spherical	17	Philip et al., 2010
Krishna tulsi	Ocimum sanctum	Leaf	Au^0	Hexagonal	30	Philip et al., 2011a
Curry tree	Murraya koenigii	Leaf	Au^0	Spherical	20	Philip et al., 2011b
Cinnamon	Cinnamomum zeylanicum	Leaf	Au^0	Nanoprism, spherical	25	Smitha et al., 2009
Mahogany	Swietenia mahogany	Leaf	Au^0	Spheroidal, triangles, hexagonals		Mondal et al., 2011
Cashew	Anacardium occidentale	Leaf	Au^0	Spherical	6.5, 17	Sheny et al., 2011
Chickpea	Cicer arietinum	Beans	Au^0	triangular prism	~ 25	Ghule et al., 2006
Markingnut Tree	Semecarpus anacardium	Leaf	Au^0	–	13–55	Raju et al., 2011
Alfalfa	Medicago sativa	Biomass	Au^0	Decahedral, icosahedral Nanoplates	30–60 500–4 µm	Montes et al., 2011
Pear	Pyrus sp.	Fruit	Au^0	Triangular, hexagonal plates	200–500, 12–20	Ghodake et al., 2010
Rose	Rosa hybrida	Petals	Au^0	Spherical, triangular, hexagonal	10	Noruzi et al., 2011

1.4.4.2.3 Synthesis of gold nanoparticles from fruit extracts

The Nanoparticle (NPs) can synthesis using the plant fruit extracts. There are many examples in the literature as mentioned in the **Table 1.7**. Fruits extracts contains many bioactive molecules which have rich content of –OH and C=C groups and can easily donate the

electron when they contact with $HAuCl_4$ in extracellular medium and thus reduce the Au^{3+} ion to Au^{o}.

Table 1.7 *Extracellular synthesis of metal nanoparticles by fruit extracts*

Plant Trivial Name	Botanical Name	NPs obtained	Size of NPs (nm)	Reference
Elephant apple	*Dilleniaindica*	Ag	40 –100	Sushmita et al., 2013
Common tansy	*Tanacetumvulgare*	Au	11	Shashi et al., 2010
Myrobalan	*Terminalia chebula*	Ag & Au	25	Jebakumar al., 2012
Sugar beet)	*Beta vulgaris*	Au	20	Godhake et al., 2010

1.4.10.2.4 Synthesis of gold nanoparticles from plant latex

There are certain reports where the nanoparticles are synthesized using plant latexes. As per the gold nanoparticles concern, we first time reported using *Calotropis procera* Latex (Das et al., 2011). However, some other nanoparticles were synthesized using plant latex as listed in the **Table1.8**.

Table 1.8 *Extracellular synthesis of gold nanoparticles by plant latex*

Botanical Name	NPs obtained	Size of NPs (nm)	Reference
Jatrophacurcas L.	TiO2	25 – 100	Laura et al.,2010
Calotropisprocera L.	Cu	15 ± 1.7	Harne et al., 2012
Jatrophacurcas	Ag	20 – 40	Harekrishna et al., 2009
Calotropis procera	Au	22 ± 10	Das et al., 2011

1.4.11 Synthesis of nanoparticles from microorganisms

Microbes produce inorganic materials either intra- or extra cellularly often in nanoscale dimensions with exquisite morphology. Microbial resistance to most toxic heavy metals is due to their chemical detoxification as well as due to energy-dependent ion efflux from the cell by membrane proteins that function either as ATP ase or as chemiosmotic cation or proton anti-transporters. Therefore, microbial systems can detoxify the metal ions by either reduction and/or precipitation of soluble toxic inorganic ions to insoluble non-toxic metal nano clusters.

1.4.11.1 Synthesis of nanoparticles from bacteria

Scientists explored the synthesis of nanoparticles by bacteria which are regarded as potent eco-friendly green nanofactories and discovered magnetite particles by magnetotactic bacteria, siliceous materials by diatoms and gypsum and calciumlayers by S-layer bacteria. Interactions between metals and microbes have been exploited for various biological applications in the fields of bioremediation, biomineralization, bioleaching, and biocorrosion and the microbial synthesis of gold nanoparticles has been emerged as a promising field of research as nanobiotechnology interconnecting biotechnology and nanotechnology. The following **Table 1.9** confronts the different bacteria involved in the synthesis of nanoparticles along with AuNPs.

Table 1.9 *Synthesis of gold nanoparticles by bacteria*

Microorganism	NPs	Localization/morphology	Size	Reference
Bacterium-intracellular Bacillus subtilis 168	Au	Octahedral inside cell wall	5–25 nm	Beveridge et al., 1980

Sulfate-reducing bacteria	Au	Cell envelope	<10 nm	Lengke et al., 2006a
Shewanella algae	Au	Periplasmic space, bacterial envelope	10–20 15–200	Konishi et al., 2007
Plectonema boryanum UTEX485	Au	Membrane vesicles/Cubic	10 nm	Lengke et al., 2006b, 2006c
Escherichia coli DH5α	Au	Cell surface/Spherical	ND	Du et al., 2007
Rhodobacter capsulatus	Au	Plasma membrane	ND	Feng et al., 2007
Bacterium-extracellular Rhodopseudomonas capsulata	Au	Spherical Triangular nanoplates Spherical nanowires	10–20 50–400 50–60	He et al., 2007, 2008
Pseudomonas aeruginosa	Au	ND	15–30	Husseiny et al., 2007
B. megatherium D01	Au	Spherical	1.9±0.8	Wen et al., 2009

1.4.11.2 Synthesis of nanoparticles from Fungi

In recent years, fungi such as *Fusarium oxysporum* (Mukherjee et al., 2002), *Colletotrichum sp.* (Shankar et al., 2003), *Trichothecium sp., Trichoderma asperellum, T. viride*, (Ahmad et al., 2005; Mukherjee et al., 2008; Fayaz et al., 2010), *Phaenerochaete chrysosporium* (Vigneshwaran et al., 2006), *F. solani USM 3799* (Ingle et al., 2009), *F. semitectum* (Basavaraja et al., 2008), *A. fumigatus* (Bhainsa et al., 2006), *Coriolus versicolor* (Sanghi et al., 2009), *Aspergillus niger* (Gade et al., 2008), *Phoma glomerata* (Birla et al., 209), *Penicillium brevicompactum* (Shaligram et al., 2009), *Cladosporium* cladosporioides (Balaji et al., 2009), *Penicillium fellutanum* (Kathiresan et al., 2009) and *Volvariella volvaceae* (Philip et al., 2009) have been explored for nanoparticles synthesis. Fungi are more advantageous compared to other microorganisms in many ways. Fungal mycelial mesh can withstand flow pressure and agitation and other conditions in bioreactors or other chambers

compared to plant materials and bacteria. These are fastidious to grow and easy to handle and easy for fabrication. The extracellular secretions of reductive proteins are more and can be easily handled in downstream processing. And also, since the nanoparticles precipitated outside the cell is devoid of unnecessary cellular components, it can be directly used in various applications. The list of fungi used for the synthesis of gold nanoparticles listed in **Table 1.10**.

Table 1.10 *Synthesis of gold nanoparticles by fungi*

Microorganism	Nanoparticle (NPs)	Localization/Morphology	Size (nm)	Reference
Fungus-intracellular Verticillium sp.	Au	Cell wall/spherical, cytoplasmic membrane/quasi-hexagonal	20±8	Mukherjee et al., 2001
Trichothecium sp.	Au	–	–	Ahmad et al., 2005
V. luteoalbum and isolate 6-3	Au	Spherical Spheres and rods	<10	Gericke et al., 2006a, 2006b
Fungus-extracellular Fusarium oxysporum	Au	Spherical, triangular	20–40	Mukherjee et al., 2002
Colletotrichum sp.	Au	Spherical	20–40	Shankar et a., 2003
Trichothecium sp.	Au	Triangle, hexagonal	5–200	Ahmad et a., 2005

1.4.11.3 Synthesis of nanoparticles from Yeast

Among the eukaryotic microorganism, yeast has been exploited mainly for the synthesis of semiconductors. *Candida glubrata* produced intracellularly monodispersed spherically shaped peptide- bound CdS quantum crystallites of 20 Å by neutralizing the toxicity of metal ions by forming metal–thiolate complex with phytochelatins (Dameron et al., 1989) and *Schizosaccharomyces pombe (*Kowshik et al., 2002*)* also produced wurtzite-typed hexagonal

lattice structured CdS nanoparticles in mid-log phase in the range of 1–1.5 nm. The list of yeast used for the synthesis of gold nanoparticles listed in **Table 1.11**.

Table 1.11 *Synthesis of gold nanoparticles by yeast*

Yeast	NPs obtained	Size of NPs (nm)	References
Schizosaccharomyces pombe and candida glabrata	CdS	35 – 75	Dameron et al.,1989 Kowshik et al., 2002 Krumov et al., 2007
Yarrowialipolytica NCIM 3589	Au	15	Agnihotri et al., 2009

1.4.11.4 Gold nanoparticles synthesis by algae

Algae used for the synthesis of the gold nanoparticles are listed in the **Table 1.12**. Mostly marine algae used for the synthesis of gold nanoparticles.

Table 1.12 *Synthesis of gold nanoparticles by algae*

Trivial name	Botanical name	Part	Particle	Morphology/localization	Size (nm)	Reference
Green alga	Chlorella vulgaris	Thallus	Au^0	Tetrahedral, decahedral, icosahedral	–	Yang et al., 2010
Green alga	Chlorella vulgaris	Thallus	Au^0	Triangular, hexagonal	–	Awadalla et al., 1992
Brown marine alga	Sargassum wightii	Thallus	Au^0	Thin planar	8–12	Hosea et al., 1986
Brown alga	Fucus vesiculosus	Biomass	Au^0	–	–	Singaravelu et al., 2007
Blue-green alga	Spirulina platensis	Dried thallus	Au^0	Spherical	7–16	Govindaraju et al., 2008

1.4.11.5 Synthesis of nanoparticles using Actinomycetes

Actinomycetes though have classified as prokaryotes as they share important characteristics of fungi. They are popularly known as ray fungi. A novel extremophilic *actinomycete, Thermomonospora sp*. was found to synthesis extracellular monodispersed spherical gold nanoparticles at an average size of 8 nm (Ahmad et al., 2003b) as listed in **Table 1.13**.

Table 1.13 *Synthesis of gold nanoparticles by Actinomycetes*

Microorganism	Nanoparticle	Localization/ morphology	Size (nm)	Reference
Actinomycete-intracellular Rhodococcus sp.	Au	Cell wall, cytoplasmic membrane	5–15	Ahmad et al., 2003a
Actinomycete-extracellular Thermomonospora sp	Au	Spherical	8	Ahmad et al., 2003b

1.4.11.6 Synthesis of nanoparticles using viruses

Tobacco mosaic virus (TMV) was used as template for the synthesis of iron oxides by oxidative hydrolysis, co-crystallization of CdS and PbS, and the synthesis of SiO2 by sol–gel condensation. The peptides like A7 and J140, which have the ability to nucleate ZnS and CdS nanocrystals were expressed as pVIII fusion proteins into the crystalline capsid of the virus, M13 bacteriophages (**Table 1.14**).

Table 1.14 *Synthesis of nanoparticles by virus*

Virus	NPs obtained	Size of NPs (nm)	Reaction
Tobacco mosaic virus (TMV)	SiO2, Fe2O3, PbS and CdS	65 – 130	Shenton et al., 1999
M13 bacteriophage	ZnS, CdS	560 x 20	Lee et al., 2002

1.4.12 Synthesis of gold nanoparticles using physical methods

Physical methods of nanoparticles synthesis comprise of methods like sonolysis, photo irradiation, laser ablation, thermolytic reduction, microwave reduction, UV irradiation.

1.4.12.1 Sonolysis

Sonolysis is the breaking of chemical bonds or formation of radicals using ultrasound. These radicals catalyze the reduction of gold ions into the gold nanoparticles. The example for the sonolysis as follows. The ultrasound is applied to the reaction mixture containing an aqueous solution of $HAuCl_4$ with glucose. Due to the ultrasound the hydroxyl radical and sugar pyrolysis radicals (forming at the interfacial region between the collapsing cavities and the bulk water) were formed and catalyze the reduction of the $HAuCl_4$ to Au^o. The morphology obtained is of nano ribbons with width 30-50 nm and length of several micrometers. These ribbons are very flexible and can bend with angles larger than 90˚. When glucose is replaced by cyclodextrin (a glucose oligomer) only spherical gold particles are obtained suggesting that glucose is essential in directing the morphology towards a ribbon (Toshio et al., 2009).

1.4.12.2 Thermolytic reduction

Thermolysis is a chemical decomposition caused by heat. The reaction is usually endothermic as heat is required to break chemical bonds in the compound undergoing decomposition. AuNPs have been fabricated via decomposition of $[AuCl(PPh_3)]$ upon reduction in a monolayer at the gas/liquid interface (Khomutov et al., 2002). Thermolysis of crude preparations of Brust's gold nanoparticles without removing the phase transfer reagent, tetraoctylammonium bromide, to 150˚-25˚C led to an increase of the particle sizes to 3.4-9.7 nm, and this size evolution was discussed on the basis of a thermodynamic model. The heat

treated gold nanoparticles formed 2D super lattices with hexagonal packing (Shimizu et al., 2003).

1.4.12.3 Photo irradiation

In this method, electrons produced during the radiolysis can reduce metal ions at the ambient temperature without using excessive reducing agents and consequent side reactions. Also, the electrons can be homogenously distributed in the solution, therefore, the AuNPs are produced in uniformly distributed, fully reduced, highly pure and stable forms. Most importantly, the size of gold nanoparticles can be controlled by varying the dose of irradiation.

AuNPs have been synthesized in a single step and a facile procedure by γ-irradiation using bovine serum albumin protein as a stabilizer (Akhavana et al., 2010). UV irradiation is another parameter that can improve the quality of gold nanoparticles including when it is used in synergy with micelles or seeds (Mallick et al., 2001). Radiolysis has been used to control gold nanoparticles size or to synthesize them in the presence of specific radicals and the mechanism of AuNPs synthesis upon γ-irradiation has been carefully examined.

1.4.12.4 Laser ablation

Laser ablation is the process of removing material from a solid (or occasionally liquid) surface by irradiating with a laser beam. Recently short-pulse laser sources have been investigated as a potential method for AuNP synthesis. The biggest influence on the nanoparticles size and distribution is the pulse duration. Femtosecond laser ablation of gold result in substantially smaller nanoparticles than during nanosecond laser ablation (Haustrup et al., 2011).

1.4.12.5 Solvothermal synthesis

Solvothermal synthesis is a method of producing chemical compounds, similar to the hydrothermal route where the synthesis is carried out in a stainless steel autoclave. The only difference being that the precursor solution is not always aqueous. Solvothermal synthesis has been used in the laboratory to make nanostructured titanium dioxide, grapheme, carbon and other materials.

The synthesis of AuNPs inside sealed vessels (steel bombs and autoclaves) can be achieved by elevating the solvent temperature above its boiling point by increasing the autogenous pressures through heating. This process increases the solubility and reactivity of most inorganic complexes and salts at such critical solvent temperatures.

1.4.12.6 Seed growth

One of the simplest most reproducible methods to synthesize gold nanorods is the seed-mediated growth method. It consists of a two step process: nucleation and the successive growth of the AuNPs. By introducing some modifications in the preparation conditions (careful control of the solution temperature, stirring, ratio of seed to metal salt, etc.), a defined aspect ratio of the gold nanorods is obtained.

1.4.12.7 Microwave reduction

In this method, AuNPs are synthesized by the use of microwave heating. The use of microwave heating for the generation of AuNPs is a rapid and effective mode of heating. The reaction mixture, chosen for nanoparticles synthesis, is subjected to microwave heating, for a

short duration of time. This method is energy saving, has unique features such as high reaction rate, rapid volumetric heating and short reaction time (Nishat et al., 2011; Das et al., 2011).

1.4.13 Synthesis of gold nanoparticles using chemical methods

All most all the chemical are traditional method where the harsh chemicals are used to synthesize the nanoparticles. The chemical methods include sonochemical method, solvolysis, chemical reduction, electrochemical, chemical vapour deposition (CVD).

1.4.13.1 Synthesis of gold nanoparticles using Citrate

This the best approach to produce size-defined gold nanoparticles through chemical reduction. The standard method, as described by Turkevich and Frens, is reduction by citrate at 100 °C. The reduction of a gold hydrochlorate solution (99%) has been initiated by sodium tris-citrate (Merck) by bringing gold solution to a boil in a double-walled reactor, which is heated by a bath thermostat. The mantle assured a very homogeneous temperature distribution within the reaction solution. The liquid is vigorously stirred by Teflon-coated magnetic bars. No refluxing was utilized in order to prevent the presence of temperature gradients in the liquid. When the solution (95 mL) started to boil, 5 mL of preheated citrate solution was added. The citrate concentration was varied to achieve different particle sizes (Kimling al., 2006).

1.4.13.2 Synthesis of gold nanoparticles using Lactic acid

This is a typical experiment where 2.5 mL of 5 mM $HAuCl_4$ aqueous solution was added to 50 mL of ultrapure water in a 100 mL of round-bottomed flask under vigorous stirring. As the solution boils, 0.34 mM lactic acid was added in different volumes. The heating was

continued to keep the solution boiling for 10 min. Then the solution was stirred for another 10 min without heating in order to form the nanoparticles (Xunjun et al., 2010).

1.4.13.3 Synthesis of gold nanoparticles using glycerol

In a typical experiment, a known amount of PVP (MW-55, 000, 0.045Min repeating unit) was dissolved in 100 ml of glycerol with effective stirring. The solution was then heated at a constant rate of 5 °C/min upto the boiling point of glycerol (290 °C). Ten millimeters of $HAuCl_4 \cdot 3H2O$ (0.0126 M) was then added to the hot PVP solution. The formation of gold nanoparticles can be visually seen by the appearance of deep wine red color during the course of the reaction (Nirmala et al., 2006).

1.4.13.4 BSA craving method

In another approach, Lee et al. demonstrated the synthesis of planar gold nanostructures in yields up to 80%, with side lengths in the range 0.6–3 mm and 19 nm thickness, using bovine serum albumin (BSA) as the reductant and stabilizer (Xie et al., 2007).

1.4.13.5 Two Phase Reduction: Burst-Schiffrin Method

In this method, AuNPs are produced in organic liquids that are normally not miscible with water. It involves the reaction of tetrachloroauric acid ($HAuCl_4$) solution with tetraoctylammoniumbromide (TOAB) solution in toluene and sodium borohydride as an anticoagulant and reducing agent, respectively. The AuNPs obtained are usually 2-6 nm in diameter (Palgave et al., 2008).

1.4.13.6 Hexadecylaniline reduction

In this method, under stationary conditions (no stirring), a biphasic mixture of hexadecylaniline, toluene and chloroaurate ions in water leads to the electrostatic complexation of reduction by the hexadecylaniline molecules. Hexadecylaniline spontaneously reduces the metal ions to yield organically dispersible spherical gold nanoparticles. Spherical gold nanoparticles of edge to edge length of 1.5 nm are obtained (Selvakannan et al., 2004).

1.4.13.7 Polyol Reduction

This method involves the reduction of a metal salt in the presence of a protecting polymer, usually poly(vinyl pyrolidone) (PVP). This method developed by Figlarz*etal.* entails refluxing the metal precursor (oxides, nitrates and acetates) in ethylene glycol or polyols (polyethylene glycol; PEG) in presence of a polymer for a specific period. The nanoparticles are formed by nucleation and growth from the solution with the polyol acting as a solvent for the inorganic compound due to its high dielectric constant.

The reaction mechanism involves two stages: (I) the conversion of the inorganic precursor into the intermediate phase in a stepwise sequence, (1) progressive dilution of the starting inorganic material, and (2) precipitation of the intermediate phase; (II) the conversion of the intermediate phase to the metal particles in a stepwise reaction involving (1) the dissolution of the intermediate phase, (2) reduction in solution, (3) evolution of the volatile products and (4) spontaneous nucleation and growth of the metal particles (Kim et al., 2004).

1.4.13.8 Sonochemical method

When substances such as water are subjected to strong ultrasound irradiation leads to the formation, expansion and collapse of cavitation bubbles by the acoustic fields. As a result, high pressure fields are produced at the centers of the bubbles, in a process called acoustic cavitation. This causes the dissociation of the interior water vapour into H and OH radicals. These radicals initiate a sequential abstraction and reduction reactions of dissolved molecules. The estimated temperature of the hot spot has been estimated to be 5000K, a temperature at which most molecules can be reduced. Sonochemical reactions generally employ alcohols such as 2-propanol or surfactants such as sodium dodecyl sulphate (SDS) or a combination of both as radical scavengers in the colloid formation (Okitsu et al., 1996).

In sonochemical synthesis of AuNPs, an aqueous solution of tetrachloroauric acid along with some reducing or stabilizing agent are subjected to strong ultrasound radiation and undergo subsequent reduction. Sonochemical reduction give rise to AuNPs with a smaller size range and higher surface area due to unique reaction routes resulting from transient high temperatures and pressures induced by the acoustic cavitation phenomenon.

1.4.13.9 Chemical Vapour Deposition (CVD)

Chemical vapour deposition (CVD) is a chemical process used to produce high –purity, high-performance solid materials. In a typical CVD process, the wafer (substrate) is exposed to one or more volatile precursors, which react and/or decompose on the substrate surface to produce the desired product.

CVD is an industrially important tool for the deposition of thin films on a variety of substrates. Formation of the nanosized film takes place in a series of steps (1) the generation

of a vapourised gaseous material source, (2) transportation of the source into the reaction chamber, (3) phase reactions of the reactants leading to the formation of the intermediate species, (4) the adsorption of the source onto the host substrate, (5) diffusion of the heated deposit along the host substrate, forming crystallization centers and subsequent film growth, (6) the removal of by-products from the boundary layer through diffusion/convection. The deposition temperature can be varied anywhere between 100-1000˚C, depending on the substrate and the target deposit. Highly monodispersed gold has been deposited with a variant of CVD; aerosol assisted CVD (AACVD), using $HAuCl_4$ as the metal precursor in the presence of tetraoctyl ammonium bromide (TOAB) (Palgave et al., 2008).

1.4.14 Synthesis of gold nanoparticles using polymers

1.4.14.1 Dextrose Reduction

In this method, AuNPs are synthesized by the reduction of Au^{3+} ions in aqueous dextrose dispersion, prepared from a medium (pH- 6.9). In a typical preparation, an aqueous stock solution of $HAuCl_4$ (0.05 M) is added to the aqueous medium containing different concentrations of dextrose. The samples are kept in an orbital shaker with a stirring speed of 150 rpm at room temperature for about 1–6 hours (Vivek et al., 2011).

1.4.14.2 Gelatin Reduction

AuNPs are prepared with a green and simple route by reducing in situ tetrachloroauric acid in gelatin. Gelatin is the thermally and hydrolytically denatured product of collagen. It has a triple-helical structure and offers distinctive advantages such as good biocompatibility, nontoxicity, remarkable affinity to proteins and excellent gel- forming ability. AuNPs with various diameters are prepared using gelatin as reducing/stabilizing agent. The aqueous

gelatin solution with 20 mL (3%) is heated at 80°C. When stirred vigorously, 2 mL of $HAuCl_4$ solution (1%, wt %) is added rapidly. The mixed solution is shaken vigorously for 30 s and left undisturbed for 2 h at 80°C, at which a red AuNPs-gelatin solution is obtained (Zhang et al., 2009).

1.4.14.3 Poly caprolactone reduction

In this method, gold-copolymer composed nanoparticles are synthesized using the triblock copolymer (PVP-PCL-PVP) and potassium tetrachloroaurate (III), both in aqueous solution. The copolymer works as a reducing as well as stabilizing agent. The reaction mixture is vigorously stirred during 2 h at 70°C (Angel et al., 2009).

1.4.8.4 Polyacrylamide reduction

In this method, to the polyacrylamide solution, equal volume of gold salt solution and tri-sodium citrate (3% of polyacrylamide volume) are added and the reaction is carried out under microwave for 10 min. The pale yellow colour transparent solution is converted to the characteristic red rose colour, indicating the formation of AuNPs (Angshuman et al., 2007).

1.4.14.5 Chitosan reduction

Chitosan is a polysaccharide that is obtained by the partial deacetylation of chitin. In a typical preparation, 100 µl of a 20 mM aqueous solution of $HAuCl_4$ is added to 3 mL of an aqueous solution of chitosan. The mixture is heated to 55°C and kept at this temperature while stirring in a water bath. After approximately 2 h, a red solution is obtained, indicating the formation of gold nanoparticles. The AuNPs prepared using chitosan as a protecting agent are of high monodispersity (Huang et al., 2004).

1.4.15 Applications of gold nanoparticles

Gold nanoparticles have been utilized for centuries by artists due to the vibrant colors produced by their interaction with visible light. More recently, these unique optical-electronics properties have been researched and utilized in high technology applications such as organic photovoltaics, sensory probes, therapeutic agents, drug delivery in biological and medical applications, electronic conductors and catalysis. **Figure 1.7** illustrates the biomedical application of the gold nanoparticles.

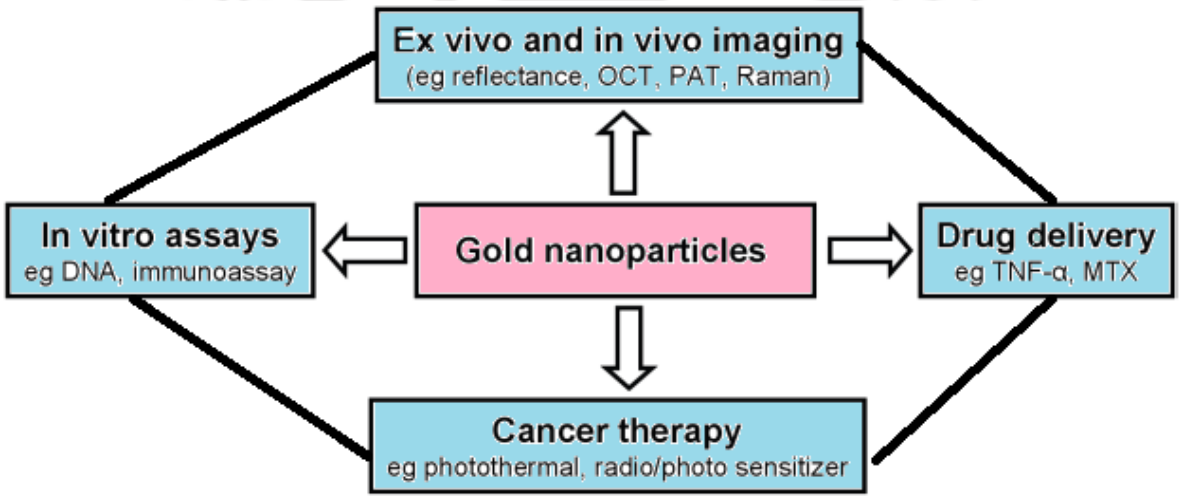

Figure 1.7 *The versatile applications of gold nanoparticles*

1.4.16 Non-analytical applications of gold nanoparticles

Gold nanoparticles are important in a diverse set of fields and they can generally be classified as two types i.e. engineered or non engineered. Engineered nanoparticles are intentionally designed and created with physical properties tailored to meet the need of specific application. They can be end product in and of themselves, as in the case of quantum dots or pharmaceutical drugs, sensor for special purposes, or they can be component later

incorporated into separate end products such as carbon black in rubber products. Either way the particle's physical properties are extremely important to their performance or the performance of any product into which they are ultimately incorporated. Non engineered nanoparticles, on the other hand, are unintentionally generated nanoparticles such as atmospheric nanoparticles created during combustion. With non engineered nanoparticles, physical properties also play importance role as they determine whether or not ill effect will occur as a result of the presence of these particles. For non analytical application nanoparticles based materials have been developed for drug and gene delivery (Panyam et al., 2003), tissue engineering (Ma et al., 2003), tumor destruction (O'Neal et al., 2004), separation and purification of biological molecules and cell (Molday et al., 1982), and also - Phagokinetic studies (Parak et al., 2002).

1.4.16.1 Tissue engineering

Natural bone surface is quite often contains features about 100 nm across. If the surface of an artificial bone implant were left smooth, the body would try to reject it. So production of a fibrous tissue covering the surface of the implant is preferable to get smooth surface. This thin layer will reduce the bone-implant contact, which may result in loosening of the implant and further inflammation. Nano-sized features can help to get smooth surface. It was demonstrated the hip or knee prosthesis which produced from nano-sized particles could reduce the chances of rejection as well as to stimulate the production of osteoblasts. The osteoblasts are the cells which are responsible for the growth of the bone matrix and are found on the advancing surface of the developing bone. The effect was demonstrated with polymeric, ceramic and, metal materials (Sato et al., 2004). More than 90% of the human bone cells from suspension adhered to the nanostructured metal surface (Adamopoulos et al., 2007). Using nano-sized

would allow to design a more durable and longer lasting hip or knee replacements and to reduce the chances of the implant getting loose.

1.4.16.2 Cancer therapy

Photodynamic cancer therapy is based on the destruction of the cancer cells by laser generated singlet oxygen, which is cytotoxic. A greater quantity of a special dye that to generate the singlet oxygen is taken in by the cancer cells when compared with a healthy tissue. Hence, a given laser radiation to the cell will only destroy the cancer cells. Unfortunately, there is a side effect of this treatment. The remaining dye molecules migrate to the skin and the eyes and make the patient very sensitive to the daylight exposure. This effect can last for up to six weeks. An attempt to avoid this affect was enclosed the dye molecules inside a porous nanoparticles (Roy et al., 2003). The dye stayed trapped inside the nanoparticles and did not spread to the other parts of the body. Even though the dye was trapped in the nanoparticles, the ability to generate oxygen was not effected due to the size of pore is about 1 nm which can freely allow the oxygen to diffuse out.

1.4.16.3 Manipulation of cells and biomolecules

Functionalized magnetic nanoparticles have found many applications including cell separation and probing (Pankhurst et al., 2003). Most of the magnetic particles studied so far are spherical, which somewhat limits the possibilities to make these nanoparticles multifunctional. Alternative cylindrically shaped nanoparticles can be created by employing metal electrodeposition into nanoporous alumina template (Reich et al., 2003). Depending on the properties of the template, nanocylinder radius can be selected in the range of 5 to 500 nm while their length can be as big as 60 μm. By sequentially depositing various thicknesses of

different metals, the structure and the magnetic properties of individual cylinders can be tuned widely. As surface chemistry for functionalization of metal surfaces is well developed, different ligands can be selectively attached to different segments. For example, porphyrins with thiol or carboxyl linkers were simultaneously attached to the gold or nickel segments respectively. Thus, it is possible to produce magnetic nanowires with spatially segregated fluorescent parts. In addition, because of the large aspect ratios, the residual magnetisation of these nanowires can be high. Hence, weaker magnetic field can be used to drive them. It has been shown that a self-assembly of magnetic nanowires in suspension can be controlled by weak external magnetic fields. This would potentially allow controlling cell assembly in different shapes and forms. Moreover, an external magnetic field can be combined with a lithographically defined magnetic pattern ("magnetic trapping").

1.4.17 Analytical applications of gold nanoparticles

The unique physical and chemical properties of nanostructured materials provide excellent prospects for interfacing biological recognition events with electronic signal transduction and for designing a new generation of bioelectronic devices with novel functions. Especially, Au nanoparticles (AuNPs) represent excellent biocompatibility and display unique structural, electronic, magnetic, optical and catalytic properties which have made them a very attractive material for biosensor, chemisensor and electrocatalyst (Andrey et al., 1997; Maye et al., 2000; Tang et al., 2006).

1.4.17.1 Enzymatic biosensor based on gold nanoparticles

The direct electron transfer (DET) from redox-protein to the electrode surface is a very important subject in bioelectrochemistry to understand the mechanism of many

bioelectrochemical reactions and construct the biochemical sensors. Therefore, many scientists have devoted their efforts to realize the direct electrochemistry of proteins. An extremely important challenge in the direct electrochemistry of proteins is the establishment of satisfactory electrical communication between the active site of the enzyme and the electrode surface (Mena et al., 2005; Andrey et al., 1997). However, the redox center of most oxidoreductase is electrically insulated by a protein shell. Because of this shell, the protein cannot be oxidized or reduced at an electrode at any potential. In order to achieve this task, mediator (discrete, electroactive intermediaries between electrodes and solution couples) have been utilized. More recently, it is interesting to find that the DET of some redox-proteins can also take place with the help of nanoparticles without need of additional mediators. Modification of electrode surfaces with the AuNPs will provide a microenvironment similar to that of the redox-proteins in native systems and gives the protein molecules more freedom in orientation, thereby reducing the insulating effect of the protein shell for the DET through the conducting tunnels of AuNPs. In 1996, Natan and co-workers (Brown et al., 1996) have reported a reversible electrochemistry of horse heart cytochrome C at SnO2 electrodes modified with 12 nm-diameter AuNPs. Since then, a great deal of literatures have been reported to complete the DET of redox-proteins using AuNPs as promoter.

1.4.17.2 Application of gold nanoparticles for genosensors

The development of electrical DNA hybridization biosensors has attracted considerable research efforts (Joseph et al., 1999; Justin et al., 2002). Such DNA sensing applications require high sensitivity through amplified transduction of the oligonucleotide interaction. Electrochemical devices offer elegant routes for interfacing, at the molecular level, the DNA recognition and signal transduction elements, and are uniquely qualified for meeting the low-

cost, low-volume, and power requirements of decentralized DNA diagnostics. The AuNPs modified electrochemical sensing interfaces offer elegant ways for interfacing DNA recognition events with electrochemical signal transduction, and for amplifying the resulting electrical response. AuNPs-based amplification schemes reports have led to improved sensitivity of bioelectronic assays by several orders of magnitude. Thus, AuNPs-based electrochemical device will provide new opportunity for gene diagnostics in the future.

Merkoci and co-workers reviewed (Castañeda et al., 2007) recent important achievements on the electrochemical sensing of DNA using AuNPs. In that review, the author discussed recent some novel strategies for geno sensors based on AuNPs. **Figure1.8** depicted a schematic of the most important strategies used to integrate AuNPs in DNA detection systems. These strategies consist of: (A) the electrochemical detection of AuNPs label by detecting the gold ions released after acidic dissolving; (B) direct detection of AuNPs anchored onto the surface of a conventional genosensor (based on stripping voltammetry); (C) silver enhancement using conductometric technique; (D) enhancement of AuNPs anchored to conventional genosensor surface by using silver or gold; (E) AuNPs as carriers of other AuNPs; (F) using AuNPs as carriers for other electroactive labels.

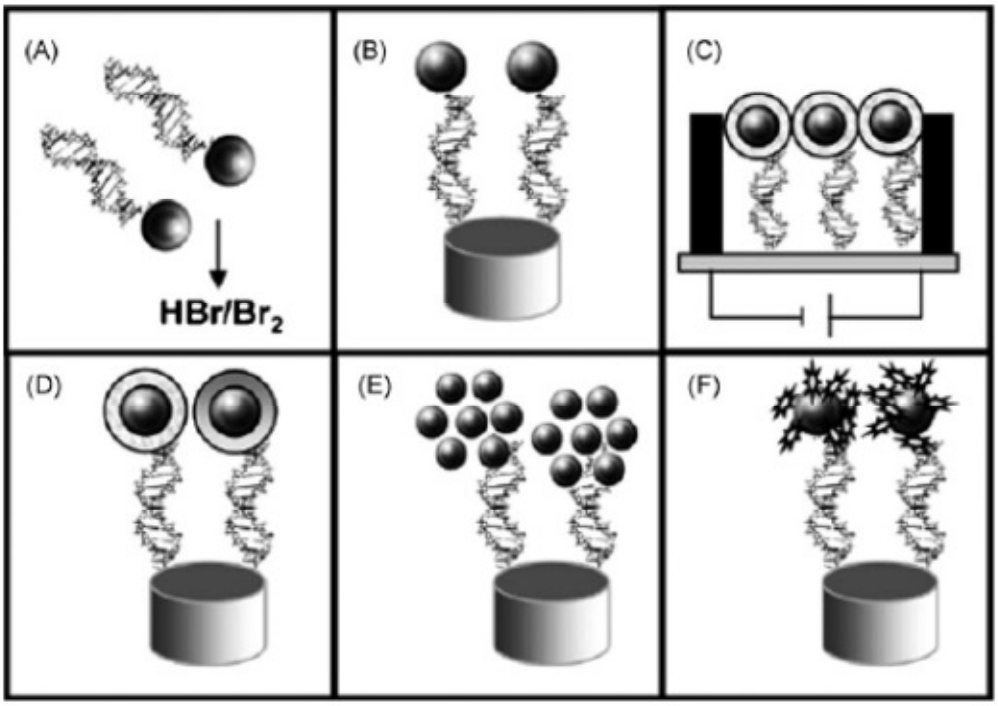

Figure 1.8 *Schematic procedure of the different strategies used for the integration of AuNPs into DNA sensing systems: (A) previous dissolving of AuNPs by using HBr/Br2 mixture followed by Au(III) ions detection, (B) direct detection of AuNPs anchored onto the surface of the genosensor, (C) conductometric detection, (D) enhancement with silver or gold followed by detection, (E) AuNPs as carriers of other AuNPs, (F) AuNPs ascarriers of other electroactive labels.(Reproduced with permission from Castañeda et al., Electroanalysis, 2007, 19(7-8):743–753).*

DNA-free ultrasensitive electrochemical immunosensors have received considerable interests because of their advantage including simplify, rapidness and high sensitivity. Yang's group (Das et al., 2006) developed an ultrasensitive and simple electrochemical method for the fabrication of a sandwich-type heterogeneous electrochemical immunosensor. **Figure 1.9** shows a typical fabrication procedure of DNA-free electrochemical immunosensor. An IgG

layer was formed on an ITO electrode via a stepwise assembly process (**Figure 1.9a**). First, partially ferrocenyltethered dendrimer (Fc-D) was immobilized to the ITO electrode by covalent bonding between dendrimer amines and carboxylic acids of a phosphonate self-assembled monolayer. Some of the unreacted amines of Fc-D were modified with biotin groups to allow the specific binding of streptavidin. Afterward, biotinylated antibodies were immobilized to the streptavidin-modified ITO electrode. An IgGnanocatalyst conjugate was prepared via direct adsorption of IgG on 10 nm AuNPs. Mouse IgG or prostate specific antigen was chosen as a target protein (**Figure 1.9b**). The IgG-nanocatalyst conjugate and the immunosensing layer sandwiched the target protein. Signal amplification was achieved by catalytic reduction of p-nitrophenol (NP) to p-aminophenol (AP) using gold nanocatalyst labels and the chemical reduction of pquinone imine (QI) by NaBH4. This novel DNA-free method could attain a very low detection limit (1 fg mL−1).

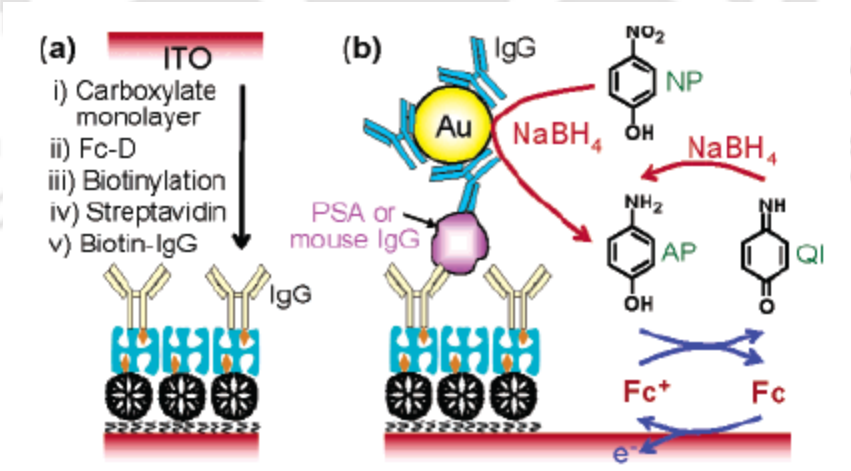

Figure 1.9 *(a) Schematic representation of the preparation of an immunosensing layer. (b) Schematic view of electrochemical detection of mouse IgG or PSA (Reproduced with permission from Das J et al., J. Am. Chem. Soc, 2006, 128(50):16022–16023).*

1.4.17.3 Application of gold nanoparticles for electrocatalytic chemosensors

Nanometer-sized AuNPs exhibiting excellent catalytic activity have received considerable attention due to their relative high surface area-to-volume ratio, and their interface-dominated properties, which significantly differ from their bulk counterparts. Thus, interest in the catalytic properties of AuNPs has increased rapidly. In particular, AuNPs have been studied extensively for the design and fabrication of electrocatalysts and using as an enhancing component of catalytic activity or selectivity. The large surface-to-volume ratios and active sites of AuNPs constitute part of the driving force in developing nanosized electrocatalysts.

AuNPs could also be employed as enhancing materials for electrochemical investigation of cell (Ding et al., 2006) and electro catalyzing of some small biomolecules such as glucose (Tominaga et al., 2005), norepinephrine (Lu et al., 2004), dopamine (Raj et al., 2003), catechol (Su et al., 2006), epinephrine (Wang et al., 2006) and ascorbic acid (Wang et al., 2007), etc. For instance, Raj and co-worker reported a nonenzymatic electrochemical method for the detection of glucose by using AuNPs self-assembled on a 3D silicate network obtained by using sol–gel processes. The nanosized Au particles have been self-assembled on the thiol tail groups of the silicate network and enlarged by hydroxylamine. The AuNPs efficiently catalyzed the oxidation of glucose at less-positive potential (0.16 V) in phosphate buffer solution (pH 9.2) in the absence of any enzymes or redox mediators. This novel non enzymatic glucose sensor showed excellent sensitivity with a detection limit of 50 nM.

1.4.17.4 Multicolor optical coding for biological assays

Increasing research in proteomics and genomic generates escalating number of sequence data and requires development of high throughput screening technologies. Various array

technologies has been used in parallel analysis are likely to reach saturation when a number of array elements exceed several millions. A three-dimensional approach, based on optical "bar coding" of polymer particles in solution, is limited only by the number of unique tags one can reliably produce and detect. Single quantum dots of compound semiconductors were successfully used as a replacement of organic dyes in various bio-tagging applications (Parak et al., 2003). By combining different sized and having different fluorescent colors quantum dots, and also combining them in polymeric microbeads will give further advantages (Han et al., 2001). A precise control of quantum dot ratios has been achieved. The selection of nanoparticles used in those experiments had 6 different colours as well as 10 intensities. It is enough to encode over 1 million combinations. The uniformity and reproducibility of beads was high letting for the bead identification accuracies of 99.99%.

1.4.17.5 Application of gold nanoparticles for signal amplification

Amanda and Coworker report a novel strategy for the high-sensitive detection of target biomolecules with very low concentrations on a quartz crystal microbalance (QCM) device using gold nanoparticles as signal enhancement probes. By employing a streptavidin–biotin interaction as a model system, we could prepare biotin conjugated gold nanoparticles maintaining good dispersion and long-term stability by controlling the biotin density on the surface of gold nanoparticles that have been investigated by UV-vis spectra and AFM images. These results showed that 10 μM *N*-(6-[biotinamido]hexyl)-3′-(2′-pyridyldithio)propionamide (biotin-HPDP) was the critical concentration to prevent the nonspecific aggregation of gold nanoparticles in this system. For sensing streptavidin target molecules by QCM, biotinylated BSA was absorbed on the Au surface of the QCM electrode and subsequent coupling of the target streptavidin to the biotin in the sensing interface followed. Amplification of the sensing

process was performed by the interaction of the target streptavidin on the sensing surface with gold nanoparticles modified with 10 μM biotin-HPDP. The biotinylated gold nanoparticles were used as signal amplification probes to improve the detection limit, which was 50 ng/ml, of the streptavidin detection system without signal enhancement, and the calibration curve determined for the net frequency changes showed good linearity over a wide range from 1 ng/ml to 10 μg/ml for the quantitative streptavidin target molecule analysis (Kim et al., 2007).

1.4.18 Commercial exploration of gold nanoparticles

Some of the companies involved in the development and commercialization of nanomaterials listed in **Table 1.15** (Salata et al., 2004).

Table 1.15 *Examples of Companies commercialising nanomaterials for bio- and medical applications.*

Company	Technology	Major Activity
Advectus Life Sciences Inc.	Polymeric nanoparticles engineered to carry antitumour drug across the blood-brain barrier	Drug delivery
Alnis Biosciences, Inc.	Biodegradable polymeric nanoparticles for drug delivery	Bio-pharmaceutical
Argonide	Nanoporous ceramic materials for endotoxin filtration, orthopaedic and dental implants, DNA and protein separation	Membrane filtration
BASF	Hydroxyapatite nanoparticles seems to improve dental surface	Toothpaste
Biophan Technologies, Inc.	Nanomagnetic/carbon composite materials to shield medical devices from RF fields	MRI shielding
Capsulution NanoScience AG	Layer-by-layer poly-electrolyte coatings, 8–50 nm	Pharmaceutical coatings to improve solubility of drugs
Dynal Biotech	Magnetic beads	–
Eiffel Technologies	Reducing size of the drug particles to 50–	Drug delivery

	100 nm	
EnviroSystems, Inc.	Nanoemulsions	Surface desinfectsant
Evident Technologies	Semiconductor quantum dots with amine or carboxyl groups on the surface, emission from 350 to 2500 nm	Luminescent biomarkers
Immunicon	magnetic core surrounded by a polymeric layer coated with antibodies for capturing cells	Tarcking and separation of different cell types
KES Science and Technology, Inc.	Nano-TiO2 to destroy airborne pathogens	AiroCide filters
NanoBio Cortporation	Antimicrobal nano-emulsions	Pharmaceutical
NanoCarrier Co., Ltd	Micellar nanoparticles for encapsulation of drugs, proteins, DNA	Drug delivery
NanoPharm AG	Polybutilcyanoacrylate nanoparticles are coated with drugs and then with surfactant, can go across the blood-brain barrier	Drug delivery
Nanoplex Technologies, Inc:	–	Nanobarcodes for Bioanalysis
Nanoprobes, Inc.	Gold nanoparticles bioconjugates for TEM and/or fluorescent microscopy	Gold nanoparticles for biological markers
Nanoshpere, Inc.	DNA barcode attached to each nanoprobe for identification purposes, PCR is used to amplify the signal; also catalytic silver deposition to amplify the signal using surface plasmon resonance	Gold biomarkers
NanoMed Pharmaceutical, Inc.	Nanoparticles for drug delivery	Drug delivery
Oxonica Ltd	Doped transparent nanoparticles to effectively absorb harmful UV and convert it into heat	Sunscreens
PSiVida Ltd	Exploiting material properties of nanostructured porous silicone	Tissue engineering, implants, drugs and gene delivery, bio-filtration
Smith & Nephew	Nanocrystal silver is highly toxic to pathogenes	Acticoat bandages
Quantum Dot Corporation	Bioconjugated semiconductor quantum dots	Luminescent biomarkers

1.5 Overall view of nanotechnology and gold nanoparticles

Nanotechnology is highly interdisciplinary, involving physics, chemistry, biology, materials science, and the full range of the engineering disciplines. The word *nanotechnology* is widely used as shorthand to refer to both the science and the technology of this emerging field. Narrowly defined, nanoscience concerns a basic understanding of physical, chemical, and biological properties on atomic and near-atomic scales. Nanotechnology, narrowly defined, employs controlled manipulation of these properties to create materials and functional systems with unique capabilities.

In contrast to recent engineering efforts, nature developed "nanotechnologies" over billions of years, employing enzymes and catalysts to organize with exquisite precision different kinds of atoms and molecules into complex microscopic structures that make life possible. These natural products are built with great efficiency and have impressive capabilities, such as the power to harvest solar energy, to convert minerals and water into living cells, to store and process massive amounts of data using large arrays of nerve cells, and to replicate perfectly billions of bits of information stored in molecules of deoxyribonucleic acid (DNA).

There are two principal reasons for qualitative differences in material behavior at the nanoscale (traditionally defined as less than 100 nanometres). First, quantum mechanical effects come into play at very small dimensions and lead to new physics and chemistry. Second, a defining feature at the nanoscale is the very large surface-to-volume ratio of these structures. This means that no atom is very far from a surface or interface, and the behaviour of atoms at these higher-energy sites have a significant influence on the properties of the

material. For example, the reactivity of a metal catalyst particle generally increases appreciably as its size is reduced—macroscopic gold is chemically inert, whereas at nanoscales gold becomes extremely reactive and catalytic and even melts at a lower temperature. Thus, at nanoscale dimensions material properties depend on and change with size, as well as composition and structure.

Using the processes of nanotechnology, basic industrial production may veer dramatically from the course followed by steel plants and chemical factories of the past. Raw materials will come from the atoms of abundant elements—carbon, hydrogen, and silicon—and these will be manipulated into precise configurations to create nanostructured materials that exhibit exactly the right properties for each particular application. For example, carbon atoms can be bonded together in a number of different geometries to create variously a fibre, a tube, a molecular coating, or a wire, all with the superior strength-to-weight ratio of another carbon material—diamond. Additionally, such material processing need not require smokestacks, power-hungry industrial machinery, or intensive human labour. Instead, it may be accomplished either by "growing" new structures through some combination of chemical catalysts and synthetic enzymes or by building them through new techniques based on patterning and self-assembly of nanoscale materials into useful predetermined designs. Nanotechnology ultimately may allow people to fabricate almost any type of material or product allowable under the laws of physics and chemistry. While such possibilities seem remote, even approaching nature's virtuosity in energy-efficient fabrication would be revolutionary.

Even more revolutionary would be the fabrication of nanoscale machines and devices for incorporation into micro- and macroscale systems. Once again, nature has led the way

with the fabrication of both linear and rotary molecular motors. These biological machines carry out such tasks as muscle contraction (in organisms ranging from clams to humans) and shuttling little packets of material around within cells while being powered by the recyclable, energy-efficient fuel adenosine triphosphate. Scientists are only beginning to develop the tools to fabricate functioning systems at such small scales, with most advances based on electronic or magnetic information processing and storage systems. The energy-efficient, reconfigurable, and self-repairing aspects of biological systems are just becoming understood.

The potential impact of nanotechnology processes, machines, and products is expected to be far-reaching, affecting nearly every conceivable information technology, energy source, agricultural product, medical device, pharmaceutical, and material used in manufacturing. Meanwhile, the dimensions of electronic circuits on semiconductors continue to shrink, with minimum feature sizes now reaching the nanorealm, under 100 nanometres. Likewise, magnetic memory materials, which form the basis of hard disk drives, have achieved dramatically greater memory density as a result of nanoscale structuring to exploit new magnetic effects at nanodimensions. These latter two areas represent another major trend, the evolution of critical elements of microtechnology into the realm of nanotechnology to enhance performance. They are immense markets driven by the rapid advance of information technology.

2.1 Introduction

The application of gold nanoparticles (AuNPs) is revolutionizing various fields like catalysis, optoelectronics, bio-imaging, photo thermal cancer therapy, and surface-enhanced Raman scattering (Taleb et al., 1998; Klaus et al., 1999; Crooks et al., 2002; Goodman et al., 1983; Haes et al., 2002; El-Sayed et al., 2001). Nanoparticles are generally synthesized by a number of chemical methods that are harmful to the environment (Tolles et al., 1996; Selvakannan et al., 2002; Okitsu et al., 2008; Sun et al., 2002). Therefore, there is a growing need to develop procedures that do not use toxic chemicals and are safe and environmentally friendly. Biological synthesis of nanoparticles using microorganisms like *Bacillus subtilis* 168, *Shewanella algae*, *Verticillium* sp., *Fusarium oxysporum*, *Thermomonospora* sp., *Rhodococcus* sp., and plant extracts has been found to be an eco-friendly alternative to chemical and physical methods (Beveridge et al., 1980; Konish et al., 2004; Mukherjee et al., 2001; Mukherjee et al., 2002; Ahmad et al., 2003a; Ahmad et al., 2003b; Mohanpuria et al., 2008). With recent synthesis of AuNPs using *Cymbopogon flexuosus*, *Coriandrum sativum*, *Cinnamomum camphora*, *Phyllanthus amarus*, *Lawsonia inermis*, and *Azadirachta indica*the, the evaluation of novel plants for AuNPs synthesis is gaining importance (Shankar et al., 2004a; Narayanan et al., 2008; Huang et al., 2007; Kasthuri et al., 2009a; Kasthuri et al., 2009b; Shankar et al., 2004b).

The Indian mint (*Mentha arvensis*, family Lamiaceae), commonly known as pudina, has been extensively used as a culinary flavoring ingredient and traditional remedy for various ailments like hiccups, sore throat, indigestion, heat stroke, dementia, neuropathies, and allergies. *Mentha* oil has been commercially used in flavoring toothpastes, cosmetics, and confectionery. *Mentha arvensis* contains various organic compounds like phenolic acids, flavonoids, terpenoids, and carotenoids, which possess

antioxidant and free radical scavenging properties (Mahishi et al., 2005; Kumar et al., 2007; Raju et al., 2007). Flavonoids are known to have antioxidant properties; we presume that they can be a possible source for the bioreduction ofAu^{3+} to Au^{o}. Here, we describe a novel use of *M. arvensis* for AuNPs synthesis.

2.2 Materials and methods

2.2.1 Materials

All chemicals used in this experiment were of highest purity and obtained from Sigma (Bangalore, India) and Merck (Mumbai, India). *M. arvensis* was grown as per traditional agronomic practice in the experimental field and healthy leaves were harvested for AuNP synthesis.

2.2.2 Preparation of leaf extract

M. arvensis leaves obtained were washed with deionized water several times to remove adsorbed dirt, chopped into small pieces (4 mm ×3 mm), and dried for at room temperature (25 ^{o}C) under shade. The dried leaves were powered in a mixer grinder (Bajaj GX 11, Mumbai, India), 4 g of which was dissolved in 40 mL of ethanol and incubated at 4 ^{o}C for 3 days. The *Mentha* leaf extract (MLE) was dried by ethanol evaporated with a rotary evaporator (Rotera Equitron, Medica Instrument Mfg. Co., Mumbai, India). One hundred milligrams of plant extract was dissolved in 1 mL of ethanol (100 μg/1 μL) and used as stock solution for further experiments.

2.2.3 Test for flavonoids and phenolic compounds

To the 5 mL of diluted ammonium solution, 2 mL of *M. arvensis* leaf extract was added, followed by a few drops of concentrated sulfuric acid. The yellowish color indicated the presence of the flavonoids. To the 2 mL of *M. arvensis* leaf extract, a few drops of 5%

ferric chloride were added. The appearance of a dark green color indicated the presence of poly phenolic compounds.

2.2.4 Synthesis of AuNPs using *Mentha arvensis* plant extract

To determine the amount of MLE required for the synthesis of AuNPs, varying concentrations (0.01%–0.05%, v/v) of MLE were mixed with 1 mM HAuCl4 aqueous solution and the final volume was made up to 10 mL with double distilled water. The resultant solution was left at 80 ^{o}C with constant stirring (200 rpm) for the change in color. The concentration of $HAuCl_4$ was optimized by reacting 0.02% leaf extract by varying the concentration (1–5 mM) of $HAuCl_4$. The reaction time for AuNPs synthesis was optimized by reacting 0.02% MLE containing 2mM $HAuCl_4$ and incubated for different time periods (10, 20, 30, 40, and 60 min), keeping other incubation conditions as above. The reaction temperature for AuNPs synthesis was optimized for the reaction involving 0.02% MLE and 2 mM $HAuCl_4$ incubated for 30 min at various temperatures (25, 40, 50, 60, 70, 80, and 90 ^{o}C). All experiments were repeated five times and the data were expressed as mean ± SD (n = 5) and absorbance recorded in a UV-Vis spectrophotometer (Cary 100 BIO, Varian, CA, USA) from 400 to 700 nm.

2.2.5 Characterization of AuNPs

2.2.5.1 UV-visible spectroscopy

All UV-visible spectroscopic measurements of the AuNPs synthesised were carried out on a Cary 100 BIO UV–Vis spectrophotometer, Varian, CA, USA.

2.2.5.2 Transmission electron microscope (TEM) studies

5 ml colloidal solution of synthesised AuNPs were centrifuged twice at 20000 rpm for 20 minutes (min) to remove the non covalently bounded molecules on the their surfaces. The

resulting pellet was redispersed in 1 ml of distilled water and few drops were placed over carbon coated copper grid and the water was evaporated in a hot air oven (Daihan Labtech Co.Ltd. model LDO-150F) at 60 ^{o}C for 4 h.TEM measurements were performed on a TEM-JEOL model 2100 instrument operated at 190 voltage of 200 kV.

2.2.5.3 X-ray Diffractrogram (XRD) analysis of AuNPs

The XRD pattern was recorded with a Bruker Advance D8 XRD machine (Bruker AXS Inc., Karlsruhe, Germany) operating at 40 kV and 40 mA with Cu-K• 1 radiation at • 1.54 A^{o}. A few drops of AuNPs solution was spread on a microscope slide to cover the total surface area and dried in a hot air oven (model LDO-150F, Daihan Labtech Co. Ltd.) at 50 ^{o}C and placed on the sample stage. The relative intensity was recorded at the scattering range (2•) of 10 to 75^{o} with a scan rate of 0.05^{o}.

2.2.5.4 FTIR analysis of AuNPs

The AuNPs solution was centrifuged at 20,000 rpm for 10 min and the resulting pellet was resuspended in 5 mL distilled water and lyophilized (model 1-4, Christ Gefriertrocknungsanlagen GmbH, Osterode Am Harz, Germany) for 14 h. The lyophilized sample was finely powdered and pressed with 200 mg of KBr and infrared spectra were recorded (Spectrum One, Perkin Elmer, MA, USA) from 450 to 4000 cm^{-1}.

2.2.5.6 EDX analysis

Elemental composition of the AuNPs was studied using a scanning electron microscope (LEO 1430 VP) equipped with an INCA Oxford EDX facility (Oxford, UK), at an acceleration voltage of 10 ke V.

2.2.6 Statistical analysis

Experiments with quantitative data were done in replicates of four independent experiments and the results were expressed as Mean ± Standard Deviation (*n = 5*)

2.3 Results

2.3.1 UV-visible spectroscopy

The formation of AuNPs was initially determined with a UV-Vis spectrophotometer. The surface plasmon resonance (SPR) band of AuNPs synthesized with 0.02% MLE showed an intense and narrow SPR peak centered at around 540 nm (**Figure 2.1A**). UV-Vis spectra of products obtained by reacting 0.02% MLE with varying concentrations (1–5 mM) displayed an intense peak at 542 nm for 2 mM $HAuCl_4$ (**Figure 2.1B**). The effect of incubation time on AuNPs formation was determined from UV-Vis spectra of reaction products synthesized by varying the reaction time from 10–60 min (**Figure 2.1C**).

The SPR peak at 539 nm with significant intensity was observed for 30 min incubation time. The experiments were conducted to identify the optimum temperature for AuNPs synthesis. We observed that except for the reaction at 25 ^{o}C, all others showed a pale to intense ruby red color. The UV-Vis absorption spectra of the AuNPs observed peaks at 538 ±7 nm The maximum peak intensity of AuNPs was attained at 80 ^{o}C at 30 min of reaction time (**Figure 2.1D**).

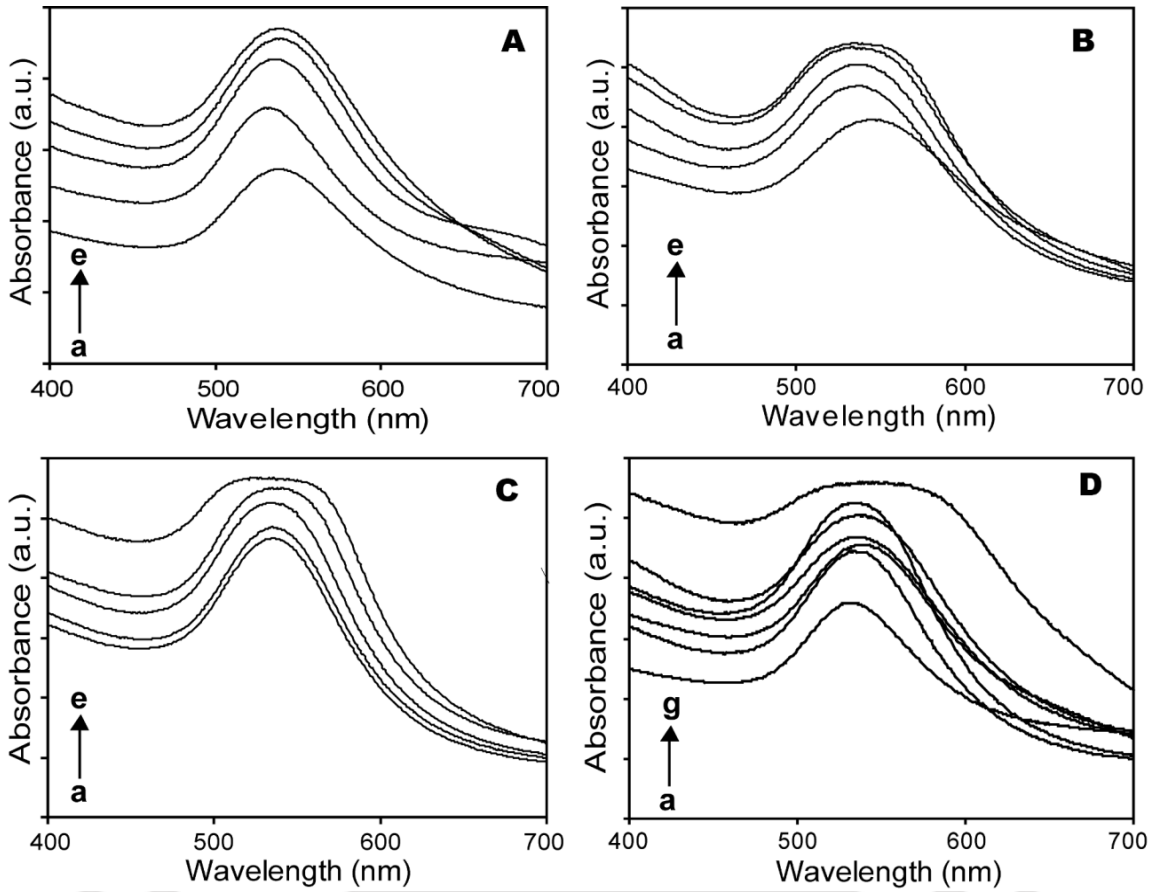

Figure 2.1 *UV-Visible absorption spectra of gold nanoparticles synthesized at 80•C with (A) 1 mM $HAuCl_4$ and M. arvensis leaf extract concentrations, viz. (a) 0.01%, (b) 0.02%, (c) 0.03%, (d) 0.04%, and (e) 0.05%; (B) 0.02% of leaf extract with different gold concentrations, viz. (a) 1 mM, (b) 2 mM, (c) 3 mM, (d) 4 mM, and (e) 5 mM; (C) 0.02% of leaf extract with 2 mM of gold concentration at different time intervals of (a) 10 min, (b) 20 min, (c) 30 min, (d) 40 min, and (e) 60 min; (D) 0.02% leaf extract containing 2 mM HAuCl4.4H2O incubated for 30 min at various temperatures, viz. (a) 25 ^oC, (b) 40 ^oC, (c) 50 ^oC, (d) 60 ^oC, (e) 70 ^oC, (f) 80 ^oC, and (g) 90 ^oC.*

2.3.2 Transmission electron microscope (TEM) studies

TEM monographs of synthesized AuNPs with optimum reaction conditions reveals the nanoparticles were of hexagonal and nearly circular shape (**Figure 2.1A**). High-resolution

image confirmed the presence fcc of the AuNPs (**Figure 2.2B**). The crystalline nature of AuNPs was confirmed form clear lattice fringes in the high-resolution image and typical selected area electron diffraction (SAED) pattern with bright circular rings corresponding to the (1 1 1), (2 0 0), and (2 2 0) planes (**Figure 2.2C**). The synthesized AuNPs were ranges from 10-55 nm with average size of 39±15 nm (**Figure 2.2D**).

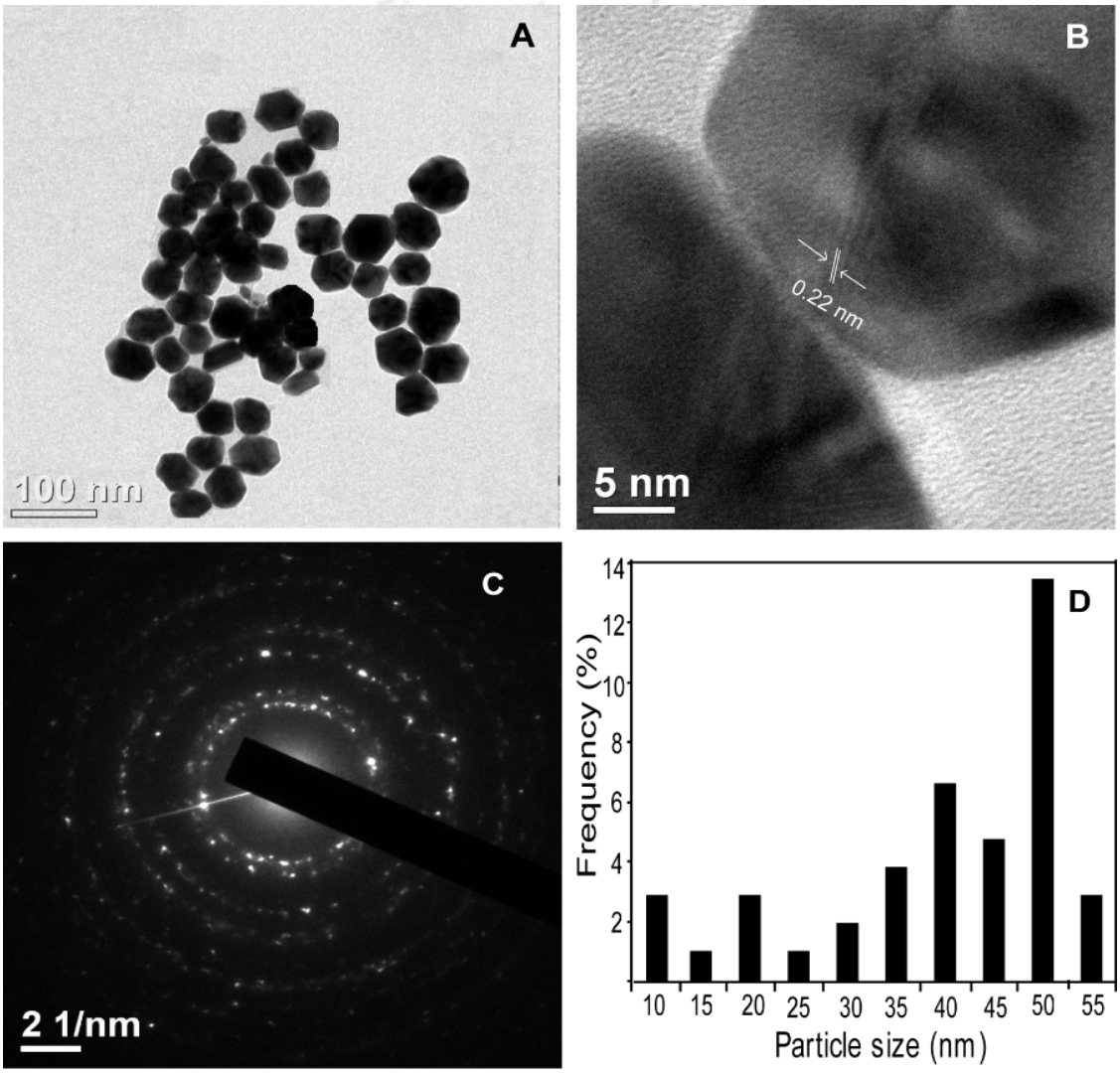

Figure 2.2 *(A) TEM, (B) HRTEM, (C) SAED pattern, and (D) size distribution of AuNPs prepared by reacting 2 mM $HAuCl_4$ solution with 0.02% M. arvensis leaf extract for 30 min at 80°C.*

2.3.3 X-ray Diffractrogram (XRD) analysis of AuNPs

The crystalline nature of AuNPs was confirmed with X-ray diffraction analysis (**Figure 2.3**). The XRD pattern of the AuNPs displayed diffraction peaks at 38.1, 44.4, and 64.5^{o} corresponding to the (1 1 1), (2 0 0), and (2 2 0) Bragg's reflections, respectively, which is due to the fcc crystal structure.

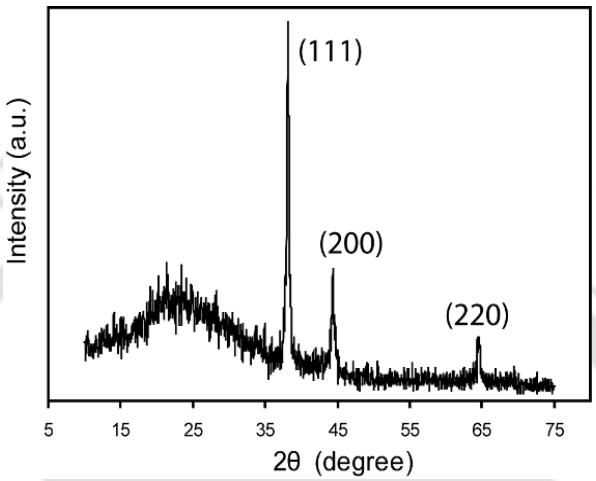

Figure 2.3 *XRD pattern of AuNPs prepared by reacting 2 mM $HAuCl_4$ solution with 0.02% M. arvensis leaf extract for 30 min at 80 ^{o}C.*

2.3.4 FTIR analysis of AuNPs

The functional groups present on the AuNPs were identified using Fourier transform infrared (FTIR). The FITR spectrum of MLE (**Figure 2.4a**) showed bands at 3330, 1629, 1227, and 1037 cm^{-1} and AuNPs synthesized by the optimum reactions condition showed infrared absorption signals at 3349, 1736, 1647, 1329, and 1024 cm^{-1} (**Figure 2.4b**).

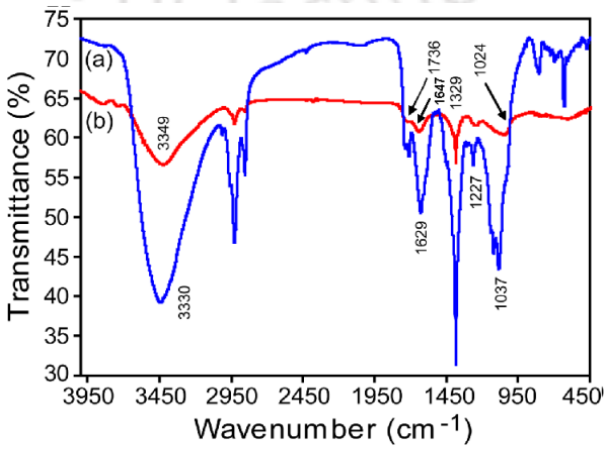

Figure 2.4 *FTIR spectrum of M. arvensis leaf extract (curve a) and AuNPs (curve b) prepared by reacting 2 mM $HAuCl_4$ solution with 0.02% M. arvensis leaf extract for 30 min at 80 ^oC.*

2.3.5 EDX analysis

Energy dispersive X-ray spectroscopy (EDX) profile of AuNPs synthesized with MLE showed a strong gold signal along with very weak carbon and oxygen peaks **(Figure 2.5).**

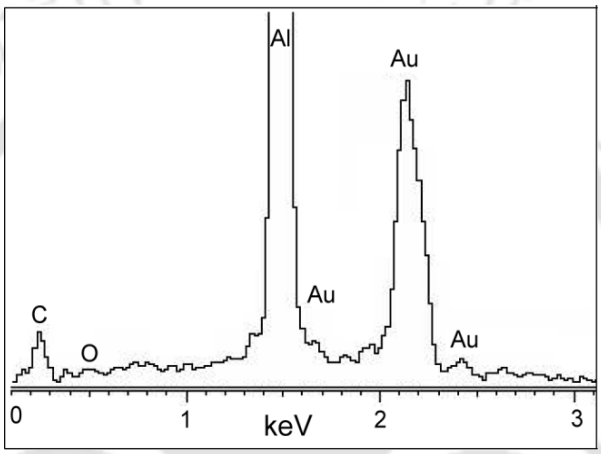

Figure 2.5 *EDX pattern of AuNPs prepared by reacting 2 mM $HAuCl_4$ solution with 0.02% M. arvensis leaf extract for 30 min at 80 ^oC.*

2.4 Discussion

The synthesis of AuNPs can be monitored easily with the naked eye by observing the appearance of color. The formation of AuNPs was initially determined with a UV-Vis spectrophotometer. The surface plasmon resonance (SPR) band of AuNPs synthesized with 0.02% MLE showed an intense and narrow SPR peak centered at around 540 nm (**Figure 2.1A**). MLE concentrations above 0.02% resulted in red-shifted SPR peaks, indicating an increase in the size of nanoparticles. From 0.04% to 0.05% of MLE, no considerable change in the SPR intensity was observed. Thus, 0.02% of MLE was considered as optimum for AuNP synthesis. UV-Vis spectra of products obtained by

reacting 0.02% MLE with varying concentrations (1–5 mM) displayed an intense peak at 542 nm for 2 mM $HAuCl_4$ (**Figure 2.1B**). The UV spectra for 4 and 5 mM of $HAuCl_4$ displayed peak flattening, whereas 1 mM was considered as suboptimal. Since no any significant gain in SPR peak intensity with 3 mM was achieved, 2 mM was taken as the optimum gold concentration for AuNPs synthesis. The effect of incubation time on AuNPs formation was determined from UV-Vis spectra of reaction products synthesized by varying the reaction time (10–60 min; **Figure 2.1C**). For 30 min incubation time, the SPR peak at 539 nm with significant intensity was observed. Incubation periods below 30 min displayed poor peak intensity and above it we observed peak flattening. Thus, 30 min was considered as the optimum incubation time for AuNPs formation. While studying the optimum temperature for AuNPs synthesis, we observed that except for the reaction at 25 ^{o}C, all others showed a pale to intense ruby red color. The UV-Vis absorption spectra of the AuNPs revealed peaks at 538 ±7 nm (**Figure 2.1D**). The maximum peak intensity of AuNPs was attained at 80 ^{o}C at 30 min of reaction time and was thus considered as the optimum reaction condition. A TEM technique was employed to visualize the size and shape of AuNPs formed.

Figure 2.2A shows a typical bright-field TEM image of AuNPs with optimum reaction conditions, which reveals that nanoparticles are of hexagonal and nearly circular shape. The clear lattice fringes of 0.22 nm in a high-resolution image revealed that the growth of the AuNPs occurred preferentially on the (1 1 1) plane (**Figure 2.2B**). The inter-plane distance of the Au (1 1 1) plane was in agreement with the (1 1 1) d-spacing of bulk Au (0.2355 nm) (Shankar et al., 2004b; Kannan et al., 2008). The clear lattice fringes in the high-resolution image and typical selected area electron diffraction (SAED) pattern with bright circular rings corresponding to the (1 1 1), (2 0 0), and (2 2 0) planes confirmed that the nanoparticles obtained were highly crystalline (**Figure 2.2C**) (Shankar

et al., 2004a; Shankar et al., 2004b; Song et al., 2009). The average size of the synthesized nanoparticles determined by TEM analysis was found to be 39±15 nm (**Figure 2.2D**).

The crystalline nature of AuNPs was confirmed with X-ray diffraction analysis (**Figure 2.3**). The XRD pattern of the AuNPs displayed diffraction peaks at 38.1, 44.4, and 64.5^{o} corresponding to the (1 1 1), (2 0 0), and (2 2 0) Bragg's reflections, respectively, which is due to the fcc crystal structure (Shankar et al., 2004b; Kannan et al., 2008). The peak corresponding to the (1 1 1) plane was more intense than the others. The ratio between the intensity of the (2 0 0) and (1 1 1) diffraction peaks was much lower than the usual value (0.52), suggesting the (1 1 1) plane as the predominant (Kannan et al., 2008). AuNPs synthesized using plant extracts are coated with a thin layer of organic material from the plant leaf extract, which acts as a capping agent (Shankar et al., 2004a; Song et al., 2009).

The Fourier transform infrared (FTIR) spectrum of MLE (**Figure 2.4a**) showed bands at 3330, 1629, 1227, and 1037 cm^{-1}. The intense broad absorbance at 3330 cm^{-1} is characteristic of the hydroxyl functional group in alcohols/phenolic compounds. The bands at 1629 can be assigned to C=C groups of aromatic rings. The 1037 cm^{-1} and corresponds to C-N stretching vibrations of aliphatic amines/alcohols/phenols (Song et al., 2009; Philip et al., 2009). AuNPs synthesized (**Figure 2.4b**) by the optimum reactions condition showed infrared (IR) absorption signals at 3349, 1736, 1647, 1329, and 1024 cm^{-1}. This represents different functional groups of the adsorbed biomolecules on the surface of the AuNPs and indicates the influence of organic moieties in synthesis and for stabilization. The flavonoids and phenolic compounds are abundant in *M. arvensis*. The biochemical test for flavonoids and phenolic compounds in MLE confirmed their presence and thus can be responsible for reductions and stabilization of AuNPs. The IR

absorption spectrum of the AuNPs at 3349, 1736, 1647, 1329, and 1024 cm^{-1} corresponded to the hydroxyl group of alcohols/phenolic compounds, conjugated ethers, •, • unsaturated ketone and esters, C=0 stretching of carboxylic acids, and C-N stretching vibration of aliphatic amines/hydroxyl groups, respectively (Philip et al., 2009). These signals were likely originated from the flavonoids and the phenolic compound present in the *M. arvensis* could have been adsorbed on the surface of the AuNPs and the same may be involved in the bioreduction of Au^{3+} to Au^{o} (Londokar et al., 2009). Flavonoids interact with Au^{3+} ions through carbonyl groups or •-electrons and then reduce into AuNPs in the extracellular medium. Because the flavonoids possess good reducing capacity, as soon as they come in contact with Au^{3+} ions in extracellular medium, they transfer their •-electrons and reduce the Au^{3+} to Au^{o}. It was understood that flavonoids also prevent agglomeration and stabilize the AuNPs (Nune et al., 2009). This gives strong evidence for the involvement of flavonoids in rapid reduction of Au^{3+} ions and as a capping agent, which gives stability to AuNPs. Phenolic compounds present in *M. arvensis* have a high capacity to reduce the Au^{3+} ions by donating their electrons. In particular, the IR absorption signals at the 1227 cm^{-1} band (**Figure 2.4a**) arise most probably from the C–O group of polyols. The appropriate disappearance of this band after the reaction with MLE may be due to the fact that the polyols are also responsible for the reduction of Au^{3+} ions, whereby they are oxidized to •, • unsaturated carbonyl groups, leading to a broad peak at 1647 cm^{-1}. This suggested that the electrons required for reduction of Au^{3+} ions were donated by different poly phenols compounds present in the MLE.

In addition to FTIR analysis, the energy dispersive X-ray spectroscopy (EDX) profile of AuNPs synthesized with MLE showed a strong gold signal along with very weak carbon and oxygen peaks. The carbon and oxygen peaks displayed may be

contributed by flavonoids or phenolic compounds bound to the surface of the AuNPs (**Figure 2.5**). The signal for Al was originated from the aluminum grid used for the analysis. FTIR and EDX analysis together suggested that the flavonoids and phenolic compounds are likely to be adsorbed on the surface of the AuNPs. On storage of the bio functionalized AuNPs synthesized using *M. arvensis*; it was observed that the colloidal solution maintains its stability and uniformity for more than 6 weeks.

2.5 Conclusions

We have synthesized AuNPs by using the *M. arvensis* ethanolic leaf extract for the first time. The different reaction parameters such as plant extract (0.02%), gold solution (2 mM), temperature (80 ^{o}C), and time (30 min) were optimized. The UV-Vis spectroscopic analysis displayed an intense peak at 530±10 nm indicating the formation of AuNPs that can be used for biomedical applications. The average size of AuNPs was found to be 39±15 nm as evident from TEM studies. The crystalline nature of AuNPs was confirmed with X-ray diffraction analysis and SAED. The XRD pattern of the AuNPs displayed diffraction peaks at 38.1, 44.4, and 64.5^{o} corresponding to the (1 1 1), (2 0 0), and (2 2 0) Bragg's reflections, respectively, which is due to the fcc crystal structure confirmed that the synthesized AuNPs were highly crystalline in nature. The strong evidence from FTIR and EDX suggested that the flavonoids and phenol compound were involved in reduction and stability of AuNPs synthesized using MLE. The flavonoids and phenolic compounds are abundant in *M. arvensis*.

---***---

3.1 Introduction

The unique plasmon resonance and small sizes associated with gold nanoparticles (AuNPs) has opened wide range of applications such as biomedicine, catalysis, biosensing, electronic and magnetic devices (Willems et al., 2005; Bhattacharya et al., 2008; Giljohann et al., 2010; Ghosh et al., 2008; Lewis et al., 1993; Lee et al., 2004; Huang et al., 2006). Various conventional synthesis methods (physical and chemical) such as seed growth, laser/photo irradiation, chemical vapour deposition, solvolysis, thermolytic reduction, solvothermal, sonochemical, electrochemical, chemical UV irradiation and microwave reduction, etc., have been employed to cater the demand of AuNPs (Anandan et al., 2008; Babu et al., 2011a; Mallick et al., 2001; He et al., 2001; Hussain et al., 2003). These methods involve usage of toxic chemicals as reducing and stabilizing agents and trace amount of these chemicals remains present on synthesized AuNPs which are potential hazards to human health (Uboldi et al., 2009). Therefore, there is growing need to develop the environmental benign method and can be achieved mostly by using plant or fruit extracts and bio organisms (Narayanan et al., 2011). In an effort to develop a green method, we found *Bacopa monnieri* ethonolic leaf *extract* (BLE) which is capable of replacing synthetic reducing, capping agents for the synthesis of AuNPs.

Bacopa monnieri (Family: Scrophulariaceae) is an emersed and sprawling herb commonly found in fresh and brackish water. It is commonly know as‘brahmi’ and has been used in Ayurvedic system of medicine for centuries. Traditionally, it was used as a brain tonic to enhance memory development, learning, concentration, bronchitis, asthma, irritable bowel syndrome gastric ulcers and providing relief to patients with anxiety or epileptic disorders. The antioxidant properties of *Bacopa monnieri* may offer protection

from free radical damage in cardiovascular disease and certain types of cancer (Anonymous et al., 2004).

In this study, we investigated the reducing and capping capabilities of BLE using UV light irradiation technique for AuNPs synthesis. The synthesized AuNPs are bounded by a stable organic coating, i.e. surface functionalized, which makes them stable over long period. This type of surface functionalization of AuNPs has not been systematically reported for most of the plant extracts previously used for the green synthesis of AuNPs but we observed unique surface functionalization phenomenon with BLE which facilitates these AuNPs for biomedical application such as drug delivery and molecular imaging.

3.2 Materials and methods

3.2.1 Materials

Bacopa monnieri was grown as per traditional agronomic practice in the experimental field and fresh leaves were harvested for AuNPs synthesis. Cell lines were obtained from the National Centre for Cell Sciences (Pune, India). 3, 4, 5-Dimethylthiazol-2-yl-2-5-diphenyltetrazolium bromide (MTT) and other reagents were obtained from sigma (Bangalore, India) and Merck (Mumbai, India).

3.2.2 Preparation of *Bacopa monnieri* Leaf Extract

B. monnieri leaves obtained were washed with deionized water several times to remove adsorbed dirt, chopped into small pieces (4 mm ×3 mm), and dried for at room temperature (25 ^{o}C) under shade. The dried leaves were powered in a mixer grinder (Bajaj GX 11, Mumbai, India), 5 g of which was dissolved in 50 mL of ethanol and incubated at 4 ^{o}C for one week to get the extract and the obtained extract was filtered using Whatman 50 mm filter papers. The *B. monnieri* leaf extract (BLE) was dried by

ethanol evaporated with a rotary evaporator (Rotera Equitron, Medica Instrument Mfg. Co., Mumbai, India). 10 mg of BLE was dissolved in 2 ml of ethanol and used as stock solution for further experiments as stock solution for further experiments.

3.2.3 Synthesis of AuNPs using *B. monnieri*

The synthesis of AuNPs was carried out by varying BFE concentration from 1-5% (100-500 µg) against 1 mM $HAuCl_4$ in a total volume of 2 ml made up with double distilled water. The resulting mixtures were placed in a UV cross linker (~254 nm) for photo irradiation for 15 min.

3.2.4 Characterization of AuNPs

3.2.4.1 UV-visible spectroscopy

All UV-visible spectroscopic measurements of the AuNPs synthesised were carried out on a Cary 100 BIO UV–Vis spectrophotometer, Varian, CA, USA.

3.2.4.2 Transmission electron microscope (TEM) studies

5 ml colloidal solution of synthesised AuNPs were centrifuged twice at 20000 rpm for 20 minutes (min) to remove the non covalently bounded molecules on the their surfaces. The resulting pellet was redispersed in 1 ml of distilled water and few drops were placed over carbon coated copper grid and the water was evaporated in a hot air oven (Daihan Labtech Co.Ltd. model LDO-150F) at 60 ^{o}C for 4 h. TEM measurements were performed on a TEM-JEOL model 2100 instrument operated at 190 voltage of 200 kV.

3.2.4.3 X-ray Diffractrogram (XRD) analysis of AuNPs

The XRD pattern was recorded with a Bruker Advance D8 XRD machine (Bruker AXS Inc., Karlsruhe, Germany) operating at 40 kV and 40 mA with Cu-K• 1 radiation at • 1.54

A•. A few drops of AuNPs solution was spread on a microscope slide to cover the total surface area and dried in a hot air oven (model LDO-150F, Daihan Labtech Co. Ltd.) at 50 ^{o}C and placed on the sample stage. The relative intensity was recorded at the scattering range (2•) of 10 to 75^{o} with a scan rate of 0.05^{o}.

3.2.4.4 FTIR analysis of AuNPs

The AuNPs solution was centrifuged at 20,000 rpm for 10 min and the resulting pellet was resuspended in 5 mL distilled water and lyophilized (model 1-4, Christ Gefriertrocknungsanlagen GmbH, Osterode Am Harz, Germany) for 14 h. The lyophilized sample was finely powdered and pressed with 200 mg of KBr and infrared spectra were recorded (Spectrum One, Perkin Elmer, MA, USA) from 450 to 4000 cm^{-1}.

3.2.4.5 EDX analysis

Elemental composition of the AuNPs was studied using a scanning electron microscope (LEO 1430 VP) equipped with an INCA Oxford EDX facility (Oxford, UK), at an acceleration voltage of 10 ke V.

3.2.5 Cyto compatibility tests of AuNPs

To maintain the HeLa (Human cervical cancer) and MCF-7 (Human breast cancer) cells, we used the Minimal Essential Medium (MEM) containing 1.0 mM sodium pyruvate, 0.1 mM nonessential amino acids, 1.5 g/L sodium bicarbonate, 2 mM L-glutamine supplemented with 10% FBS (heat inactivated) and 1% antibiotic-antimycotic solution (1000 U/mL penicillin G, 10 mg/mL streptomycin sulphate, 5 mg/mL gentamycin, and 25 μg/mL amphotericin B). The cells were cultured at 37 °C in a humidified incubator (Heal Force, HF 160 W, China) supplemented with 5% CO_2.

To examine the proliferation of AuNPs on cancer cells, monocultures of the HeLa and MCF-7 cell lines were incubated with increasing concentrations of filter (0.2 micron) sterilized AuNPs for 24 h and the cell viability was estimated by MTT dye conversion assay. Cells not exposed to AuNPs were taken as control. Cells were seeded and maintained (1×10^4) in a 96-well plate (Cell Bind, Corning) using MEM medium with serum. After 24 h of growth, the medium was replaced with the serum free medium that contained varied concentrations of AuNPs (10 - 100 µM). The media was removed after 24 h of treatment and cells were washed with phosphate-buffered saline (PBS, 0.01M, pH-7.2). This was followed by addition of 100 µl of MTT (0.5 mg/mL) prepared in serum free medium to each well and incubated for 4 h at 37 °C. After incubation the medium was removed and 100 µl of dimethyl sulphoxide (DMSO) was added to each well to solubilise the formazan crystals and the concentration of formazan was determined by measuring its absorbance at 70 nm using a multiwell plate reader (Tecon micro plate reader, model 680, CA, USA). The cell viability was calculated with the following equation.

$$\text{Cell viability (\%)} = (A_{\text{treated}} / A_{\text{control)}}) \times 100$$

Where A_{treated} and A_{control} are the absorbance's of the treated and untreated cells, respectively.

3.2.6 Statistical analysis

Experiments with quantitative data were done in replicates of four independent experiments and the results were expressed as Mean ± Standard Deviation ($n = 5$)

3.3. Results

3.3.1 UV-visible spectroscopy analysis

We performed the experiments varying the concentrations of BLE form 1-5% (100-500 µg) against 1 mM $HAuCl_4$ gold solution and the final volume was made up to 2 ml with distilled water. We found that 4% of BLE was sufficient to reduce 1 mM $HAuCl_4$ as there was insignificant peak intensity with 5% BLE. The SPR peaks corresponding to 1-3% of BLE exhibited poor intensity and red shift which indicates, respectively, negligible and large sized nanoparticles formation. Thus, we considered the 4% BLE (400 µg) as an optimum to reduce 1 mM $HAuCl_4$ gold solution (**Figure 3.1**). Schematic representation of AuNPs synthesis was shown in **scheme 1**. Furthermore, we have investigated the optimized time for the synthesis of AuNPs and found to be 15 min of UV irradiation as shown in **Table 3.1**.

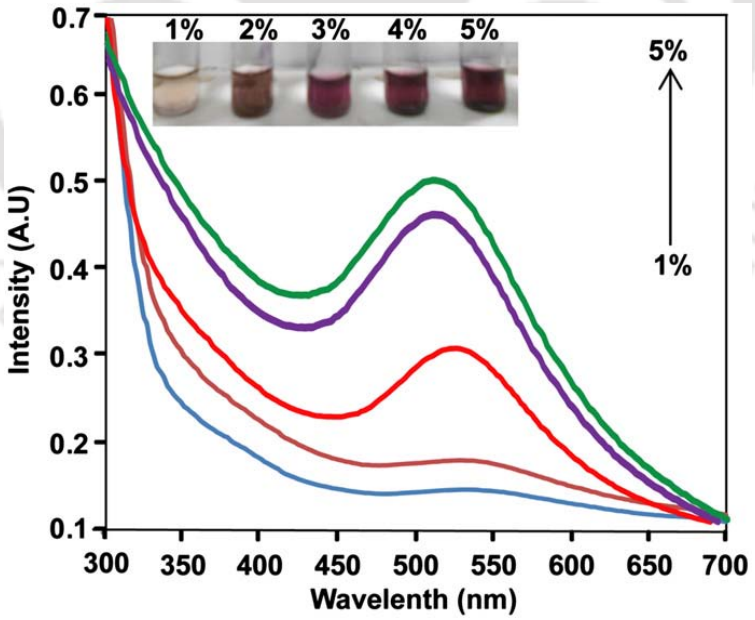

Figure 3.1 *UV–visible absorption spectra of AuNPs synthesized by different concentrations of BLE (a=1%, b=2%, c=3%, d=4%, e=5%) against 1mM $HAuCl_4$ for 15 min of UV light irradiation.*

Table 3.1 *Optimization of time for the synthesis of AuNPs*

No. Of Runs	$HAuCl_4$ (mM).	BLE (%)	Time (min)	AuNPs ($\bullet_{max}$)
1	1	4	5	No formation
2	1	4	10	No formation
3	1	4	15	Appearance of ruby red colour 529
4	1	4	25	537
5	1	4	30	542

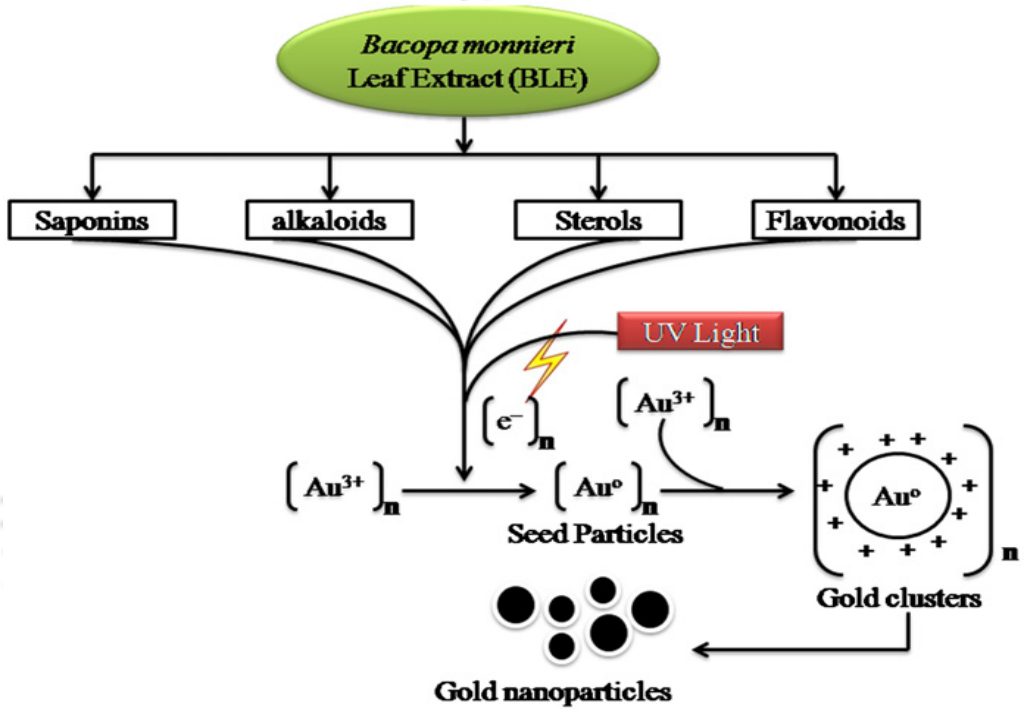

Scheme 1 *Schematic representation of stable AuNPs synthesis using Bacopa monnieri Leaf Extract.*

We have compared UV irradiation with the conventional heating and found importantly that later method required 80 min to reduce the 1mM $HAuCl_4$ gold salt with 4% of BLE (400 mg) which is significant time difference with respective to UV irradiation. The detailed comparison was shown in **Table 3.2**

Table 3.2 *Comparison of UV irradiation with conventional heating method.*

Reaction parameters/properties	Method of AuNPs synthesis	
	Conventional Heating	UV Light irradiation
BLE concentration (v/v)	4%	4%
$HAuCl_4$ concentration	1mM	1mM
Time	80 minutes	15 Min
Predominant Shape of AuNPs	Spherical, Hexagonal	Spherical, Hexagonal
Peak Position	557	525
Particle range	5-100	3-45
Mean Diameter of AuNPs (nm)	21	11
Capping	Yes	Yes
Biocompatibility against tested cell lines	Yes	Yes

3.3.2 Characterization studies of AuNPs

3.3.2.1 Transmission Electron Microscope (TEM)

TEM monographs showed that the AuNPs were predominantly adopted a spherical shape with narrow range of 3-45nm (**Figure 3.2a, 3.2b**). High resolution TEM image revealed clear fcc (0.23 nm) indicating that the growth of the AuNPs occurred preferentially on the (1 1 1) plane (**Figure 3.2c**). Bright circular rings and diffraction peaks (1 1 1), (2 0 0), (2 2 0) of SAED (**Figure 3.2d**) confirmed the crystalline nature of the AuNPs.

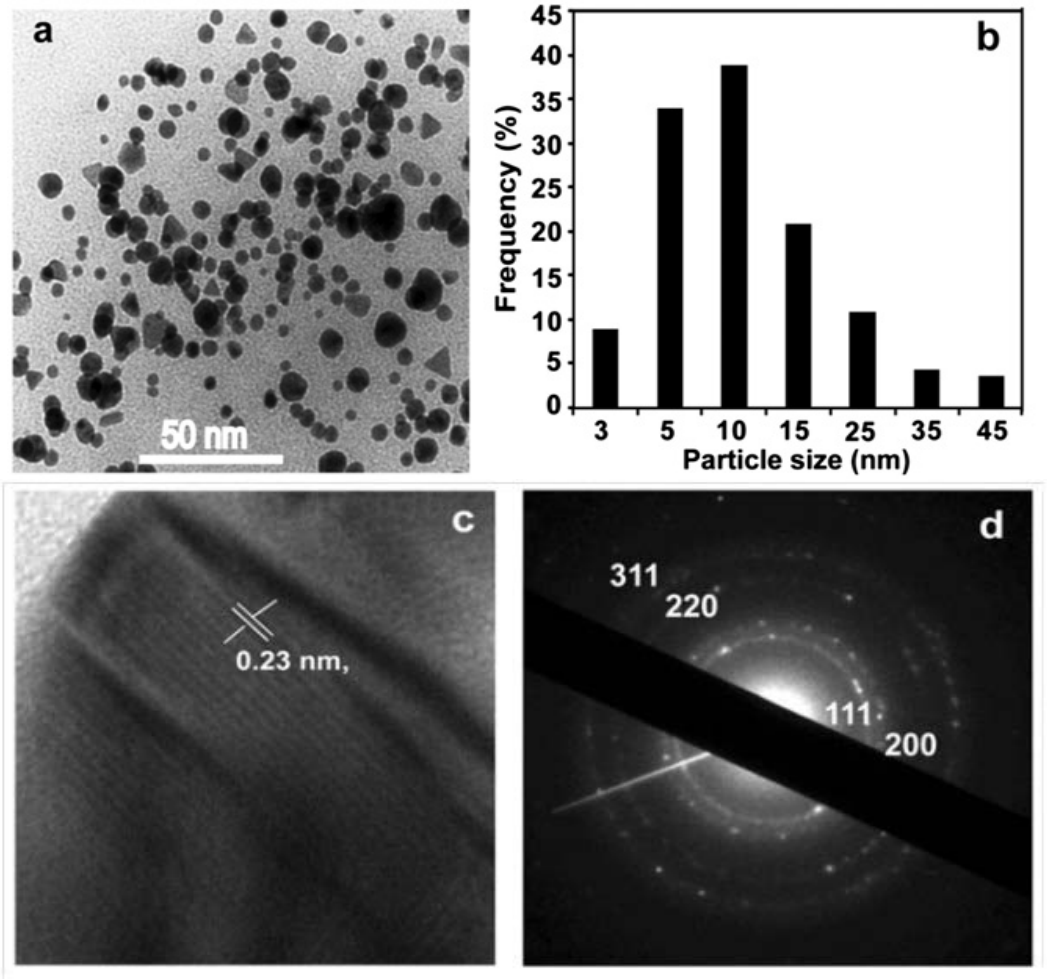

Figure 3.2 *TEM images of (a) AuNPs synthesized with 4% BLE and 1mM $HAuCl_4$ for 15 min and (b) size distribution histogram(c) HRTEM (d) SAED pattern.*

3.3.2.2 X-ray Diffractrogram (XRD) analysis of AuNPs

The crystalline nature of AuNPs was confirmed with X-ray diffraction analysis **(Figure 3.3)**. The XRD pattern of the AuNPs displayed diffraction peaks at 38.1, 44.4, and 64.5^{o} corresponding to the (1 1 1), (2 0 0), and (2 2 0) Bragg's reflections, respectively, which is due to the fcc crystal structure.

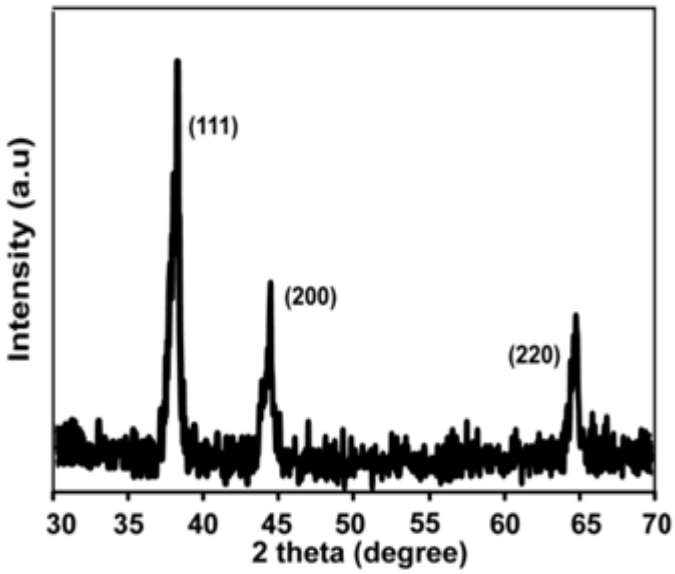

Figure 3.3 *XRD patterns of the AuNPs synthesized using BLE (4%) and $HAuCl_4$ (1mM) for 15 min of UV light irradiation.*

3.3.2.3 FTIR analysis of AuNPs

The FTIR spectra of AuNPs showed sharp transmittance peaks at 3394 (–OH group arising from hydroxyl group containing compounds), 1632 (amide I bond of proteins), 1377 (methyl group of alkanes) and 1085c1 (C–N stretching vibrations of amide bond) (**Figure 3.4**). These functional groups (N–H, N=H, C–CH_3 and OH) attributed to the bioactive molecules present in BLE which facilitated the reduction of the Au^{3+} ions to Au^{o} and capped on AuNPs during the synthesis process.

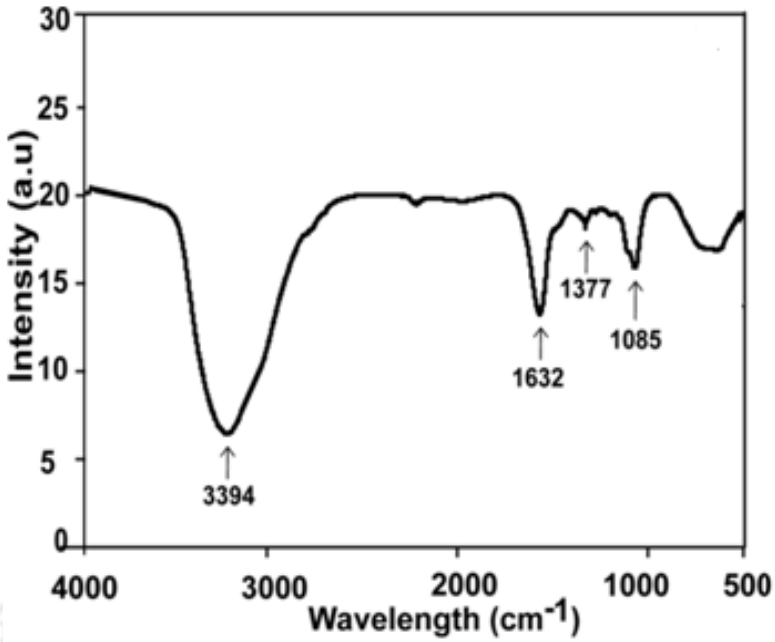

Figure 3.4 FT-IR spectra of AuNPs synthesized using BLE (4%) and $HAuCl_4$ (1mM) for 15 min of UV light irradiation.

3.3.2.4 TGA analysis

TGA spectrum of AuNPs occurs over a wide temperature range (225–580 ^{o}C) which revealed the significant weight loss (5%) of AuNPs (**Figure 3.5**). This clearly indicated that bioactive molecules were capped on the AuNPs and were completely degraded due to high temperature. Hence, it was deduced that AuNPs were capped with bioactive molecules originated from BLE.

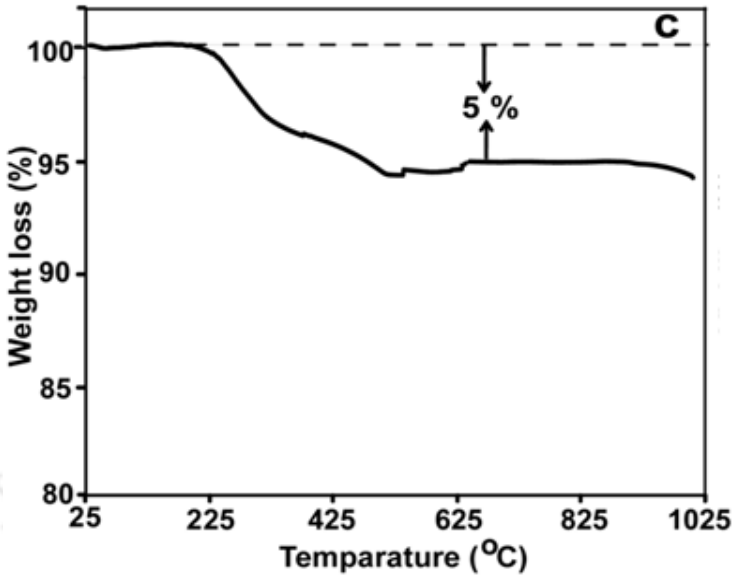

Figure 3.5 *TGA spectra of the AuNPs synthesized using BLE (4%) and $HAuCl_4$ (1mM) for 15 min of UV light irradiation.*

3.3.3 Cyto-compatibility assay

To examine the cytotoxicity of AuNPs, monocultures of the HeLa and MCF-7 cell lines were incubated with increasing concentrations of filter (0.2 micron) sterilized GNPs for 24 h and the cell viability was estimated by MTT dye conversion assay. After 24 h of post treatment, the three cell lines (HeLa and MCF-7) showed excellent viability up to as high as 100 µ mol/L of AuNPs (**Figure 3.6**). The cellular morphologies of three cell lines were unaltered after treatment with AuNPs suggesting that treatment with GNPs did not induce any cytotoxic effect causing significant damage or death of the treated cells.

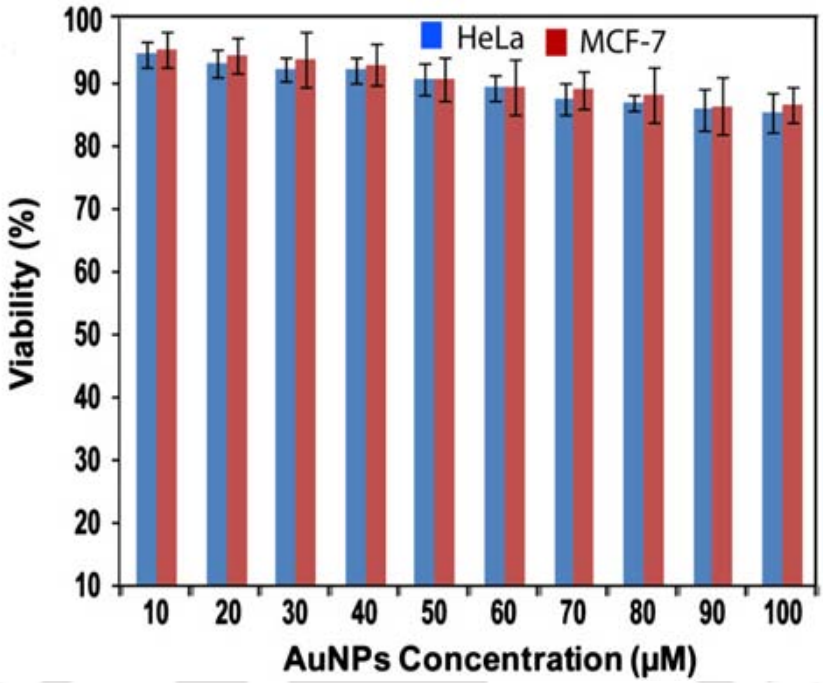

Figure 3.6 Cyto toxicity assay: Cell viabilities of HeLa and MCF-7cells exposed to different concentrations of AuNPs (10–100 mM) over a 24 h treatment.

3.4 Discussion

We observed the solution containing gold ions (Au^{3+}) and BLE turned into ruby red after 15 min of UV irradiation (~254 nm). We found that 4% BLE (400 µg) was sufficient to reduce 1 mM $HAuCl_4$ as there was insignificant peak intensity with 5% BLE. The SPR peaks corresponding to 1-3% of BLE exhibited poor intensity and red shift which indicates, respectively, negligible and large sized nanoparticles formation. Thus, we considered the 4% BLE as an optimum to reduce 1 mM $HAuCl_4$ gold solution **(Figure. 3.1)**. Furthermore, we investigated the optimum time as 15 min for the synthesis of AuNPs **(Table 1)**.

UV irradiation in aqueous reaction mixtures containing BLE generates hydroxyl radicals from aqueous solution (Wang et al., 1999) and free electrons from bioactive molecules. The bioactive molecules present in BLE include alkaloids (brahmine, nicotine

and herpestine), saponins (d-mannitol and hersaponin, acid A, and monnierin), bacopasaponins (bacosides A1, A2, A3, A4, N1,N2), flavonoids (luteolin and apigenin), betulic acid, stigma sterol and beta-sitosterol (Gohil et al., 2010; Anbarsi et al., 2006). These bioactive molecules are known to act as potential reduction agents and we speculated that they are involved in the reduction of the $HAuCl_4$ to AuNPs by donating the free electrons or •-electrons. The mechanism involves two-step process, i.e. nucleation and particle development. Firstly, gold ions (Au^{3+}) were reduced to 'seed' particles (Au^{o}) which undergoes agglomerations and form the gold cluster. Secondly, these clusters act as nucleation centers and catalyze the reduction of the remaining metal ions. The result is autocatalytic growth of the gold cluster and attains particular size and addressed as particle development. The possible mechanism of these molecules in the reduction of gold salt (Au^{3+}) to gold nanoparticles (Au^{o}) was shown in **Scheme 1**.

We have compared UV irradiation with the conventional heating and found importantly that later method required 80 min to reduce the 1 mM $HAuCl_4$ gold salt with 4% of BLE (400 µg) which is significant time difference with respective to UV irradiation. The detailed comparison was shown in **Table 2**.

TEM images showed that the AuNPs were predominantly adopted a spherical shape with narrow range of 3-45nm **(Figure 3.2a, 3.2b)**. High resolution TEM image revealed clear fcc (0.23 nm) indicating that the growth of the AuNPs occurred preferentially on the (1 1 1) plane **(Figure 3.2c)**. Bright circular rings and diffraction peaks (1 1 1), (2 0 0), (2 2 0) of SAED confirmed crystalline nature of AuNPs **(Figure 3.2d)**. Furthermore, XRD pattern of the AuNPs showed three prominent Bragg reflections that were indexed on the basis of fcc structure of gold. The intensities of the (1 1 1), (2 0 0), (2 2 0) and (3 1 1) diffraction peaks corresponding to 38.1°, 44.5°, 64.8° and 77.5°,

respectively, confirmed that the synthesized AuNPs were of crystalline in nature **(Figure. 3.3)** (Pradeep et al., 2011; Shankar et al., 2004; Babu et al., 2011b).

The FTIR spectra of AuNPs showed sharp transmittance peaks at 3394 (–OH group arising from hydroxyl group containing compounds), 1632 (amide I bond of proteins), 1377 (methyl group of alkanes) and 1085 cm^{-1} (C–N stretching vibrations of amide bond) **(Figure 3.4)** (Babu et al., 2011b; Babu et al., 2012). These functional groups (N–H, N=H, C–CH_3 and OH) attributed to the bioactive molecules present in BLE which facilitated the reduction of the Au^{3+} ions to Au^{o} and capped on AuNPs during synthesis process. TGA spectrum of AuNPs occurs over a wide temperature range (225-580 ^{o}C) which revealed the significant weight loss (5%) of AuNPs **(Figure. 3.5)**. This clearly indicated that bio active molecules were capped on the AuNPs and were completely degraded due to high temperature. Hence, it was deduced that AuNPs were capped with bioactive molecules originated from BLE. These capped AuNPs were tested on the human cancer cell lines (HeLa, MCF-7) and found to be biocompatible, thus provides opportunities for the delivery, molecular imaging and therapy **(Figure 3.6).**

3.5 Conclusions

We investigated the reduction and stabilizing capabilities of BLE for AuNPs synthesis. We found that 4% of BLE was sufficient to reduce 1 mM $HAuCl_4$ as there was insignificant peak intensity with 5% BLE. The SPR peaks corresponding to 1-3% of BLE exhibited poor intensity and red shift which indicates, respectively, negligible and large sized nanoparticles formation. Thus, we considered the 4% BLE (400 µg) optimum for the AuNPs synthesis. Furthermore, we have investigated the optimized time for the synthesis of AuNPs and found to be 15 min of microwave irradiation. We have compared UV irradiation with the conventional heating and found importantly that later method

required 80 min to reduce the 1mM $HAuCl_4$ gold salt with 4% of BLE (400 mg) which is significant time difference with respective to UV irradiation. SAED and XRD analysis revealed the crystalline nature of AuNPs. FTIR and TGA analyses confirmed the capping of bioactive molecules on AuNPs. TGA spectrum of AuNPs occurs over a wide temperature range (225–580 ^{o}C) which revealed the significant weight loss (5%) of AuNPs. This clearly indicated that bioactive molecules were capped on the AuNPs and were completely degraded due to high temperature. Hence, it was deduced that AuNPs were capped with bioactive molecules originated from BLE. This method has advantages such as eco-friendly, cost effectiveness; large scale commercial production and most importantly, resulting in biocompatible AuNPs which can be used for biomedical applications.

---***---

4.1 Introduction

Gold nanoparticles (AuNPs) have been of immense interest for their unique chemical and physical properties and potential technological applications in various fields ranging from catalysis to disease diagnosis (Azzazy et al., 2006; Bhattacharya et al., 2008; Han et al., 2007a; Han et al., 2007b; Jain et al., 2005). Conventional methods of AuNPs synthesis mostly rely on the use of synthetic chemicals and prolonged heating (Esumi et al., 2001; Feitz et al., 2004; Lin et al., 2001; Beveridge et al., 1980;). Owing to the increased awareness for potential toxicity of AuNPs associated with biological applications, alternative methodologies for biocompatible AuNPs synthesis are gaining importance. Replacement of toxic chemicals as a reducing and stabilizing agent is the prime concern of this new approach. Reports about the successful synthesis and subsequent stability of AuNPs by using different biomaterials sourced from plant and microbes are now increasing day by day (Mohanpuria et al., 2008; Raveendran et al., 2003; Huang et al., 2004; Mukherjee et al., 2001a; Mukherjee et al., 2001b; Xiao et al., 2004). Currently, nano fabrication is laying emphasis on the principle of 'green' nanotechnology which advocates the application of environmentally sound and non-polluting methods for synthesis of nanoparticles and their derivatives. In our continuous effort of screening new plant material we have screened the plants, fruits extract and plant latex for the synthesis of the AuNPs, includes *Fagopyrum esculentum*, *Piper betle,* (plant extracts), *Cocos nucifera*, *Solanum indicum* and *Sapindus mukorossi* (fruit extracts) and *Calotropis procera* (latex).

F. esculentum (Family: Polygonaceae), commonly known as douron bon in the north-eastern part of India, is widely spread in the Himalayan region. It has been reported to be extensively used for strengthening of capillary walls for reducing hemorrhaging in people with high blood pressure and increasing microcirculation in people with chronic

venous insufficiency (Ihme et al., 1996; Nestler et al., 1999; Iuorno et al., 2002; Tomotake et al., 2001). We observed that it is used as traditional medicine for respiratory diseases by the people of Assam and Meghalaya, India. It contains antioxidants molecules (rutins and tannins), proteins, amino acids, fagopyrins and inositol derivatives which have potential capability to acts as reducing agents (Bonafaccia et al., 2003; Kreft et al., 1999; Horbowicz et al., 1998; Kreft et al., 2002). We planned the present work by hypothesizing that these molecules can facilitate the reduction of various metal salts to their corresponding nanoparticles. For the first time, we describe the novel use of F. esculentum for the synthesis of AuNPs.

P. betle Linn (family: Piperaceae) leaves are widely used as a post-meal mouth freshener, and the crop is extensively grown in India, Sri Lanka, Malaysia, Thailand, Taiwan, and other Southeast Asian countries. The leaves of this plant are economically and medicinally important and have been traditionally used in India, China. In Thailand leaves are used to prevent oral malodor since it has an antibacterial activity against obligate oral anaerobes responsible for halitosis (Niranjan et al., 2002). Aqueous extracts of *P. betle* have also been shown to reduce the adherence of early dental plaque bacteria (Razak et al., 2006). The leaves of *P. betle* have a strong pungent and aromatic flavor and are used as a mouth freshener, in wound healing (Santhanam et al., 1990), as a digestive and pancreatic lipase stimulant (Prabhu et al., 1995), antioxidant (Dasgupta et al., 2004; Choudhury et al., 2002), antifungal, antibacterial (Tappayuthpijarn et al., 1982; Boonyaratanakornkit et al., 1990; Pongpech et al., 1993), anti-inflammatory, bioprotective (Bhattacharya et al., 2005), and antidiabetic (Arambewela et al., 2005) agent. In Chinese folk medicine, it is used for curing wind-cold cough, bronchial asthma, rheumatism, stomachalgia, and pregnancy edema (Nanjing zhonhyiyao Univerersity; 2006). *P. betel* leaves contain a significant amount of antioxidants such as

hydroxychavicol, eugenol, ascorbic acid, and •-carotene (Capdeviella-Pardies et al., 1985). We have successfully synthesized AuNPs by hypothesizing that the presence of strong antioxidants and flavonoids would assist in the reduction of gold ions to AuNPs.

C. nucifera (family: Arecaceae) is the only accepted species in the genus *Cocos*. The term coconut can refer to the entire coconut palm, the seed, or the fruit, which, botanically, is a drupe, not a nut. possesses antioxidant property and shows a wide spectrum of medicinal use (Cooke et al., 1992; Da fonseca et al., 2009; Singh et al., 2002; Adams et al., 1992; Anurag et al., 2003; Jenssen et al., 2006). *C. nucifera* is a large palm, growing up to 30 meters (98 ft) tall, with pinnate leaves 4–6 meters (13–20 ft) long, and pinnae 60–90 cm long; old leaves break away cleanly, leaving the trunk smooth. Coconuts are generally classified into two general types: tall and dwarf. On very fertile land, a tall coconut palm tree can yield up to 75 fruits per year, but more often yields less than 30 mainly due to poor cultural practices. In recent years, improvements in cultivation practices and breeding have produced coconut trees that can yield more. The biochemical profiling showed that it has a high sugar (fructose, glucose, and sucrose), vitamin C, sorbitol, and mannitol contents, which are good reducing Agents (Young et al., 2009). We investigated the reducing and stabilizing potentials of coconut water (CW) collected from the ripened fruits for the AuNPs synthesis.

S. indicum is an indigenous plant grown widely in Taiwan and has many biomedical applications such as anti-inflammatory, wound-healing agents, analgesic, rhinitis treatment, cough, and breast cancer. In Thailand, fruits of *S. indicum* are used as vegetables and as essential ingredients in anticarcinogens (Syu et al., 2001 ; Kao et al., 1988). In a continuous effort to search for desirable plant material for the eco-friendly synthesis of the AuNPs, we found *Solanum indium* fruits which have both reducing and stabilizing capabilities.

S. mukorossi is famous as the soap-nuts, mostly extend in the Shivalik Hill regions of Himalayas in India. It is a deciduous tree, growing to 25 m tall and flowers are borne in panicle. Fruit are fleshy, round nuts (2-2.5 cm diameter) and yellowish brown in color. The fleshy portion contains different types of saponins, containing sesquiterpene oligoglycoside (Kasai et al., 1986), hederagenin saponins (Huang et al., 2003), dammarane-type triterpenoids (Kuo et al., 2005) and triterpenoids saponins. Saponins from this plant possess various pharmacological activities such as anti bacterial, anti fungal, anti viral, antidermatophytic, antiinflammatory, antitussive, cytotoxic, molluscicidal and haemolytic (Gupta et al., 2005; Talwar et al., 2008; Ibrahim et al., 2006; Ibrahim et al., 2008; Dobhal et al., 2007; Huang et al., 2007; Quetin-Leclercq et al., 1992; Takagi et al., 1980). We investigated the reducing, capping and dispersing capabilities *S. mukorossi* for the synthesis of AuNPs. We hypothesized that the saponins present in *S. mukorossi* can be potential reducing agents for AuNPs synthesis, which at the same time serves as the capping and stabilizing agents. The synthesized AuNPs are tested on cancer lines for their biocompatibility and found to be non toxic, providing an opportunity for biomedical applications.

C. procera (Family: Apocynaceae) known by the common names apple of Sodom, Sodom apple, mudar, or osheror stabragh, is a species of flowering plant, that is native to North Africa, Tropical Africa, Western Asia, South Asia, and Indochina. It is commonly known as apple of Sodom, a name derived from the Hebrew *Tapuah Sdom*. The green globes are hollow but the flesh contains a toxic milky sap that is extremely bitter and turns into a gluey coating resistant to soap. *C. procera*, a multifarious plant having many remedial properties, can act as both reducing and capping agent in the AuNPs synthesis through conventional heating which motivated us to further explore the synthesis of AuNPs through MW irradiation (Das et al., 2011).

We have synthesized AuNPs using microwave irradiation (900W, 2.45 GHz, LG MO- MC-767W/WS). Microwave (MW) dielectric heating is a fast emerging and widely accepted new processing technology for a variety of inorganic synthesis and biomedical applications (Wada et al., 1999; Wada et al., 2001; Yin et al., 2004; Patel et al., 2005; Nahar et al., 2004; Sahu et al., 2009). The water molecule is the target for microwave ovens, like any other molecule with a dipole, it absorbs microwave radiation. Microwave radiation is converted into heat with high efficiency, so that "superheating" (external link) becomes possible at ambient pressure. Enormous accelerations in reaction time can be achieved, if superheating is performed in closed vessels under high pressure; a reaction that takes several hours under conventional conditions can be completed over the course of minutes. Compared to the conventional heating, MW irradiation shortens reaction times and improve yield without causing any appreciable alteration in the composition of products of a chemical reaction. In contrast to general heating treatment, MW synthesis favors homogeneous heating through the entire bulk of the reaction mixture in a container, leading to a more homogeneous and easy nucleation of noble metal nanoparticles (Thiebaut et al., 1993; Correa et al., 1998; Yin et al., 2004; Patel et al., 2005).

4.2 Materials and methods

4.2.1 Materials

F. esculentum was collected from vicinity of Indian Institute of Technology Guwahati, Guwahati, India. *P. betel*, C. nucifrea and *S. mukorossi* were collected from a local market in Guwahati, India. *S. indium* was grown as per traditional agronomic practice in the experimental field and healthy leaves of all plant were harvested for AuNPs synthesis. The reagents were of analytical grade obtained either from Merck (Mumbai, India) or

Sisco Research Laboratories (Mumbai, India). 3,4,5-Dimethylthiazol-2-yl-2-5-diphenyltetrazolium bromide (MTT) was purchased from Hi Media (Bangalore, India). Cell lines were obtained from the National Centre for Cell Sciences (Pune, India). Chloro auric acid and cell culture-related plasticware were obtained from Sigma-Aldrich (Bangalore, India).

4.2.2 Preparation of plant leaf extracts

F. esculentum leaves were washed with deionised water several times to remove adsorbed dirt, chopped into small pieces and dried at room temperature (25 °C) under shade. The dried leaves were powered in a mixer grinder (Bajaj Model GX 11, India). 10 g of powder was dissolved in 50 mL of ethanol and then kept at 4 °C for one week to get the leaf extract. The *F. esculentum* leaf extract (FLE) was filtered and dried by evaporating ethanol with a rotary evaporator (Rotera Equitron, Medica Instrument Mfg. Co., Mumbai, India). 100 mg of FLE was dissolved in 1 mL ethanol and used as stock solution for various experiments.

P. betel leaves were washed with deionized water to remove adsorbed dirt. The leaves were chopped into small pieces (2×2 cm) and dried at room temperature (25 °C) under shade. The dried leaves were powered in a mixer grinder (Bajaj Model GX 11, Mumbai, India). Five grams of powder was dissolved in 50 ml of ethanol and kept at 4 °C for 1 week to get the leaf extract. The *P. betle* leaf extract (PLE) was filtered using a Whatman (50 mm; Sigma, Bangalore, India) filter paper, and the filtrate was stored at 4 °C for various experiments.

4.2.3 Preparation of fruit extracts

Coconut water (CW) was collected from locally purchased mature coconut fruit and filtered before using it for AuNPs synthesis.

S. indium fruits were washed with deionised water to remove adsorbed dirt. About 50 g of fruits were chopped, taken in to 25 ml of distilled water and grinded (Bajaj Model GX 11, India) for 15 minutes (min). The grinding *S. indium* fruits extract (SFE) was filtered with whatman filter paper (50 mm) and the filtrate was stored at 4 ^{o}C for various experiments.

S. mukorossi fruits were picked when they were in yellowish orange in color and shade dried until they turned reddish brown color. The fruit were then de-seeded and crushed and powdered. 5g of powder was dissolved in 50 ml of distilled water and kept at 4 ^{o}C for one week to get the extract. *S. mukorossi* fruit extract (SmFE) was filtered using whatman (50mm) filter paper and the filtrate stored at 4 ^{o}C for various experiments.

4.2.4 Preparation of plant latex

Crude latex of *C. procera* was collected in distilled water (1:1 ratio) and centrifuged at 5000 $\times$g at 4 ^{o}C for 10 min to separate the water insoluble rubber. The supernatant constituting the aqueous fraction (AF) was collected and used for AuNPs synthesis.

4.2.5 Synthesis of AuNPs using plant extracts

4.2.5.1 Synthesis of AuNPs using *F. esculentum* Leaf extract (FLE)

AuNPs synthesis was carried out by varying FLE concentration (from 0.1% to 0.5%) against 1 mmol/L $HAuCl_4$ in a total volume of 2 mL made up with double distilled water. The resulting mixtures were placed in a domestic microwave oven (900W, 2.45

GHz, LG MO- MC-767W/WS) and irradiated for 15 s. The optimum time for synthesis was determined by incubating 0.4% of FLE by varying irradiation time from 10 to 20 s with an interval of 2 s.

4.2.5.2 Synthesis of AuNPs using *P. betle* Leaf extract (PLE)

The synthesis of AuNPs was carried out by varying the PLE concentration (0.5% to 4%) against 0.5 mM $HAuCl_4$ in a total volume of 2 ml made up with double distilled water. The resulting mixtures were placed in a domestic microwave oven (900 W, 2.45 GHz, LG MO- MC-767 W/WS, LG Corp., Noida, India) and irradiated for 15 s. To obtain the optimum concentration of $HAuCl_4$, the experiments were carried out by varying the gold solution concentration against 2% of PLE. The optimum time for synthesis was determined by incubating 2% of PLE with 0.5 mM by varying the MW irradiation time from 12 to 30 s with an interval of 2 s.

4.2.6 Synthesis of AuNPs using fruit extracts

4.2.6.1 Synthesis of AuNPs using coconut water (CW)

Coconut water (CW) was mixed with different concentrations (0.1–0.275 mM) of $HAuCl_4$ and the final volume was made up to 2 mL with distilled water. The reaction mixture was placed in a domestic microwave oven (900 W, 2.45 GHz, LG MO-MC-767W/WS [LG Electronics Pvt. Ltd., India]) and irradiated for 15 s. With the optimum concentration of $HAuCl_4$, experiments were repeated for 5 to 21 s. About 10 mL of the colloidal solution was centrifuged at 20,000 rpm for 10 min to obtain the AuNPs as a pellet.

4.2.6.2 Synthesis of AuNPs using *S. indicum* fruit extract (SFE)

The syntheses of AuNPs were carried out by varying the SFE (0.005-0.05%) against to 0.5 mM $HAuCl_4$ and the final volume was made up to 2 ml with double distilled water. To all the resulting mixture, we applied microwave irradiation for 15 sec. To find out the optimum concentration of $HAuCl_4$, the experiments were carried out by varying the gold solution (0.1-1 mM) concentration against 0.03% of the SFE. 30 ml of 0.1% SFE mixed with 10 ml of the 5 mM $HAuCl_4$ solution and the final volume was made up to 100 ml with the distilled water to get the concentrations as 0.03% SFE and 0.5 mM $HAuCl_4$. A fixed amount of the working solution (2 ml) was taken and exposed to the microwave irradiation for respective time intervals (5-25) incubating 0.03% of SFE with 0.5 mM $HAuCl_4$ by varying microwave irradiation time from 5-25 sec with an interval of 3 sec.

4.2.6.3 Synthesis of AuNPs using *SmFE* (SmFE)

The synthesis of AuNPs was carried out by varying SmFE concentration (1-10%) against 1 mM $HAuCl_4$ in a total volume of 10 ml made up with double distilled water. To find out optimum concentrations of $HAuCl_4$, we carried out the reactions varying the $HAuCl_4$ solution (0.2-1 mM) against 0.8% SmFE. We used 0.6% SmFE and 0.6 mM $HAuCl_4$ to narrow down the particle size distribution of synthesized AuNPs. The resulting mixtures were placed in a domestic microwave oven (900W, 2.45 GHz, LG MO- MC-767W/WS) and irradiated for 25 seconds (sec).

4.2.7 Synthesis of AuNPs using *C. procera* latex aqueous faction (AF)

AuNPs synthesis was carried out in a domestic microwave oven (900W, 2.45 GHz, LG MO- MC-767W/WS). To optimize AF concentration, different volumes (for final concentration of 1–5%, v/v) of AF were reacted with 1 mM of $HAuCl_4$ aqueous solution and irradiated with MW for 40 seconds. To see the effect of MW irradiation time on the

AuNPs synthesis process, reaction mixture was irradiated for different time duration (10-60 s) at the maximum power output (900W) of the microwave oven.

4.2.8 Characterization of AuNPs

4.2.8.1 UV-visible spectroscopy

All UV-vis spectroscopic measurements of synthesized AuNPs were carried out on a Cary 100 BIO UV-vis spectrophotometer (Varian, CA, USA).

4.2.8.2 Transmission Electron Microscope (TEM) studies

A volume of 10 mL of the AuNP solution was centrifuged at 20,000 rpm for 20 min. The resulted pellet was resuspended in 3 mL of distilled water and centrifuged at 20,000 rpm for 20 min. This process was repeated thrice and the resultant pellet was resuspended in 1 mL of distilled water. Few drops of the redispersed colloidal solution were placed over carbon coated copper grid and the water was evaporated in hot air oven (Daihan Labtech Co. Ltd. model LDO-150F) at 60 °C for 4 h. TEM measurements were performed on a transmission electron microscope (TEM-JEOL model 2100) operated at 190 Vof 200 kV.

4.2.8.3 X-ray Diffractrogram (XRD) analysis of AuNPs

The colloidal solution mixtures obtained in Section 2.6 were centrifuged at 20,000 rpm and resulted pellets were resuspended in appropriate volume (3 mL) of double distilled water. This process was repeated for three times to obtain the pure nanoparticles of the respective type. Finally, each resulted pellets was redispersed in 5 mL of double distilled water and freeze dried in a lyophiliser (Christ Gefriertrocknungsanlagen GmbH Model 1-4) for 16 h. The fine dried powder samples were analyzed with the help of an XRD instrument (Bruker Advance D8 XRD machine) with Cu source at the wavelength of 1.5406 A^{o} in thin film mode.

4.2.8.4 FTIR analysis of AuNPs

About 50 mL of AuNPs suspension was lyophilized for 24 h. The lyophilized samples were pressed into pellet with 200mgof potassium bromide and the infrared spectrum was recorded in an FTIR spectroscope (Spectrum One, Perkin Elmer, Massachusetts, USA), from 4000 to 450 cm^{-1} with a resolution of 2 cm^{-1} and five scans per sample.

4.2.8.5 EDX analysis

The elemental composition of the intact AuNPs were obtained by using EDX spectroscopy (LEO 1430 VP) at variable pressure scanning electron microscope equipped with INCA Oxford EDX facility, at an acceleration voltage of 10 keV.

4.2.9 Biochemical test for flavonoids and phenolic compounds

0.5 mL of ethanolic extract (10 mg/mL) of both FLE and SLE were mixed with Folin-Ciocalteu reagent (2 mL, 1:1 diluted with distilled water) and aqueous sodium carbonate (2 mL, 1 mol/L). The mixture was allowed to stand for 15 min and the absorbance recorded in a spectrophotometer at 765 nm (SHEMADZU, Japan). The standard curve was prepared using 0, 50, 100, 150, 200, 250 g/L solutions of gallic acid in methanol:water (50:50, v/v). Total phenol was expressed in terms of gallic acid equivalent (mg/g of dry mass).

FLE and SLE (0.5 mL of 10 mg/mL) in ethanol was separately mixed with 1.5 mL of methanol, 0.1 mL of 10% aluminium chloride, 0.1 mL of 1 mol/L potassium acetate, and 2.8 mL of distilled water. The mixture was left at room temperature for 30 min after

which the absorbance of the reaction mixture was measured at 415 nm. The calibration curve was plotted by using quercetin (10 to 100 mg/mL in methanol) as a standard.

4.2.10 Effect of pH and salt concentration on stability of AuNPs

AuNPs was synthesized with optimized parameters (0.4% FLE and 16 s) and the pH of the solution was measured. To find out limits of the pH value, 2 mL of AuNPs solution was taken into a series of test tubes and the pH value of the solution was adjusted between 2 and 10. The final volume was made up to 3 mL with distilled water. The solution was then allowed to stand for 6 h and observed for the change in colour visually and finally the absorbance recorded.

To find out the effect of salt concentration on AuNPs stability, we carried out a set of experiments by varying the concentration of NaOH from 0.01 to 0.5 mol/L. In a test tube containing 2 mL of AuNPs solution, a calculated amount of salt was added and the final volume made up to 3 mL with distilled water to get the desired molarity. The change in colour was observed visually.

4.2.11 Cytotoxicity assay

HeLa (Human cervical cancer), MCF-7 (Human breast cancer) and IMR-32 (Human neuroblastoma cell line) cells were maintained in the Minimal Essential Medium (MEM) containing 1.0 mmol/L sodium pyruvate, 0.1 mmol/L nonessential amino acids, 1.5 g/L sodium bicarbonate, 2 mmol/L L-glutamine supplemented with 10% FBS (heat inactivated) and 1% antibiotic-antimycotic solution (1000 U/mL penicillin G, 10 mg/mL streptomycin sulphate, 5 mg/mL gentamycin, and 25 µg/mL amphotericin B). The cells were cultured at 37 °C in a humidified incubator (Heal Force, HF 160W, China) supplemented with 5% CO_2. To examine the cytotoxicity of AuNPs, monocultures of the

HeLa, MCF-7 and IMR-32 cell lines were incubated with increasing concentrations of filter (0.2 micron) sterilized AuNPs for 24 h and the cell viability was estimated by MTT dye conversion assay. Cells not exposed to AuNPs were taken as control. For MTT assay, HeLa, MCF-7 and IMR-32 cells were seeded (1_104) in a 96-well plate (Cell Bind, Corning). After 24 h of growth, the medium was replaced with the serum free medium that contained varied concentrations of AuNPs (from 10 to 100 µmol/L). After 24 h of treatment the media was removed and cells were washed with phosphate-buffered saline (PBS, 0.01 mol/L, pH = 7.2). This was followed by the addition of 100 µL of MTT (0.5 mg/mL) prepared in serum free medium to each well and incubated for 4 h at 37 °C. After incubation, the medium was removed and 100 µL of dimethyl sulphoxide (DMSO) was added to each well to solubilize the formazan crystals. The concentration of formazan was determined by measuring its absorbance at 70 nm using a multi well plate reader (Tecon micro plate reader, model 680, CA, USA). The cell viability was calculated with the following equation:

$$\text{Cell viability}/\% = \frac{A_{\text{treated}}}{A_{\text{control}}} \times 100$$

4.2.12 Statistical analysis

Experiments with quantitative data were done in replicates of four independent experiments and the results were expressed as Mean ± Standard Deviation ($n = 5$)

4.3 Results

4.3.1 Optimization of plant and fruit extracts for AuNPs synthesis

4.3.1.1 Optimization of FLE

We have investigated the optimum plant and fruit extract concentrations for the AuNPs synthesis. The formation of AuNPs can be easily visualized by appearance of ruby red

colour due to longitudinal excitation of surface plasmon vibrations of AuNPs at (538±4) nm in the visible range of spectra. The conditions for the synthesis of AuNPs were optimized by varying percentage of FLE and incubation time against 1 mmol/L gold salts. We observed that 0.4% FLE completely reduced the 1 mmol/L $HAuCl_4$ as there was no significant change in peak intensity with 0.5% FLE (**Figure 4.1A**).

4.3.1.2 Optimization of PLE

The SPR peak of 2% PLE against 0.5 mM gold solution showed intense and narrow peak centered around 544 nm, as shown in **Figure 4.1B**, whereas the SPR peaks above the 2% PLE concentration were flattening and redshifted, indicating the formation of large-size AuNPs and those below the 2% concentration were considered as suboptimal. Thus, 2% PLE was considered as optimal for the synthesis of AuNPs.

4.3.1.3 Optimization of SFE

The reaction mixtures of SFE (0.005-0.025%) showed the gradual increment in the formation of the AuNPs whereas the reaction mixtures above 0.03% of SFE showed flattered peaks. These results revealed that 0.03% of SFE was sufficient to reduce the 0.5 mM of $HAuCl_4$. Thus, we considered that 0.03% of SFE was optimum for the AuNPs synthesis (**Figure 4.1C**).

4.3.1.4 Optimization of SmFE

The SPR peak of 8% SmFE against 1 mM $HAuCl_4$ showed intense and narrow peak centred at 542 nm (**Figure 4.1D**). The SPR peak above 8% SmFE was flattening, indicating that 8% SmFE was sufficient to reduce the 1 mM $HAuCl_4$. Thus, we consider 8% SmFE as an optimum concentration against 1 mM $HAuCl_4$ for AuNPs synthesis.

4.3.2 Optimization of *a*queous fraction (AF) of *C. procera* latex for AuNPs synthesis

The SPR peaks corresponding to 1 and 2% of AF against 1mM of $HAuCl_4$ were located at around 600 and 550 nm, respectively, suggesting the formation of larger AuNPs. For 3–5% of AF, SPR peaks were blue-shifted and located at around 527±2 nm which was characteristic of spherical AuNPs. At 3–5% AF, differences in SPR peaks and intensity were seen to be negligible and thus 3% of AF was considered as the optimum concentration for efficient reduction of 1mM $HAuCl_4$ to AuNPs (**Figure 4.1E**). We have synthesized AuNPs using the aqueous fraction of *C. procera* by conventional heating. We made a comparison of the two methods, namely, "conventional heating" and "MW irradiation" as shown in **Table 4.1**

Table 4.1. *Comparison of the results obtained in conventional heating and MW irradiation of AuNPs synthesis.*

Reaction parameters/properties	Method of AuNPs synthesis	
	Conventional Heating	Microwave irradiation
AF concentration (v/v)	4%	3%
$AuCl_4$ concentration	1mM	1mM
Time	20 minutes	40 seconds
Shape	Spherical	Spherical
Mean Diameter of AuNPs (nm)	22 ± 10	13 ± 5
Protein capping	Yes	Yes
Biocompatibility against tested cell lines	Yes	Yes

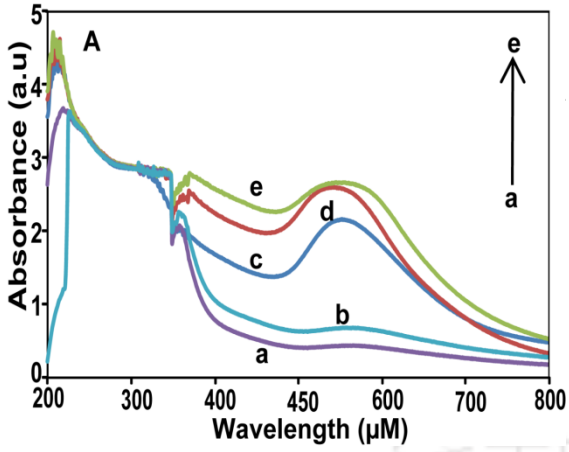

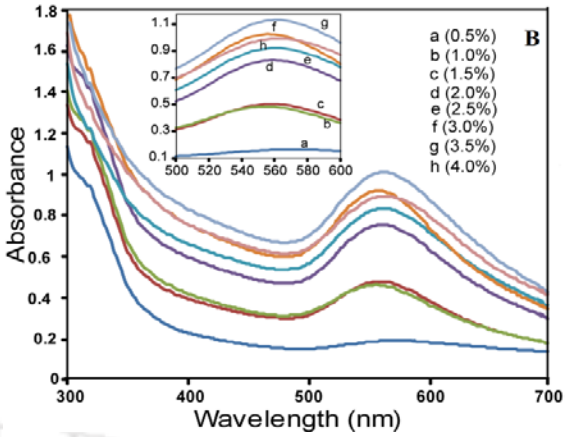

(A) FLE (B) PLE

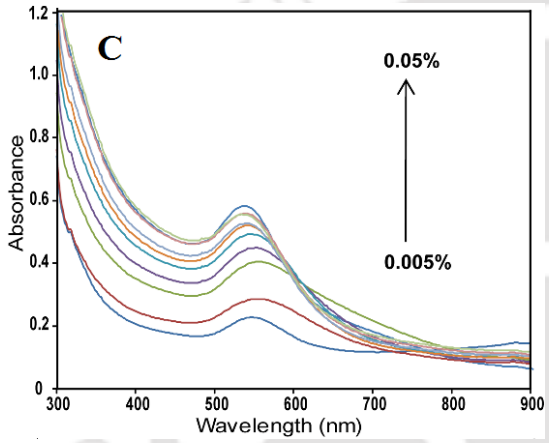

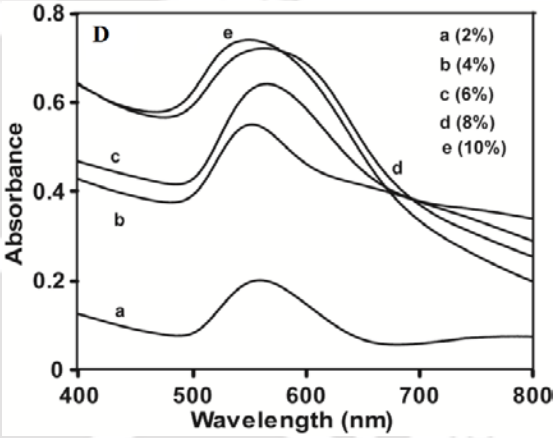

C (SFE) D (SmFE)

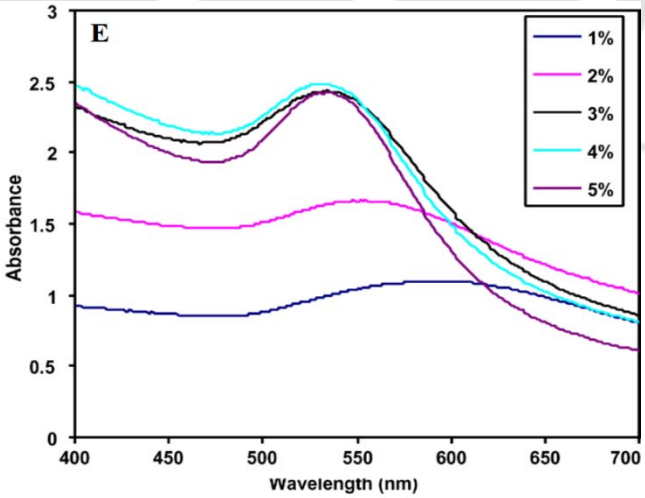

E (C. procere AF)

Figure 4.1 *UV-visible absorption spectra of AuNPs synthesized by (A) (different concentrations of FLE (a — 0.1%, b — 0.2%, c — 0.3%, d—0.4%, e—0.5%) for 15 s*

against 1 mmol/L $HAuCl_4$), (B) (different concentrations of PLE (a = 0.5%, b = 1%, c = 1.5%, d = 2%, e = 2.5%, f = 3%, g = 3.5%, and h = 4%) for 15 s against 0.5 mM $HAuCl_4$), (C) (different concentrations of SFE (0.005-0.05%) for 15 sec against 0.5 mM $HAuCl_4$. (D) (synthesized by different concentrations of SmFE (a = 2%, b = 4%, c = 6%, d = 8%, e = 10) against 1 mM $HAuCl_4$ for 25 sec of microwave irradiation time) (E) (AuNPs synthesized using 1mM $HAuCl_4$ with different concentrations (1–5%) of AF).

4.3.3 Optimization of $HAuCl_4$ for AuNPs synthesis

4.2.3.1 Optimization of $HAuCl_4$ for AuNPs synthesis using PLE

UV–Vis spectra of products obtained by reacting 2% PLE with various concentrations of $HAuCl_4$ (0.1-1 mM), which displayed an intense peak at 547 nm for 0.5 mM $HAuCl_4$. However, the SPR peaks displayed by the 0.3 mM $HAuCl_4$ were suboptimal, whereas those of 0.7 and 1 mM $HAuCl_4$ were red shifted. Since there was no significant formation of the peak with 0.1 mM, 0.5 mM $HAuCl_4$ was taken as the optimum for the synthesis of the AuNPs (**Figure 4.2A**). UV Visible spectral analysis of the different reaction products exhibited sharp SPR peaks presented in **Table 4.2** indicating the successful formation of AuNPs.

Table 4.2 *UV-visible spectral analysis of the reaction mixtures and their* $\bullet_{max}$ *peak positions.*

No of Runs	$HAuCl_4$ Concentration	PLE Extract	MW Irradiation Time	Observed $\bullet_{max}$ Peak position
1	0.5 mM	0.50%	15 Sec	538
2	0.5 mM	1.00%	15 Sec	534
3	0.5 mM	1.50%	15 Sec	530
4	0.5 mM	2.00%	15 Sec	544
5	0.5 mM	2.50%	15 Sec	550
6	0.5 mM	3.00%	15 Sec	558
7	0.5 mM	3.50%	15 Sec	548
8	0.5 mM	4.00%	15 Sec	548
9	0.1 mM	2.00%	15 Sec	544
10	0.3 mM	2.00%	15 Sec	542
11	0.5 mM	2.00%	15 Sec	547
12	0.7 mM	2.00%	15 Sec	558
13	1.0 mM	2.00%	15 Sec	564
14	0.5 mM	2.00%	12 Sec	550
15	0.5 mM	2.00%	14 Sec	552
16	0.5 mM	2.00%	16 Sec	550
17	0.5 mM	2.00%	18 Sec	556
18	0.5 mM	2.00%	20 Sec	552
19	0.5 mM	2.00%	22 Sec	554
20	0.5 mM	2.00%	24 Sec	552
21	0.5 mM	2.00%	26 Sec	548
22	0.5 mM	2.00%	28 Sec	548
23	0.5 mM	2.00%	30 Sec	548

4.2.3.2 Optimization of $HAuCl_4$ for AuNPs synthesis using coconut water (CW)

For 0.250 mM $HAuCl_4$, the SPR peak was located at around 530 nm (**Figure 4.2B**). Above this concentration, the SPR peak was red-shifted, indicating the formation of larger AuNPs. Thus, 0.250 mM was considered as optimum for the AuNPs synthesis.

4.2.3.3 Optimization of $HAuCl_4$ for AuNPs synthesis using SFE

UV-Vis spectra of products obtained by reacting 0.03 % SFE with varying concentration (0.1-1 mM) displayed an intense peak at 547 nm for 0.5 mM $HAuCl_4$. However, the SPR peaks displayed by the 0.1 and 0.3 mM $HAuCl_4$ were suboptimal, whereas 0.7 and 1 mM $HAuCl_4$ were flattered indicating the insignificant formation of the AuNPs. Thus, 0.5 mM $HAuCl_4$ was taken as the optimum for the synthesis of the AuNPs (**Figure 4.2C**).

4.2.3.4 Optimization of $HAuCl_4$ for AuNPs synthesis using SmFE

We carried out the various reactions to find out the optimum $HAuCl_4$ concentration and observed the slight red shifted peaks corresponding to 0.2, 0.8 and 1 mM $HAuCl_4$ concentrations which were an indication of formation of large size particles (Fig. 1b). The reaction mixtures containing 0.4 and 0.6 mM $HAuCl_4$ concentration exhibited sharp SPR peaks at 525± 4 nm which signifies the formation of ideal size particles. However, as more number of particles were achieved with 0.6 mM $HAuCl_4$ concentration in contrast to 0.4 mM, thus we consider 0.6 mM as optimum (**Figure 4.2D**)

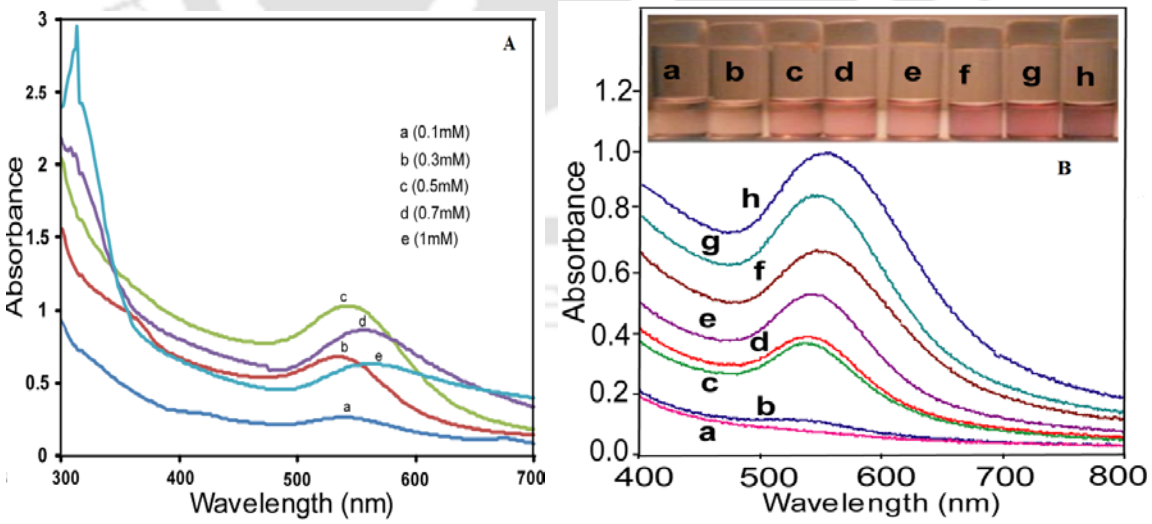

(A) PLE (B) CW

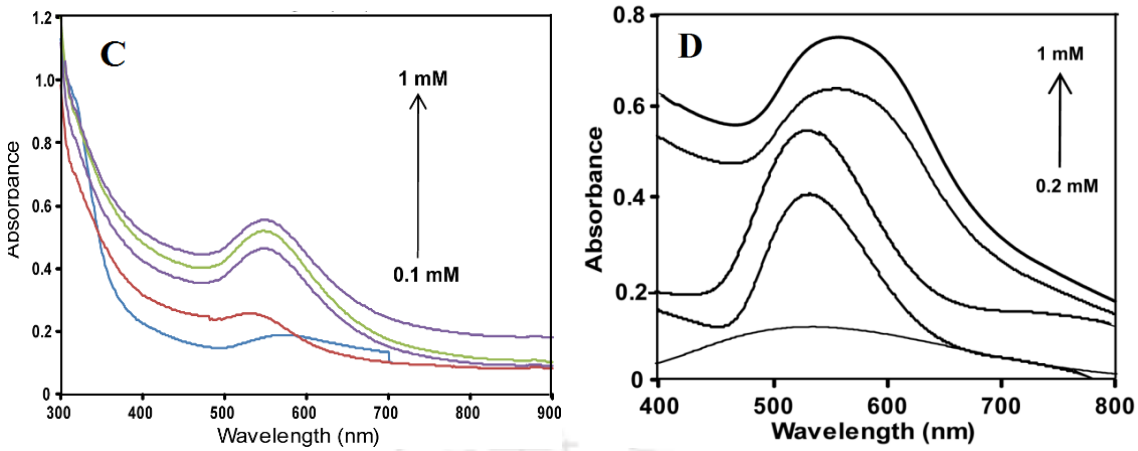

(C) SFE (D) SmFE

Figure 4.2 *UV-Visible absorption spectra of AuNPs synthesized by (A) varying concentrations of $HAuCl_4$ (a = 0.1 mM, b = 0.3 mM, c = 0.5 mM, d = 0.7 mM, and e = 1 mM) against 2% PLE. (B) different concentrations (a = 0.1 mM, b = 0.125 mM, c = 0.150 mM, d = 0.175 mM, e = 2 mM, f = 0.225, g = 0.250, h = 0.275 mM) of HAuCl4 for 15 s; (C) varying concentrations of $HAuCl_4$ (0.1- 1 mM) against to the 0.03% SFE. (D) SPR peaks of AuNPs synthesized by varying the $HAuCl_4$ concentrations (0.2-1 mM) against 8% SmFE for 25 sec.*

4.3.4 Optimization of time for AuNPs synthesis

4.3.4.1 Optimization of time for AuNPs synthesis using FLE

We found 16 s as the optimum time required for complete reduction of 1 mmol/L $HAuCl_4$ with 0.4% of FLE. This was evident from the flattening peak intensity associated with 18 and 20 s (**Figure 4.3A**).

4.3.4.2 Optimization of time for AuNPs synthesis using PLE

We performed various experiments carried out to determine the optimum time for the synthesis of AuNPs by incubating the 2% PLE and 0.5 mM gold solution at different time intervals (12 to 30 s) of microwave irradiation. We found that the peaks above 18 s were flattening, indicating no further significant formation of AuNPs. The peaks below 18 s

were considered as suboptimal as they displayed poor intensity. Thus we consider 18 s as optimum time for the synthesis of AuNPs (**Figure 4.3B**).

4.3.4.3 Optimization of time for AuNPs synthesis using coconut water

We repeated the reaction for different MW irradiation time period (Figure 1B). From 9 to 17 s, the formation of AuNPs was enhanced, as can be seen from the respective SPR intensities. Above 17 s, changes in the SPR intensities and peaks were negligible (**Figure 4.3C**).

4.3.4.4 Optimization of time for AuNPs synthesis using SFE

Various experiments were performed to determine the optimum time for the synthesis of the AuNPs by incubating the 0.03% SFE and 0.5 mM $HAuCl_4$ solution at different microwave irradiation time intervals from 5-25 seconds (sec) of microwave irradiation. We found that the peaks above 20 sec were flattering, indicating no further significant formation of AuNPs. Below 20 sec considered as the suboptimal for the synthesis of AuNPs (**Figure 4.3D**).

4.3.4.5 Optimization of time for AuNPs synthesis using *C. procera* (AF)

We carried out the different experiments to identify the optimum time for the synthesis of the AuNPs. For 10, 20 and 25 s no SPR peaks were observed. At 30 s the intensity of SPR band of AuNPs was found to be low with a peak around 536 nm, which indicated the formation of spherical particles. With increased MW irradiation from 30 to 40 s, the intensities of SPR bands increased considerably with narrow peaks shifted to 525– 530 nm. For 40–60 s irradiations, increase in the SPR band intensities was very low which indicated complete reduction of gold ions (**Figure 4.3E**).

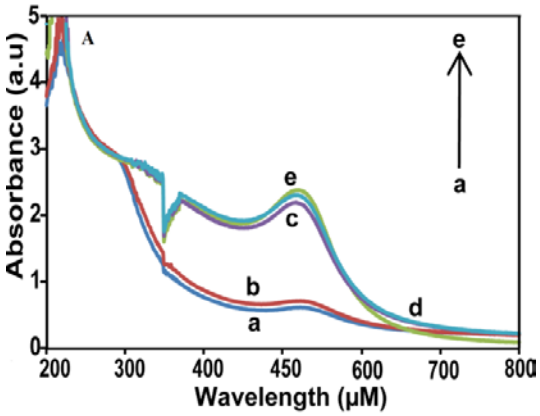

(A) FLE

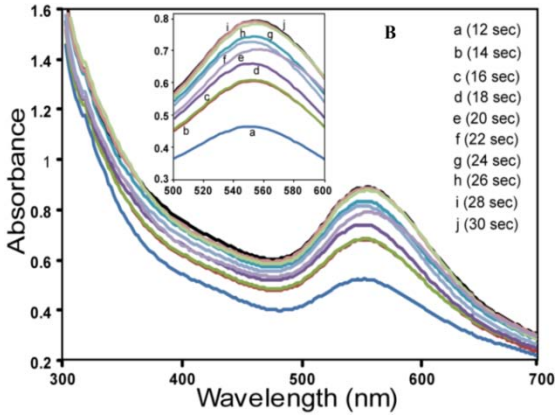

(B) PLE

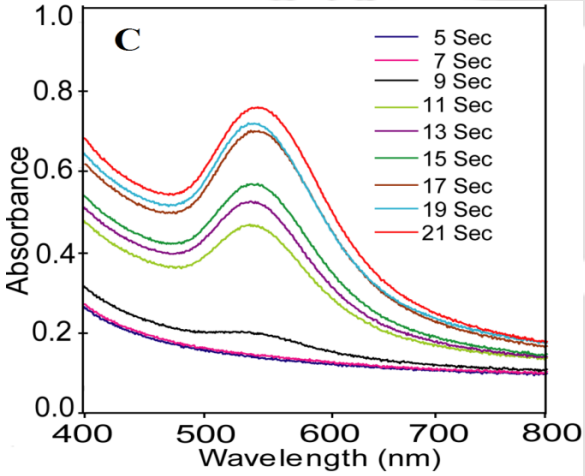

(C) CW

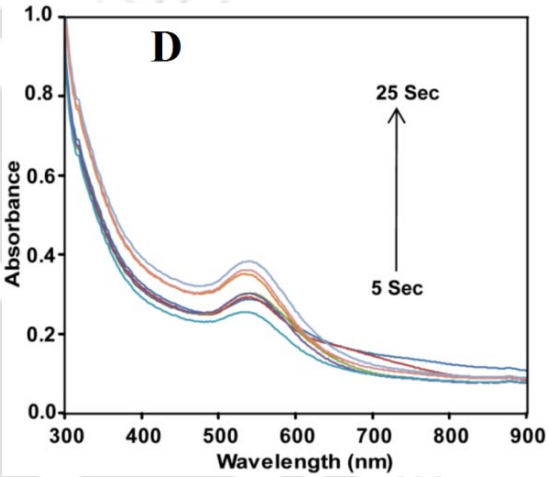

(D) SFE

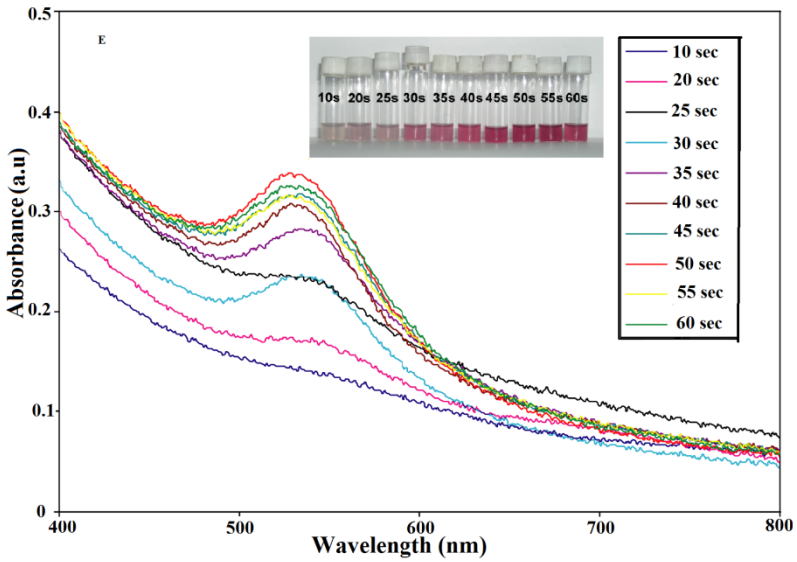

(E) *C. procera* (AF)

Figure 4.3 *UV-Visible absorption spectra of AuNPs synthesized at (A) varying MW irradiation time (a—12 s, b—14 s, c—16 s, d—18 s, e— 20 s) with 0.4% FLE and 1 mmol/L $HAuCl_4$. (B) MW irradiation time (with 2% PLE and 0.5 mM HAuCl4) a = 12 s, b = 14 s, c = 16 s, d = 18 s, e = 20 s, f = 22 s, g = 24 s, h = 26 s, i = 28 s, and j = 30 s (C) at varying MW irradiation times (5, 7, 9, 11, 13, 15, 17, 19, and 21 s) with 0.250 mM $HAuCl_4$. (D) MW irradiation time (5-25 sec) with 0.03 % SFE and 0.5 mM $HAuCl_4$. (E) at different MW irradiation time duration (10–60 sec), the inset photo shows respective colour of gold colloidal solution.*

4.3.5 Characterization of AuNPs

4.3.5.1 Transmission Electron Microscope (TEM) analysis of AuNPs

We have employed the TEM technique to visualize the size and shape of formed AuNPs. The AuNPs obtained from FLE, PLE, CW, SFE, SmFE *and C. procera* (AF) were of different shapes and sizes and the average sizes of the AuNPs were 8.3 nm (3-20), 6 nm (10-35), 10±5 (5-20), 7.4 nm (5-50), 25 nm (3-50) and 8.2 nm (5-20), respectively. The morphology of the AuNPs synthesized using above plant materials were given in the **Figure 4.4**.

Most of the synthesized AuNPs were of spherical and hexagonal in nature. We also observed the triangular, rod, oval and polygonal shapes. In particular, typical TEM images of AuNPs synthesized using SmFE with 0.8% SmFE and 1 mM $HAuCl_4$ showed that majority nanoparticles of hexagonal and spherical in shape. We observed the wide range of particles size distribution (3-50 nm) with optimized parameters (0.8% SFE and 1 mM $HAuCl_4$) (**Figure 4.4Ea**). Furthermore, we wanted to narrow down the particles size distribution by changing the parameters. This was achieved with 0.6% SmFE and 0.6 mM $HAuCl_4$ with predominant particles size as 25 nm (**Figure 4.4Eb**).

We observed the significant change in the peak position (red-shifted peaks) of the reaction mixture obtained by using 4% PLE and 0.7 mM $HAuCl_4$ for 30 s, indicating the formation of large-size AuNPs, which was confirmed using TEM technique. The TEM images shown in **Figure 4.5** revealed the formation of large-size AuNPs, which agreed with the results obtained in **Figure 4.1B**. The detailed morphology of all synthesized AuNPs was showed in the **Table 4.3.**

Table 4.3 *Morphology of AuNPs synthesized with different plant and fruits extracts.*

S. No	Plant or Fruit material /Fruit Extract	AuNPs size Range	Average Size	AuNPs Shapes	Predominant Shapes
1	*F. esculentum*	3-20	8.3	Hexagonal, Triangular, Circular and Rod shaped	Hexagonal
2	*P.betle*	10-35	6	Circular, Hexagonal, Rod shaped, Cylindrical, Diamond and Triangular	Hexagonal
3	Coconut Water *(C. nucifera)*	5-20	10.5±5	Circular, Hexagonal, and Triangular	Circular
4	*S. indicum*	5-50	7.4	Circular, triangular, Rod shaped and Hexagonal	Circular and Hexagonal
5	*SmFE*	3-50	25	Circular, Hexagonal, Rod shaped, Cylindrical, Diamond and Triangular	Circular Hexagonal
6	*C. procera* (AF)	5-20	8.2	Circular, Hexagonal, and Triangular	Circular Hexagonal

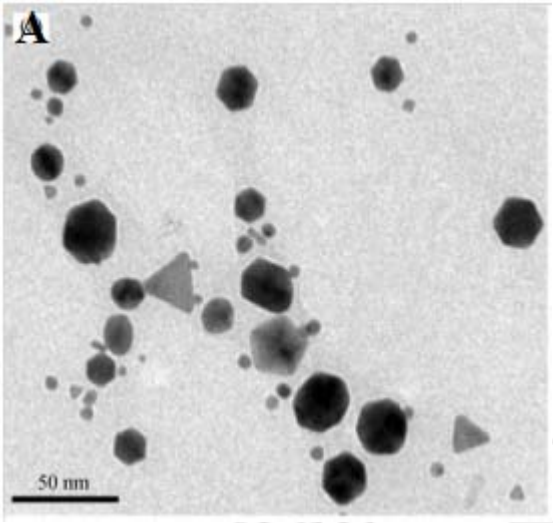

(A) FLE

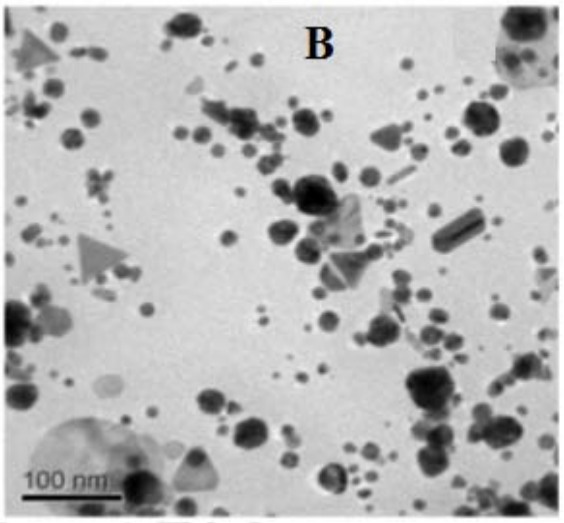

(B) PLE

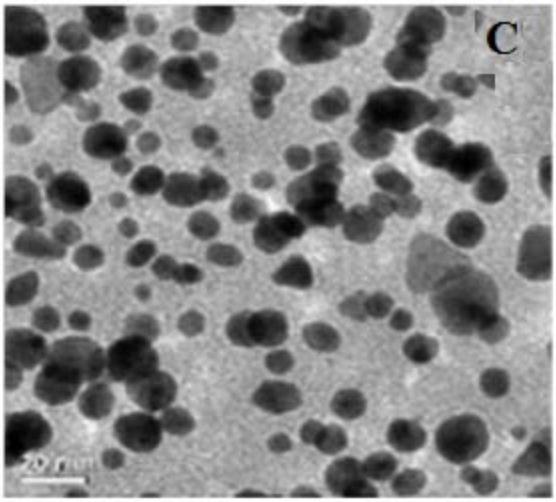

(C) Coconut water (CW)

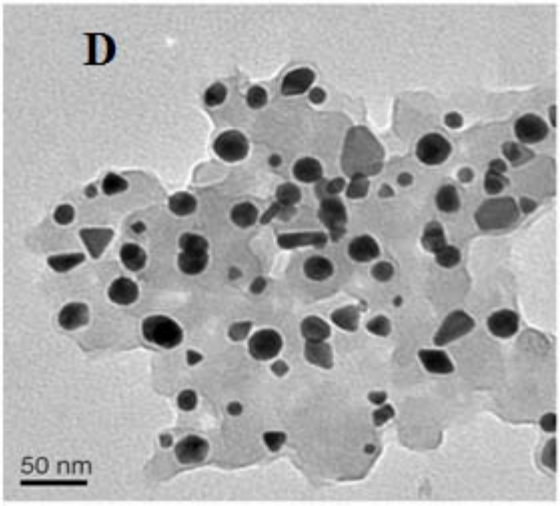

(D) SFE

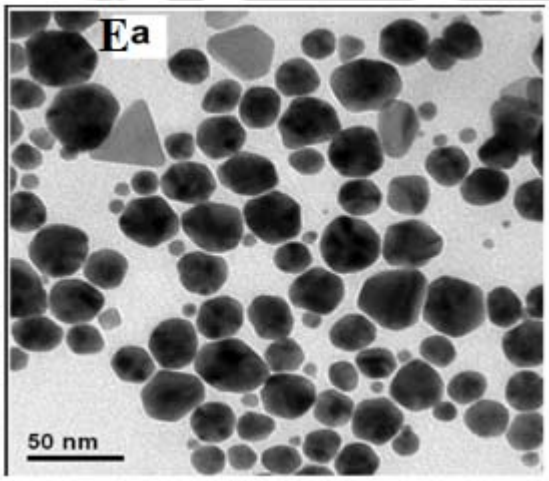

E (a) SmFE

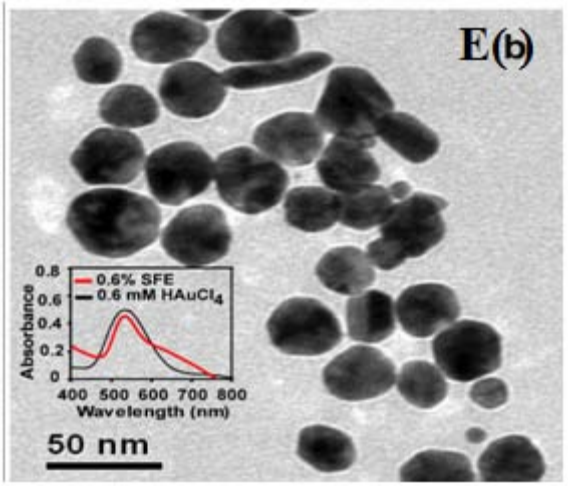

E (b) SmFE

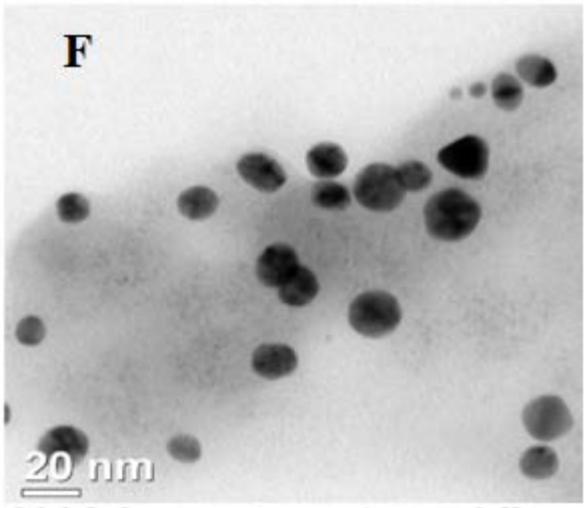

(F) *C. procera* (AF)

Figure 4.4 *TEM Images of (A) FLE, (B) PLE, (C) CW (D) SFE (E) SmFE (a, b) (F) C. Procera (AF) (synthesized from 3% procera latex with 1mM $HAuCl_4$ at 40 sec MW irradiation).*

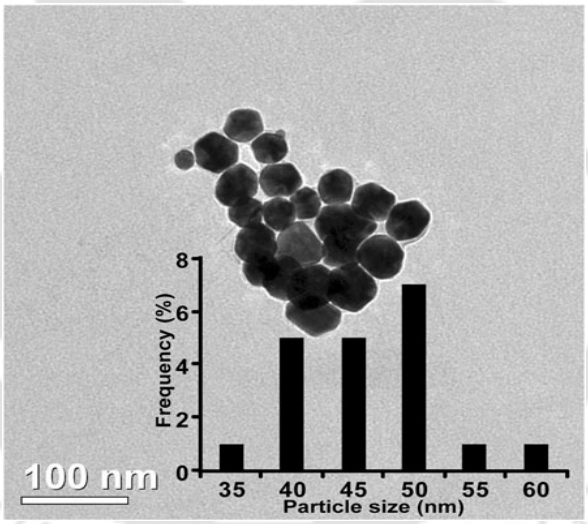

Figure 4.5 *TEM analysis of AuNPs synthesized at higher concentrations. TEM image of AuNPs synthesized with 4% PLE and 0.7 mM $HAuCl_4$ for 30 s.*

AFM analysis of AuNPs synthesized using CW with 0.250 mM with varying MW irradiation times was done in noncontact mode. At 9 s, the formation of AuNPs was negligible, whereas at 11and 17 s the process of AuNPs formation was accelerated, as can be seen from the AFM image (**Figure 4.6**).With the increase in MW irradiation time,

there was no considerable alteration in the morphology of AuNPs. AFM analysis for 9, 11, and 17 s supported the results of UV-Vis spectroscopic studies (**Figure 4.3C**).

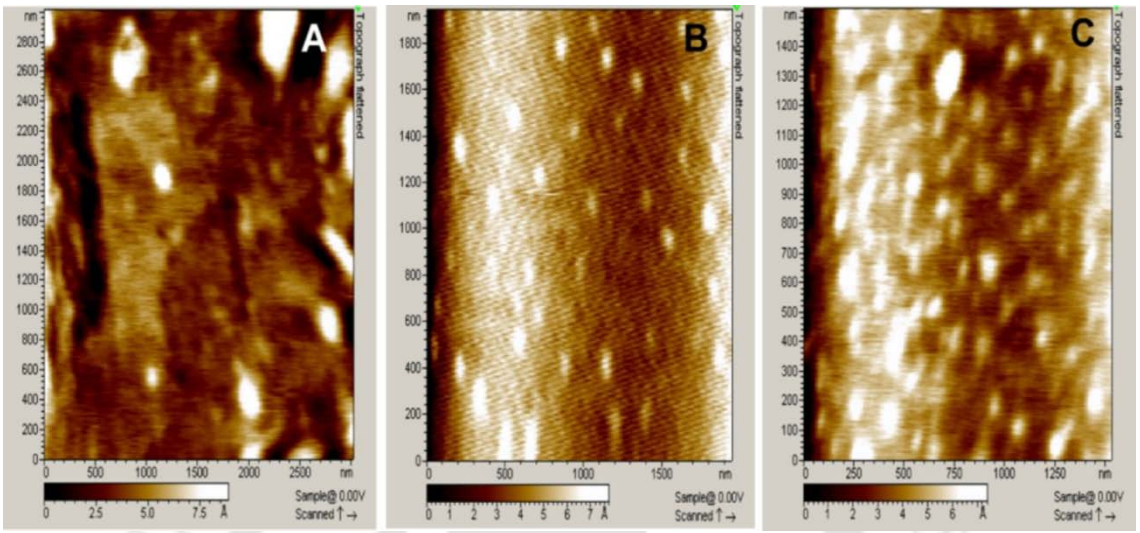

Figure 4.6 *AFM images of AuNPs synthesized by reacting 0.250 mM $HAuCl_4$ at different MW irradiation times: A = 9 s, B = 11 s, and C = 17 s.*

4.3.5.2 ***High Resolution Transmission Electron Microscope analysis***

The HRTEM images using FLE, PLE, CW, SFE, SmFE, and *C. procera (*AF) revealed clear lattice fringes of 0.22 nm revealed that the growth of the AuNPs occurred preferentially on the (1 1 1) plane (**Figure 4.7**). The inter planer distance of the Au (1 1 1) plane was in agreement with the (1 1 1) d-spacing of bulk Au (0.2355 nm).

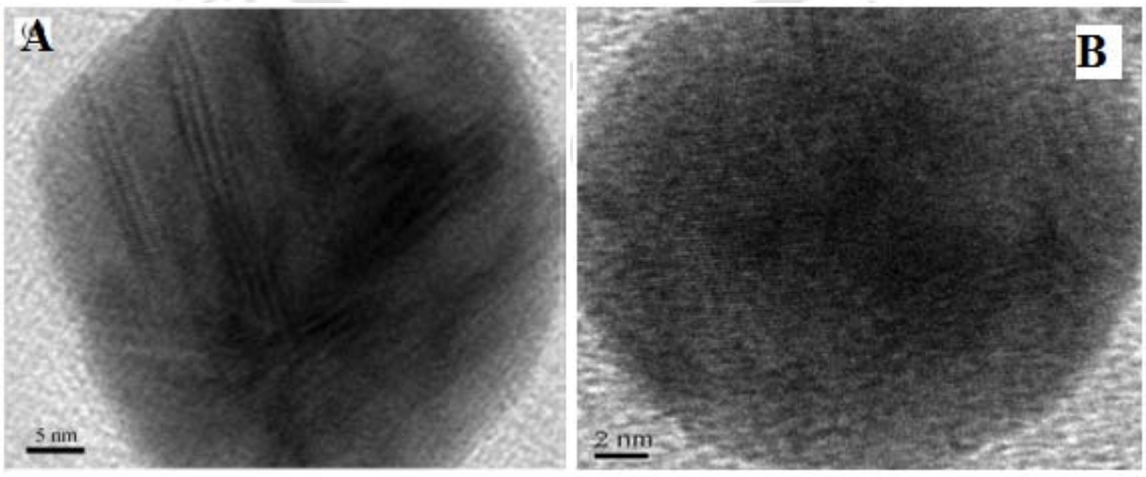

(A) FLE (B) PLE

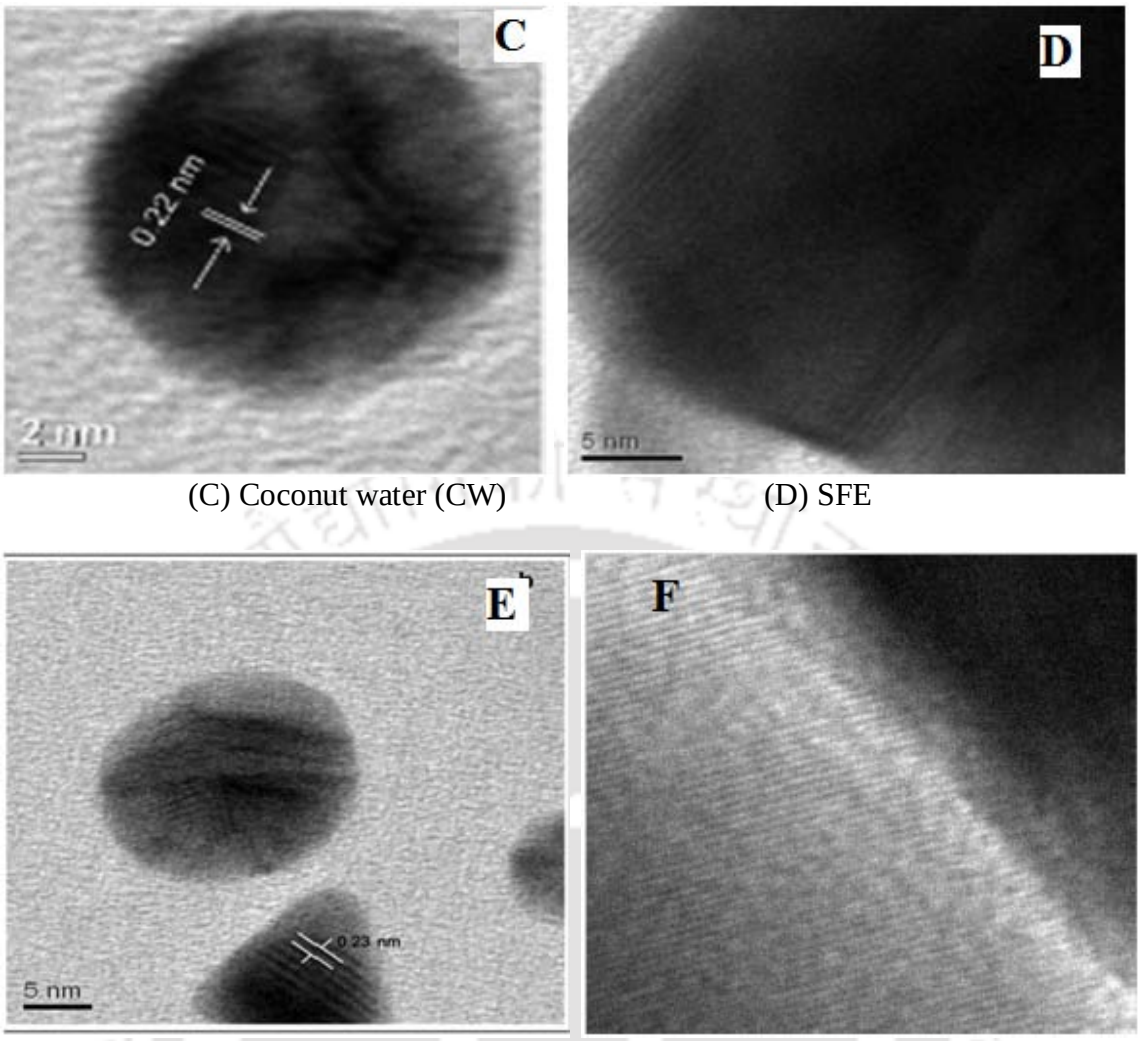

(C) Coconut water (CW) (D) SFE

(E) SmFE (F) (F) *C. procera* (AF)

Figure 4.7 *HRTEM of AuNPs synthesized with optimized parameters (A) FLE, (B) PLE, (C) CW (D) SFE (E) SmFE (F) C. procera (AF).*

4.3.5.3 ***Selected area electron diffraction (SAED) pattern***

Selected-area electron diffraction pattern (SAED) of a single-spherical particle confirmed its crystalline nature (Figure 3(c)). Three Debye-Scherrer's rings corresponding to strong (1 1 1), (2 0 0), and weak (2 2 0) planes of an fcc crystalline lattice were observed for AuNPs synthesized using FLE, PLE, CW, SFE, SmFE and C. procera (AF) (**Figure 4.8).**

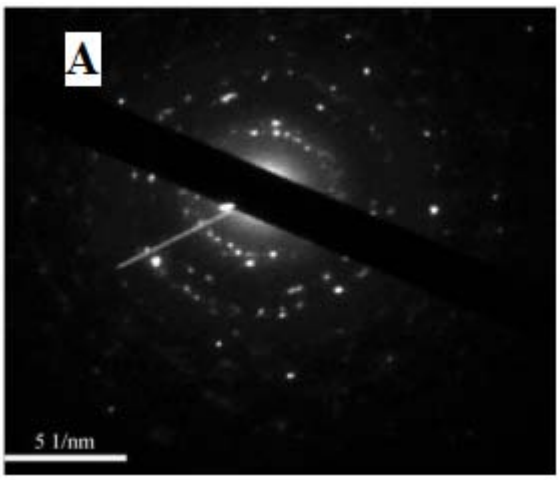

(A) FLE

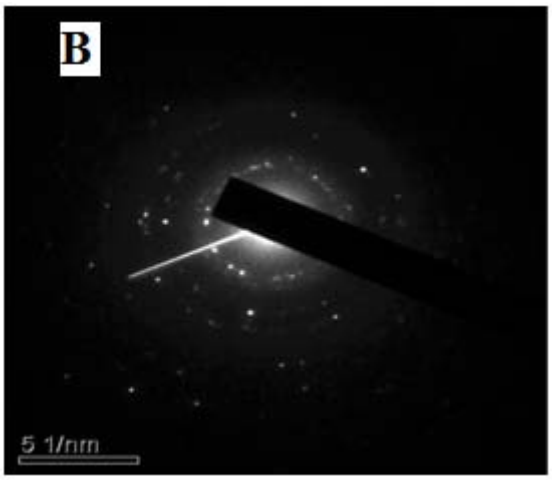

(B) PLE

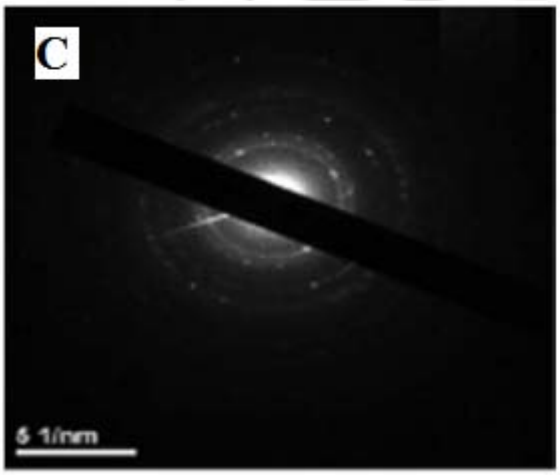

(C) Coconut water (CW)

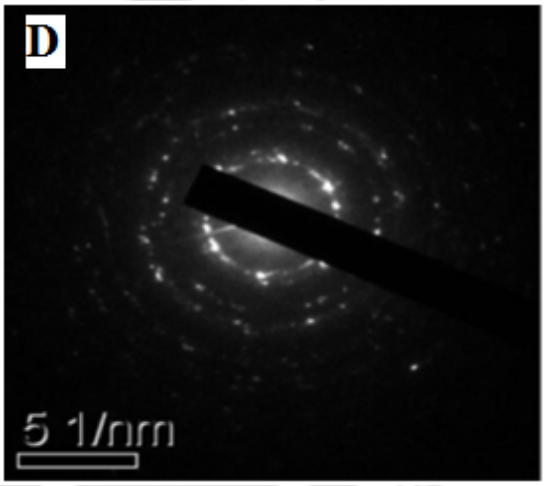

(D) SFE

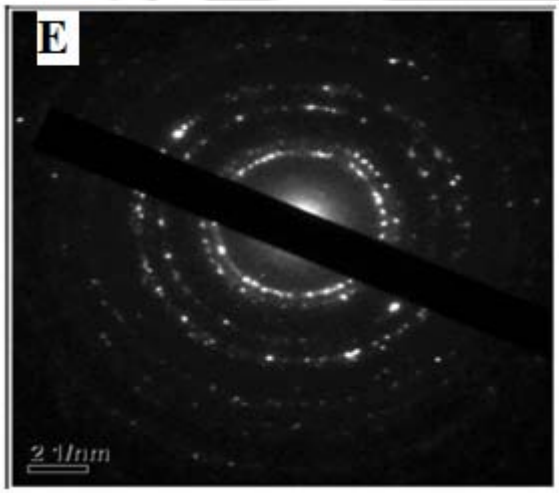

(E) SmFE (F)

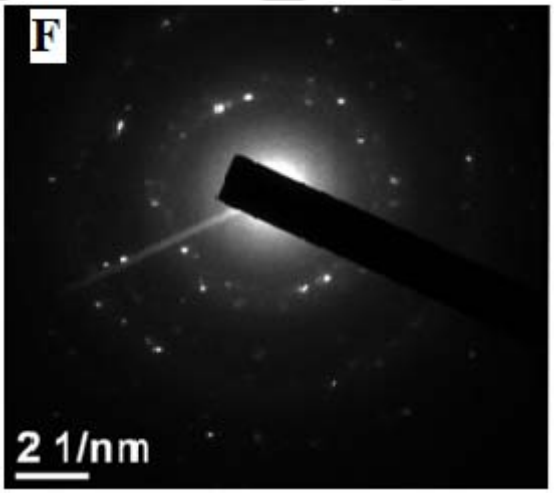

(F) *C. procera* (AF)

Figure 4.8 *SAED pattern of AuNPs synthesized with optimized parameters using (A) FLE, (B) PLE, (C) CW (D) SFE (E) SmFE (F) C. procera (AF).*

4.3.5.4 Histograms of the AuNPs

The synthesized AuNPs were of different shapes and sizes i.e anisotropic. The histograms represent the ranges of AuNPs formed from different plants materials. The size ranges of AuNPs synthesized using FLE, PLE, CW, SFE, SmFE and C. procera (AF) and were of 3-20, 10-35, 5-20, 5-50, 3-50 and 5-20, respectively (**Figure 4.9)**.

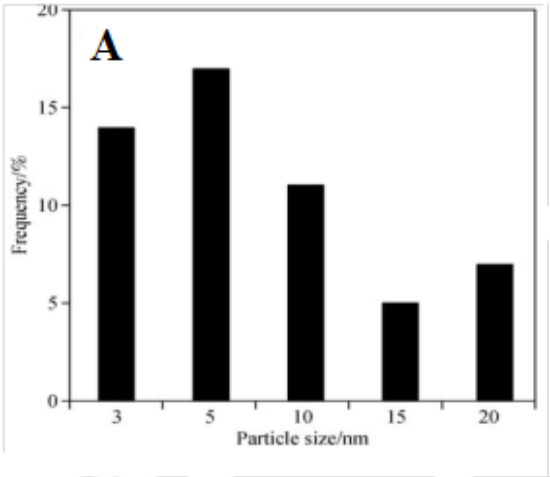

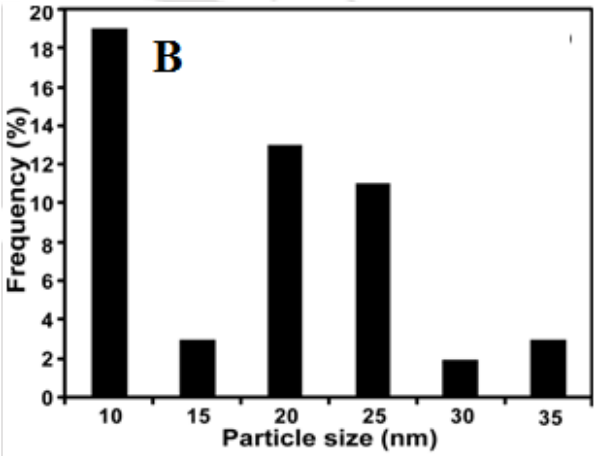

(A) FLE (B)PLE

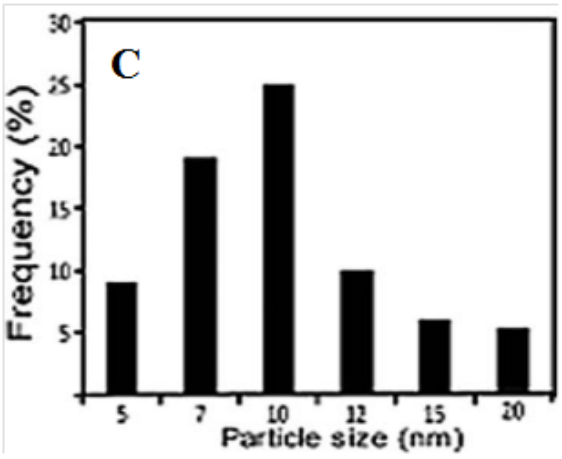

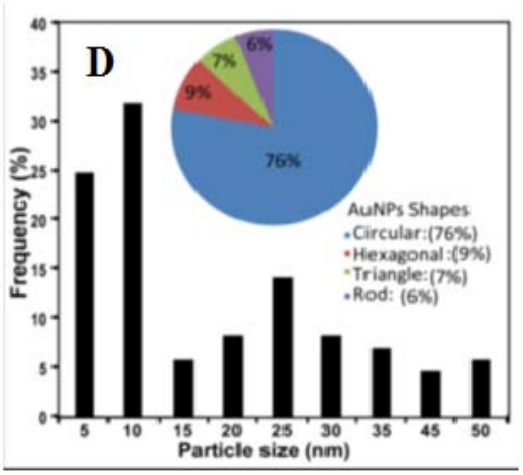

(C) Coconut water (CW) (D) SFE

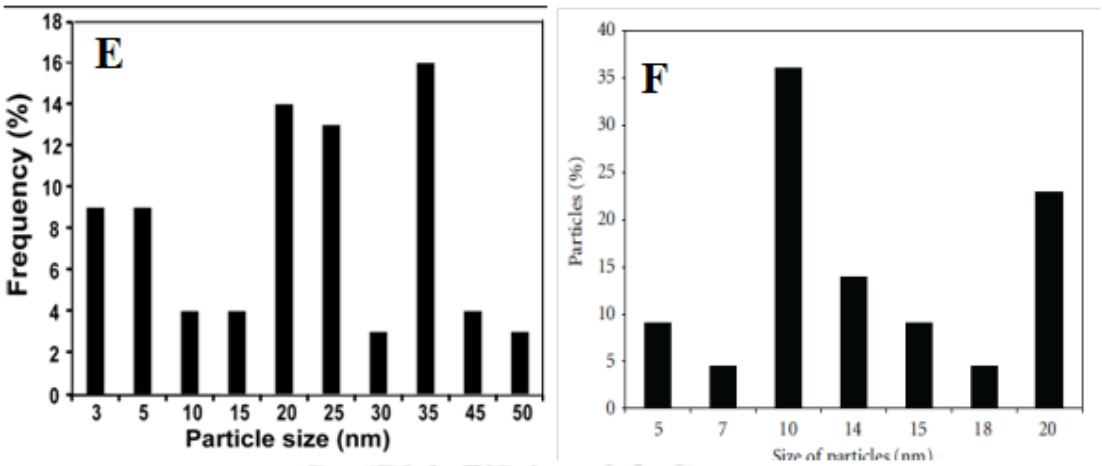

(E) SmFE (F) (F) *C. procera* (AF)

Figure 4.9 *Histogram patterns of AuNPs synthesized with optimized parameters using (A) FLE, (B) PLE, (C) CW (D) SFE (E) SmFE (F) C. procera (AF).*

4.3.5.5 X-ray Diffraction pattern

The crystalline nature of AuNPs synthesized using FLE, PLE, CW, SFE, SmFE and C. procera (AF) was confirmed with X-ray diffraction analysis (**Figure 4.10**). The XRD pattern of the AuNPs synthesized from FLE, PLE, CW, SFE, SmFE and *C. procera* (AF) displayed diffraction peaks at 38.1, 44.4, and 64.5• corresponding to the (1 1 1), (2 0 0), and (2 2 0) Bragg's reflections, respectively, which is due to the fcc crystal structure. These results confirmed the synthesized AuNPs were of crystalline in nature.

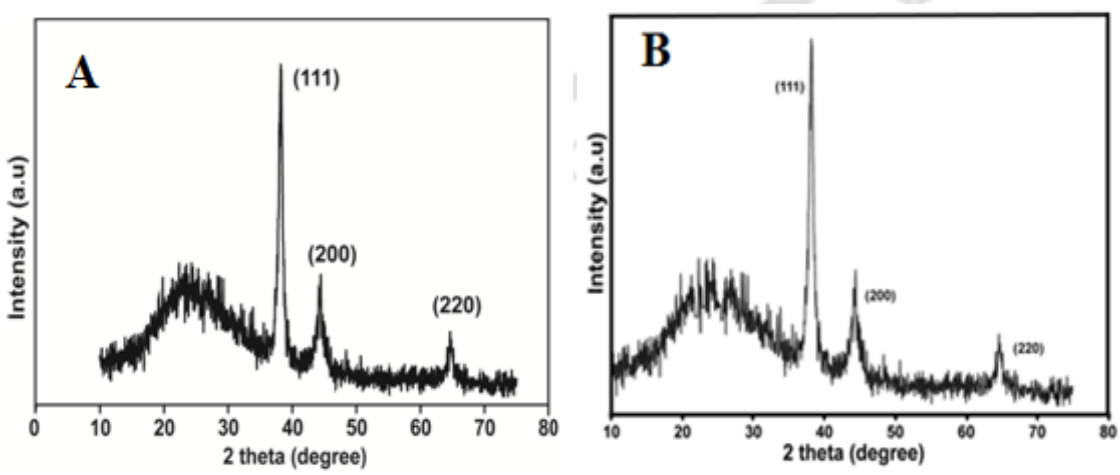

(A) FLE (B) PLE

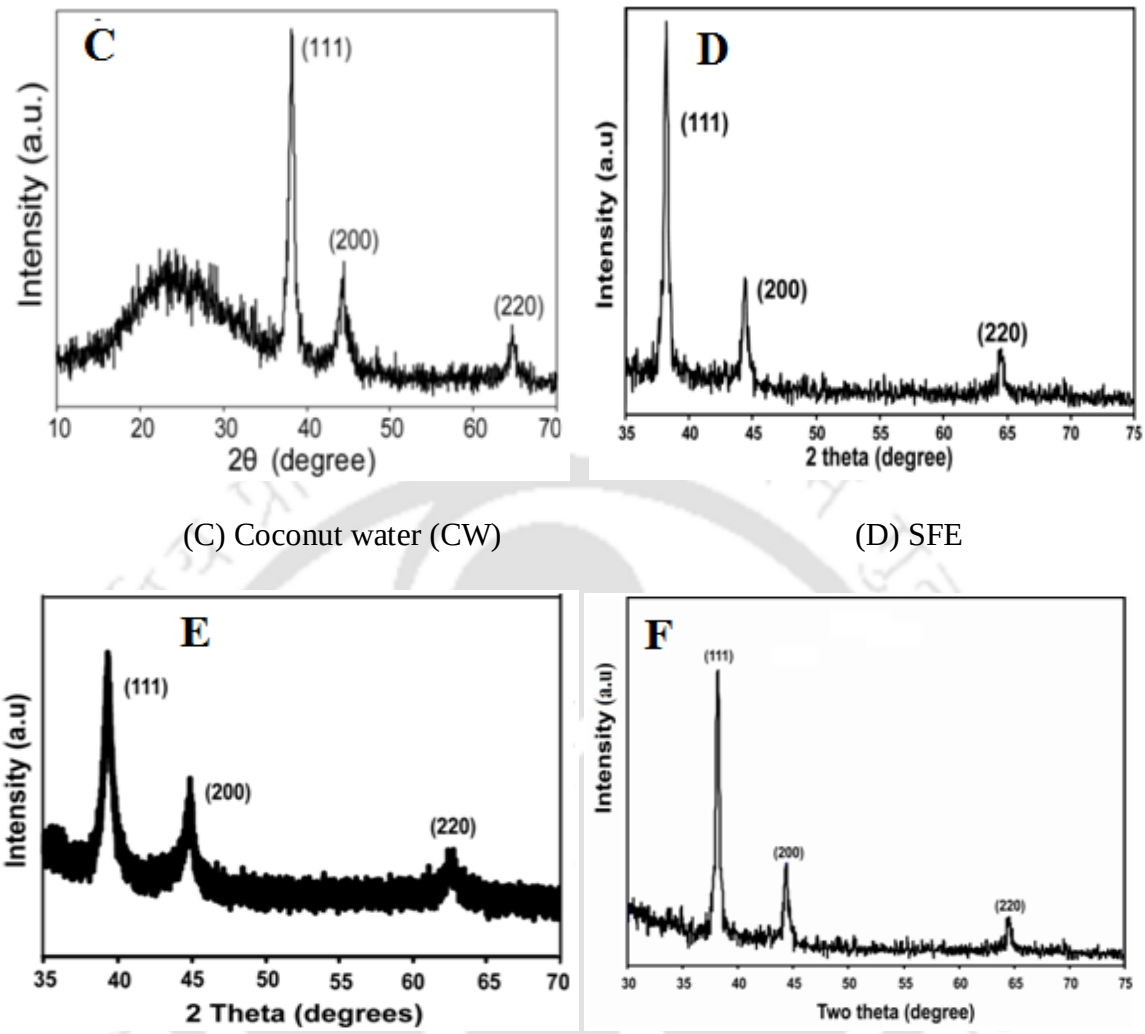

(C) Coconut water (CW) (D) SFE

(E) SmFE (F) (F) *C. procera* (AF)

Figure 4.10 *XRD patterns of AuNPs synthesized with optimized parameters using (A) FLE, (B) PLE, (C) CW (D) SFE (E) SmFE (F) C. procera (AF).*

4.3.5.6 FT-IR analysis of AuNPs

FT-IR spectra of AuNPs synthesized with optimized conditions indicated the presence of the biomolecules on the AuNPs. The biomolecules were originated from the plant extracts and adsorbed on to the AuNPs which further provides the stability to the synthesized AuNPs. We have observed the functional groups on AuNPs synthesized using FLE. FT-IR spectra of FLE showed strong signals at 3330, 2927, 1637, 1475, and 1084 cm^{-1} corresponding to hydroxyl group arising from alcohols and phenolic compounds,

secondary amine, amide I bond of proteins, asymmetric deformation of CH_3 from alkenes, and C–N stretching vibrations of amide bond, respectively. The vibrational absorption band at 1384 cm^{-1} was assigned to rocking of methyl group (Curve a in **Figure 4.11A**). FT-IR spectra of AuNPs showed strong signals at 3414 cm^{-1} (hydroxyl group of alcohols or phenols), 2418 cm^{-1} (hydroxyl group of carboxylic acids), 1668 cm^{-1} (amide I bond of proteins), 1390 cm^{-1} (methyl group of alkanes). The intense band that appeared at 1154 cm^{-1} can be ascribed to C–O–C or C–O stretching modes in phenolic compound or phenolic derivatives (Curve b in **Figure 4.11A**).

The FT-IR spectra of PLE, as shown in **Figure 4.11B** (curve a), showed peaks at 3,495 cm^{-1} (hydroxyl group arising from alcohols and phenolic compounds), 2,865 cm^{-1} (secondary amine), 1,651 cm^{-1} (amide I bond of proteins), 1,422 cm^{-1} (C =C groups from alkenes), 1,328 cm^{-1} (C–CH3 group), and 1,083 cm^{-1} (C–N stretching vibrations of amide bond), whereas the AuNPs showed peaks at 3,402, 2,865, 1,637, 1,365, and 1,046 cm^{-1}, as indicated in **Figure 4.11B (**curve b**).**

An FTIR spectrophotometer (range 500–4000 cm^{-1}; Perkin-Elmer, Norwalk, CT) showed the spectra of AuNPs formed with different MW irradiation times (9, 11, and 17 s) and filtered CW. Both AuNPs and CW showed strong signals at 1042, 1627, and 3014 cm^{-1} corresponding to C–N stretching vibrations of amine, amide bond, and hydroxyl groups, respectively (**Figure 4.11C**). AuNPs showed intense transmittance at 1042 cm^{-1} due to C–N stretching vibrations of amine originating from the protein molecules adsorbed on AuNPs.

FT-IR spectra of SFE showed strong signals at 3454, 2951, 1649, 1431 and 1082 cm^{-1} corresponding to hydroxyl group arising from alcohols and phenolic compounds, secondary amine, amide I bond of proteins, asymmetric deformation of CH_3 from alkenes, and C–N stretching vibrations of amide bond, respectively (**Figure 4.11D,** curve

a). FT-IR spectra of AuNPs showed strong signals at 3440 cm^{-1} (hydroxyl group of alcohols or phenols), 2949 cm^{-1} (secondary amine), 1668 cm^{-1} (amide I bond of proteins), 1425 cm^{-1} (deformation of the -CH3 from alkanes) 1082 cm^{-1} (stretching vibrations of C–N from amide bond) (**Figure 4.11D,** curve b).

The FTIR spectra of SmFE, showed peaks at 3374 (hydroxyl group arising from hydroxyl group containing compounds), 2917 (secondary amine), 1641 (amide I bond of proteins), 1415 (C=C groups from alkenes), 1241 (C-CH_3 group) and 1025 cm^{-1} (C–N stretching vibrations of amide bond) as showed in **Figure 4.11E,** curve a**,** where as the AuNPs showed the peaks at 3419, 1647, 1241 and 1049 cm^{-1}) (**Figure 4.11E,** curve b).

The FTIR spectrum (**Figure 4.11F,** curve a) of AF showed characteristic IR bands belonging to protein, alcoholic, or phenolic compounds. Broad band at 3360 cm^{-1} was due to the hydroxyl functional group. Strong absorption bands at 1617 and 1080 cm^{-1} were characteristic of amide I and C–N stretching vibrations of amine, respectively where as the AuNPs showed at) strong bands for amide I (1625 cm^{-1}), C=O stretching mode of carboxylic acid, and C–N stretching of amines (1373 cm^{-1} and 1086 cm^{-1}) (**Figure 4.11F,** curve b**)**.

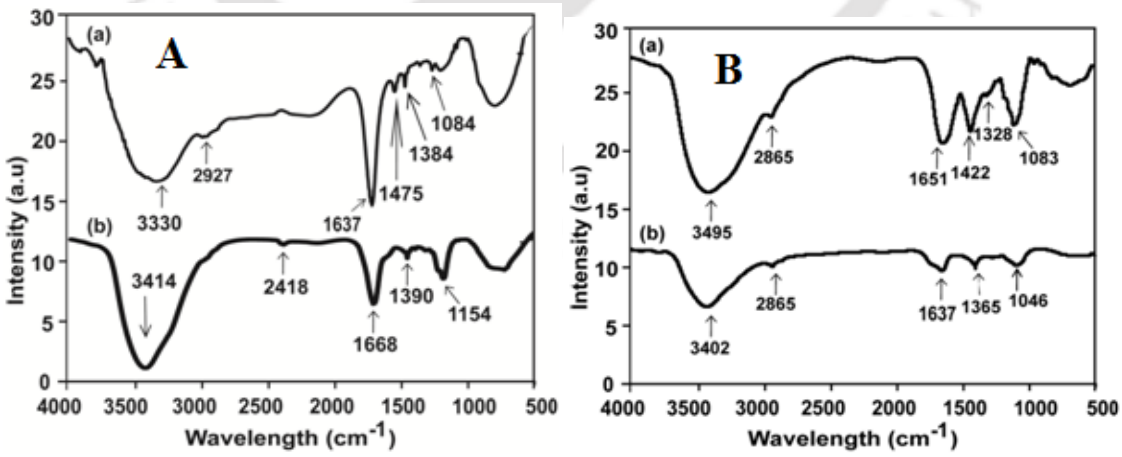

(A) FLE (B) PLE

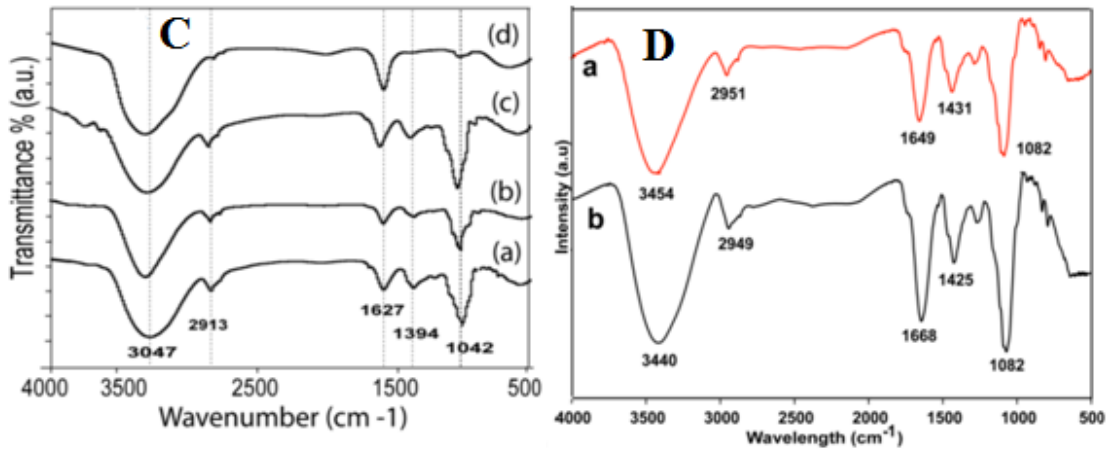

C) Coconut water (CW) (D) SFE

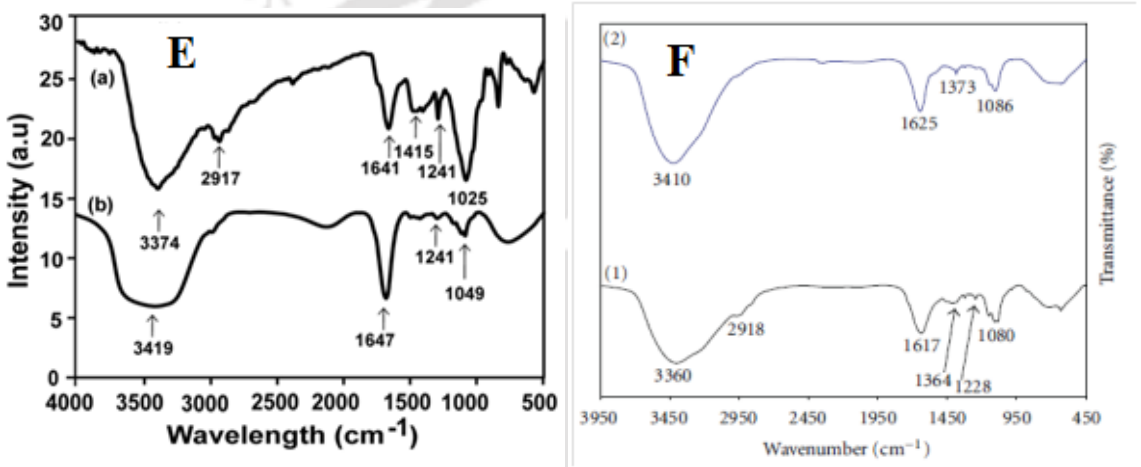

(E) SmFE (F) c. procera (AF)

Figure 4.11 *FTIR spectra of AuNPs synthesized with optimized parameters using (A) FLE, (B) PLE, (C) CW (D) SFE (E) SmFE (F) C. procera (AF).*

We performed the thermal gravimetric analysis to determine the content of the capping agents on the AuNPs synthesized using SmFE. The thermal degradation (TGA spectrum) of AuNPs occurs over a wide temperature range (200-480 ^{o}C) which revealed the significant weight loss of AuNPs. This now clearly indicates that biomolecules were capped on the AuNPs and were completely degraded due to high temperature (200-480 ^{o}C). It is worthwhile to mention that there was further fall of spectrum beyond 885 ^{o}C as the temperature was attaining to melting point of gold 1,064 °C (**Figure 4.12**).

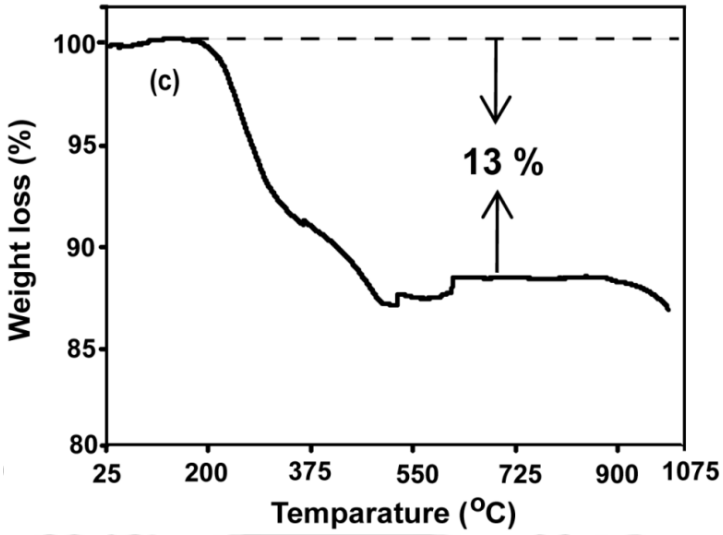

Figure 4.12 *Thermal gravimetric analysis of AuNPs synthesized with 8% PFE against 1 mM $HAuCl_4$ for 25 sec of microwave irradiation time.*

NMR spectrum of the purified and lyophilized AuNPs confirmed the inclusion of biomolecules on AuNPs surfaces NMR signals at 7.98 and 1.79 ppm correspond to the protons of aromatic environment and alkyl/allylic groups, respectively. The signals at 2.84 and 2.92 were due to chemical environments belonging to acetylenic compounds **(Figure 4.13)**.

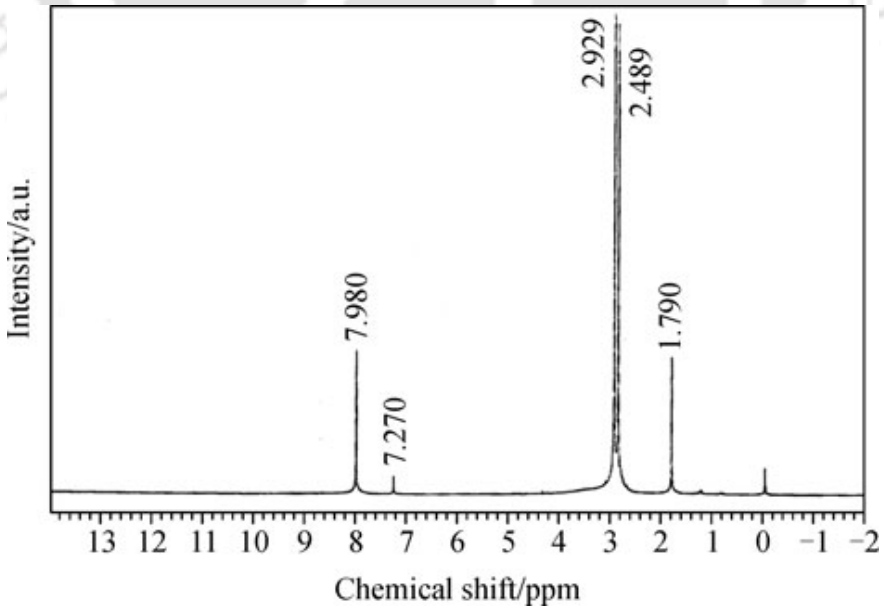

Figure 4.13 *^{1}H NMR spectrum of AuNPs synthesized with 0.4% FLE, 1 mmol/L $HAuCl_4$ and 16 s as MW irradiation time.*

4.3.5.7 Elemental composition

The elemental composition of the AuNPs synthesized using (A) FLE, (B) PLE, (C) CW (D) SFE (E) SmFE (F) C. procera (AF) were obtained by using Energy-Dispersive X-ray Spectroscopy (LEO 1430 VP) at variable pressure scanning electron microscope equipped with INCA Oxford EDX facility, at an acceleration voltage of 10 keV. The EDX profile of SFE, PLE, SFE and SmFE showed the different elements on the synthesized AuNPs. (**Figure 4.14**)

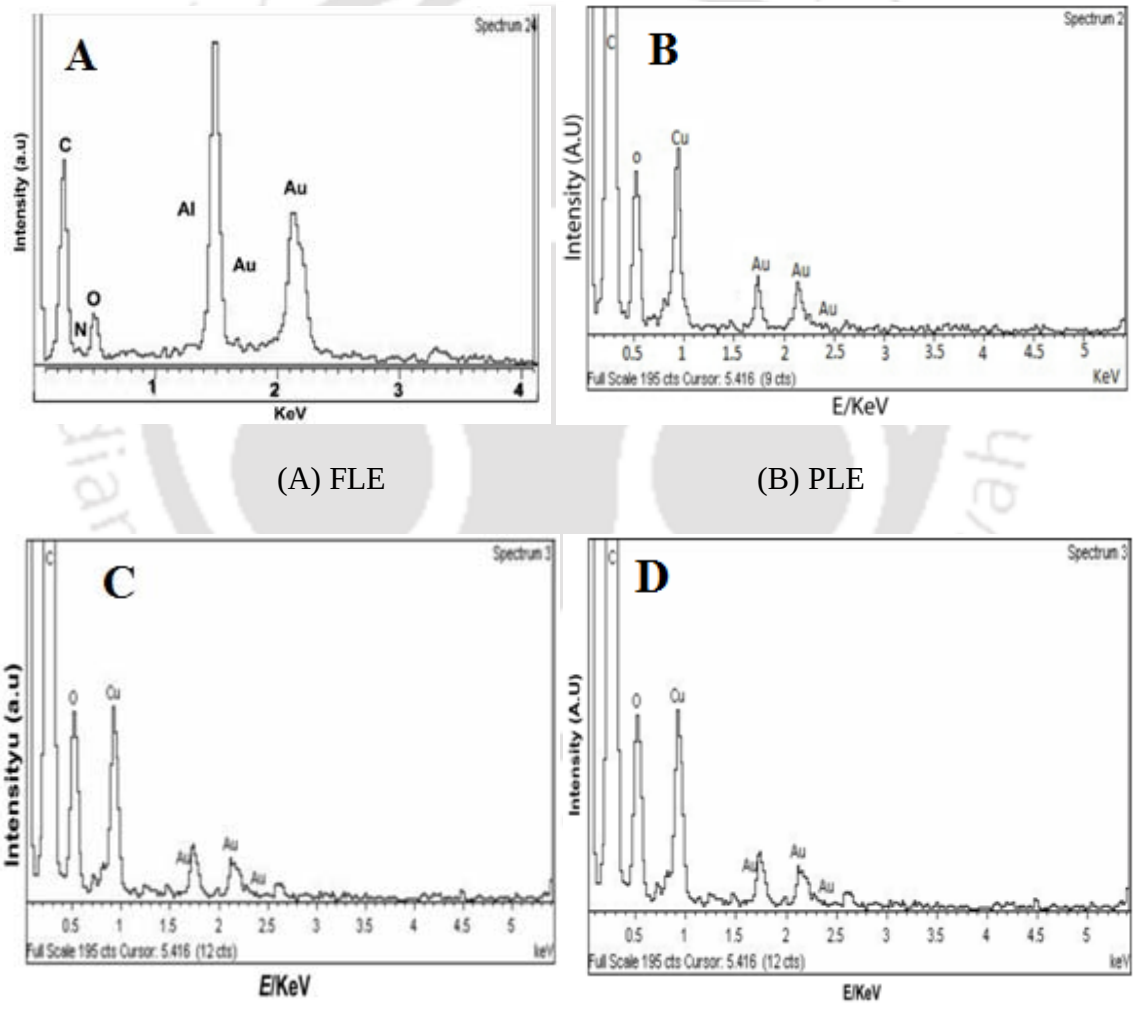

(A) FLE (B) PLE

(C) SFE (D) SmFE

Figure 4.14 *EDX profile of AuNPs synthesized with optimized parameters using (A) FLE, (B) PLE, (C) SFE (D) SmFE.*

4.3.5.8 Cytotoxicity Tests

The cytotoxicity of AuNPs on cancer cells were evaluated by MMT assay. The monocultures of the HeLa, IMR-32 and MCF-7 cells were incubated with increasing concentrations of filter (0.2 micron) sterilized AuNPs for 24 hrs. The cytotoxicity test revealed the synthesized AuNPs using FLE, PLE, CW, SFE, SmFE and C. procera (AF) were biocompatible thereby using them in the biomedical applications (**Figure 4.15**).

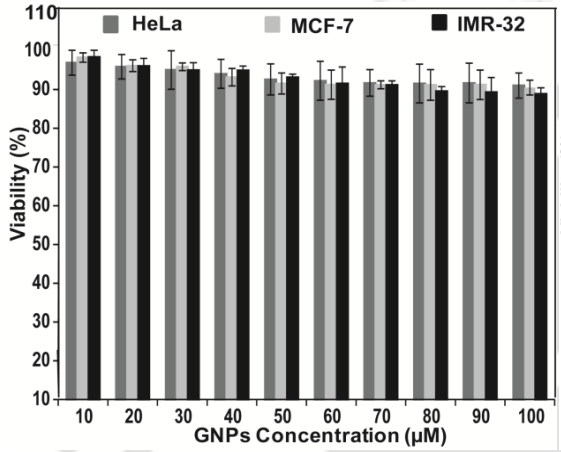

(A) FLE

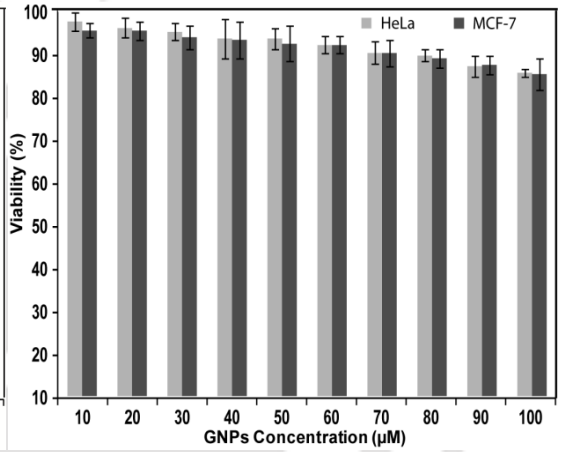

(B) PLE

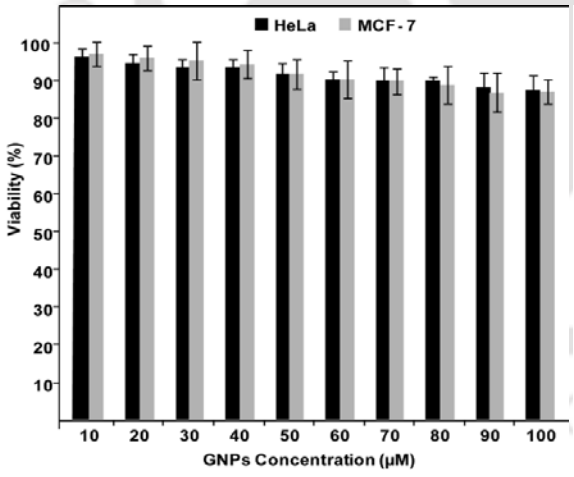

(C) CW

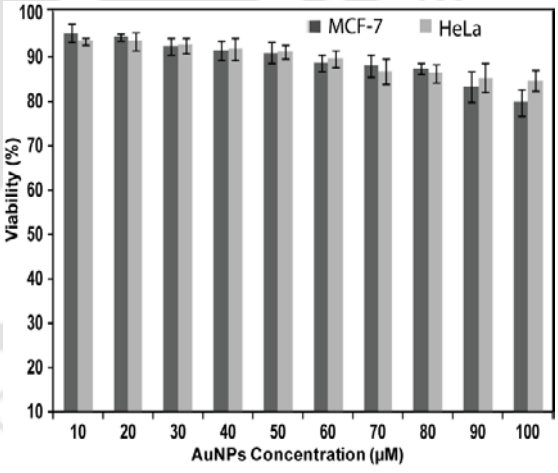

(D) SFE

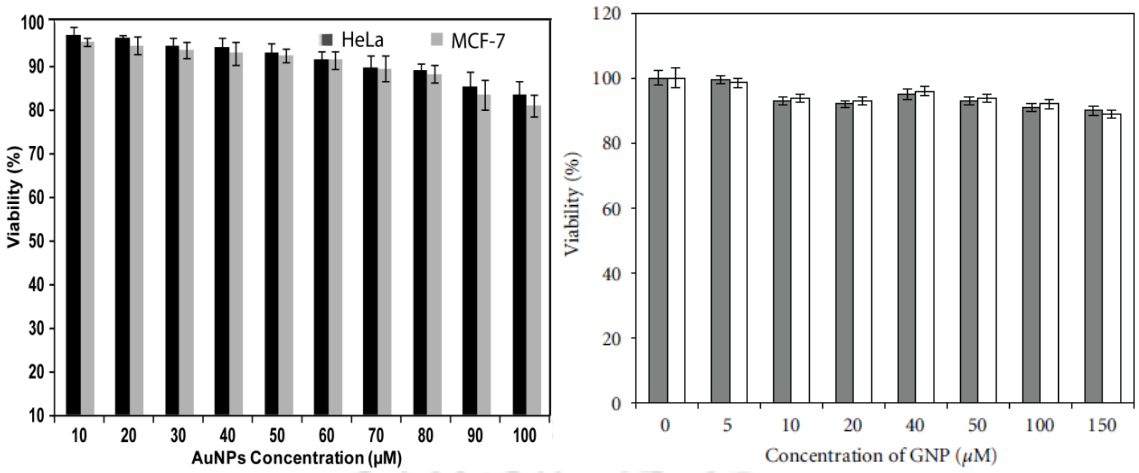

(E) SmFE (F) C. procera (AF)

Figure 4.15 Cytotoxicity assay: *Cell viability of HeLa, MCF-7 and IMR-32 cells exposed to different concentrations of AuNPs (10 to 100 µM) synthesized using (A) FLE (B) PLE (C) CW (D) SFE (E) SmFE (F) C. procera (AF) over a 24-h treatment.*

The cytotoxicity of AuNPs synthesized using PLE under in vitro conditions in HeLa and MCF-7 cells was examined by MTT assay for 24 h in terms of effect of AuNPs on cell proliferation. Only cells that are viable after 24-h exposure to the AuNPs can metabolize MTT efficiently and produce purple colored crystal which is soluble in DMSO. **Figure 4.16** shows unaltered cellular morphologies of two cell lines after treatment with AuNPs, suggesting that treatment with AuNPs did not induce any cytotoxic effect causing significant damage or death of the treated cells. **Table 4.4** shows the cytotoxicity of the AuNPs synthesized using FLE, PLE, CW, SFE, SmFE and *C. procera* (AF).

Table 4.4 C*ytotoxic effect of synthesized AuNPs using FLE, PLE, CW, SFE, SmFE and C. procera (AF)*

S. No	Plant or Fruit material /Fruit Extract	Human Cancer Lines Used	Concentration of AuNPs (in µM)									
1	*F. esculentum*	HeLa	10	20	30	40	50	60	70	80	90	100
		Viability%)	97	97	97	96	95	95	94	94	94	93
		MCF-7	10	20	30	40	50	60	70	80	90	100
		Viability (%)	99	97	97	96	95	95	95	95	94	92
		IMR-32	10	20	30	40	50	60	70	80	90	100
		Viability (%)	99	98	98	98	96	95	95	94	92	90
2	*P. betle*	HeLa	10	20	30	40	50	60	70	80	90	100
		Viability (%)	98	97	96	94	94	93	92	92	91	89
		MCF-7	10	20	30	40	50	60	70	80	90	100
		Viability (%)	96	96	94	94	93	93	91	91	91.5	89
3	*S. indicum*	HeLa	10	20	30	40	50	60	70	80	90	100
		Viability (%)	96	96	94	94	94.5	90	90	88	84	83
		MCF-7	10	20	30	40	50	60	70	80	90	100
		Viability (%)	95	95	94	94.5	95	91	88	86	85	85
4	Coconut Water *(C. nucifera)*	HeLa	10	20	30	40	50	60	70	80	90	100
		Viability (%)	95	94	94	93.5	93	91	91	91	90	88
		MCF-7	10	20	30	40	50	60	70	80	90	100
		Viability (%)	96	95	95	94.5	93	91	91	89	88	87
5	*C. procera*	HeLa	0	5	10	20	40	50	100	150	-	-
		Viability (%)	100	99	94	94	96	95	94	93	-	-
		A549	0	5	10	20	40	50	100	150	-	-
		Viability (%)	100	100	97	97	98	97	96	95	-	-
6	*S. mukorassi*	HeLa	10	20	30	40	50	60	70	80	90	100
		Viability (%)	98	98	97	97	96	95	94	94	87	82
		MCF-7	10	20	30	40	50	60	70	80	90	100
		Viability (%)	95	94	93	93	92	92	91	90	87	85

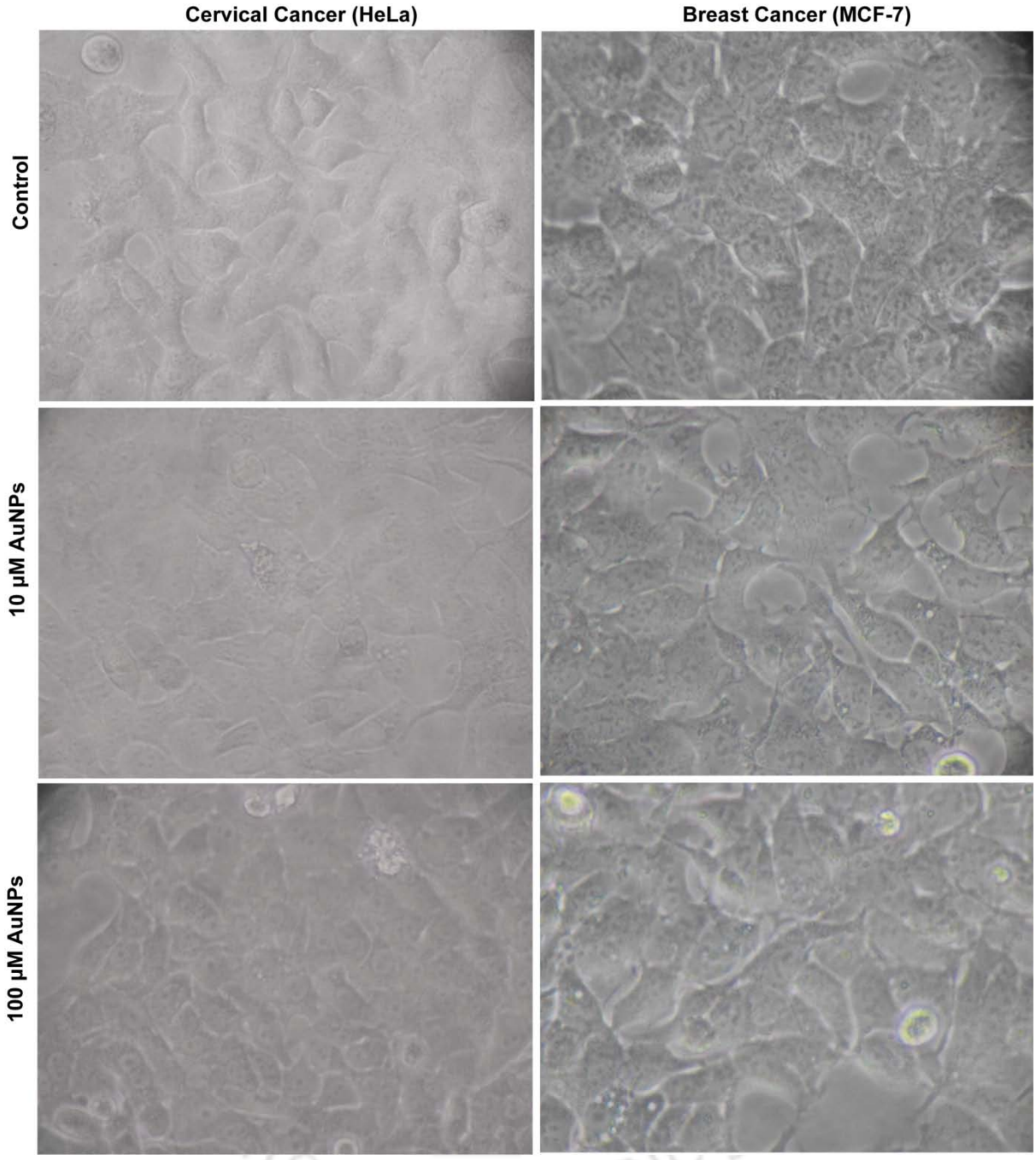

Figure 4.16 *Images of cancer cell lines (HeLa and MCF-7). Over 24-h AuNPs treatment; control, 10, and 100 µM.*

The cytotoxicity of AuNPs synthesized using CW under in vitro conditions in HeLa and MCF-7 cells was examined by MTT assay for 24 h in terms of effect of AuNPs on cell proliferation. Both cell lines retained their cellular morphologies, suggesting that

treatment with AuNPs did not induce any cytotoxic effect causing significant damage or death of the treated cells (**Figure 4.17**).

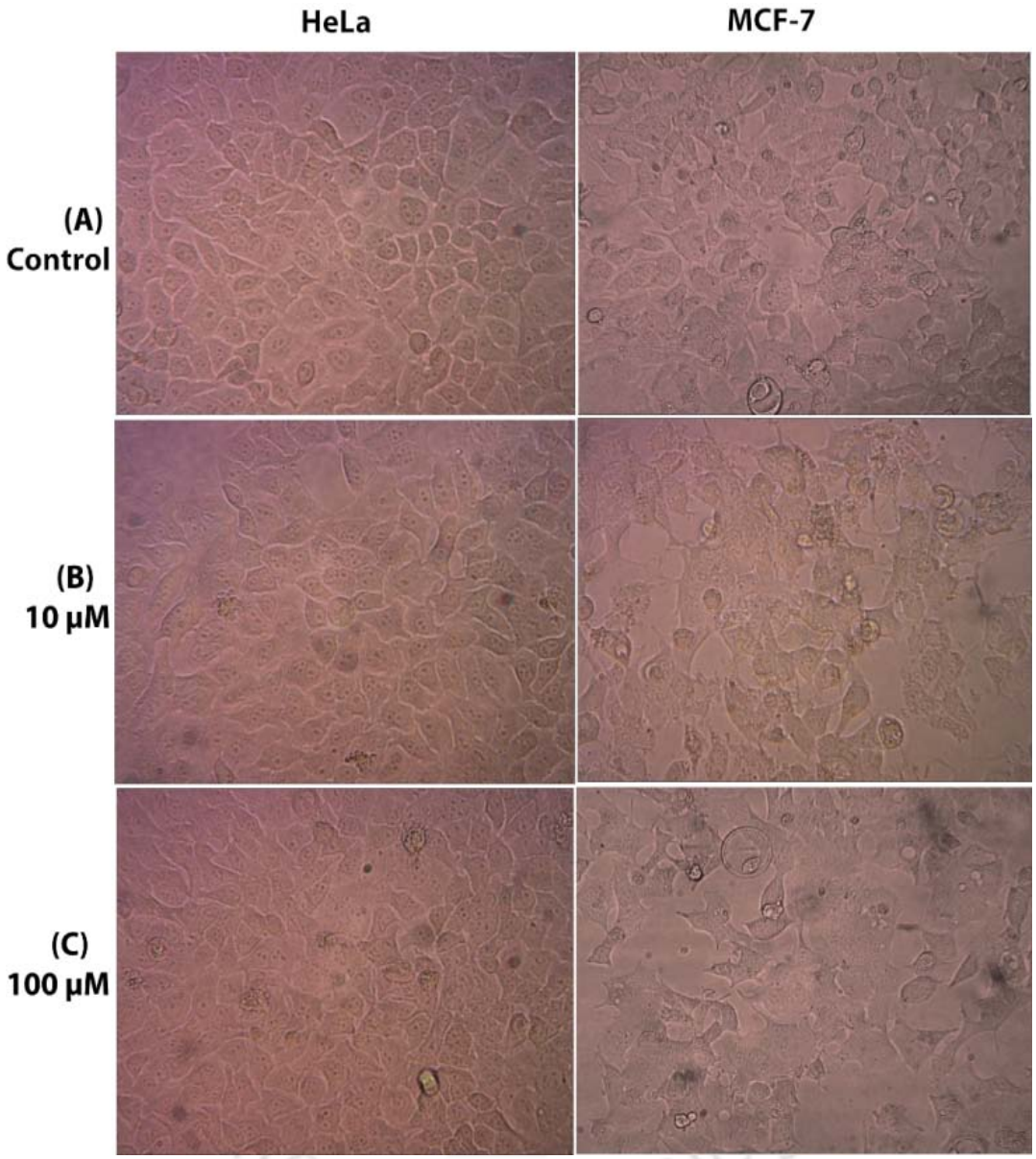

Figure 4.17 *Images of HeLa and MCF-7 cells over 24-h AuNPs (synthesized using CW) treatment: (A) control, (B) 10 µM, and (C) 100 µM.*

4.3.6 Effect of P^H and salt concentrations on AuNPs synthesized using FLE

We performed a set of experiments to find out the effect of the pH on the stability of AuNPs. AuNPs was synthesized with optimized parameters (0.4% FLE and 16 s) and it was found that the pH of the solution under these optimized conditions was 7.81. After 6 h, we found the formation of AuNPs clusters in all test tubes except at pH 7 which was

evident from visual observation and the hypo chromic decrease in the intensity of the SPR band (data not shown). To find out the effect of salt concentration on stability of AuNPs, we carried out different experiments by varying the concentration of NaOH from 0.1 to 0.5 mol/L and saw immediate increase in the blue colour indicating the rapid growth of size due to agglomeration. Thus, we narrowed down our test ranging from 0.01 to 0.1 mol/L wherein we observed a change in the colour from ruby red to intense blue. We performed various experiments to identify the effect of the salt and 0.1 mol/L NaOH was considered as the threshold concentration beyond which the AuNPs are unstable.

The biochemical tests revealed that FLE contained phenolic compounds (3.169 mg/mL) and flavonoids (2.95 mg/mL). Although the exact mechanism of synthesis of AuNPs by FLE is still not clear, our current observation suggested that the presence of highly potential reducing molecules such as phenolic compounds, flavonoids and antioxidant molecules (rutins and tannins) has reduced $HAuCL_4$ to AuNPs through the transfer of •-electrons to Au^{3+} and reduced to Au^0 in the extracellular medium. The possible mechanisms of phenolic compounds and flavonoids mediating the synthesis of AuNPs are shown in **Figure 4.18.** The synthesized AuNPs were stored at room temperature and found to be stable over a period of three months in aqueous solution. This suggested that the synthesis method reported herein provided stabilization of AuNPs without the involvement of any synthetic harsh chemicals.

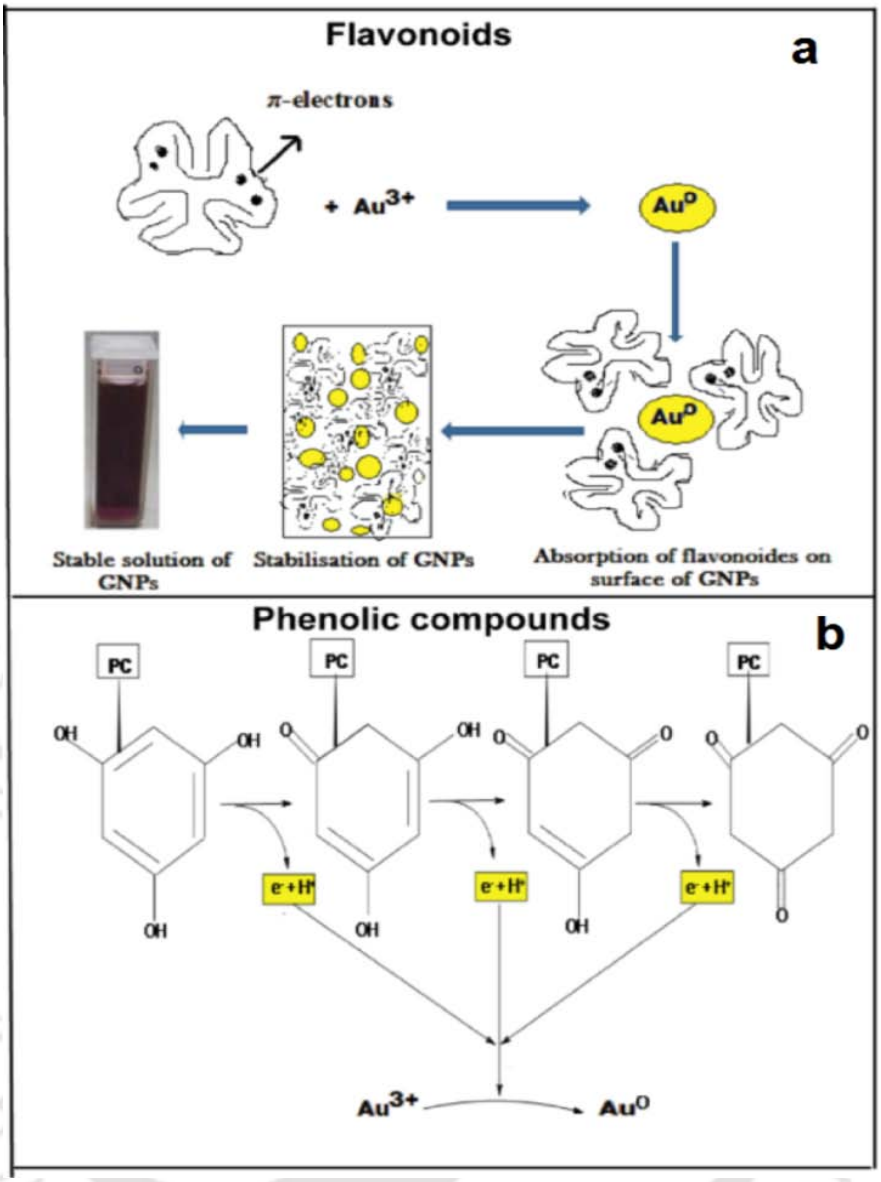

Figure 4.18 *Tentative mechanisms of (a) flavonoids and (b) phenolic compounds.*

4.4 Discussion

The conditions for the synthesis of AuNPs were optimized by varying percentage of FLE and incubation time against 1 mmol/L gold salts. The formation of AuNPs can be easily visualized by appearance of ruby red colour due to longitudinal excitation of surface plasmon vibrations of AuNPs at (538±4) nm in the visible range of spectra. We observed that 0.4% FLE completely reduced the 1 mmol/L $HAuCl_4$ as there was no significant change in peak intensity with 0.5% FLE (**Figure 4.1A).** We found 16 s as the optimum time required for complete reduction of 1 mmol/L $HAuCl_4$ with 0.4% of FLE. This was

evident from the flattening peak intensity associated with 18 and 20 s (**Figure 4.3A).** The surface plasmon resonance (SPR) peaks observed at 325 nm were due to organic moieties in the reaction mixture (**Figure 4.1A**) The width of SPR peak may be attributed to the change in refractive index of medium and change in the size and shape of AuNPs in the aqueous solution (Raghunandan et al., 2009).

We performed a set of experiments to find out the effect of the pH on the stability of AuNPs synthesized using FLE. AuNPs was synthesized with optimized parameters (0.4% FLE and 16 s) and it was found that the pH of the solution under these optimized conditions was 7.81. After 6 h, we found the formation of AuNP clusters in all test tubes except at pH 7 which was evident from visual observation and the hypo chromic decrease in the intensity of the SPR band (data not shown). The formation of particle clusters was due to the agglomeration of the AuNPs. Thus, the range from pH 7 to pH 8 was the ideal for the stability of the AuNPs.

To find out the effect of salt concentration on stability of AuNPs, we carried out different experiments by varying the concentration of NaOH from 0.1 to 0.5 mol/L and saw immediate increase in the blue colour indicating the rapid growth of size due to agglomeration. Thus we narrowed down our test ranging from 0.01 to 0.1 mol/L wherein we observed a change in the colour from ruby red to intense blue. There was no considerable change in the SPR peak intensity and colour of solution mixtures containing 0.01– 0.09 mol/L of NaOH (data not shown). However, we observed pale blue colour in the AuNPs solution containing 0.1 mol/L NaOH while intense blue in the solution containing 0.2 mol/L NaOH which reveals the aggregation of AuNPs indicating that the stability is decreased. Hence, 0.1 mol/L NaOH was considered as the threshold concentration beyond which the AuNPs are unstable.

The biochemical tests revealed that FLE contained phenolic compounds (3.169 mg/mL) and flavonoids (2.95 mg/mL). Although the exact mechanism of synthesis of AuNPs by FLE is still not clear, our current observation suggested that the presence of highly potential reducing molecules such as phenolic compounds, flavonoids and antioxidant molecules (rutins and tannins) has reduced $HAuCL_4$ to AuNPs through the transfer of •-electrons to Au^{3+} and reduced to Au^0 in the extracellular medium. The possible mechanisms of phenolic compounds and flavonoids mediating the synthesis of AuNPs are shown in **Figure 4.18**. The synthesized AuNPs were stored at room temperature and found to be stable over a period of three months in aqueous solution. This suggested that the synthesis method reported herein provided stabilization of AuNPs without the involvement of any synthetic harsh chemicals.

The formation of AuNPs was monitored with the naked eye by observing the appearance of the ruby red color, as shown in **Figure 4.1B**. *P. betel* has a high content of phenolic acids, antioxidants, and flavonoids. The abundant hydroxyl groups available in these compounds could participate in the gold bioreduction. The bioreduction of gold could occur through the oxidation of hydroxyl (R–OH) to carbonyl groups (R–C= O), as shown in following equation:

$$AuCl_4^- + 3R\text{-}OH \longrightarrow Au^o + 3R{=}O + 3H^+ + 4Cl^-$$

The SPR peak of 2% PLE against 0.5 mM gold solution showed intense and narrow peak centered around 544 nm, as shown in **Figure 4.1B**, whereas the SPR peaks above the 2% PLE concentration were flattening and redshifted, indicating the formation of large-size AuNPs and those below the 2% concentration were considered as suboptimal. Thus, 2% PLE was considered as optimal for the synthesis of AuNPs. **Figure 4.2B** shows the UV– Vis spectra of products obtained by reacting 2% PLE with various concentrations of $HAuCl_4$ (0.1 to 1 mM), which displayed an intense peak at 547 nm for

0.5 mM $HAuCl_4$. However, the SPR peaks displayed by the 0.3 mM $HAuCl_4$ were suboptimal, whereas those of 0.7 and 1 mM $HAuCl_4$ were red shifted. Since there was no significant formation of the peak with 0.1 mM, 0.5 mM $HAuCl_4$ was taken as the optimum for the synthesis of the AuNPs. UV visible spectral analysis of the different reaction products exhibited sharp SPR peaks presented in **Table 4.2**, indicating the successful formation of AuNPs.

Figure 4.3B shows the various experiments carried out to determine the optimum time for the synthesis of AuNPs by incubating the 2% PLE and 0.5 mM gold solution at different time intervals (12 to 30 s) of microwave irradiation. We found that the peaks above 18 s were flattening, indicating no further significant formation of AuNPs. The peaks below 18 s were considered as suboptimal as they displayed poor intensity. This revealed that 18 s was sufficient to reduce the 0.5 mM gold solution to AuNPs, thereby proving it as optimum for the synthesis. Also, we observed the significant change in the peak position (red-shifted peaks) of the reaction mixture obtained by using 4% PLE and 0.7 mM $HAuCl_4$ for 30 s, indicating the formation of large-size AuNPs, which was confirmed using TEM technique. The TEM images shown in **Figure 4.5** revealed the formation of large-size AuNPs, which agreed with the results obtained in **Figure 4.1B**.

The synthesis of AuNPs using CW was visually confirmed from the change in color of the reaction mixture from yellow to ruby red. UV-Visible spectral analysis of the reaction products exhibited sharp surface plasmon resonance (SPR) peaks, indicating the successful formation of AuNPs. For 0.250 mM $HAuCl_4$, the SPR peak was located at around 530 nm (**Figure 4.1C**). Above this concentration, the SPR peak was red-shifted, indicating the formation of larger AuNPs. Thus, 0.250 mM was considered as optimum for the AuNPs synthesis. With this optimized $HAuCl_4$ concentration, we repeated the reaction for different MW irradiation time period (**Figure 4.3C**). From 9 to 17 s, the

formation of AuNPs was enhanced, as can be seen from the respective SPR intensities. Above 17 s, changes in the SPR intensities and peaks were negligible. Thus, maximum reduction of 0.250 mM of $HAuCl_4$ occurred in the first 17 s of the reaction time.

AFM analysis of AuNPs synthesized with 0.250 mM with varying MW irradiation times was done in noncontact mode. At 9 s, the formation of AuNPs was negligible, whereas at 11 and 17 s the process of AuNPs formation was accelerated, as can be seen from the AFM image (**Figures 4.6A–C**).With the increase in MW irradiation time, there was no considerable alteration in the morphology of AuNPs. AFM analysis for 9, 11, and 17 s supported the results of UV-Vis spectroscopic studies (**Figure 4.3C**).

The syntesis of AuNPs using SFE was confirmed from the change of reaction mixtures from pale yellow to ruby red under microwave irradiation. The reaction mixtures (0.005-0.025%) showed the gradual increment in the formation of the AuNPs whereas the reaction mixtures above 0.03% of SFE showed flattered peaks. These results revealed that 0.03% of SFE was sufficient to reduce the 0.5 mM of $HAuCl_4$. Thus, we considered that 0.03% of SFE was optimum for the AuNPs synthesis (**Figure 4.1D**). UV-Vis spectra of products obtained by reacting 0.03 % SFE with varying concentration (0.1-1 mM) displayed an intense peak at 547 nm for 0.5 mM $HAuCl_4$. However, the SPR peaks displayed by the 0.1 and 0.3 mM $HAuCl_4$ were suboptimal, whereas 0.7 and 1 mM $HAuCl_4$ were flattered indicating the insignificant formation of the AuNPs. Thus, 0.5 mM $HAuCl_4$ was taken as the optimum for the synthesis of the AuNPs (**Figure 4.2C**).

Various experiments were performed to determine the optimum time for the synthesis of the AuNPs by incubating the 0.03% SFE and 0.5 mM $HAuCl_4$ solution at different microwave irradiation time intervals from 5-25 seconds (sec) of microwave irradiation. We found that the peaks above 20 sec were flattering, indicating no further significant formation of AuNPs. The peaks below to 20 sec were considered as

suboptimal as they displayed poor intensity. This revealed that 20 sec were sufficient to reduce the 0.5 mM of gold solution to AuNPs there by proving it as the optimum for the synthesis (**Figure 4.3D**).

UV-visible spectral analysis of the reaction products obtained from SmFE exhibited sharp surface plasmon resonance (SPR) peaks, indicating the successful formation of AuNPs. The SPR peak of 8% SmFE against 1 mM $HAuCl_4$ showed intense and narrow peak centred at 542 nm (**Figure 4.1E**). The SPR peak above 8% SFE was flattening, indicating that 8% SFE was sufficient to reduce the 1 mM $HAuCl_4$. Thus, we consider 8% SmFE as an optimum concentration against 1 mM $HAuCl_4$ for AuNPs synthesis. We carried out the various reactions to find out the optimum $HAuCl_4$ concentration and observed the slight red shifted peaks corresponding to 0.2, 0.8 and 1 mM $HAuCl_4$ concentrations which were an indication of formation of large size particles (**Figure 4.2D**). The reaction mixtures containing 0.4 and 0.6 mM $HAuCl_4$ concentration exhibited sharp SPR peaks at 525± 4 nm which signifies the formation of ideal size particles. However, as more number of particles were achieved with 0.6 mM $HAuCl_4$ concentration in contrast to 0.4 mM, thus we consider 0.6 mM as optimum.

Saponins are major chemical constituents of SFE, involved in the reduction of the gold salt to their corresponding nanoparticles by transferring •-electrons. Saponins have rich content of –OH and C=C groups and can easily donate the electron when they contact with $HAuCl_4$ in extracellular medium and thus reduce the Au^{3+} ion to Au^{o}. To aid the synthesis process we employed the microwave irradiation for synthesis of AuNPs which has an advantage of homogeneous nucleation of nanoparticles and thereby facilitating the rapid formation of AuNPs (Yin et al., 2004).

We observed that the solution containing unreduced gold ions (Au^{3+}) and AF turned into ruby red after around 40 sec of MW irradiation. UV-Vis scanning of the

colored solution in the range of 400–700 nm exhibited bands for surface plasmon resonance (SPR) indicating the formation of AuNPs (**Figure 4.1E**). The SPR peaks corresponding to 1 and 2% of AF against 1mM of $HAuCl_4$ were located at around 600 and 550 nm, respectively, suggesting the formation of larger AuNPs. For 3–5% of AF, SPR peaks were blue-shifted and located at around 527±2 nm which were characteristic of spherical AuNPs. As SPR peak position and intensity are indicative of particle size and concentration, respectively, we concluded that AF above 3% can form AuNPs with spherical shape. At 3–5% AF, differences in SPR peaks and intensity were seen to be negligible and thus 3% of AF was considered as the optimum concentration for efficient reduction of 1mM $HAuCl_4$ to AuNPs.

MW irradiation time was optimized with this optimized AF concentration. A gradual transition of change in the colour of the reaction mixture obtained at different time of MW irradiation can be seen in the inset of **Figure 2.3E**. For 10, 20 and 25 s no SPR peaks were observed. At 30 s the intensity of SPR band of AuNPs was found to be low with a peak around 536 nm, which indicated the formation of spherical particles. With increased MW irradiation from 30 to 40 s, the intensities of SPR bands increased considerably with narrow peaks shifted to 525–530 nm. For 40–60 s irradiations, increase in the SPR band intensities was very low which indicated complete reduction of gold ions. Thus we considered 40 s of MW irradiation to be optimum for the AuNPs synthesis (**Figure 2.3E**).

We have synthesized AuNPs using the aqueous fraction of *C. procera* by conventional heating. We made a comparison of the two methods, namely, “conventional heating” and “MW irradiation” as shown in **Table 4.1**. It can be seen that MW irradiation incredibly took less time, produced smaller sized AuNPs, and consumed less AF, while

there was no major effect on the shape and biocompatibility. Thus MW irradiation offered a method of rapid synthesis of the finer AuNPs over conventional heating.

TEM analysis of the AuNPs synthesized in 16 s MW irradiation time with 0.4% FLE showed the dominance of spherical and hexagonal particles which were well dispersed without any agglomeration (**Figure 4.4A).** The shapes of AuNPs were triangular, hexagonal, rod shaped and spherical. A histogram representing the size distribution of AuNPs corresponding to TEM image exhibited the variation in the particle size ranging from 3 to 20 nm with the average of 8.3 nm. AuNPs having 5 and 20 nm as an average size were spherical and hexagonal, respectively. We have employed the TEM technique to visualize the size and shape of formed AuNPs synthesized using PLE. **Figure 4.4B** shows the typical bright-field TEM image of AuNPs obtained with optimum reaction conditions and reveals that the majority of AuNPs formed were circular in shape. TEM analysis of the AuNPs synthesized using CW with 0.250 mM for 17 s of MW irradiation showed the dominance of nearly spherical particles, which were well dispersed without any agglomeration (**Figure 4.4C**). Typical bright-field TEM image of AuNPs synthesized using SFE with optimum reaction conditions showed diverse shaped nanoparticles. The size of the AuNPs synthesized was ranges from 5-50 nm and the average size was found to be 7.4 nm (**Figure 4.4D**). Typical TEM images of AuNPs synthesized using 0.8% SmFE and 1 mM $HAuCl_4$ showed that majority nanoparticles of hexagonal and spherical in shape (**Figure 4.4E**). We observed the wide range of particles size distribution (3-50 nm) with optimized parameters (0.8% SFE and 1 mM $HAuCl_4$). Furthermore, we wanted to narrow down the particles size distribution by changing the parameters. This was achieved with 0.6% SFE and 0.6 mM $HAuCl_4$ with predominant particles size as 25 nm (**Figure 4.5**). TEM analysis also revealed that the AuNPs were showed excellent dispersion which was due to the fact that the biomolecules mainly saponins are bounded

on nanoparticles and facilitating the repulsion of AuNPs thereby dispersing AuNPs in aqueous medium. A representative TEM image and corresponding size distribution histogram of AuNPs synthesized with optimized conditions (3% AF, 40 s MW irradiation time) is shown in **Figure 4.4F**. Spherical particles were more abundant than particles of other shapes. **Table 4.3** shows the morphologies of all synthesized AuNPs using FLE, PLE, CW, SFE, SmFE and C.procera (AF).

AFM analysis of AuNPs synthesized using CW with 0.250 mM with varying MW irradiation times was done in noncontact mode. At 9 s, the formation of AuNPs was negligible, whereas at 11and 17 s the process of AuNPs formation was accelerated, as can be seen from the AFM image (**Figure 4.6**).With the increase in MW irradiation time, there was no considerable alteration in the morphology of AuNPs. AFM analysis for 9, 11, and 17 s supported the results of UV-Vis spectroscopic studies (**Figure 4.3C**).

The ultra high resolution TEM (UHRTEM) image all AuNPs synthesized using FLE, PLE, CW, SFE, SmFE, and *C. procera (*AF) displayed clear lattice fringes on the particle surface (**Figure 4.7**). TEM (HRTEM) image showing clear lattice fringes of 0.22 nm, revealing that the growth of the AuNPs occurred preferentially on the (1 1 1) plane. The interplaner distance of the Au (1 1 1) plane was in agreement with the (1 1 1) d-spacing of bulk Au (0.2355 nm) (Shankar et al., 2004; Kannan et al., 2008; Babu et al., 2012c; Babu et al., 2012d).

Selected-area electron diffraction (SAED) pattern of AuNPs synthesized using FLE, PLE, CW, SFE, SmFE, and *C. procera (*AF) showed bright circular rings corresponding to Bragg's diffraction peaks which confirmed the crystalline nature of particles (Babu et al., 2010). The crystalline nature of the synthesized AuNPs was confirmed from the selected area electron diffraction (SAED) pattern with bright circular

rings corresponding to the (1 1 1), (2 0 0), and (2 2 0) planes (Babu et al., 2012e), as shown in (**Figure 4.8**).

The synthesized AuNPs were of different shapes and sizes i.e anisotropic. The histograms represent the ranges of AuNPs formed from different plants materials. The size ranges of AuNPs synthesized using FLE, PLE, CW, SFE, SmFE and C. procera (AF) and were of 3-20, 10-35, 5-20, 5-50, 3-50 and 5-20, respectively (**Figure 4.9)**.

XRD pattern suggested that the AuNPs synthesized using FLE, PLE, CW, SFE, SmFE and C. procera (AF) were crystalline in nature. Intense diffraction peaks were clearly observed at (1 1 1), (2 0 0) and (2 2 0) corresponding to the Bragg's angles at 38.1°, 44.4° and 64.5°, respectively. The ratio between the intensity of (2 0 0) and (1 1 1) diffraction peaks was much lower than the usual value (0.52), suggesting the (1 1 1) as the predominant plane (Babu et al., 2010; Das et al., 2010; Babu et al., 2011) (**Figure 4.10**).

FT-IR spectra of AuNPs synthesized with 0.4% FLE and 16 s of MW irradiation time indicated the presence of the bioorganic molecules on the AuNPs. FT-IR spectra of FLE showed strong signals at 3330, 2927, 1637, 1475, and 1084 cm^{-1} corresponding to hydroxyl group arising from alcohols and phenolic compounds, secondary amine, amide I bond of proteins, asymmetric deformation of CH3 from alkenes, and C–N stretching vibrations of amide bond, respectively. The vibrational absorption band at 1384 cm^{-1} was assigned to rocking of methyl group (Curve a in **Figure 4.11A**). FT-IR spectra of AuNPs showed strong signals at 3414 cm^{-1} (hydroxyl group of alcohols or phenols), 2418 cm^{-1} (hydroxyl group of carboxylic acids), 1668 cm^{-1} (amide I bond of proteins), 1390 cm^{-1} (methyl group of alkanes). The intense band that appeared at 1154 cm^{-1} can be ascribed to C–O–C or C–O stretching modes in phenolic compound or phenolic derivatives (Babu et

al., 2010; Das et al., 2010; Babu et al., 2011; Brugnerotto et al., 2001) (Curve b in **Figure 4.11A**).

NMR spectrum of the purified and lyophilized AuNPs confirmed the inclusion of biomolecules on AuNPs surfaces NMR signals at 7.98 and 1.79 ppm correspond to the protons of aromatic environment and alkyl/allylic groups, respectively. The signals at 2.84 and 2.92 were due to chemical environments belonging to acetylenic compounds **(Figure 4.13)**. NMR signals at 7.98 and 1.79 ppm correspond to the protons of aromatic environment and alkyl/allylic groups, respectively. The signals at 2.84 and 2.92 were due to chemical environments belonging to acetylenic compounds.

The involvement of functional groups in synthesized AuNPs was studied by FT-IR. The FT-IR spectra of PLE, as shown in **Figure 4.11B** (curve a), showed peaks at 3,495 cm^{-1} (hydroxyl group arising from alcohols and phenolic compounds), 2,865 cm^{-1} (secondary amine), 1,651 cm^{-1} (amide I bond of proteins), 1,422 cm^{-1} (C =C groups from alkenes), 1,328 cm^{-1} (C–CH_3 group), and 1,083 cm^{-1} (C–N stretching vibrations of amide bond), whereas the AuNPs showed peaks at 3,402, 2,865, 1,637, 1,365, and 1,046 cm−1, as indicated in **Figure 4.11B** (curve b) (Babu et al., 2011; Babu et al., 2010). The main significant difference between the spectrum of intact PLE before and after gold reduction is the disappearance peak at 1,328 cm^{-1} (curve a) and appropriate alteration of 1,422 to 1,365 cm^{-1}. This phenomenon revealed that biomolecules in the PLE, such as antioxidants, phenols, and flavonoids, that contain abundant aromatic C=C groups (1,422 cm^{-1}) may play an important role in the bioreduction and stabilization of AuNPs and may be responsible for the appearance of the significant peak at 1,365 cm^{-1} corresponding to the C–C bond. The three absorption peaks of AuNPs at 1,637, 2,865, and 3,042 cm^{-1} are attributed to the primary amines, alkyl, and OH groups, respectively. The reappearance of these groups in the spectrum of AuNPs suggested the attachment of some N– H, N=H,

and OH groups onto AuNPs during the biosynthesis process. Hence, it was deduced that AuNPs might be capped and stabilized by biomolecules (antioxidants, flavonoids, and polyphenols) originating from PLE (Babu et al., 2012a; Babu et al., 2012b).

An FTIR spectrophotometer (range 500–4000 cm^{-1}; Perkin-Elmer, Norwalk, CT) showed the spectra of AuNPs formed with different MW irradiation times (9, 11, and 17 s) and filtered CW. Both AuNPs and CW showed strong signals at 1042, 1627, and 3014 cm^{-1} corresponding to C–N stretching vibrations of amine, amide bond, and hydroxyl groups, respectively (**Figure 4.11C**) (Narayanan et al., 2008). AuNPs showed intense transmittance at 1042 cm^{-1} due to C–N stretching vibrations of amine originating from the protein molecules adsorbed on AuNPs. FTIR analyses suggested the presence of some proteins on the surface of the AuNPs and are perhaps responsible for the stability of the synthesized AuNPs. The adsorption pattern of biomolecules seems to be less influenced by the MW irradiation time as resulted by FTIR analysis (**Figure 4.11C, b-d)**. As confirmed from biochemical tests, CW was found to contain glucose (6.25 mg/mL), fructose (4.95 mg/mL), and about 1.9mg/100Gof ascorbic acid. These compounds could be responsible for the bioreduction of $HAuCl_4$ to AuNPs. Thus, the CW is a naturally occurring balanced cocktail for the synthesis of AuNPs that is readily available.

FT-IR spectra of AuNPs synthesized using SFE with optimized conditions indicated the presence of the biomolecules on the AuNPs. FT-IR spectra of SFE showed strong signals at 3454, 2951, 1649, 1431 and 1082 cm^{-1} corresponding to hydroxyl group arising from alcohols and phenolic compounds, secondary amine, amide I bond of proteins, asymmetric deformation of CH_3 from alkenes, and C–N stretching vibrations of amide bond, respectively (**Figure 4.11D** curve a). FT-IR spectra of AuNPs showed strong signals at 3440 cm^{-1} (hydroxyl group of alcohols or phenols), 2949 cm^{-1} (secondary amine), 1668 cm^{-1} (amide I bond of proteins), 1425 cm^{-1} (deformation of the -CH_3 from

alkanes) 1082 cm^{-1} (stretching vibrations of C–N from amide bond) (**Figure 4.11D,** Curve b) (Patel et al., 2005). These results confirmed the association of bioactive molecules in both SFE and AuNPs. The biochemical tests revealed that the presence of phenolic compounds and flavonoids in SFE. These bioactive molecules (phenolic compounds and flavonoids) reduced the Au^{3+} ion into Au^{o} nanoparticles by oxidizing hydroxyl (R-OH) to carbonyl groups (R-C=O) or transfer their •-electrons. During microwave irradiation process the bioactive molecules adsorbed onto the AuNPs and stabilize the synthesized AuNPs.

The involvement of surface functional groups on AuNPs was studied by FTIR. The FTIR spectra of SmFE, showed peaks at 3374 (hydroxyl group arising from hydroxyl group containing compounds), 2917 (secondary amine), 1641 (amide I bond of proteins), 1415 (C=C groups from alkenes), 1241 (C-CH_3 group) and 1025 cm^{-1} (C–N stretching vibrations of amide bond) (**Figure 4.11E,** curve a) where as the AuNPs showed the peaks at 3419, 1647, 1241 and 1049 cm^{-1} (**Figure 4.11E,** curve b). These peaks are attributed to the biomolecules such as saponins and triterpenoid present in SmFE. The main significant difference between the spectrum of intact SmFE (curve a) and AuNPs is the disappearance peak at 2917 and 1415 cm^{-1} (curve b). This phenomenon revealed that biomolecules (saponins, triterpenoid) that contain aromatic C=C groups (1415 cm^{-1}) might play an important role in the bioreduction and stabilization of AuNPs during the synthesis process. The absorption peaks on the AuNPs at 1647 and 3419 cm^{-1} attributed to the primary amines, alkyl and OH groups respectively (Babu et al., 2011; Babu et al., 2012). The reappearance of these groups in the spectrum of AuNPs suggested the attachment of some N–H, N=H and OH groups onto AuNPs during the biosynthesis process. Hence, it was deduced that AuNPs might be capped and stabilized by molecules originated from SmFE.

The FTIR spectrum of AF showed characteristic IR bands belonging to protein, alcoholic, or phenolic compounds (**Figure 4.11F,** curve a). Broad band at 3360 cm^{-1} was due to the hydroxyl functional group. Strong absorption bands at 1617 and 1080 cm^{-1} were characteristic of amide I and C–N stretching vibrations of amine, respectively. The band at 1228 cm^{-1} belongs to amide III. The characteristic peak for amide II seemed to have merged with the intense band of amide I. Band at 2918 cm^{-1} was assigned to secondary amine and band arising from the C=O stretching mode of carboxylic acid can be seen at 1364 cm^{-1}. FTIR spectrum of Au-NP (**Figure 4.11F,** curve b) showed strong bands for amide I (1625 cm^{-1}), C=O stretching mode of carboxylic acid, and C–N stretching of amines (1373 cm^{-1} and 1086 cm^{-1}). A comparative analysis of both FTIR spectra (**Figure 4.11F,** curve a,b) suggested active participation of AF proteins in the bioreduction of chlorauric acid to AuNPs. Changes in IR absorption bands and shifts in band positions at 1617 to 1625, 1080 to 1086, and 1364 to 1373 cm^{-1} supported a dominant role of protein molecules in the synthesis of AuNPs. Protein estimation (8 mgL^{-1}) of AF and retention of original colour of AuNPs solution even after treatment with strong electrolyte solution (10% NaCl), indicated for adsorption of proteins on AuNPs surfaces.

We performed the thermal gravimetric analysis to determine the content of the capping agents on the AuNPs. **Figure 4.12** shows the thermal degradation (TGA spectrum) of AuNPs occurs over a wide temperature range (200-480 ^{o}C) which revealed the significant weight loss of AuNPs (13%). This now clearly indicates that biomolecules were capped on the AuNPs and were completely degraded due to high temperature (200-480 ^{o}C). It is worthwhile to mention that there was further fall of spectrum beyond 885 ^{o}C as the temperature was attaining to melting point of gold 1,064 °C.

The elemental composition of the AuNPs synthesized using (A) FLE, (B) PLE, (C) CW (D) SFE (E) SmFE (F) *C. procera* (AF) were obtained by using Energy-Dispersive X-ray Spectroscopy (LEO 1430 VP) at variable pressure scanning electron microscope equipped with INCA Oxford EDX facility, at an acceleration voltage of 10 keV. The EDX profile of SFE, PLE, SFE and SmFE showed the different elements on the synthesized AuNPs. The X-ray EDX profile of AuNPs showed a strong signal for gold and aluminium along with very weak carbon, nitrogen and oxygen peaks. The signal for Al originated from the aluminium grid used for the analysis. The signal for Cu originated from the grid used for the analysis. The resulting carbon and oxygen peaks may have originated from the antioxidants/flavonoids/phenolic or organic biomolecules bound to the surface of the AuNPs (**Figure 4.14**).

The cytotoxicity of AuNPs synthesized using FLE under in vitro conditions in HeLa, MCF-7 and IMR-32 cells was examined in terms of effect of AuNPs on cell proliferation by MTTassay for 24 h. In this assay, only cells that are viable after 24 h exposure to the AuNPs can metabolize MTT efficiently and produce purple coloured crystal which is soluble in DMSO. After 24 h of post treatment, the three cell lines (HeLa, MCF-7 and IMR-32) showed excellent viability up to as high as 100 µmol/L of AuNPs (**Figure 4.15A)**. The cellular morphologies of three cell lines were unaltered after treatment with AuNPs suggesting that treatment with AuNPs did not induce any cytotoxic effect causing significant damage or death of the treated cells. This indicated that the FLE provided a nontoxic coating on the surface of AuNPs. It is also important to notice that a vast majority of gold (I) and gold (III) compounds exhibit varying degrees of cytotoxicity to a variety of cells (Kreft et al., 2002; Patel et al., 2005). The lack of any noticeable toxicity of AuNPs synthesized with FLE provides an opportunity for application in delivery and molecular imaging. Furthermore, the average sizes of AuNPs were 8.3 nm

while the living sub cellular parts are in the sub-micron sized domain for which the synthesized AuNPs can be used for targeting and delivery.

The cytotoxicity of AuNPs synthesized suing PLE under in vitro conditions in HeLa and MCF-7 cells was examined by MTT assay for 24 h in terms of effect of AuNPs on cell proliferation. Only cells that are viable after 24-h exposure to the AuNPs can metabolize MTT efficiently and produce purple colored crystal which is soluble in DMSO. **Figure 4.15B** shows the viability of both HeLa and MCF-7 cancer cell lines after 24 h post treatment and showed excellent viability as high as 100 µmol/L of AuNPs. **Figure 4.16** shows unaltered cellular morphologies of two cell lines after treatment with AuNPs, suggesting that treatment with AuNPs did not induce any cytotoxic effect causing significant damage or death of the treated cells. This indicated that the PLE provided a nontoxic coating on the surface of AuNPs. This revealed that the synthesized AuNPs were of insignificant toxicity on cancer line, providing an opportunity for application in drug delivery and molecular imaging.

In the MTT-based cytotoxicity assay, after 24 h of post treatment, HeLa and MCF-7 cells showed high viabilities, 87±4% and 85±3.2% for HeLa and MCF-7, respectively, at maximum dose (100 μM) of AuNPs synthesized using CW (**Figure 4.15C**). Both cell lines retained their cellular morphologies, suggesting that treatment with AuNPs did not induce any cytotoxic effect causing significant damage or death of the treated cells (**Figure 4.17**). It is worth mentioning that a vast majority of gold (I) and gold (III) compounds exhibit varying degrees of cytotoxicity to a variety of cells (Basset et al., 2003; Shaw et al., 1999). The lack of any noticeable toxicity of the present AuNPs proves them to be highly biocompatible.

The cytotoxicity of AuNPs synthesized using SFE under in vitro conditions in HeLa and MCF-7 cells was examined using MTT assay for 24 hrs. The principle

involves, only cells that are viable after 24 h exposure to the AuNPs can metabolize MTT efficiently and produce purple coloured crystal which is soluble in DMSO. The cellular morphologies of two cell lines were unaltered after treatment with AuNPs suggesting that treatment with AuNPs did not induce any cytotoxic effect causing significant damage or death of the treated cells. Both HeLa and MCT-7 cell lines showed excellent viability upto as high as 100 µ mol/L of AuNPs after 24 h of post treatment (**Figure 4.15D**). HeLa cell showed more resistance to synthesized AuNPs, comparatively with MCF-7. These results indicated that the SFE provided a nontoxic coating on the surface of AuNPs. Therefore, the synthesized AuNPs were of insignificant toxicity on cancer line provides an opportunity for applications in molecular imaging and drug delivery.

The cytotoxicity of AuNPs synthesized using SmFE under in vitro conditions in HeLa and MCF-7 cells was examined in terms of effect of AuNPs on cell toxicity by MTT assay for 24 h. Only cells that are viable after 24 h exposure to the AuNPs can metabolize MTT efficiently and produce purple coloured crystal which is soluble in DMSO. The cellular morphologies of two cell lines were unaltered after treatment with AuNPs suggesting that treatment with AuNPs did not induce any cytotoxic effect causing significant damage or death of the treated cells. The two cancer cell lines (HeLa and MCF-7) after 24 h of post treatment showed excellent viability up to as high as 100 µ mol/L of AuNPs (**Figure 4.15E**). This indicated that the SmFE provided a nontoxic coating on the surface of AuNPs. This revealed that the synthesized AuNPs were of insignificant toxicity on cancer line provides an opportunity for application in delivery and molecular imaging.

The cytotoxicity of AuNPs synthesized using *C. procera* (AF) under in vitro conditions in HeLa and MCF-7 cells was examined in terms of effect of AuNPs on cell toxicity by MTT assay for 24 h. Only cells that are viable after 24 h exposure to the

AuNPs can metabolize MTT efficiently and produce purple coloured crystal which is soluble in DMSO. The cellular morphologies of two cell lines were unaltered after treatment with AuNPs suggesting that treatment with AuNPs did not induce any cytotoxic effect causing significant damage or death of the treated cells. The two cancer cell lines (HeLa and MCF-7) after 24 h of post treatment showed excellent viability up to as high as 100 µ mol/L of AuNPs (**Figure 4.15F**). This indicated that the SFE provided a nontoxic coating on the surface of AuNPs. This revealed that the synthesized AuNPs were of insignificant toxicity on cancer line provides an opportunity for application in delivery and molecular imaging. **Table 4.4** shows the cytotoxicity of the AuNPs synthesized using FLE, PLE, CW, SFE, SmFE and *C. procera* (AF).

4.5 Conclusions

The method of employed for AuNPs synthesis has advantages such as rapidness, use of biologically benign biomaterial, and most importantly, resulting in biocompatible AuNPs. We have investigated the optimum parameter for synthesizing the AuNPs using FLE (0.4% FLE, 1 mmol/L $HAuCl_4$ and 16 s), PLE (4% PLE and 0.7 mM $HAuCl_4$ for 30 s.), CW (0.250 mM $HAuCl_4$ and 17 s), SFE (0.03% FLE, 0.5 mM $HAuCl_4$ and 20 sec), SmFE (8% SFE and 1mM $HAuCl_4$ for 25 s) and *C. procera* (3% AF, 1mM $HAuCl_4$ and time 40 sec). Biomolecules such as flavonoids and phenolic compounds found in plant and fruits extracts are involved in the reduction of gold ions to AuNPs. AuNPs synthesized using *C. procera* (AF) were stabilized by protein capping as confirmed from coagulation test. The crystallinity of AuNPs was confirmed by XRD analysis. FT-IR, NMR and EDX analyses demonstrated the presence of biomolecules on the surface of AuNPs arising from the strong reducing molecules such as phenolic compounds, flavonoids and antioxidants which are involved in the reduction of gold salts to AuNPs. The cellular morphologies of cell lines were unaltered after treatment with AuNPs

suggesting that treatment with AuNPs did not induce any cytotoxic effect causing significant damage or death of the treated cells. The cancer cell lines (HeLa, IMR-32 and MCF-7) after 24 h of post treatment showed excellent viability up to as high as 100 µ mol/L of AuNPs. This indicated that the plant and fruits extracts provided a nontoxic coating on the surface of AuNPs. This revealed that the synthesized AuNPs were of insignificant toxicity on cancer line provides an opportunity for application in delivery and molecular imaging.

---***---

5.1 Introduction

Synthesis of gold nanoparticles (AuNPs) using plant extract has gained importance as they possess unique chemical, physical, biological and optoelectronic properties which depend on shape and size of nanoparticles and are exploited in a wide range of applications such as in biology, chemical sensing of single molecule, controlled release, catalysis, and immunoassays (Giljohann et al., 2010; Ghosh et al., 2008; Lewis et al., 1993; Lee et al., 2004; Bhattacharya et al., 2008). The conventional synthesis of AuNPs involves the application of strong reducing and stabilizing agents, which remain in the products and are potential hazards to human health (uboldi et al., 2009). Therefore, there is a continuous attempt to use green synthetic methods whereby, nanoparticles can be synthesized by using biological resources that are capable of replacing synthetic reducing and stabilizing agents. There are numerous research articles emphasized on the plant extract for the synthesis of AuNPs (Narayanan et al., 2011). As a part of an effort to screen new plants for synthesizing AuNPs, we found that the ethanolic leaf extract of Andrographis paniculata (A. paniculata) can be successfully used for the synthesis of stable AuNPs.

A. paniculata, a native of India and Sri Lanka, is an annual herbaceous plant (family: Acanthaceae), extremely bitter, about 3 feet high and one of the most commonly used plants in traditional systems of Unani and Ayurvedic medicines. This herb is popularly known as ‘Maha-tita’ (king of bitters) or ‘Chirota-tita’ in the northeast of India. It can be found in variety of habitats such as planes, hill sides, coastlines, roadsides, farms, and wastelands. It has been revealed that A. paniculata leaf extract (ALE) contains diterpenes, flavonoids and stigma sterols (Siripong et al., 1992). The extract possesses ent-labdane diterpenoids and andrographolide as the main bioactive compounds which have wide spectrum of biological applications such as antibacterial (Singha et al., 2003),

antimalarial (Dua et al., 2004), antithrombotic (Thisoda et al., 2006), antitumor (Yang et al., 2009), immunostimulatory (Puri et al., 1993) properties. A. paniculata has been reported to have anti-inflammatory (Sheeja et al., 2008) and antiallergic activities. The anti-inflammatory action of the plant is attributed to andrographolide, the major active principle ingredient of the plant (Madav et al., 1996). A. paniculata also helps in boosting the immune system, protects against cancer and HIV (Chang et al., 1988), prevents blood clots, diabetes and hypertension (Ahmad et al., 1993), and maintains efficient digestive functioning (Jarukamjorn et al., 2008). It has many applications, including treatment of dyspepsia, influenza, dysentery, malaria, respiratory infections and as antidote for snake-bite and poisonous stings of some insects (kirtikar et al., 1975). It is also considered to be used as antiphlogistic antipyretic, detoxicant, analgesic and an agent for the treatment of acute infections of the respiratory organs and urinary system and gastrointestinal tract (Nazimudeen et al., 1978). We designed the current work by considering the bioactive molecules present in A. paniculata such as andrographolide, flavonoids, antioxidants, diterpenes and stigma sterols which can facilitate the reduction of various metal salts to their corresponding nanoparticles. For the rapid synthesis of AuNPs, we applied ultrasonication (sonics, VC 505 Vibra Cell), which has an advantage of formation of the acoustic bubble and generation of immense heat (Suslick et al., 1990) thereby influencing the nucleation process of AuNPs. Further, we have functionalized AuNPs with polycaprolactone (PCL), gelatin (GL) and PCL–GL which are named as AuNP–PCL, AuNP–GL and AuNP–PCL–GL composites, respectively. The as-synthesized intact AuNPs were tested for their cytotoxicity using human cancer cell lines HeLa and MCF-7. However, AuNPs showed insignificant effect on cell viability, indicating their biocompatibility. Therefore, this green approach is a successful method for the synthesis

of stabilized AuNPs and the functionalization with natural polymers without the involvement of chemical agents.

5.2 Materials and Methods

5.2.1 Materials

A. paniculata was grown as per traditional agronomic practice in the experimental field and healthy leaves were harvested for the AuNPs synthesis. Cell lines were obtained from National Centre for Cell Sciences (Pune, India). Cell culture related plasticwares were obtained from the Sigma-Aldrich (Bangalore, India). All the reagents were of analytical grade obtained from either Sisco Research Laboratories (Mumbai, India) or E. Merck India Ltd. (Mumbai, India). 3-(4, 5-dimethylthiazol-2-yl)-2, 5-diphenyltetrazolium bromide (MTT) was purchased from HiMedia (Bangalore, India).

5.2.2 Preparation of leaf extract

A. paniculata leaves were washed with deionised water to remove adsorbed dirt. The leaves were chopped into small pieces (2 cm _ 2 cm) and dried at room temperature (25 °C) under shade. Then the dried leaves were powdered in a mixer grinder (Bajaj Model GX 11, India). About 5 g of powder was dissolved in 50 mL of ethanol and kept at 4 °C for one week to get the leaf extract. The ALE was filtered using Whatman 50 mm filter papers and the filtrate was stored at 4 °C for various experiments.

5.2.3 Test for flavonoids and phenolic compounds

To the 5 mL of diluted NH_3 solution, 2 mL of ALE was added, followed by few drops of concentrated H_2SO_4. The yellow colour indicated the presence of the flavonoids. To the 2 mL of ALE, few drops of 5% $FeCl_3$ were added. The appearance of dark green colour indicated the presence of polyphenolic compounds.

5.2.4 Synthesis of AuNPs using *A. paniculata* plant extract (ALE)

Synthesis of AuNPs was carried out by varying the ALE (0.5%–5%) against to 1 mmol/L $HAuCl_4$ and the final volume was made up to 2 mL with double distilled water. To all the resulting mixtures, we applied ultrasonication for 2 min with 30% amplitude at room temperature. To find out the optimum concentration of $HAuCl_4$, the experiments were carried out by varying the gold solution concentration in the range of 0.5–3 mmol/L against 3.5% of the ALE. The optimum time for synthesis was determined by incubating 3.5% of ALE with 1 mmol/L $HAuCl_4$ by varying the sonication time in the range of 1–4 min with an interval of 30 s. All the reactions were done with pulse off and on 4 s each.

5.2.5 Effect of amplitude and pH on the synthesis of AuNPs

To identify the effect of amplitude and pH, we applied the ultrasonication for 120 s to the reaction mixtures comprising of ALE (3.5%) and $HAuCl_4$ (1 mmol/L) by varying the amplitude from 21% to 35% and adjusting the pH value of reaction mixtures from 1 to 11.

5.2.6 Functionalization of AuNPs with PCL, GL, and PCL–GL

Both PCL and GL, 0.25% of each, separately, was added to the 5 mL of dimethyl formamide (DMF) and 5 mL of the pre-warmed water, respectively, and the total volume of each reaction mixture was adjusted to 20 mL with distilled water containing ALE (3.5%) and $HAuCl_4$ (1 mmol/L). For functionalization of PCL–GL, the reaction mixtures (0.25% of PCL in 5 mL of DMF and 0.25% of GL in 5 mL of pre-warmed water) were mixed together and the total volume was adjusted to 20 mL of distilled water containing ALE (3.5%) and $HAuCl_4$ (1 mmol/L). For all the reaction mixtures we applied ultrasonication for 10 min at the 35% amplitude.

5.2.7 Characterization of AuNPs

5.2.7.1 Ultraviolet-visible (UV-vis) spectroscopy

All UV-vis spectroscopic measurements of synthesized AuNPs were carried out on a Cary 100 BIO UV-Vis spectrophotometer (Varian, CA, USA).

5.2.7.2 Transmission electron microscopy (TEM)

A volume of 10 mL of the AuNP solution was centrifuged at 20,000 rpm for 20 min. The resulted pellet was resuspended in 3 mL of distilled water and centrifuged at 20,000 rpm for 20 min. This process was repeated thrice and the resultant pellet was resuspended in 1 mL of distilled water. Few drops of the redispersed colloidal solution were placed over carbon coated copper grid and the water was evaporated in hot air oven (Daihan Labtech Co. Ltd. model LDO-150F) at 60 °C for 4 h. TEM measurements were performed on a transmission electron microscope (TEM-JEOL model 2100) operated at 190 Vof 200 kV.

5.2.7.3 X-ray diffraction (XRD), Fourier transform infrared (FT-IR) spectroscopy and energy dispersive X-ray (EDX) spectroscopy.

The colloidal solution mixtures obtained in Section 5.2.6 were centrifuged at 20,000 rpm and resulted pellets were resuspended in appropriate volume (3 mL) of double distilled water. This process was repeated for three times to obtain the pure nanoparticles of the respective type. Finally, each resulted pellets was redispersed in 5 mL of double distilled water and freeze dried in a lyophiliser (Christ Gefriertrocknungsanlagen GmbH Model 1-4) for 16 h. The fine dried powder samples were analyzed with the help of an XRD instrument (Bruker Advance D8 XRD machine) with Cu source at the wavelength of 1.5406 A^{o} in thin film mode. Infrared spectra were recorded using a FTIR spectroscope (Spectrum One, Perkin Elmer, MA, USA), from 4000 to 450 cm^{-1}, with a resolution of 2 cm^{-1} and 5 scans/sample by pressing the 1 mg of each finely powdered AuNP, AuNP–PCL, AuNP–GL, and AuNP–PCL–GL powders with 200 mg KBr.

The elemental composition of the intact AuNPs were obtained by using EDX spectroscopy (LEO 1430 VP) at variable pressure scanning electron microscope equipped with INCA Oxford EDX facility, at an acceleration voltage of 10 keV.

5.2.8 Cytotoxicity studies

The minimal essential medium (MEM) containing 1.0 mmol/L $C_3H_3NaO_3$, 0.1 mmol/L nonessential amino acids, 1.5 g/L $NaHCO_3$, 2 mmol/L L-glutamine supplemented with 10% fetal bovine serum (FBS; heat inactivated) and 1% antibiotic-antimycotic solution (1000 U/mL penicillin G, 10 mg/mL streptomycin sulphate, 5 mg/mL gentamycin, and 25 µg/mL amphotericin B) was used to maintain the HeLa (human cervical cancer) and MCF-7 (human breast cancer) cells. The cells were cultured at 37 °C in a humidified incubator (Heal Force, HF 160W, China) supplemented with 5% CO_2.

The cytotoxicity of AuNPs on cancer cells was evaluated by the MTT assay, which is a widely used screening method to measure cell viability and proliferation. The monocultures of the HeLa and MCF-7 cells were incubated with increasing concentrations of filter (0.2 µm) sterilized AuNPs for 24 h. The cell viability was estimated by MTT dye conversion assay. Cells not exposed to AuNPs were considered as control. About 1_104 cells were seeded and maintained in a 96-well plate (Cell Bind, Corning) using MEM containing serum. After 24 h of incubation, the medium was replaced with the serum free medium containing various concentrations of AuNPs (10–100 µmol/L). The media was removed after 24 h of treatment and cells were washed with phosphate-buffered saline (PBS; 0.01 mol/L, pH = 7.2) followed by the addition of 100 µL of MTT (0.5 mg/mL) prepared in serum free medium to each well and incubated for 4 h in an incubator. Subsequently, medium was removed and 100 µL of dimethyl sulphoxide (DMSO) was added to each well to solubilise the formazan crystals. The concentration of formazan was determined using a multiwell plate reader (Tecon micro-

plate reader, model 680, CA, USA) at 470 nm absorbance. The cell viability was calculated with the following equation:

$$\text{Cell viability (\%)} = (A_{\text{treated}}/A_{\text{control}}) \text{ X } 100$$

Where A_{treated} and A_{control} are the absorbance's of treated and untreated cells, respectively.

5.2.9 Statistical analysis

Experiments with quantitative data were done in replicates of four independent experiments and the results were expressed as Mean ± Standard Deviation ($n = 5$)

5.3. Results

5.3.1 Formation of spherical AuNPs from ALE in the ultrasonication process under optimum conditions

In an effort to optimize parameters for the synthesis of spherical AuNPs, different reactions were carried out by varying the concentration of ALE (0.5%–5%) against 1 mmol/L $HAuCl_4$ for 120 s of the ultrasonication time, which resulted in appearance of ruby red colour in all the reaction mixtures indicating the synthesis of AuNPs. We found that 3.5% ALE reduced the 1 mmol/L of $HAuCl_4$ and considered as optimum for AuNPs synthesis. To find out the optimum concentration of $HAuCl_4$, we carried out various experiments with 3.5% ALE by changing the concentration of the gold salts from 0.5 to 1 mmol/L and observed the maximum peak intensity associated with 1 mmol/L $HAuCl_4$ and thus we considered as an optimum (**Figure 5.1**).

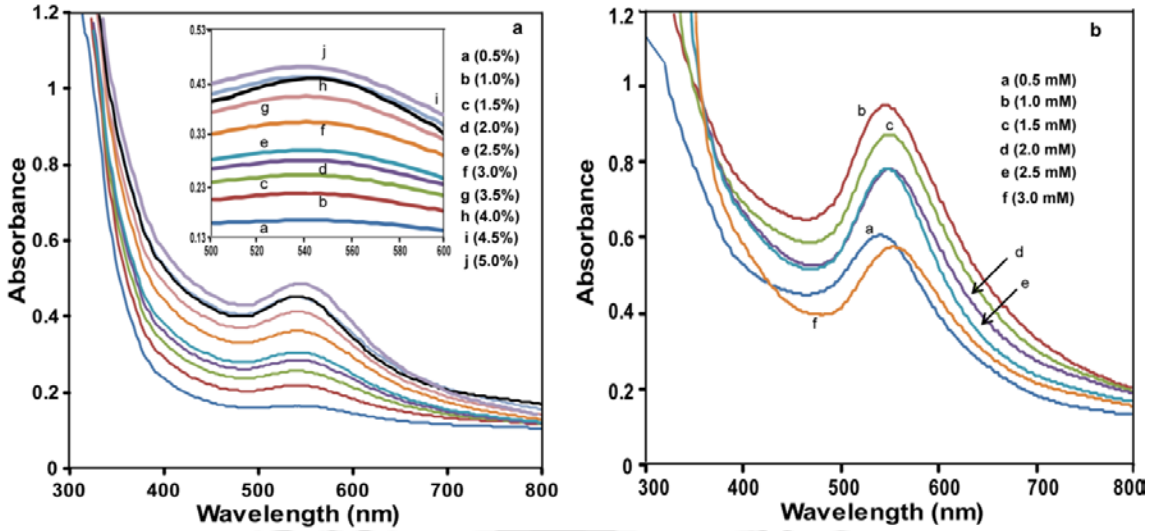

Figure 5.1 *UV-Vis absorption spectra of AuNPs synthesized by (a) varying ALE concentrations (a — 0.5%, b — 1%, c — 1.5%, d — 2%, e—2.5%, f—3%, g—3.5%, h—4%, i—4.5%, j—5%) for 2 min against 1 mmol/L $HAuCl_4$ and (b) varying $HAuCl_4$ concentrations (a — 0.5 mmol/L, b — 1 mmol/L, c — 1.5 mmol/L, d — 2 mmol/L and e — 2.5 mmol/L, f — 3 mmol/L) against 3.5% ALE.*

The optimum ultrasonication time required for the AuNPs synthesis was determined by performing various experiments with 3.5% ALE and 1 mmol/L $HAuCl_4$ for different ultrasonication time from 60 to 240 s with an interval of 30 s and we found 120 s to be the optimum time.

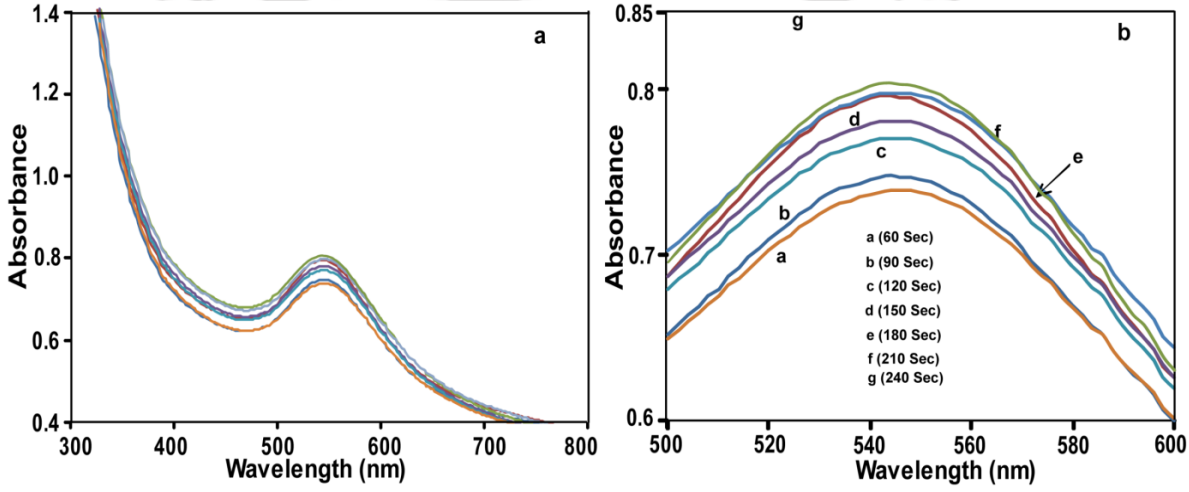

Figure 5.2 *UV-Vis absorption spectra of AuNPs synthesized with 3.5% ALE and 1 mmol/L $HAuCl_4$ by different ultrasonication time (a —60 s, b—90 s, c—120 s, d—150 s,*

e—180 s, f—210 s, g—240 s): (a) wavelength range from 300 to 800 nm; (b) wavelength range from 500 to 600 nm.

Figure 5.3 represent the schematic representation of sonocatalytic synthesis of AuNPs under optimized conditions (3.5% ALE, 120 s ultrasonication time, 1 mmol/L $HAuCl_4$, 35% amplitude and pH 5). The gradual increment in the formation of AuNPs was observed with the increase of the amplitude (**Figure 5.4**). We found that the peak pertaining to 35% amplitude showed the maximum intensity out of the various experiments performed with 3.5% ALE and 1 mmol/L of $HAuCl_4$ by varying the different amplitudes from 21% to 35% for 120 s of the ultrasonication time and was, thus, considered as the optimum.

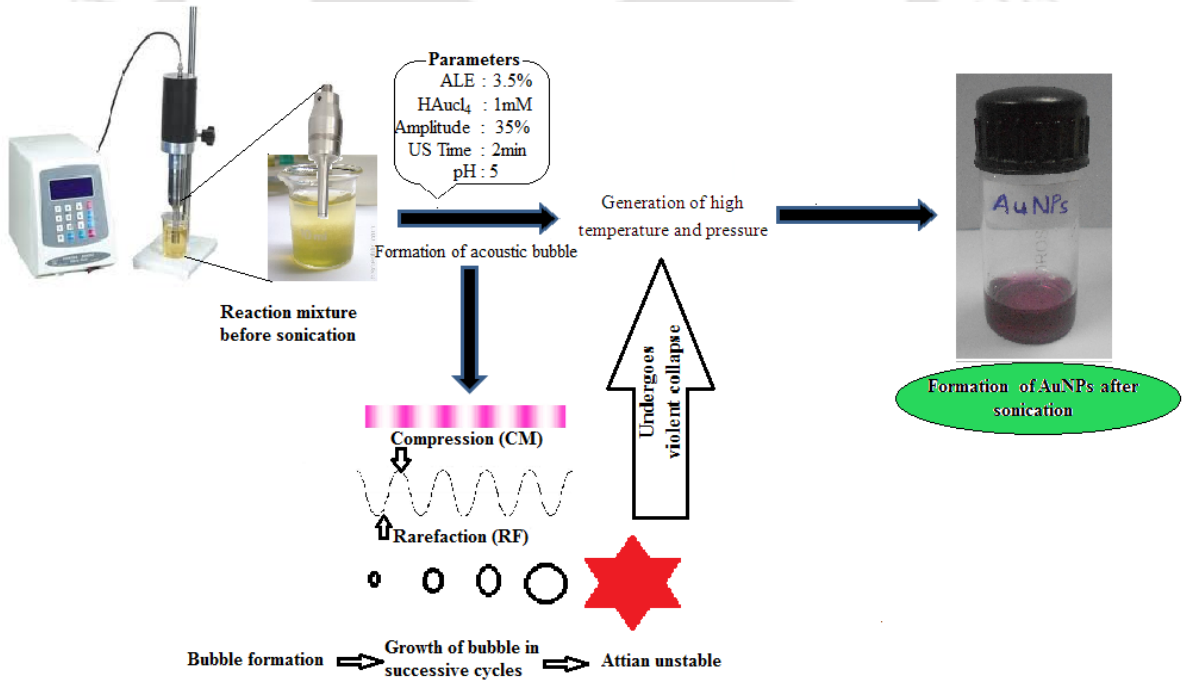

Figure 5.3 *Schematic representation of sonocatalytic synthesis of AuNPs under optimized conditions (3.5% ALE, 120 s ultrasonication time, 1 mmol/L $HAuCl_4$, 35% amplitude and pH 5).*

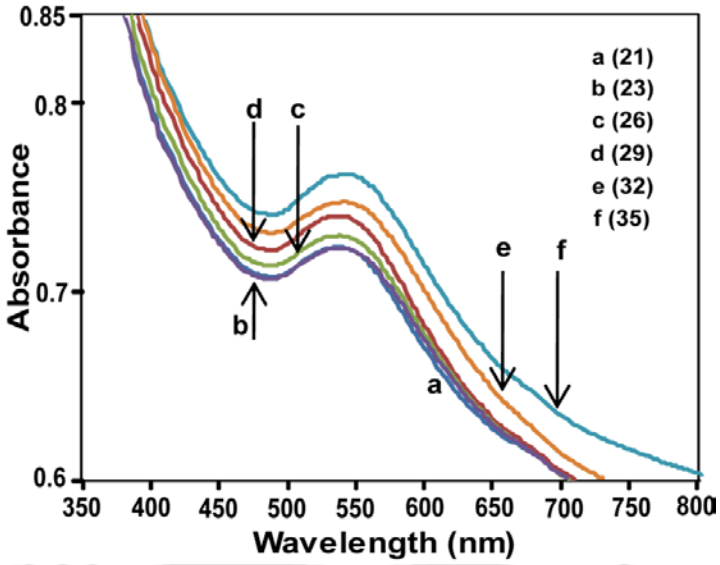

Figure 5.4 *UV-Vis absorption spectra of AuNPs synthesized with 3.5% ALE and 1 mmol/L* $HAuCl_4$ *for 120 s of the ultrasonication time by varying the ultrasonication amplitude (a — 21%, b —23%, c — 26%, d — 29%, e — 32%, f — 35%).*

The pH of the intact reaction mixture before embarking into experiments was found to be 4.87. We observed pH 5 as an optimum from the experiments performed with 3.5% ALE, 1 mmol/L of $HAuCl_4$ by adjusting the pH (1–11) for 120 s of ultrasonication (**Figure 5.5**).

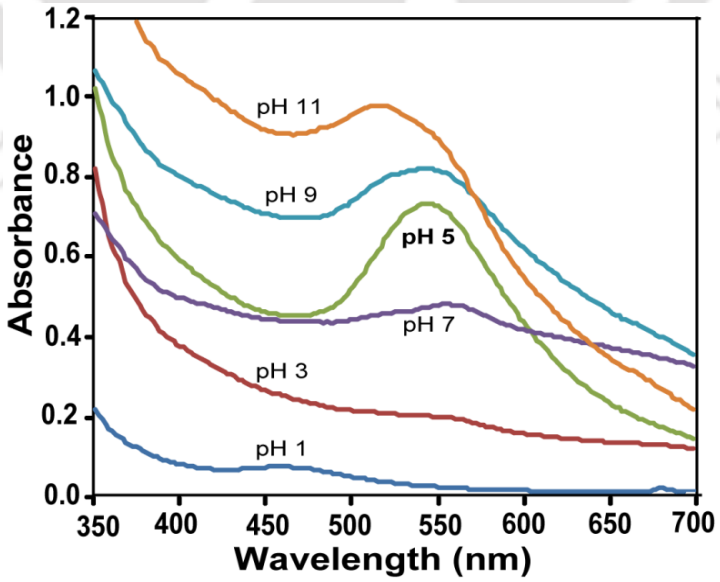

Figure 5.5 *UV-Vis absorption spectra of AuNPs synthesized with 3.5% ALE and 1 mmol/L $HAuCl_4$ for 120 s of the ultrasonication time by varying the pH value.*

We found that optimum parameters for the synthesis of spherical AuNPs are ALE (3.5%), $HAuCl_4$ (1 mmol/L), amplitude (35%), pH 5 and ultrasonication time (120 s). All these parameters resulted in the intense and narrow peaks ranging from 520 to 547 nm (**Figure 5.6**) which is an indication of the formation of nanoparticles ranging from 5-100 nm. The values of experiments (N=35) corresponding to a full experimental design with five variable factors such as $HAuCl_4$, ALE, sonication time, sonication amplitude and pH as shown in **Table 5.1.**

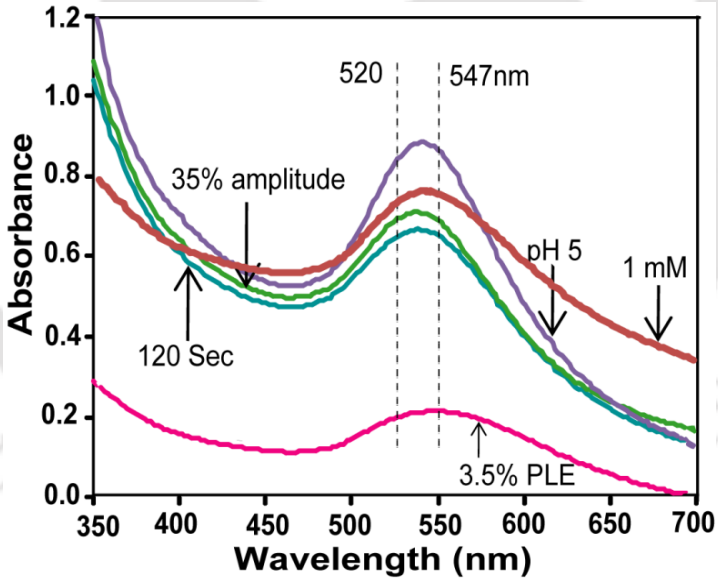

Figure 5.6 *UV-vis absorption spectra of AuNPs synthesized with optimized parameters: 3.5% ALE, 1 mM $HAuCl_4$, 120 s of the ultrasonication time, 35% amplitude and pH 5.*

Flavonoids interact with Au^{3+} ions through carbonyl groups or •-electrons and then reduced into AuNPs in the extracellular medium. As soon as they come in contact with Au^{3+} ions in extracellular medium, their •-electrons are transferred and Au^{3+} ions are

reduced to Au^{o}, as shown in **Scheme 5.1**. Flavonoids can also prevent agglomeration and stabilize AuNPs. Thus the involvement of flavonoids in the rapid reduction of Au^{3+} ions and as capping agent gives stability to AuNPs.

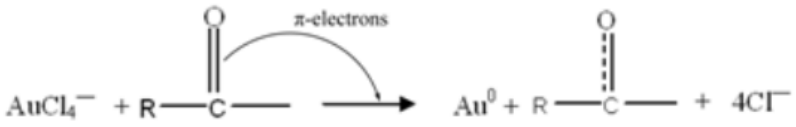

Scheme 5.1 *The reduction of Au^{3+} to Au^{o} by the transfer of carbonyl group •-electrons.*

Table 5.1 *The λ_{max} values of experiments (N = 35) corresponding to a full experimental design with five variable factors such as $HAuCl_4$, ALE, sonication time, sonication amplitude and pH.*

No of Runs	$HAuCl_4$ Concetration	ALE Extract	Sonication Time	Sonication Amplitude	pH of reaction mixture	Observed Peak position
1	1mM	0.50%	120 Sec	30	4.87	541
2	1mM	1%	120 Sec	30	4.87	541
3	1mM	1.50%	120 Sec	30	4.87	542
4	1mM	2.00%	120 Sec	30	4.87	538
5	1mM	2.50%	120 Sec	30	4.87	541
6	1mM	3.00%	120 Sec	30	4.87	539
7	1mM	3.50%	120 Sec	30	4.87	541
8	1mM	4%	120 Sec	30	4.87	541
9	1mM	4.50%	120 Sec	30	4.87	541
10	1mM	5%	120 Sec	30	4.87	541
11	0.5mM	3.50%	120 Sec	30	4.87	556
12	1.0mM	3.50%	120 Sec	30	4.87	541
13	1.5mM	3.50%	120 Sec	30	4.87	552
14	2.0mM	3.50%	120 Sec	30	4.87	552
15	2.5mM	3.50%	120 Sec	30	4.87	552
16	3mM	3.50%	120 Sec	30	4.87	548
17	1mM	3.50%	60 Sec	30	4.87	544
18	1mM	3.50%	90 Sec	30	4.87	544

19	1mM	3.50%	120 Sec	30	4.87	545
20	1mM	3.50%	150 Sec	30	4.87	544
21	1mM	3.50%	180 Sec	30	4.87	542
22	1mM	3.50%	210 Sec	30	4.87	544
23	1mM	3.50%	240 Sec	30	4.87	542
24	1mM	3.50%	120 Sec	21	4.87	540
25	1mM	3.50%	120 Sec	23	4.87	540
26	1mM	3.50%	120 Sec	26	4.87	540
27	1mM	3.50%	120 Sec	29	4.87	540
28	1mM	3.50%	120 Sec	32	4.87	544
29	1mM	3.50%	120 Sec	35	4.87	544
30	1mM	3.50%	120 Sec	35	1	No Peak observed
31	1mM	3.50%	120 Sec	35	3	No Peak observed
32	1mM	3.50%	120 Sec	35	5	563
33	1mM	3.50%	120 Sec	35	7	546
34	1mM	3.50%	120 Sec	35	9	547
35	1mM	3.50%	120 Sec	35	11	520

5.3.2 Characterization studies

5.3.2.1 Transmission Electron Microscope (TEM)

We performed TEM experiment to visualize the size and shape of AuNPs. Typical bright-field TEM image of AuNPs obtained with optimum reaction conditions showed that 96% of nanoparticles were of spherical in shape (**Figure 5.7a**). The size of the AuNPs synthesized ranged from 5 to 75 nm and the average size was found to be 9.97 nm (**Figure 5.7b**). The crystalline nature of the synthesized AuNPs was confirmed from the selected area electron diffraction (SAED) pattern with bright circular rings corresponding to the (1 1 1), (2 0 0), and (2 2 0) planes (**Figure 5.8a**). High-resolution TEM (HRTEM) image shown in (**Figure 5.8b**) revealed clear lattice fringes of 0.22 nm, indicating that the growth of the AuNPs occurred preferentially on the (1 1 1) plane.

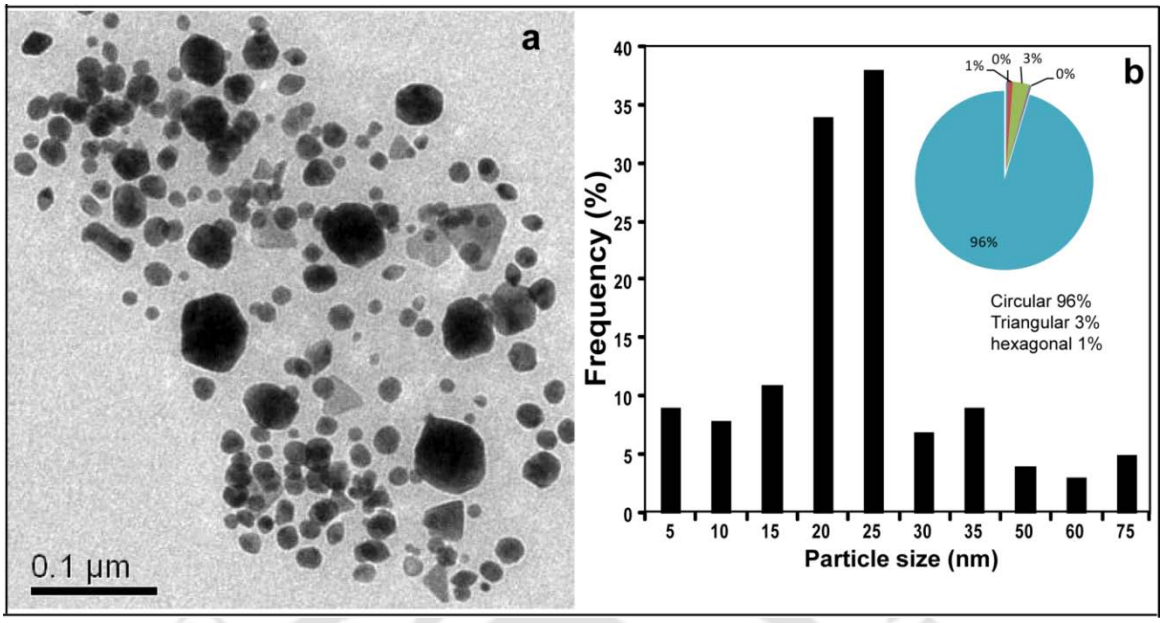

Figure 5.7 *(a) TEM image and (b) particle size distribution histogram of AuNPs synthesized with 3.5% ALE and 1 mmol/L $HAuCl_4$ for 120 s of the ultrasonication time at the 35% amplitude.*

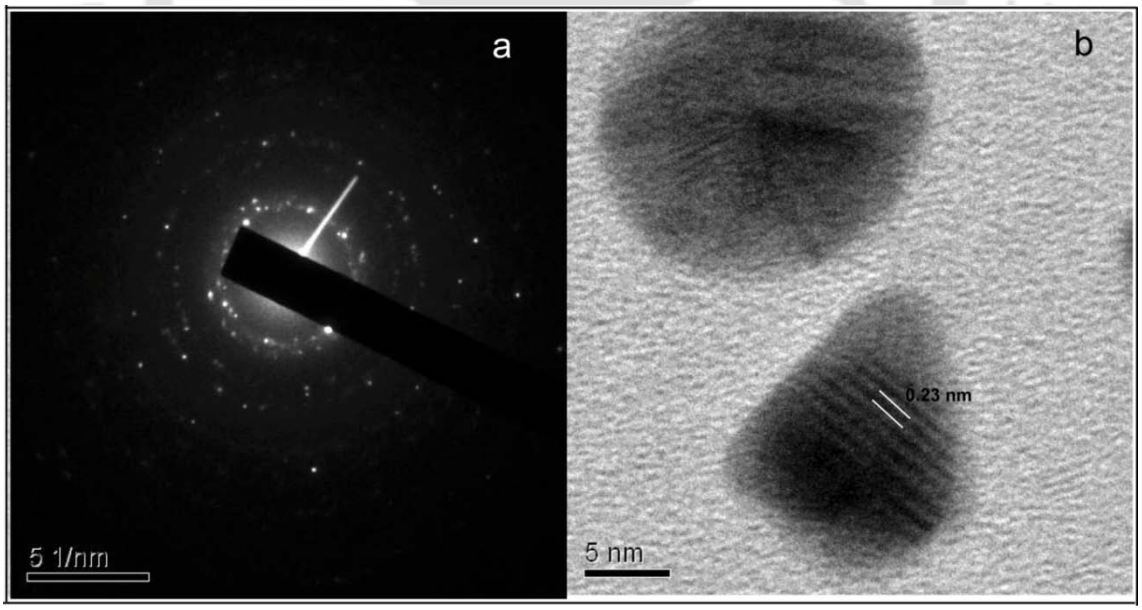

Figure 5.8 *(a) HRTEM image and (b) SAED pattern of AuNPs synthesized with optimized parameters (3.5% ALE, 1 mmol/L $HAuCl_4$, 35% amplitude and 120 s).*

5.3.2.2 EDX analysis

EDX profile of AuNPs revealed a strong signal for gold and copper along with very strong carbon, nitrogen and oxygen peaks. The EDX pattern suggested the presence of biomolecules on the surface of the synthesized AuNPs **(Figure 5.9)**.

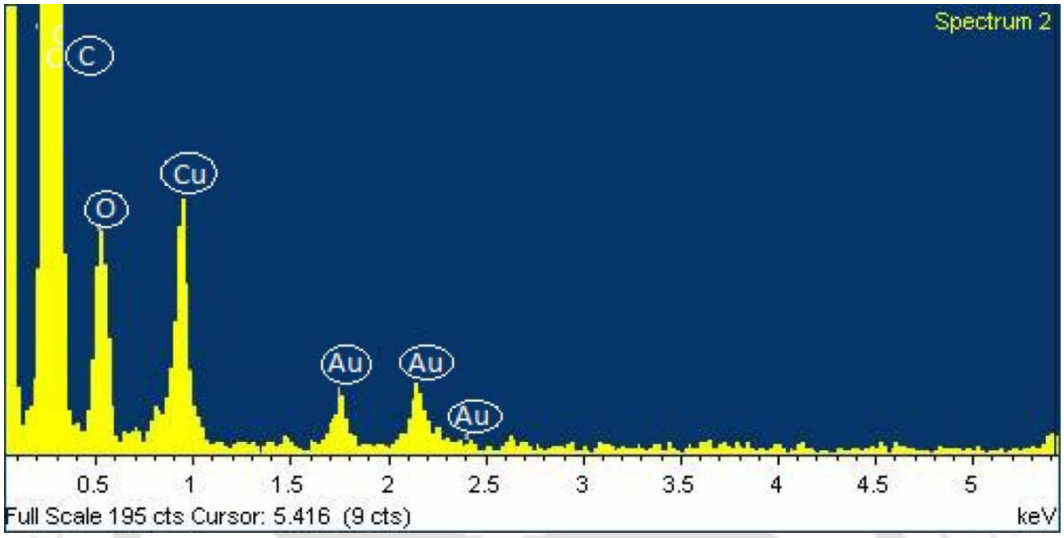

Figure 5.9 *EDX patterns of AuNPs synthesized with 3.5% ALE and 1 mmol/L $HAuCl_4$ at the 35% amplitude for the ultrasonication time of 120 s.*

5.3.2.3 X-ray Diffractrogram (XRD) analysis of AuNPs

The successful functionalization of PCL, GL, and PCL–GL onto the AuNPs was confirmed from XRD and FT-IR analyses. We observed the different coloured colloidal solutions for AuNP–PCL, AuNP–GL, and AuNP–PCL–GL composites (**Figure 5.10**).

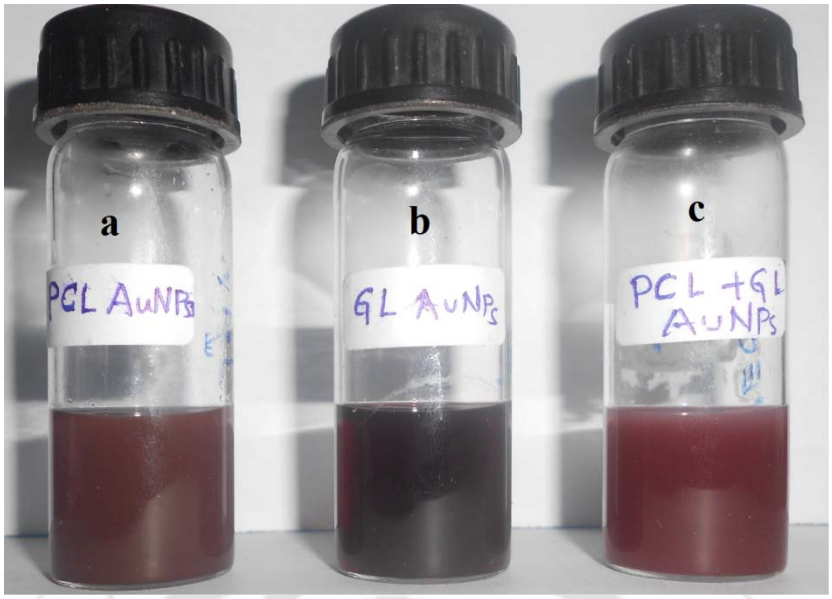

Figure 5.10 *Colloidal solutions synthesized with 3.5% ALE and 1 mmol/L $HAuCl_4$ at the 35% amplitude for 10 min: AuNP–PCL (a), AuNP–GL (b), AuNP–PCL–GL (c).*

XRD pattern of the AuNPs showed three prominent Bragg reflections that were indexed on the basis of fcc structure of gold. The intensities of the (1 1 1), (2 0 0), (2 2 0) and (3 1 1) diffraction peaks corresponding to 38.1°, 44.5°, 64.8° and 77.5°, respectively, confirmed that the synthesized AuNPs were of crystalline in nature (**Figure 5.11**). Moreover, we also observed the additional peaks at 19.73° and 24.97°, indicating the functionalization of PCL onto AuNPs (**Figure 5.11c**). We also we observed the characteristic peak representing GL at 20° along with the peaks corresponding to the AuNPs which indicates the functionalization of the GL on to the AuNPs (**Figure 5.11d**). The XRD spectrum of AuNP–PCL–GL showed the characteristic peak of PCL, whereas peaks corresponding to AuNPs and GL were absent. The results revealed that GL was initially bounded to AuNPs and then covered by PCL (**Figure 5.11e**).

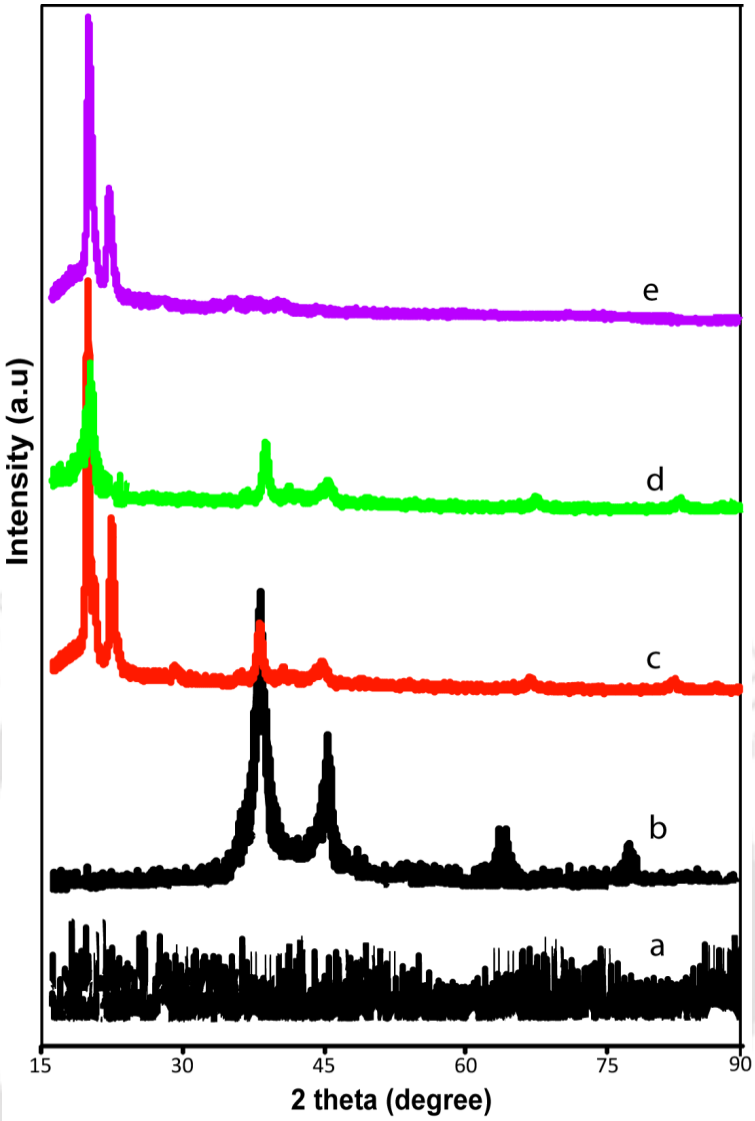

Figure 5.11 *XRD patterns of ALE (a), AuNP (b), AuNP–PCL (c), AuNP–GL (d), and AuNP–PCL–GL (e). AuNPs were synthesized using 3.5% ALE and 1 mmol/L $HAuCl_4$ at the 35% amplitude for 120 s, and AuNP–PCL, AuNP–GL and AuNP–PCL–GL colloidal solutions were synthesized using 3.5% ALE and 1 mmol/L $HAuCl_4$ at the 35% amplitude for 10 min.*

5.3.2.4 FTIR analysis of AuNPs

The FT-IR spectra in **Figure 5.12** revealed the functional groups associated with ALE, AuNPs, PCL, AuNP–PCL, GL, AuNP–GL and AuNP–PCL–GL. The FT-IR spectra of ALE showed the characteristic peaks at 3492, 2934, 1629 cm^{-1} corresponding to hydroxyl group arising from phenolic compounds and alcohols, secondary amine, amide I bond of proteins respectively (**Figure 5.12a**). The FT-IR spectra of AuNPs (**Figure 5.12b**) synthesized with the optimized conditions (3.5% ALE, 1 mmol/L $HAuCl_4$ and 120 s) showed strong peaks at 3457 cm^{-1} (hydroxyl group of alcohols or phenols), 2932 cm^{-1} (secondary amine or methylene C –H asym./sym. stretch), 1740 cm^{-1} (alkyl carbonate), 1645 cm^{-1} (amide bond of protein), 1387 cm^{-1} (methyl group of alkanes or sulfur-oxygen compounds) and 1041 cm^{-1} (cyclohexane ring vibrations). This suggests the absorption of the bioactive compounds on the surface of the AuNPs.

The characteristic peaks for pure PCL and GL were observed at 1751 and 1655 cm^{-1} respectively (**Figure 5.12c, 5.12e**). We observed an intense peak at 1722 cm^{-1} (**Curve d in Figure 5.12d**) corresponding to PCL that confirms the functionalization of the PCL on to AuNPs. The intense stretching modes observed at 1655 cm^{-1} (**Figure 5.12e**) and 1641 cm^{-1} (**Figure 5.12f**) were assigned to GL confirmed the functionalization of the GL on to AuNPs. We also observed a peak at 1738 cm^{-1} corresponding to PCL and the peaks corresponding to both AuNPs and GL were absent (**Figure 5.12g**) which indicated that during the sonication process GL was initially bound to the AuNPs and later on it was covered by PCL. Tentative mechanisms involved in the functionalization of (a) PCL, (b) GL, and (c) PCL–GL composites onto AuNPs as shown in **Scheme 5.2**.

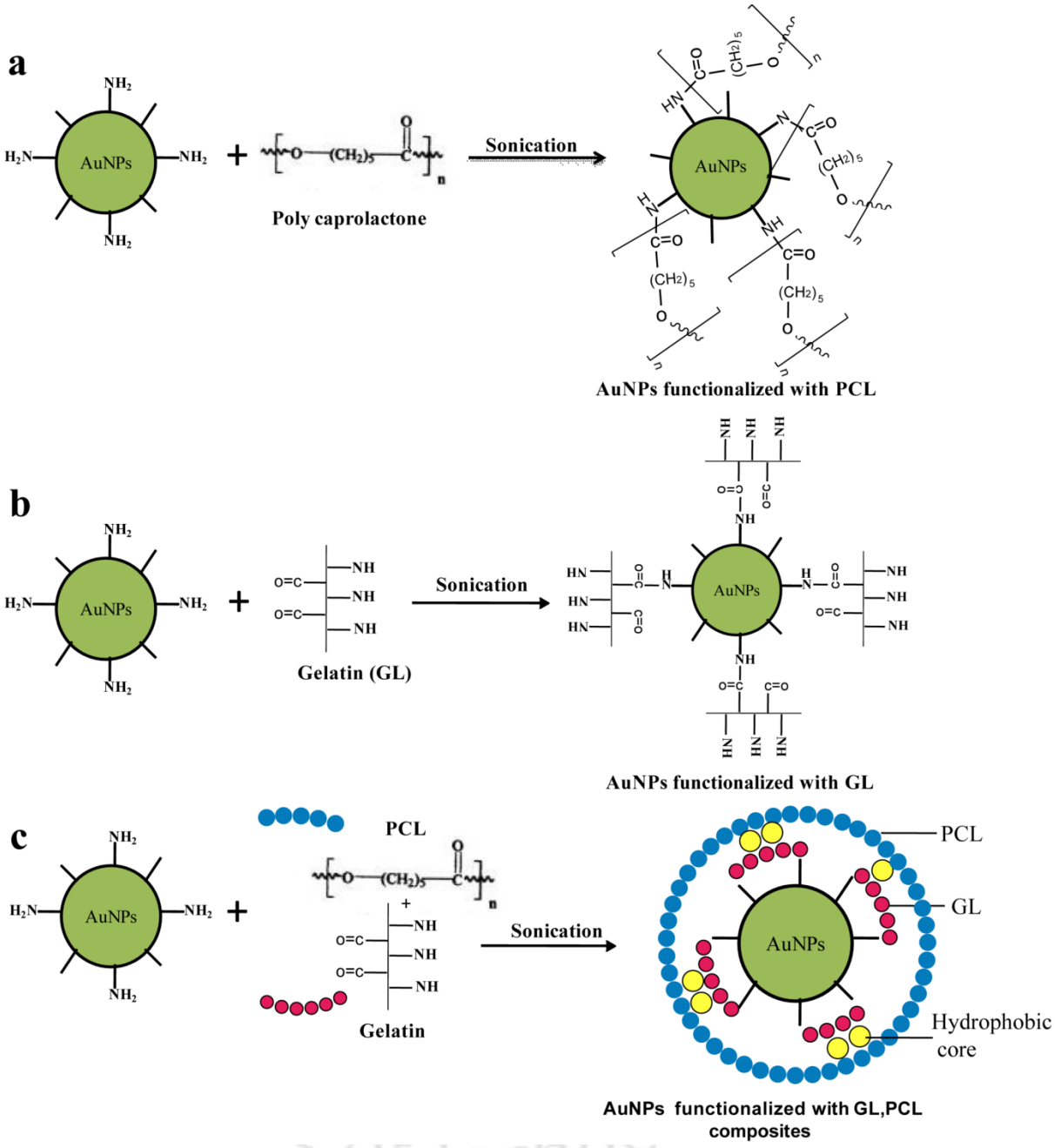

Scheme 5.2 Tentative mechanisms involved in the functionalization of (a) PCL, (b) GL, and (c) PCL–GL composites onto AuNPs.

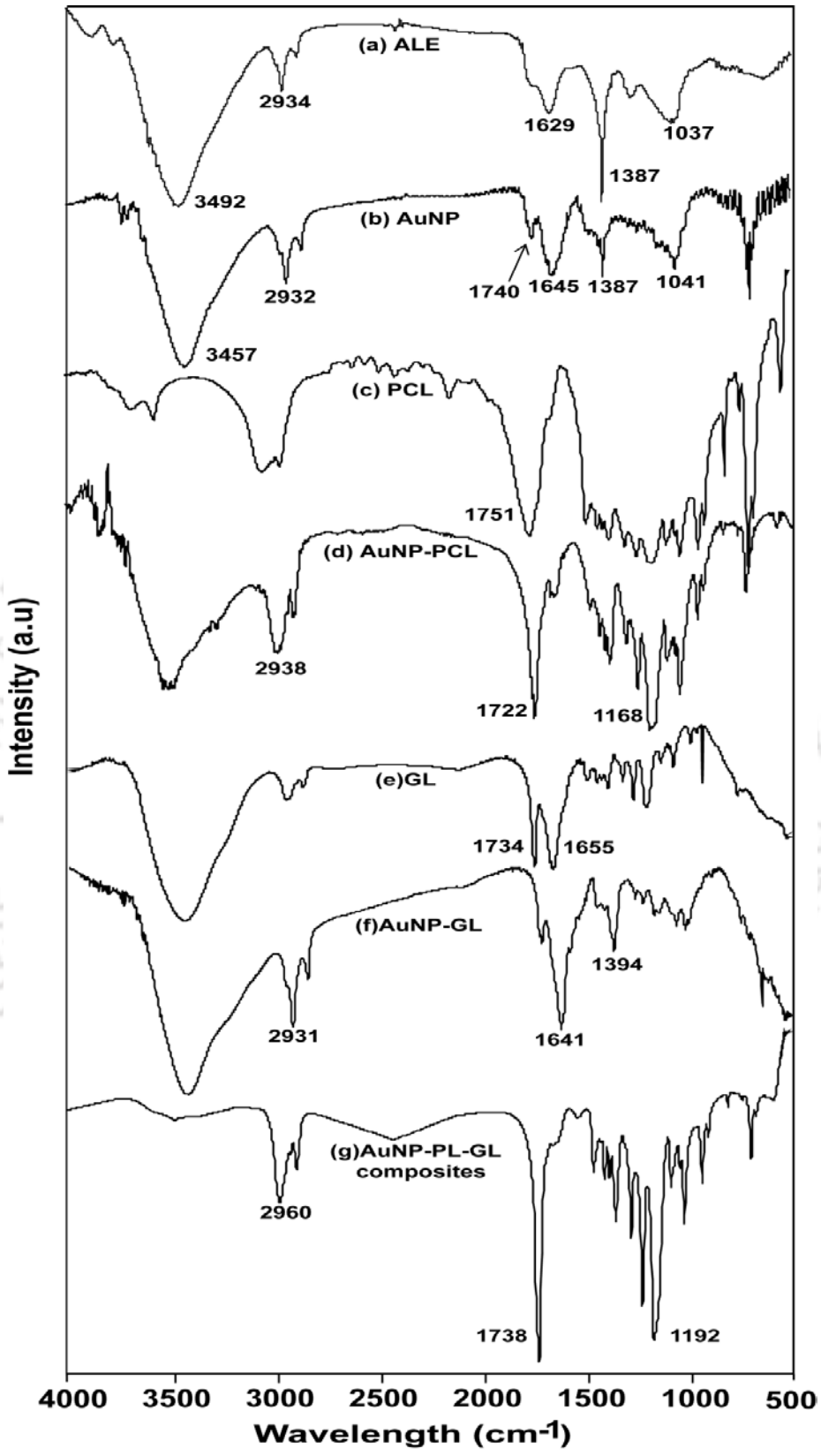

Figure 5.12 *FT-IR spectra of ALE (a), AuNPs (b), PCL (c), AuNP–PCL (d), GL (e), AuNP–GL (f), and AuNP–PCL–GL (g).*

5.3.3 Cyto compatibility assay

The cytotoxicity of intact AuNPs under in vitro conditions in HeLa and MCF-7 cells was examined in terms of effect of AuNPs on cell viability by MTT assay for 24 h. Only cells that are viable after 24 h exposure to the AuNPs can metabolize MTT efficiently and produce purple coloured crystal that is soluble in DMSO. There was no change in morphology of both HeLa and MCF-7 after AuNP treatment. This suggests that AuNPs did not induce any cytotoxic effect for causing significant damage or death of the cells (**Figure 5.13**).

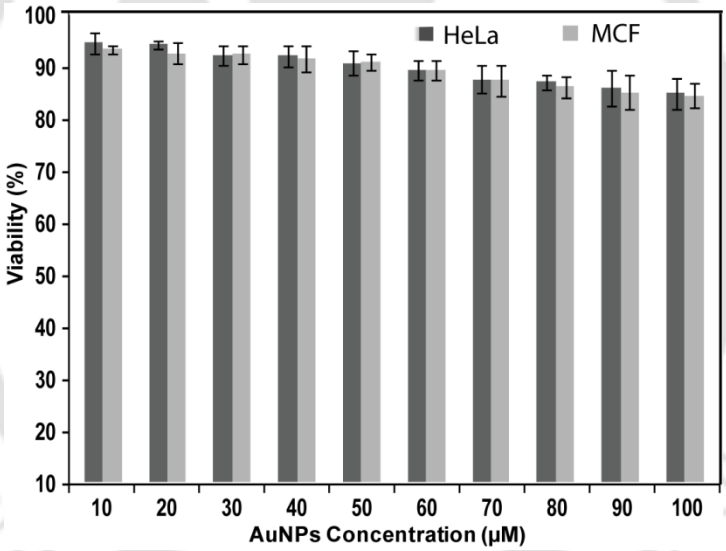

Figure 5.13 *Cytotoxicity assay: Cell viability of HeLa and MCF-7 cells exposed to different concentrations of AuNPs (10–100 μmol/L) over a period of 24 h treatment.*

5.4 Discussion

In an effort to optimize parameters for the synthesis of spherical AuNPs, different reactions were carried out by varying the concentration of ALE (0.5%–5%) against 1 mmol/L $HAuCl_4$ for 120 s of the ultrasonication time, which resulted in appearance of ruby red colour in all the reaction mixtures indicating the synthesis of AuNPs. The peak intensities of reaction mixtures with above 3.5% of ALE were flattened, indicating the insignificant increment in the formation of AuNPs. This infers that the 3.5% ALE reduces the total 1 mmol/L of $HAuCl_4$. Thus we consider the 3.5% of ALE as optimum for the AuNP synthesis **(Figure 5.1a)**. To find out the optimum concentration of $HAuCl_4$, we carried out various experiments with 3.5% ALE by changing the concentration of the gold salts from 0.5 to 1 mmol/L and observed the maximum peak intensity associated with 1 mmol/L $HAuCl_4$ that we considered as an optimum **(Figure 5.1b)**. The peaks associated with 2 mmol/L and above showed the gradual decrease in their intensities, revealing that 3.5% of the ALE is adequate for the total reduction of $HAuCl_4$. The optimum ultrasonication time required for the AuNPs synthesis was determined by performing various experiments with 3.5% ALE and 1 mmol/L $HAuCl_4$ for different ultrasonication time from 60 to 240 s with an interval of 30 s and we found 120 s to be the optimum time. We observed the progression in the intensities of peaks with respect to time. As there is no significant change in the peak intensities associated above 120 s, we considered it as an optimum time **(Figure 5.2a, 2b)**.

We applied ultrasonication for the rapid synthesis of AuNPs, which can generate the acoustic cavities in the medium (H_2O). These acoustic cavities release immense energy in the form of high temperature (5000 K) and high pressure (20,000 pounds per square inch (psi)) by undergoing implosive collapse (Suslick et al., 1990; Maisonhaute et al., 2002; Mason et al., 2011). The enormous energy released during the sonication

process assisted reducing agents (phenolic compound and flavonoids) to reduce gold ions to AuNPs **(Figure 5.3)**.

A. paniculata has a high content of phenolic acids, antioxidants and flavonoids which can act as strong reducing agents. The biochemical test revealed that flavonoids and phenolic compounds are present in ALE and may be responsible for reductions and stabilisation of AuNPs. The abundant free hydroxyl groups available in these compounds participate in the gold bioreduction. Phenolic compounds reduce through the oxidation of hydroxyl (R – OH) to carbonyl groups (R – C = O) as shown in the following reaction:

$$AuCl_4^- + 3R\text{-}OH \longrightarrow Au^o + 3R{=}O + 3H^+ + 4Cl^-$$

Flavonoids interact with Au^{3+} ions through carbonyl groups or •-electrons and then reduced into AuNPs in the extracellular medium. As soon as they come in contact with Au^{3+} ions in extracellular medium, their •-electrons are transferred and Au^{3+} ions are reduced to Au^o, as shown in **Scheme 5.1**. Flavonoids can also prevent agglomeration and stabilize AuNPs (Nune et al., 2009). Thus the involvement of flavonoids in the rapid reduction of Au^{3+} ions and as capping agent gives stability to AuNPs.

The gradual increment in the formation of AuNPs was observed with the increase of the amplitude **(Figure 5.4)**. We found that the peak pertaining to 35% amplitude showed the maximum intensity out of the various experiments performed with 3.5% ALE and 1 mmol/L of $HAuCl_4$ by varying the different amplitudes from 21% to 35% for 120 s of the ultrasonication time and was, thus, considered as the optimum. The pH of the intact reaction mixture before embarking into experiments was found to be 4.87. We observed pH 5 as an optimum from the experiments performed with 3.5% ALE, 1 mmol/L of $HAuCl_4$ by adjusting the pH (1–11) for 120 s of ultrasonication **(Figure 5.5)**. We observed insignificant peaks corresponding to the reaction mixtures with pH 1 and 3. The reaction mixture with pH 5 resulted in the formation of the intense and narrow peak at

541 nm whereas the reaction mixtures with pH 9 and 11 resulted in broad peaks which indicate the formation of the different size and shape of AuNPs, and thus, pH 5 was considered as optimum.

We found that optimum parameters for the synthesis of spherical AuNPs are ALE (3.5%), $HAuCl_4$ (1 mmol/L), amplitude (35%), pH 5 and ultrasonication time (120 s). All these parameters resulted in the intense and narrow peaks ranging from 520 to 547 nm **(Figure. 5.6)** which is an indication of the formation of nanoparticles ranging from 5 to 100 nm (Mody et al., 2010). These results are in accordance with the observation from **Figure 5.7a**, which proved the controlled synthesis of the AuNPs in terms of size. The λ_{max} values of all reactions are shown in **Table 1**.

We performed TEM experiment to visualize the size and shape of AuNPs. Typical bright-field TEM image of AuNPs obtained with optimum reaction conditions showed that 96% of nanoparticles were of spherical in shape **(Figure 5.7a).** The size of the AuNPs synthesized ranged from 5 to 75 nm and the average size was found to be 9.97 nm **(Figure 5.7b)**.

The crystalline nature of the synthesized AuNPs was confirmed from the selected area electron diffraction (SAED) pattern with bright circular rings corresponding to the (1 1 1), (2 0 0), and (2 2 0) planes **(Figure 5.8a)** (Babu et al., 2010; Shankar et al., 2004a). High-resolution TEM (HRTEM) image shown in **Figure 5.8b** revealed clear lattice fringes of 0.22 nm, indicating that the growth of the AuNPs occurred preferentially on the (1 1 1) plane. The inter planer distance of the Au (1 1 1) plane was in agreement with the (1 1 1) dspacing of bulk Au (0.2355 nm) (Babu et al., 2010).

EDX profile of AuNPs revealed a strong signal for gold and copper along with very strong carbon, nitrogen and oxygen peaks. The signal for copper originated from the grid used for the TEM analysis. We found molecular carbon and oxygen which may be

originated from antioxidants, flavonoids, phenolic or organic biomolecules bound to the surface of the AuNPs. The EDX pattern suggested the presence of biomolecules on the surface of the synthesized AuNPs **(Figure 5.9)**. The successful functionalization of PCL, GL, and PCL–GL onto the AuNPs was confirmed from XRD and FT-IR analyses. We observed the different coloured colloidal solutions for AuNP–PCL, AuNP–GL, and AuNP–PCL–GL composites **(Figure 5.10)**.

XRD pattern of the AuNPs showed three prominent Bragg reflections that were indexed on the basis of fcc structure of gold. The intensities of the (1 1 1), (2 0 0), (2 2 0) and (3 1 1) diffraction peaks corresponding to 38.1°, 44.5°, 64.8° and 77.5°, respectively, confirmed that the synthesized AuNPs were of crystalline in nature **(Figure 5.11b)** (Babu et al., 2010; Shankar et al., 2004a; Kannan et al., 2008). Moreover, we also observed the additional peaks at 19.73° and 24.97°, indicating the functionalization of PCL onto AuNPs **(Figure 11c)** (Hiremath et al., 2011). Also, we observed the characteristic peak representing GL at 20° along with the peaks corresponding to the AuNPs **(Figure. 5.11d)** (Nagahama et al., 2009). The XRD spectrum of AuNP–PCL–GL showed the characteristic peak of PCL, whereas peaks corresponding to AuNPs and GL were absent. The results revealed that GL was initially bounded to AuNPs and then covered by PCL **(Figure 5.11e)**.

The FT-IR spectra in **Figure 5.12** revealed the functional groups associated with ALE, AuNP, PCL, AuNP–PCL, GL, AuNP–GL and AuNP–PCL–GL. The FT-IR spectra of ALE showed the characteristic peaks at 3492, 2934, 1629 cm^{-1} corresponding to hydroxyl group arising from phenolic compounds and alcohols, secondary amine, amide I bond of proteins respectively **(Figure 5.12a)**. The intense peak observed at 1387 cm^{-1} is due to rocking of methyl groups (alkanes) of bioactive molecules present in the ALE (Babu et al., 2011). We observed a band at 1037 cm^{-1} attributed to C –N stretching

vibrations of aliphatic amines or alcohols or phenols (Kannan et al., 2008; Hiremath et al., 2011). It is well known that the AuNPs synthesized using plant extract are coated with thin layer of the organic biomolecules, which can acts as capping agents to provides stability of AuNPs (Shankar et al., 2004b; Song et al., 2009). The FT-IR spectra of AuNPs **(Figure 5.12b)** synthesized with the optimized conditions (3.5% ALE, 1 mmol/L $HAuCl_4$ and 120 s) showed strong peaks at 3457 cm^{-1} (hydroxyl group of alcohols or phenols), 2932 cm^{-1} (secondary amine or methylene C –H asym./sym. stretch), 1740 cm^{-1} (alkyl carbonate), 1645 cm^{-1} (amide bond of protein), 1387 cm^{-1} (methyl group of alkanes or sulfur-oxygen compounds) and 1041 cm^{-1} (cyclohexane ring vibrations). This suggests the absorbtion of the bioactive compounds on the surface of the AuNPs.

The characteristic peaks for pure PCL and GL were observed at 1751 and 1655 cm^{-1} respectively **(Figure 5.12c, 5.12e)** (Hiremath et al., 2011; Nagahama et al., 2009; Shah et al., 2010). We observed an intense peak at 1722 cm^{-1} **(Figure 5.12d)** corresponding to PCL that confirms the functionalization of the PCL on to AuNPs. We observed the shift of peak from 1041 cm^{-1} **(Figure 5.12b)** to 1168 cm^{-1} **(Figure 5.12d)** which may be due to the slight change in confirmations of functional groups such as C–O, C–O–C and C–H stretches during the synthesis process. Infrared spectra related to stretching modes were observed for GL and AuNP–GL. The intense stretching modes observed at 1655 cm^{-1} **(Figure 5.12e)** and 1641 cm^{-1} **(Figure 5.12f)** were assigned to GL (Ghasemi-Mobarakeh et al., 2008; Ki et al., 2005). In general, the common bands of protein appeared at approximately 1545 cm^{-1} (amide II) and 1657 cm^{-1} (amide I). The former band appeared due to the stretching of C – N bond whereas later band was due to either stretching vibrations of C – O bond or coupling of bending of N – H bonds. It is known that amide I band contains significant information about the secondary structures of proteins. The •-sheets of the protein absorb in the range 1640–1623 cm^{-1} and near

1675 cm^{-1}, •-helices in the range 1660–1653 cm^{-1}, unordered structures and •-helices 1650–1641 cm^{-1} and •-turns in the range 1695–1659 cm^{-1} (Krimm et al., 1986). The characteristic peak of GL reappeared at 1641 cm^{-1} in **Figure 5.12f** which confirmed the functionalization of the AuNPs with GL. Interestingly, in the FT-IR spectra of AuNP–PCL–GL composites, we noticed the peak at 1192 cm^{-1} attributed to the secondary amine and C – N stretch which may have originated due to the reaction between C = O functional group of PCL and amine group of GL. We also observed a peak at 1738 cm^{-1} corresponding to PCL and the peaks corresponding to both AuNPs and GL were absent **(Figure 5.12g).** This suggests that during the sonication process, GL was initially bound to the AuNPs and later on it was covered by PCL. Both the polymers (PCL and GL) can form nanocomposites with the hydrophobic void space inside when they mixed in appropriate amounts. Paclitaxel, an anticancer drug, was successfully delivered into cancer cell line by using the nanocomposites synthesized with PCL and GL (Sahoo et al., 2011). The current study revealed that these polymers formed into composites during the sonication process and were not removed from the AuNPs even after repeated washing, which confirmed that they were bound covalently. The tentative mechanisms involved in the binding of PCL–GL composites are shown in **Scheme 5.2**. The hydrophobic void space developed inside the polymers can be used as a vehicle for carrying different drugs for different diseases.

The cytotoxicity of intact AuNPs under in vitro conditions in HeLa and MCF-7 cells was examined in terms of effect of AuNPs on cell viability by MTT assay for 24 h. Only cells that are viable after 24 h exposure to the AuNPs can metabolize MTT efficiently and produce purple coloured crystal that is soluble in DMSO. There was no change in morphology of both HeLa and MCF-7 after AuNPs treatment. This suggests that AuNPs did not induce any cytotoxic effect for causing significant damage or death of

the cells. Both HeLa and MCF-7 cells after 24 h of post-treatment showed excellent viability up to as high as 100 µmol/L of AuNPs **(Figure 5.13)**.

5.5 Conclusions

We determined the optimum conditions for synthesis of AuNPs by ultrasonication using ethanolic extract of *A. paniculata* as ALE (3.5%), $HAuCl_4$ (1 mmol/L), amplitude (35%), pH 5 and ultrasonication time (120 s) for the spherical synthesis of the AuNPs. Biomolecules such as flavonoids and phenolic compounds found in *A. paniculata* are involved in the reduction of gold ions to AuNPs. TEM analysis revealed that ultrasonic catalysis resulted in the formation of spherical AuNPs with an average size of 9.97 nm. EDX profile of AuNPs revealed a strong signal for gold and copper along with very strong carbon, nitrogen and oxygen peaks which indicated the adsorption of the biomolecules on the AuNPs. XRD pattern of the AuNPs showed three prominent Bragg reflections that were indexed on the basis of fcc structure of gold. The intensities of the (1 1 1), (2 0 0), (2 2 0) and (3 1 1) diffraction peaks corresponding to 38.1°, 44.5°, 64.8° and 77.5°, respectively, confirmed that the synthesized AuNPs were of crystalline in nature. The synthesized AuNPs were characterized using biophysical tools such as XRD, FT-IR and EDX spectroscopy which confirmed the functionalization with PCL, GL and PCL–GL. The characterization studies (XRD and FT-IR) also revealed that during the sonication process GL was initially bound to the AuNPs and later on it was covered by PCL. The cytotoxic studies revealed that the maximum dose (100 µmol/L) of synthesized AuNPs showed insignificant toxicity on HeLa and MCF-7 cells. The rapidness and eco-friendly method mentioned here for the synthesis of AuNPs provides an opportunity for application in drug delivery and molecular imaging.

---***---

6.1 Summary

The present investigation was focused on the screenings the reducing, capping and dispersing capabilities of plants and fruits extracts for the synthesis of AuNPs and the AuNPs were extensively characterized with biophysical tools. We have synthesized AuNPs using some indigenous medicinal plant and fruit extracts from North East India, includes *Fagopyrum esculentum* leaf extract (FLE), *Piper betle* Leaf Extract (PLE), *Cocos nucifera* (coconut water; CW), *Solanum indicum* fruit extract (SFE) and *Sapindus mukorossi* fruit extracts (SmFE) and *Calotropis procera* Aqueous fraction of latex. We applied various methods to mediate the synthesis of AuNPs such as heat, UV irradiation, microwave irradiation and sonocatalysis.

6.1.1 Heat Mediated Synthesis of AuNPs using *Mentha arvensis* leaf extract (MLE).

We synthesized AuNPs using ethanolic extract of *Mentha arvensis* leaves, an edible plant used as a condiment and traditional medicine in India. UV-Vis spectroscopy analysis confirmed the formation of gold nanoparticles. The different reaction parameters such as plant extract (0.02%), gold solution (2 mM), temperature (80 ^{o}C), and time (30 min) were optimized for the synthesis of AuNPs. A TEM technique was employed to visualize the size and shape of AuNPs formed. Typical bright-field TEM image of AuNPs with optimum reaction conditions, which reveals that nanoparticles are of hexagonal and nearly circular shape with an average size of 39±15 nm and were stable even after 6 weeks of storage at room temperature. The clear lattice fringes of 0.22 nm in a high-resolution image revealed that the growth of the AuNPs occurred preferentially on the (1 1 1) plane. The crystalline nature of AuNPs was confirmed with X-ray diffraction analysis. The XRD pattern of the AuNPs displayed diffraction peaks at 38.1, 44.4, and 64.5◦ corresponding to the (1 1 1), (2 0

0), and (2 2 0) Bragg's reflections, respectively, which is due to the fcc crystal structure. The crystallinity of AuNPs also confirmed from the typical selected area electron diffraction (SAED) pattern with bright circular rings corresponding to the (1 1 1), (2 0 0), and (2 2 0) planes corresponding to gold lattice fringes. In addition to gold, energy-dispersive X-ray analysis (EDX) showed the presence of carbon and oxygen elements. The evidence from Fourier transform infrared (FTIR) spectroscopy and EDX suggested that flavonoids and phenol compounds were involved in reduction and stability of AuNPs synthesized using *Mentha arvensis*. The UV-Vis spectroscopic analysis displayed an intense peak at 530±10 nm indicating the formation of AuNPs that can be used for biomedical applications.

6.1.2 Sonocatalytic UV Light Mediated Synthesis of Gold Nanoparticles Using *Boccopa monneri* Leaf Extract

For the first time we have introduced UV irradiation in 'green synthesis' field for AuNPs synthesis using *Bacopa monnieri* leaf extract (BLE). The reducing and capping functions provided by BLE can replace synthetic reducing and stabilizing agents required for nanoparticles synthesis. We observed the solution containing gold ions (Au^{3+}) and BLE turned into ruby red after 15 min of UV irradiation (~254 nm). We found that 4% BLE (400 mg) was sufficient to reduce 1 mM HAuCl4 as there was insignificant peak intensity with 5% BLE. Furthermore, we found the optimum time for the synthesis of AuNPs as 15 min. TEM images showed that the AuNPs were predominantly spherical in shape with size distribution range of 3–45 nm. High resolution TEM image revealed clear fcc (0.23 nm) indicating that the growth of the AuNPs occurred preferentially on the (1 1 1) plane. Bright circular rings and diffraction peaks (1 1 1), (2 0 0), (2 2 0) of both SAED and XRD patterns, confirmed the crystalline nature of AuNPs. FTIR studies revealed that the bioactive

molecules present in BLE facilitated the reduction of the $Au3^{+}$ ions to Au^{0} and later capped the AuNPs during the particle growth termination process. TGA spectrum of AuNPs occurs over a wide temperature range (225–580 ^{o}C) which revealed the significant weight loss (5%) of AuNPs. This clearly indicated that bioactive molecules were capped on the AuNPs and were completely degraded due to high temperature. These capped AuNPs were tested on the human cancer cell lines (HeLa, MCF-7) and were found to be biocompatible opportunities for use in drug delivery, molecular imaging and therapy.

6.1.3 Microwave Mediated Synthesis of Gold Nanoparticles using Plant and Fruit extracts

We have successfully investigated the reducing and stabilizing capabilities *Fagopyrum esculentum* leaf extract (FLE), *Piper betle* leaf extract (PLE), *Cocos nucifera* (CW), *Solanum indicum* fruit extract (SFE) and *Sapindus mukorossi* fruit extracts (SmFE) and Aqeous fraction (AF) of *Calotropis procera* latex for the synthesis of the AuNPs. UV-visible spectroscopy analysis indicated the successful formation of gold nanoparticles. We have optimized the parameters for the synthesis of AuNPs using FLE (0.4% FLE, 1 mmol/L $HAuCl_4$ and 16 s MW irradiation time), PLE (2% PLE, 0.5 mM $HAuCl_4$, and 18 s MW irradiation time), CW (0.250 mM HAuCl4 for 17 s), SFE (0.03% FLE, 0.5 mM $HAuCl_4$ and 20 sec MW irradiation time), SmFE (8% PFE, 1 mM $HAuCl_4$ and 25 sec of MW irradiation time) and *C. procera* (AF) (3% procera latex, 1mM $HAuCl_4$ and 40 sec MW irradiation).

We have employed the TEM technique to visualize the size and shape of formed AuNPs. AuNPs obtained by FLE showed shapes of triangular, hexagonal, rod shaped and spherical. A histogram representing the size distribution of AuNPs corresponding to TEM

image exhibited the variation in the particle size ranging from 3 to 20 nm with the average of 8.3 nm. The size of the synthesized AuNPs obtained by PLE ranges from 10 to 35 nm, and the average size was found to be 6 nm. TEM analysis of the AuNPs synthesized with CW (0.250 mM for 17 s of MW irradiation) showed the dominance of nearly spherical particles, which were well dispersed without any agglomeration. The particle size distribution ranged from 5 to 20 nm with average particle diameter of 10.5 ±5 nm, which was revealed from the size distribution histogram. The size of the AuNPs synthesized using SFE, was ranges from 5-50 nm and the average size was found to be 7.4 nm. The AuNPs obtained suing SmFE showed wide range of particles size distribution (3-50 nm) with optimized parameters (0.8% SFE and 1 mM $HAuCl_4$). A representative TEM image and corresponding size distribution histogram of AuNPs synthesized with C. procera (AF) exhibited abundant spherical particles than particles of other shapes. HRTEM images revealed clear lattice fringes of 0.22 nm, indicating that the growth of the AuNPs occurred preferentially on the (1 1 1) plane. The interplanar distance of the Au (1 1 1) plane was in agreement with the (1 1 1) d-spacing of bulk Au (0.2355 nm). The nanoparticles obtained were highly crystalline, as evident from the SAED pattern with bright concentric rings corresponding to the (1 1 1), (2 0 0), and (2 2 0) planes.

XRD pattern suggested that the AuNPs synthesized by plant materials were crystalline in nature. Intense diffraction peaks were clearly observed at (111), (200) and (220) corresponding to the Bragg's angles at 38.1°, 44.4° and 64.5°, respectively. The ratio between the intensity of (200) and (111) diffraction peaks was much lower than the usual value (0.52), suggesting the (111) as the predominant plane. FT-IR, NMR and EDX analyses demonstrated the presence of biomolecules on the surface of AuNPs arising from the strong

reducing molecules such as phenolic compounds, flavonoids and antioxidants which are involved in the reduction of gold salts to AuNPs. Cytotoxicity studies revealed that there is no significant toxicity of AuNPs on the proliferation of cells. The small size of AuNPs synthesized with FLE provides an opportunity for safe delivery to sub cellular organelles and applications in molecular imaging and therapy. This approach for the synthesis of AuNPs synthesis provides a 'green' opportunity for the production of nanoparticles with a very less time.

6.1.4 Sonocatalytic Synthesis of Gold Nanoparticles and Functionalized with PCL, GL and PCL-GL composites.

In this study, we determined the optimum conditions for synthesis of AuNPs by ultrasonication using ethanolic extract of *A. paniculata* as ALE (3.5%), HAuCl4 (1 mmol/L), amplitude (35%), pH 5 and ultrasonication time (120 s) for the spherical synthesis of the AuNPs. Biomolecules such as flavonoids and phenolic compounds found in *A. paniculata* are involved in the reduction of gold ions to AuNPs. We performed TEM experiment to visualize the size and shape of AuNPs. Typical bright-field TEM image of AuNPs obtained with optimum reaction conditions showed that 96% of nanoparticles were of spherical in shape. The size of the AuNPs synthesized ranged from 5 to 75 nm and the average size was found to be 9.97 nm. High-resolution TEM (HRTEM) image revealed clear lattice fringes of 0.22 nm, indicating that the growth of the AuNPs occurred preferentially on the (1 1 1) plane. The inter planer distance of the Au (1 1 1) plane was in agreement with the (1 1 1) dspacing of bulk Au (0.2355 nm). The crystalline nature of the synthesized AuNPs was confirmed from the selected area electron diffraction (SAED) pattern with bright circular rings corresponding to the (1 1 1), (2 0 0), and (2 2 0) planes. We observed the different coloured colloidal

solutions for AuNP–PCL, AuNP–GL, and AuNP–PCL–GL composites. The successful functionalization of PCL, GL, and PCL–GL onto the AuNPs was confirmed from XRD and FT-IR analyses. The cytotoxic studies revealed that the maximum dose (100 µmol/L) of synthesized AuNPs showed insignificant toxicity on HeLa and MCF-7 cells. The rapidness and eco-friendly method mentioned here for the synthesis of AuNPs provides an opportunity for application in drug delivery and molecular imaging.

8.2 FUTURE PROSPECTS

Our attempt to synthesize AuNPs using indigenous plant materials yielded screening of many plants from North East India. We have successfully characterized the synthesized AuNPs with biophysical techniques. However at the end of the investigations we could foresee many areas in which further studies could yield potentially new and beneficial information as summarized below.

- The AuNPs synthesized using plant materials demonstrated to be non toxic. However, *in vivo* studies of these AuNPs are required to understand their true potential. Information on the toxicity and tolerability of the AuNPs in animal models *in vivo* would be crucial for biomedical applications.
- The synthesized AuNPs could be fabricated with natural polymers for potential drugs carriers for the treatment of the cancer.
- These AuNPs are highly axisable for functionalization of aptamers thereby providing the opportunity to treat the diseases with aptamers based therapy.
- The ability of these AuNPs to carry the potential drugs in stem cells can be evaluated for potential applications in stem cell based therapy.

Adamopoulos O, Papadopoulos T. Nanostructured bioceramics for maxillofacial applications. Journal of Materials Science: Materials in Medicine. 2007; 18(8):1587–1597.

Adams W, Bratt DE. Young coconut water for home rehydration in children with mild gastroenteritis. Trop Geogr Med. 1992; 44: 149–153.

Agnihotri M, Joshi S, Kumar AR, Zinjarde S, Kulkarni S. Biosynthesis of gold nanoparticles by the tropical marine yeast Yarrowia lipolytica NCIM 3589. Materials Letters. 2009; 63:1231–1234.

Ahmad A, Senapati S, Khan MI, Kumar R, Ramani R, Srinivas V, et al. Intracellular synthesis of gold nanoparticles by a novel alkalotolerant actinomycete, Rhodococcus species. Nanotechnol. 2003a; 14a:824–828.

Ahmad A, Senapati S, Khan MI, Kumar R, Sastry M. Extra-/Intracellular Biosynthesis of Gold Nanoparticles by an Alkalotolerant Fungus, Trichothecium sp. J Biomed Nanotechnol. 2005; 1:47–53.

Ahmad A, Senapati S, Khan MI, Kumar R, Sastry M. Extracellular Biosynthesis of Monodisperse Gold Nanoparticles by a Novel Extremophilic Actinomycete Thermomonospora sp. Langmuir. 2003b; 19:3550–3553.

Ahmad M, Asmawi MZ. Some pharmacological effects of aqueous extract of Andrographis paniculata Nees. In: Gan E K ed. The International Conference on the Use of' Traditional Medicine & Other Natural Products in Health Care (Abstract). Penang, Malaysia: School of Pharmaceutical Sciences. University of Science Malaysia. 1993.

Ajayan PM, Schadler LS, Braun PV 2003. Nanocomposite science and technology. Wiley. ISBN 3-527-30359-6.

Akhavana A, Kalhorb HR, Kassaeea MZ, Sheikhc N, Hassanloub M. Radiation synthesis and characterization of protein stabilized gold nanoparticles. Chemical Engineering Journal. 2010; 159:230–235.

Anandan S, Grieser F, Ashokkumar M. Sonochemical synthesis of Au–Ag core–shell bimetallic nanoparticles. J Phys Chem C. 2008; 112: 15102–5.

Anbarsi K, Vani G, Balakrishna K, Devi CS. Effect of bacoside A on brain antioxidant status in cigarette smoke exposed rats. Life Sci. 2006; 78(12): 1378–84.

Andrey LG. Enzyme-catalyzed direct electron transfer: Fundamentals and analytical applications. Electroanalysis. 1997; 9(9):661–674.

Angel L, Caterina Q, Francisco J, Ligia G, Deodato R. Gold-copolymer nanoparticles: Poly(•-caprolactone)/poly(N-vinyl-2-pyrrolydone) Biodegradable triblock copolymer as stabilizer and reductant. European Polymer Journal. 2009; 45:3035–3042.

Angshuman P, Sunil S, Surekha D. Synthesis of Au Ag and Au–Ag alloy nanoparticles in aqueous polymer solution. Colloids and Surfaces A: Physiochem Eng Aspects. 2007; 302:51–57.

Ankamwar B, Chaudhary M, Sastry M. Gold Nanotriangles Biologically Synthesized using Tamarind Leaf Extract and Potential Application in Vapor Sensing. Nanometal Chem. 2005b; 35:19–26.

Ankamwar B, Chinmay D, Absar A, Murali S. Biosynthesis of Gold and Silver Nanoparticles Using Emblica Officinalis Fruit Extract, Their Phase Transfer and Transmetallation in an Organic Solution. J Nanosci Nanotechnol. 2005a; 5:1665–1671.

Ankamwar B. Biosynthesis of gold nanoparticles (green-gold) using leaf extract of. Terminozlia catozppoa. E-J Chem. 2010; 7:1334–1339.

Anonymous. Monigraphs of Bacopa monnieri Altern Med Rev. 2004; 9(1): 79–85.

Anurag P, Rajamohan T. Cardioprotective effect of tender coconut water in experimental myocardial infarction. Plant Foods Hum Nutr. 2003; 58: 1–12.

Appenzeller T. The man who dared to think small. Science. 1991; 254:1300–1301.

Arambewela LSR, Arawwawala LDAM, Ratnasooriya WD. Antidiabetic activities of aqueous and ethanolic extracts of Piper betle leaves in rats. J Ethnopharmacol. 2005; 102: 239–245.

Armendariz V, Jose-Yacaman M, Moller AD, Peralta-Videa JR, Troiani H, Herrera I, Gardea-Torresdey JL, Revista Mexicana De Fisica 50 Supplemento. 2004; 1: 7.

Arulkumar S, Sabesan M. Int J Res Pharm Sci. 2010; 1:417.

Avgoustakis K. Pegylated poly(lactide) and poly(lactide-co-glycolide) nanoparticles: preparation, properties and possible applications in drug delivery. Curr Drug Deliv. 2004; 1:321–333.

Awadalla FT, Pesic B. Biosorption of cobalt with the AMT metal removing agent. Hydrometallurgy. 1992; 28:65–80.

Azzazy HM, Mansour MM, Kazmierczak SC. Nanodiagnostics: a new frontier for clinical laboratory medicine. Clinical Chemistry. 2006; 52(7): 1238–1246.

Babu PJ, Das RK, Gogoi N, Sharma P, Bora U. Microwave mediated rapid synthesis of gold nanoparticles using *Calotropis procera* latex and study of optical properties. ISRN Nanomaterials. 2012a: 1–6.

Babu PJ, Das RK, Kumar A, Bora U. Microwave Mediated Synthesis of Gold Nanoparticles Using Coconut Water. Int J Green Nanotechnol Biomed. 2011a; 3: 13–21.

Babu PJ, Saranya S, Sharma P, Tamuli R, Bora U. Sonocatalytic Synthesis of Gold Nanoparticles Using Ethnolic Extract of *Andrographis paniculata* and Functionalization with Gelatin-Polycaprolactone Composites. Front Mater Sci. 2012b; 6(3): 236–249.

Babu PJ, Sharma P, Bora U. *Sapindus mukorossi* aqueous fruit extract as reducing, capping and dispersing agents in synthesis of gold nanoparticles. (In press, Accepted for publication in Micro and Nano Letters, 2012c).

Babu PJ, Sharma P, Borthakur BB, et al. Synthesis of gold nanoparticles using Mentha arvensis leaf extract. International Journal of Green Nanotechnology: Physics and Chemistry. 2010; 2 (2): 62–68.

Babu PJ, Sharma P, Kalita MC, et al. Green synthesis of biocompatible gold nanoparticles using Fagopyrum esculentum leaf extract. Frontiers of Materials Science. 2011b; 5(4): 379–387.

Babu PJ, Sharma P, Saranya S, Bora U. Piper betle Mediated Green Synthesis of Biocompatible Gold Nanoparticles. Int Nano Letters. 2012d; 2: 18–27.

Babu PJ, Sharma P, Saranya S, Bora U. UV Light mediated synthesis of gold nanoparticles using ethonolic leaf extract of *Bacopa monnieri*. Materials Letters. 2012e; 93: 431–434.

Bakshi SR , Lahiri D, Argawal A. Carbon nanotube reinforced metal matrix. International Materials Reviews. 2010; 55, 41–64.

Balaji DS, Basavaraja S, Deshpande R, Mahesh BD, Prabhakar BK, Venkataraman A. Extracellular biosynthesis of functionalized silver nanoparticles by strains of Cladosporium cladosporioides fungus. Coll Surf B: Biointerf. 2009; 68:88–92.

Bankar A, Joshi B, Kumar AR, Zinjarde S. Banana peel extract mediated synthesis of gold nanoparticles. Colloids Surf B Biointerfaces. 2010; 80:45–50.

Basavaraja S, Balaji SD, Lagashetty A, Rajasab AH, Venkataraman A. Extracellular biosynthesis of silver nanoparticles using the fungus Fusarium semitectum. Mat Res Bull. 2008; 43:1164–1170.

Basset C, Vadrot J, Denis J, Poupon J, Zafrani ES. Prolonged cholestasis and uctopenia following gold salt therapy. Liver Int. 2003; 23: 89–93.

Batlle X, Labarta A. Finite-size effects in fine particles: magnetic and transport properties. J Phys D: Apply Phys. 2002; 35:R15–R42.

Bean CP, Livingston JD. J Appl Phys. 1959; 30:1205

Berkovsky BM, Medvedev VF, Krokov MS. Magnetic Fluids: Engineering Applications. 1993; (Oxford: Oxford University Press)

Beveridge TJ, Murray RGE. Sites of metal deposition in the cell wall of Bacillus subtilis. J Bacteriol. 1980; 141: 876–887.

Bhainsa KC, D'Souza SF. Extracellular biosynthesis of silver nanoparticles using the fungus Aspergillus fumigatus. Coll Surf B: Interf. 2006; 47:160–164.

Bhattacharya R, Mukherjee P. Biological properties of "naked" metal nanoparticles. Advanced Drug Delivery Reviews. 2008; 60(11): 1289–1306.

Bhattacharya S, Subramanian M, Roychowdhury S, Bauri AK, Kamat JP, Chattopadhyay SJ. Radioprotective property of the ethanolic extract of *Piper betel* leaf. Radiat Res. 2005; 46: 165–171.

Birla SS, Tiwari VV, Gade AK, Ingle AP, Yadav AP, Rai MK. Fabrication of silver nanoparticles by Phoma glomerata and its combined effect against Escherichia coli, Pseudomonas aeruginosa and Staphylococcus aureus. Lett Appl Microbiol. 2009; 48:173–179.

Bonafaccia G, Marocchini M, Kreft I. Composition and technological properties of the flour and bran from common and tartary buckwheat. Food Chemistry, 2003, 80(1): 9–15.

Boonyaratanakornkit L, Pothiyanont P, Noppakun N, Sinhaseni P, Laorpaksa A, Virunhaphol S. Activity of betle leaf ointment on skin diseases. Thai J Pharm Sci. 1990; 15: 277–287.

Brill RH, Cahill ND. A Red Opaque Glass from Sardis and Some Thoughts on Red Opaques in General. J Glass Study. 1988; 30: 16–27.

Brown CL, Bushell G, Whitehouse MW, Agrawal DS, Tupe SG, Paknikar KM, Tiekink ERT. Nanogoldpharmaceutics. Gold Bull. 2007; 40: 245–250.

Brown KR, Fox AP, Natan MJ. Morphology-Dependent Electrochemistry of Cytochrome c at Au Colloid-Modified SnO2 Electrodes. J Am Chem Soc. 1996; 118(5):1154–1157.

Brugnerotto J, Lizardi J, Goycoolea F M. An infrared investigation in relation with chitin and chitosan characterization. Polymer. 2001; 42(8): 3569–3580.

Capdevielle-Pardies P, David J, Miquel JL, Le Bras M. Quid of betel. Med Trop, 1985, 45: 299–307.

Castañeda MT, Alegret S. Electrochemical Sensing of DNA Using Gold Nanoparticles. Electroanalysis. 2007; 19(7-8):743–753.

Castro L, Blazquez ML, Gonzalez F, Munoz JA, Ballester A. Extracellular biosynthesis of gold nanoparticles using sugar beet pulp. Chem Eng J. 2010; 164: 92–97.

Castro L, Blazquez ML, Munoz JA, Gonzalez F, Garcia-Balboa C, Ballester A. Biosynthesis of gold nanowires using sugar beet pulp. Proc Biochem. 2011; 46:1076–1082.

Catherine L. Gold Nanoparticles for physics, chemistry and biolgy (Gold nanoparticles in the Past: Before the Nanotechnology Era). ISBN–13:9781848168060. 2012.

Chandran SP, Chaudhary M, Pasricha R, Ahmad A, Sastry M. Synthesis of Gold Nanotriangles and Silver Nanoparticles Using Aloevera Plant Extract. Biotechnol Prog. 2006; 22:577–583.

Chang RS, Yeung HW. Inhibition of growth of human immunodeficiency virus in vitro by crude extracts of Chinese medicinal herbs. Antiviral Research. 1988; 9(3): 163–175.

Charles SW, Popplewell J. Properties and applications of magnetic liquids. Hand Book of Magnetic Materials. , ed K H J Buschow, 1986.

Chen MS, Goodman DW. The Structure of Catalytically Active Gold on Titania. Science. 2004; 306:252–255.

Choi SK, Chun KY, Lee SB. Selective decoration of silver nanoparticles on the defect sites of single-walled carbon nanotubes. Diamond Relat Mater. 2009; 18:637–641.

Choudhury D, Kale RK. Antioxidant and non-toxic properties of *Piper betle* leaf extract: in vitro and in vivo studies. Phytother Res, 2002, 16: 461–466.

Chouzouri G, Xanthos M. In vitro bioactivity and degradation of polycaprolactone composites containing silicate fillers. Acta Biomater. 2007; 3:745–56.

Christophe A, Jacqueline T, Géraldine LD, Céline M, Claire B, Alice Le MH, Thierry B, Francis Vo, Marc J, Pascal P, Stéphane R, Olivier T. Gadolinium Chelate Coated Gold Nanoparticles As Contrast Agents for Both X- ay Computed Tomography and Magnetic Resonance Imaging. J. AM. CHEM. SOC. 2008; 130: 5908–5915

Collins PG, Avouris P. Scientific American. 2000; 62:283.

Cooke JP, Singer AH, Tsao P, Zera P, Rowan RA, Billingham M E. Antiatherogenic effects of L-arginine in the hypercholesterolemic rabbit. J Clin Invest. 1992; 90: 1168–1172.

Correa R, Gonzalez G, Dougar V. Emulsion polymerization in a microwave reactor. Polymer. 1998; 39(6-7): 1471–1474.

Cozzoli PD, Pellegrino T, Manna L. Synthesis, properties and perspectives of hybrid nanocrystal structures. Chem Soc Rev. 2006; 35:1195–1208.

Crooks RM, Zhao M, Sun L, Chechik V, Yeung LK. Dendrimer-encapsulated metal nanoparticles: Synthesis, characterization, and applications to catalysis. Accounts Chem. Res. 2002; 34: 181–190.

Da Fonseca AM, Bizerra AMC, De Souza JSN, Monte JCF, De Oliveira MCF, De Mattos, MC, Cordell GA, Braz-Filho R, Lemos TLG. Constituents and antioxidant activity of two varieties of coconut water (*Cocos nucifera* L.). Braz J Pharmacogn. 2009; 19(1B): 193–198.

Dameron CT, Reese RN, Mehra RK, Kortan AR, Carroll PJ, Steigerwald ML, et al. Biosynthesis of cadmium sulphide quantum semiconductor crystallites. Nature. 1989; 338:596–597.

Daniel MC, Astruc D. Gold Nanoparticles:• Assembly, Supramolecular Chemistry, Quantum-Size-Related Properties, and Applications toward Biology, Catalysis, and Nanotechnology. Chem ReV. 2004; 104:293–346.

Das J, Aziz MA, Yang HA. Nanocatalyst-Based Assay for Proteins: DNAFree Ultrasensitive Electrochemical Detection Using Catalytic Reduction of p-Nitrophenol by Gold-Nanoparticle Labels. J Am Chem Soc. 2006; 128(50):16022–16023.

Das RK, Borthakur BB, Bora U. Green synthesis of gold nanoparticles using ethanolic leaf extract of Centella asiatica. Materials Letters. 2010; 64(13): 1445–1447.

Das RK, Pragya S, Pradip N, Utpal B. Synthesis of gold nanoparticles using aqueous extract of Calotropis procera latex. Materials Letters. 2011; 65:610–613.

Das RK, Sharma P, Nahar P, Bora U. Synthesis of gold nanoparticles using aqueous extract of Calotropis procera latex. Materials Letters. 2011; 65(4): 610–613.

Dasgupta N, De B. Antioxidant activity of *Piper betel* L. leaf extract in vitro. Food Chem. 2004; 88: 219–224.

Dieter Vollath. Nanomaterials: An Introduction to Synthesis, Properties and Application; WILEY-VCH Verlag GmbH&Co. KGaA, Weinheim, Germany ISBN: 978-3-527-31531-4.

Ding L, Hao C, Xue Y, Ju H. A Bio-Inspired Support of Gold Nanoparticles-Chitosan Nanocomposites Gel for Immobilization and Electrochemical Study of K562 Leukemia Cells. Biomacromolecules. 2007; 8(4):1341–1346.

Dobhal U, Bisht NS, Bhandari SL. Traditional Values of Sapindus mukorossi gaertn. vern. Ritha: A Review. Plant Arch, 2007, 7: 485–486.

Dobson J. Gene therapy progress and prospects: magnetic nanoparticle-based gene delivery. Gene Ther. 2006; 13:283–287.

Du L, Jiang H, Xiaohua H, Wang E. Biosynthesis of gold nanoparticles assisted by Escherichia coli DH5• and its application on direct electrochemistry of hemoglobin. Electrochem Commun. 2007; 9:1165–1170.

Dua VK, Ojha VP, Roy R. Anti-malarial activity of some xanthones isolated from the roots of Andrographis paniculata. Journal of Ethnopharmacology. 2004; 95(2–3): 247–251.

Dubey SP, Lahtinen M, Sarkka H, Sillanpaa M. Bioprospective of Sorbus aucuparia leaf extract in development of silver and gold nanocolloids. Colloids Surf B Biointerfaces. 2010a; 80:26–33.

Dubey SP, Lahtinen M, Sillanpaa M. Green synthesis and characterizations of silver and gold nanoparticles using leaf extract of Rosa rugosa. Colloid Surf A Physicochem Eng Asp. 2010; 364:34–41.

Dubey SP, Lahtinen M, Sillanpaa M. Tansy fruit mediated greener synthesis of silver and gold nanoparticles. Proc Biochem. 2010; 45:1065–1071.

Dwivedi AD, Gopal K. Plant-Mediated Biosynthesis of Silver and Gold Nanoparticles. J Biomed Nanotechnol. 2011; 7:163–164.

Elghanian R, Storhoff JJ, Mucic RC, Letsinger RL, Mirkin CA. Selective Colorimetric Detection of Polynucleotides Based on the Distance-Dependent Optical Properties of Gold Nanoparticles. Science. 1997; 277:1078–1081.

El-Sayed MA. Some interesting properties of metals confined in time and nanometer space of different shapes. Accounts Chem Res. 2001; 34: 257–264.

Esumi K, Suzuki KA, Torigoe K. Preparation of gold nanoparticles in formamide and N,N dimethylformamide in the presence of poly(amidoamine) dendrimers with surface methyl ester groups. Colloids and Surfaces A: Physicochemical and Engineering Aspects. 2001; 189(1–3): 155–161.

Fan H, Lu Y, Stump A, Reed ST, Baer T, Schunk R, Perez-Luna V, Lopez GP, Brinker CJ. Rapid prototyping of patterned functional nanostructures. Nature. 2000; 405:56–60.

Faraday M, Phil. Trans. Roy. Soc. London. 1857; 147: 145–181.

Farokhzad OC, Cheng J, Teply BA, Sherifi I, Jon S, Kantoff PW, et al. Targeted nanoparticle-aptamer bioconjugates for cancer chemotherapy in vivo. Proc Natl Acad Sci. 2006; 103(16):6315–20.

Farokhzad OC, Jon SY, Khadelmhosseini A, Tran TNT, LaVan DA, Langer R. Nanopartide-aptamer bioconjugates: a new approach for targeting prostate cancer cells. Cancer Res. 2004; 64(21):7668–72.

Fayaz M, Balaji K, Girilal M, Yadav R, Kalaichelvan PT, Venketesan R. Biogenic synthesis of silver nanoparticles and their synergistic effect with antibiotics: a study against gram-positive and gram-negative bacteria. Nanomedicine. 2010; 6:103–109.

Feitz AGJ, Waite D. Process for producing a nanoscale zerovalent metal by reduction of inorganic salts with dithionite or borohydride. Australia: CRC for Waste Management and Pollution Control Limited, 2004.

Feldheim DL, Foss CAJ. Metal Nanoparticles: Synthesis, Characterization and Applications Eds. Marcel Dekker: New York. 2002.

Feng Y, Yu Y, Wang Y, Lin X. Biosorption and Bioreduction of Trivalent Aurum by Photosynthetic Bacteria Rhodobacter capsulatus. Curr Microbiol. 2007; 55:402–408.

Feynman RP. There's plenty of room at the bottom. Eng Sci. 1960; 23(5): 22–36.

Frenkel J, Dorfman J. Spontaneous and Induced Magnetisation in Ferromagnetic Bodies. Nature. 1930; 126:274.

Fricker SP. Medical uses of gold compounds: Past present and future. Gold Bull. 1996; 29: 53–60.

Gade AK, Bonde PP, Ingle AP, Marcato P, Duran N, Rai MK. Exploitation of Aspergillus niger for synthesis of silver nanoparticles. J Biobased Mater Bioenergy 2008; 2:1–5.

Gao HJ, Ji BH, Jager IL, Arzt E, Fratzl P. From the Cover: Materials become insensitive to flaws at nanoscale: Lessons from nature. Proc Natl Acad Sci. 2003; 100:5597–5600.

Gardea-Torresdey JL, Parsons JG, Gornez E, Peralta-Videa J, Troiani HE, Santiago P, et al. Formation and Growth of Au Nanoparticles inside Live Alfalfa Plants. Nano Lett. 2002; 2:397–401.

Gardea-Torresdey JL, Tiemann KJ, Gamez G, Dokken K, Tehuacanero S, Jose-Yacaman M. Gold Nanoparticles Obtained by Bio-precipitation from Gold(III) Solutions. J Nanopart Res. 1999; 1:397–404.

Gauthier O, Bouler JM, Aguado E, Pilet P, Daculsi G. Macroporous biphasic calcium phosphate ceramics: influence of macropore diameter and macroporosity percentage on bone ingrowth. Biomaterials. 1998; 19:133–9.

Georgakilas V, Gournis D, Tzitzios V, Pasquato L, Guldi DM, Prato M. Decorating carbon nanotubes with metal or semiconductor nanoparticles. J Mater Chem. 2007; 17:2679–2694.

Gericke M, Pinches A. Biological synthesis of metal nanoparticles. Hydrometallurgy. 2006a; 83:132–140.

Gericke M, Pinches A. Microbial production of gold nanoparticles. Gold Bull. 2006b; 39:22–28.

Ghasemi-Mobarakeh L, Prabhakaran MP, Morshed M, et al. Electrospun poly(•-caprolactone)/gelatin nanofibrous scaffolds for nerve tissue engineering. Biomaterials. 2008; 29(34): 4532– 4539.

Ghodake GS, Deshpande NG, Lee YP, Jin ES. Pear fruit extract-assisted room-temperature biosynthesis of gold nanoplates. Colloids Surf B Biointerfaces. 2010; 75: 584–589.

Ghosh P, Han G, De M, et al. Gold nanoparticles in delivery applications. Advanced Drug Delivery Reviews. 2008; 60(11): 1307–1315.

Ghule K, Ghule AV, Liu JY, Ling YC. Microscale Size Triangular Gold Prisms Synthesized Using Bengal Gram Beans (Cicer arietinum L.) Extract and $HAuCl_4 \cdot 3H_2O$: A Green Biogenic Approach. J Nanosci Nanotechnol. 2006; 6:3746–3751.

Giljohann DA, Seferos DS, Daniel WL. Gold nanoparticles for biology and medicine. Angew Chem Int Ed. 2010; 49(19): 3280–3294.

Gohil KJ, Patel JA. A review on Bacopa monniera: Current research and future prospects. Altern Med Rev. 2010; 4(1): 1–9.

Goodman SL. Collateral immunoprecipitation and localization of cellular antigens using monoclonal antibody-gold conjugates. Exp Cell Res. 1983; 144: 209–214.

Govindaraju K, Basha SK, Kumar VG, Singaravelu G. Silver, gold and bimetallic nanoparticles production using single-cell protein (Spirulina platensis) Geitler. J Mater Sci. 2008; 43:5115–5122.

Gref R, Domb A, Quellec P, et al. The controlled intravenous delivery of drugs using peg-coated sterically stabilized nanospheres. Adv Drug Deliver Rev. 1995; 16:215–233.

Griffith LG. Emerging design principles in biomaterials and scaffolds for tissue engineering. Ann NY Acad Sci. 2002; 961:83–95.

Grobmyer SR, Moudgil BM. Cancer Nanotechnology: Methods in Molecular Biology 624, DOI 10.1007/978-1-60761-609-2_11, © Springer Science+Business Media, LLC 2010.

Guo SJ, Pan XL, Gao HL, Yang ZQ, Zhao JJ, Bao XH. Probing the Electronic Effect of Carbon Nanotubes in Catalysis: NH_3 Synthesis with Ru Nanoparticles. Chem Eur J. 2010; 16:5379–5384.

Gupta G. Review: Microbicidal Spermicide or Spermicidal Microbicide. Eur. J. Contracept. Reprod. Health Care. 2005; 10: 212–218.

Gupta N, Singh HP, Sharma RK. Single-pot synthesis: Plant mediated gold nanoparticles catalyzed reduction of methylene blue in presence of stannous chloride. Colloid Surf A Physicochem Eng Asp. 2010; 367:102–107.

Haes AJ, van Duyne RP. A nanoscale optical biosensor: Sensitivity and selectivity of an approach based on the localized surface plasmon resonance spectroscopy of triangular silver nanoparticles. J Am Chem Soc. 2002; 124: 10596–10604.

Hamley IW. Nanotechnology with Soft Materials. Angew Chem Int Ed. 2003; 42:1692–1712.

Han G, Ghosh P, Rotello V M. Functionalized gold nanoparticles for drug delivery. Nanomedicine, 2007b, 2(1): 113–123.

Han G, Ghosh P, Rotello VM. Multi-functional gold nanoparticles for drug delivery. Advances in Experimental Medicine and Biology, 2007a, 620: 48–56.

Han M, Gao X, Su JZ, Nie S. Quantum-dot-tagged microbeads for multiplexed optical coding of biomolecules. Nature Biotechnology. 2001; 19:631–635.

Harekrishna B, Dipak KB, Gobinda PS, Priyanka S, Shankar PD, Ajay M. Green synthesis of silver nanoparticles using latex of Jatropha curcas. Colloids and Surfaces A: Physiochem Eng Aspects. 2009; 339:134–139.

Harne S, Sharma A, Dhaygude M, Joglekar S, Kodam K, Hudlikar M. Novel route for rapid biosynthesis of copper nanoparticles using aqueous extract of Calotropis procera L. latex and their cytotoxicity on tumor cells. Colloids and Surfaces B Biointerfaces. 2012; 95: 284–288.

Harrell JA, Brown VM. J Am Res Center Egypt. 1992; 29: 81.

Haustrup N, O'Connor GM. Nanoparticle Generation During Laser- ablation and Laser-Induced Liquifaction. Physics Procedia. 2011; 12: 46–53.

He S, Guo Z, Zhang Y, Zhang S, Wang J, Gu N. Biosynthesis of gold nanoparticles using the bacteria Rhodopseudomonas capsulata. Mater Lett. 2007; 61:3984–3987.

He S, Zhang Y, Guo Z, Gu N. Biological Synthesis of Gold Nanowires Using Extract of Rhodopseudomonas capsulate. Biotechnol Prog. 2008; 24:476–480.

He T, Ma Y, Cao Y, Jiang P, Zhang X, Yang W, et al. Enhancement Effect of Gold Nanoparticles on the UV-Light Photochromism of Molybdenum Trioxide Thin Films. Langmuir. 2001; 17: 8024–7.

Hench LL. Bioceramics. J Am Ceram Soc. 1998; 81:1705–28.

Hench LL. Ceramics glasses and glass–ceramics. In: Ratner BD, Hoffman AS, Schoen FJ, Lemons JE, editors. Biomaterials science: an introduction to materials in medicine. San Diego, CA: Academic Press; 1996. p. 84.

Hench LL. Sol–gel materials for bioceramic applications. Curr Opin Solid State Mater Sci. 1997; 2:604–10.

Hilbert I, Andra W, Bahring R, Daum A, Hergt R, Kaiser WA. Evaluation of Temperature Increase with Different Amounts of Magnetite in Liver Tissue Samples. Invest Radiol. 1997; 32:705–712.

Hiremath JG, Devi VK. Preparation and in vitro characterization of poly(epsilon-caprolactone)-based tamoxifen citrate-loaded cylindrical subdermal implant for breast cancer. Asian Journal of Pharmaceutics. 2011; 5(1): 9–14.

Hodes G. When Small Is Different: Some Recent Advances in Concepts and Applications of Nanoscale Phenomena. Adv Mater. 2007; 19:639–655.

Horbowicz M, Brenac P, Obendorf R L. Fagopyritol B1, O-• -Dgalactopyranosyl-(1!2)-D-chiro-inositol, a galactosyl cyclitol in maturing buckwheat seeds associated with desiccation tolerance. Planta, 1998, 205(1): 1–11.

Hosea M, Greene B, Mcpherson R, Henzl M, Alexander MD, Darnall DW. Accumulation of elemental gold on the alga Chlorella vulgaris. Inorg Chim Acta. 1986; 123:161–165.

Huang H, Yang X. Synthesis of polysaccharide-stabilized gold and silver nanoparticles: a green method. Carbohydrate Research. 2004; 339(15): 2627–2631.

Huang HC, Liao SC, Chang FR, Kuo YH, Wu Y C. Molluscicidal Saponins from Sapindus mukorossi, Inhibitory Agents of Golden Apple Snails: Pomacea Canaliculata. J Agric Food Chem. 2003; 51: 4916–4919.

Huang HC, Tsai WJ, Liaw CC, Wu SH, Wu YC, Kuo YH. Anti-platelet Aggregation Triterpene Saponins from the Galls of Sapindus mukorossi. Chem Pharm Bull. 2007; 55: 1412–1415.

Huang J, Li Q, Sun D, Lu Y, Su Y, Yang X, et al. Biosynthesis of silver and gold nanoparticles by novel sundried Cinnamomum camphora leaf. Nanotechnology. 2007; 18:105104–105115.

Huang J, Li Q, Sun D, Lu Y, Su Y, Yang X. Biosynthesis of silver and gold nanoparticles by novel sundried Cinnamomum camphora leaf. Nanotechnology. 2007; 18: 105104.

Huang SH. 'Gold nanoparticle-based immunochromatographic test for identification of taphylococcus aureus from clinical specimens. Clin Chim Acta. 2006; 373: 139–43.

Huang Y, Duan X, Lieber CM. Directed Assembly of One-Dimensional Nanostructures into Functional Networks. Science. 2001; 291:630–633.

Hunt LB. The true story of Purple of Cassius. Gold Bull. 1976; 9: 134–139.

Hunt LB. The oldest metallurgical handbook. Gold Bull. 1976; 9: 24–31.

Hussain I, Brust M, Papworth AJ, Cooper AI. Preparation of Acrylate-Stabilized Gold and Silver Hydrosols and Gold-Polymer Composite Films. Langmuir. 2003; 19: 4831–5.

Husseiny MI, Abd El-AM, Badr Y, Mahmoud MA. Biosynthesis of gold nanoparticles using Pseudomonas aeruginosa. SpectrochimActaA. 2007; 67:1003–1006.

Ibrahim M, Khan AA, Tiwari SK, Habeeb MA, Khaja MN., Habibullah CM. Antimicrobial Activity of Sapindus mukorossi and Rheum emodi Extracts Against H. pylori: in vitro and in vivo Studies. World J. Gastroenterol, 2006, 12: 7136–7142.

Ibrahim M, Mohammed NK., Anjum A, Aleem AK, Mohammed AH, Yalavarthy PD, Mangamoori LN, Chitoor MH. Hepatoprotective Activity of Sapindus mukorossi and Rheum Emodi Extracts. World J Gastroenterol, 2008, 14(16): 2566–2571.

Ihme N, Kiesewetter H, Jung F. Leg oedema protection from a buckwheat herb tea in patients with chronic venous insufficiency: a single-centre, randomised, double-blind, placebo-controlled clinical trial. European Journal of Clinical Pharmacology, 1996, 50(6): 443–447.

Ingle A, Rai M, Gade A, Bawaskar M. Fusarium solani: a novel biological agent for the extracellular synthesis of silver nanoparticles. J Nanopart Res. 2009; 11:2079–2085.

Iuorno M J, Jakubowicz D J, Baillargeon JP. Effects of Dchiro- inositol in lean women with the polycystic ovary syndrome. Endocrine Practice. 2002; 8(6): 417–423.

Jain KK. Role of nanobiotechnology in developing personalized medicine for cancer. Technology in Cancer Research and Treatment. 2005; 4(6): 645–650.

Jarukamjorn K, Nemoto N. Pharmacological aspects of Andrographis paniculata on health and its major diterpenoid constituent Andrographolide. Journal of Health Science. 2008; 54(4): 370– 381.

Jebakumar IET, Sethuraman MG. Instant green synthesis of silver nanoparticles using Terminalia chebula fruit extract and evaluation of their catalytic activity on reduction of methylene blue. Process Biochemistry. 2012; 47:1351–1357.

Jenssen H, Hamill P, Hancock RE. Peptide antimicrobial agents. Clin Microbiol Rev. 2006; 19: 491–511.

Ji BH, Gao HJ. Mechanical properties of nanostructure of biological materials. J Mech Phys Solids. 2004; 52:1963–1990.

Jiang G, Shi D. Coating of HA on porous alumina substrate through a thermal decomposition method. J Biomed Mater Res. 1999; 48:117–20.

Jin RC, Cao YW, Mirkin CA, Kelly KL, Schatz GC, Zheng JG. Science. 2001; 294: 1901–1903.

Joseph W. Towards Genoelectronics: Electrochemical Biosensing of DNA Hybridization. Chemistry - A European Journal. 1999; 5(6):1681–1685.

Justin G. Electrochemical DNA Hybridization Biosensors. Electroanalysis. 2002; 14(17):1149–1156.

Kachenko AG, Xie H, Coleman D, Glomm W, Ryan J, Anderson MF, Franzen S, Feldheim DL. Multifunctional Gold Nanoparticle–Peptide Complexes for Nuclear Targeting. J Am Chem Soc. 2003; 125: 4700–4701.

Kamigaito O, What can be improved by nanometer composites? J. Jpn. Soc. Powder Powder Metall. 38:315-21, 1991 in Kelly, A, Concise encyclopedia of composites materials, Elsevier Science Ltd, 1994.

Kang YS, Risbud S, Rabolt JF, Stroeve P. Synthesis and characterization of nanometer-size Fe3O4 and •-Fe2O3 Particles. Chem Mater. 1996; 8:2209–2211.

Kannan P, Abraham John S. Synthesis of mercaptothiadiazolefunctionalized gold nanoparticles and their self-assembly on Au substrates. Nanotechnology. 2008; 19(8): 085602.

Kannan P, John SA. Synthesis of mercaptothiadiazole-functionalized gold nanoparticles and their self-assembly on Au substrates. Nanotechnology. 2008; 19: 085602.

Kao MT, Popular Herbal Remedies of Taiwan (2); Southern Materials Center, Inc: Taipei, 1988; p 139.

Kasai R, Fujino H, Kuzuki T, Wong WH, Goto C, Yata N, Tanaka O, Yasuhara F, Yamaguchi S. Acyclic Sesquiterpene Oligoglycosides from Pericarps of Sapindus mukurossi. Phytochemistry. 1986; 25: 871–876.

Kasthuri J, Kathiravan K, Rajendiran N. Phyllanthin-assisted biosynthesis of silver and gold nanoparticles: a novel biological approach. J Nanopart Res. 2009b; 11:1075–1085.

Kasthuri J, Veerapandian S, Rajendiran N. Biological synthesis of silver and gold nanoparticles using apiin as reducing agent. Colloids Surf B Biointerfaces. 2009a; 68:55–60.

Kathiresan K, Manivanan S, Nabeel MA, Dhivya B. Studies on silver nanoparticles synthesized by a marine fungus, Penicillium fellutanum isolated from coastal mangrove sediment. Coll Surf B: Biointerf. 2009; 71:133–137.

Katz E, Willner I. Integrated Nanoparticle–Biomolecule Hybrid Systems: Synthesis, Properties, and Applications. Angew Chem Int Ed Engl. 2004; 43:6042–6108.

Khalil MMH, Ismail EH, El-Magdoub F. Arab J Chem, in press, doi:10.1016/j. arabjc.2010.11.011.

Khomutov GB. Two-Dimensional Synthesis of Anisotropic Nanoparticles. Colloids Surf. 2002; 202:243–267.

Ki CS, Baek DH, Gang KD, et al. Characterization of gelatin nanofiber prepared from gelatin–formic acid solution. Polymer. 2005; 46(14): 5094–5102.

Kim F, Connor S, Song H, Kuykendall T, Yang P. Platonic Gold Nanocrystals. Angew Chem Int Ed. 2004; 43:3673–3677.

Kim NH, Baek TJ, Park HG, Seong GH. Highly Sensitive Biomolecule Detection on a Quartz Crystal Microbalance Using Gold Nanoparticles as Signal Amplification Probes. Analytical Sciences. 2007; 23(2):177–181.

Kimling J, Maier M, Okenve B, Kotaidis V, Ballot H, Plech A. Turkevich Method for Gold Nanoparticle Synthesis Revisited. J Phys Chem B. 2006; 110:15700–15707.

Kirtikar KR, Basu BD. Indian medicinal plants. Periodical Experts. 1975; 3: 1884–1886.

Klaus T, Joerger R, Olsson E, Granqvist CG. Silver-based crystalline nanoparticles, microbially fabricated. Proc Natl Acad Sci. 1999; 96: 13611–13614.

Knosp H, Holliday RJ, Corti CW. Gold in dentistry: Alloys, uses and performance. Gold Bull. 2003; 36: 93–102.

Kokubo T, Kim HM, Kawashita M. Novel bioactive materials with different mechanical properties. Biomaterials. 2003; 24:2161–75.

Konish Y, Deshmukh N, Tsukiyama T, Saitoh N. Microbial preparation of gold nanoparticles by anaerobic bacterium. Trans Mater Res Soc Jpn. 2004; 29: 2341–2343.

Konishi Y, Tsukiyama T, Tachimi T, Saitoh N, Nomura T, Nagamine S. Microbial deposition of gold nanoparticles by the metal-reducing bacterium Shewanella algae. Electrochim Acta. 2007; 53:186–192.

Kowshik M, Vogel W, Urban J, Kulkarni SK, Paknikar KM. Microbial Synthesis of Semiconductor PbS Nanocrystallites. Adv Mater. 2002; 14:815–818.

Kreft S, Knapp M, Kreft I. Extraction of rutin from buckwheat (Fagopyrum esculentum Moench) seeds and determination by capillary electrophoresis. Journal of Agricultural and Food Chemistry. 1999; 47(11): 4649–4652.

Kreft S, Strukelj B, Gaberscik A, et al. Rutin in buckwheat herbs grown at different UV-B radiation levels: comparison of two UV spectrophotometric and an HPLC method. Journal of Experimental Botany. 2002; 53(375): 1801–1804.

Krimm S, Bandekar J. Vibrational spectroscopy and conformation of peptides, polypeptides, and proteins. Advances in Protein Chemistry. 1986; 38: 181–364.

Krpetic Z, Scari G, Caneva E, Speranza G, Porta F. Gold Nanoparticles Prepared Using Cape Aloe Active Components. Langmuir. 2009; 25:7217–7221.

Kruis FE, Fissan H, Peled A. Synthesis of nanoparticles in the gas phase for electronic, optical and magnetic applications. J Aerosol Sci. 1998; 29(5–6):511–535.

Krumov N., Stephanie O, Perner NI, Angel A, Clemens P. Journal of Biotechnology. 2007; 132:481–486.

Kumar A, Chattopadhyay S. DNA damage protecting activity and antioxidant potential of pudina extract. Food Chem. 2007; 100: 1377–1384.

Kumar P, Singh P, Kumari K, Mozumdar S, Chandra R. A green approach for the synthesis of gold nanotriangles using aqueous leaf extract of Callistemon viminalis. Mater Lett. 2011; 65:595–597.

Kuo YH, Huang HC, Yang Kuo LM, Hsu YW, Lee KH, Chang FR, Wu YC. New Dammarane-type Saponins from the Galls of Sapindus mukorossi. J Agric Food Chem. 2005; 53: 4722–4727.

Laura C, Blazquez ML, Felisa G, Jesus AM, Antonio B. Extracellular biosynthesis of gold nanoparticles using sugar beet pulp. Chemical Engineering Journal. 2010; 164:92–97.

Law M, Sibuly DJ, Johnson JC, Goldberger J, Saykally RJ, Yang P. Nanoribbon Waveguides for Subwavelength Photonics Integration. Science. 2004; 305:1269–1273.

Lee KB, Kim EY, Mirkin CA, et al. The use of nanoarrays for highly sensitive and selective detection of human immunodeficiency virus type 1 in plasma. Nano Letters. 2004; 4(10): 1869– 1872.

Lee SW, Mao C, Flynn CE, Belcger AM. Ordering of Quantum Dots Using Genetically Engineered Viruses. Science. 2002; 296:892–895.

Lengke M, Fleet ME, Southam G. Morphology of Gold Nanoparticles Synthesized by Filamentous Cyanobacteria from Gold(I)−Thiosulfate and Gold(III)−Chloride Complexes. Langmuir. 2006b; 22:2780–2787.

Lengke M, Ravel B, Fleet ME, Wanger G, Gordon RA, Southam G. Mechanisms of Gold Bioaccumulation by Filamentous Cyanobacteria from Gold(III)−Chloride Complex. Environ Sci Technol. 2006c; 40:6304–6309.

Lengke M, Southam G. Bioaccumulation of gold by sulfate-reducing bacteria cultured in the presence of gold(I)-thiosulfate complex. Geochim Cosmochim Acta. 2006a; 70:3646–3661.

Leonard K, Ahmmad B, Okamura H, Kurawaki J. In situ green synthesis of biocompatible ginseng capped gold nanoparticles with remarkable stability. Colloids Surf B Biointerfaces. 2011; 82:391–396.

Lewis LN. Chemical catalysis by colloids and clusters. Chem Rev. 1993; 93: 2693–730.

Lewis LN. Chemical catalysis by colloids and clusters. Chemical Reviews. 1993; 93(8): 2693–2730.

Lin J, Zhou W, O'Connor C J. Formation of ordered arrays of gold nanaoparticles from CTAB reverse micelles. Materials Letters. 2001; 49(5): 282–286.

Londokar RL, Poddar PV. Studies on activity of various extract of Mentha arvensis Linn against drug induced gastric ulcer in mammals. Gastrointest Oncol. 2009; 15(1): 82–88.

Lu LP, Wang SQ, Lin XQ. Fabrication of layer-by-layer deposited multilayer films containing DNA and gold nanoparticle for norepinephrine biosensor. Analytica Chimica Acta. 2004; 519(2):161–166.

Lupold SE, Hicke BJ, Lin Y, Coffey DS. Identification and characterization of nuclease-stabilized RNA molecules that bind human prostate cancer cells via the prostate-specific membrane antigen. Cancer Res. 2002; 62(14):4029–33.

Ma J, Wong H, Kong LB, Peng KW. Biomimetic processing of nanocrystallite bioactive apatite coating on titanium. Nanotechnology. 2003; 14(6):619–623.

Madav S, Tandan SK, Lal J, et al. Anti-inflammatory activity of andrographolide. Fitoterapia. 1996; 67(5): 452–458.

Mahishi P, Srinivasa BH, Shivanna MB. Medicinal plant wealth of local communities in some villages in ShimogaDistrict of Karnataka, India. J Ethnopharmacol. 2005; 98: 307–312.

Mai, Yu Z, 2006. Polymer Nanocomposites. Woodhead Publ.. ISBN 978-1-85573-969-7. "Polymer-Clay Nanocomposites", T. J. Pinnavaia, G. W. Beall (eds.), Wiley, 2001; ISBN 978-0-471-63700-4.

Maier SA, Brongersma ML, Kik PG, Meltzer S, Requichia AAG, Atwater H. Plasmonics—A Route to Nanoscale Optical Devices. AdV Mater. 2001; 13:1501–1505.

Maier SA, Kik PG, Atwater HA, Meltzer S, Harel E, Koel BE, Requicha AA. Local detection of electromagnetic energy transport below the diffraction limit in metal nanoparticle plasmon waveguides. Nature Mater. 2003; 2:229–232.

Maisonhaute E, Prado C, White PC, et al. Surface acoustic cavitation understood via nanosecond electrochemistry. Part III: Shear stress in ultrasonic cleaning. Ultrasonics Sonochemistry. 2002; 9(6): 297–303.

Mallick K, Wang ZL, Pal T. Seed- Mediated Successive Growth of Gold Particles Accomplished by UV Irradiation: A Photochemical Approach for Size-Controlled Synthesis. J Photochem Photobiol. 2001; 140:75–80.

Mallick K, Wang ZL, Pal T. Seed-Mediated Successive Growth of Gold Particles Accomplished by UV Irradiation: a Photochemical Approach for Size-Controlled Synthesis. J Photochem Photobiol. 2001; 140:75–80.

Mallouk TE, Kovtyukhova NI. Nanowires as Building Blocks for Self-Assembling Logic and Memory Circuits. Chem Eur J. 2002; 8:4354–4363.

Manias, Evangelos. Nanocomposites: Stiffer by design. Nature Materials. 2007; 6(1):9–11.

Mano JF, Sousa RA, Boesel LF, Neves NM, Reis RL. Bioinert, biodegradable and injectable polymeric matrix composites for hard tissue replacement: state of the art and recent developments. Compos Sci Technol. 2004; 64:789–817.

Maquet V, Boccaccini AR, Pravata L, Notingher I, Je´roˆme R. Porous poly(a-hydroxyacid)/bioglass composite scaffolds for bone tissue engineering. I: Preparation and in vitro characterization. Biomaterials. 2004; 25:4185–94.

Marshall AT, Haverkamp RG, Davies CE, Parsons JG, Gardea-Torresdey JL, Agterveld. Accumulation of gold nanoparticles in Brassic juncea. Int J Phytoremediation, 2007, 9(3):197–206.

Mason TJ, Cobley AJ, Graves JE, et al. New evidence for the inverse dependence of mechanical and chemical effects on the frequency of ultrasound. Ultrasonics Sonochemistry. 2011; 18(1): 226–230.

Maye MM, Lou Y, Zhong CJ. Core-Shell Gold Nanoparticle Assembly as Novel Electrocatalyst of CO Oxidation. Langmuir. 2000; 16(19):7520–7523.

Mena ML, Yanez-Sedeno P, Pingarron JM. A comparison of different strategies for the construction of amperometric enzyme biosensors using gold nanoparticle-modified electrodes. Analytical Biochemistry. 2005; 336(1):20–27.

Mishra AN, Bhadauria S, Gaur MS, Pasricha R, Kushwah BS. Synthesis of Gold Nanoparticles by Leaves of Zero-Calorie Sweetener Herb (Stevia rebaudiana) and Their Nanoscopic Characterization by Spectroscopy and Microscopy. Int J Green Nanotechnol Phys Chem. 2010; 1:118–124.

Mody VV, Siwale R, Singh A, et al. Introduction to metallic nanoparticles. Journal of Pharmacy and Bioallied Sciences. 2010; 2(4): 282–289.

Mohanpuria P, Rana NK, Yadav SK. Biosynthesis of nanoparticles: technological concepts and future applications, Journal of Nanoparticle Research, 2008, 10 (3): 507–517.

Molday RS, Mackenzie D. Immunospecific ferromagnetic iron-dextran reagents for the labeling and magnetic separation of cells. Journal ofImmunological Methods. 1982; 52(3):353–367.

Mondal S, Roy N, Laskar RA, Ismail SK, Basu S, Mandal D, et al. Biogenic synthesis of Ag, Au and bimetallic Au/Ag alloy nanoparticles using aqueous extract of mahogany (Swietenia mahogani JACQ.) leaves. Colloids Surf B Biointerfacesaces. 2011; 82:497–504.

Montes MO, Mayoral A, Deepak FL, Parsons JG, Jose-Yacaman M, Peralta-Videa JR, et al. Anisotropic gold nanoparticles and gold plates biosynthesis using alfalfa extracts. J Nanopart Res. 2011; 13:3113–3121.

Mukherjee P, Ahmad A, Mandal D, Senapati S, Sainkar SR, Khan MI, et al. Bioreduction of $AuCl_4^-$ Ions by the Fungus Verticillium sp. and Surface Trapping of the Gold Nanoparticles Formed. Angew Chem Int Ed. 2001; 40:3585–3588.

Mukherjee P, Ahmad A, Mandal D. Fungus-mediated synthesis of silver nanoparticles and their immobilization in the mycelial matrix: a novel biological approach to nanoparticle synthesis. Nano Letters, 2001a, 1(10): 515–519.

Mukherjee P, Ahmad A, Mandal M, Senapati S, Sainkar SR, Khan MI, Parischa R, Ajayakumar V. Bioreduction of $AuCl_4$-ions by the fungus Verticillium sp. And surface trapping of the gold nanoparticle formed dquote. Angew Chem Int Ed. 2001; 40: 3585–3588.

Mukherjee P, Roy M, Mandal BP, Dey GK, Mukherjee PK, Ghatak J, et al. Green synthesis of highly stabilized nanocrystalline silver particles by a non-pathogenic and agriculturally important fungus T. asperellum. Nanotechnology. 2008; 19:075103.

Mukherjee P, Senapati S, Ahmad A, Khan MI, Sastry M. Extracellular Synthesis of Gold Nanoparticles by the Fungus Fusarium oxysporum. ChemBiochem. 2002; 5: 461–463.

Mukherjee P, Senapati S, Mandal D, et al. Extracellular Synthesis of Gold Nanoparticles by the Fungus Fusarium oxysporum. ChemBioChem. 2002; 3:461–463.

Mukherjee P, Senapati S, Mandal D, et al. Extracellular Synthesis of Gold Nanoparticles by the Fungus Fusarium oxysporum. ChemBioChem. 2002; 3:461–463.

Nagahama H, Maeda H, Kashiki T, et al. Preparation and characterization of novel chitosan/gelatin membranes using chitosan hydrogel. Carbohydrate Polymers. 2009; 76(2): 255–260.

Nagaraj B, Agnieszka SK, Dagmara M, Yathirajan HS, Keerthi VR, Chandrashekar N, Salman D, Liny P. Plant mediated synthesis of gold nanoparticles using fruit extracts of Ananas comosus (L.) (Pineapple) and evaluation of biological activities. 2012; DOI:10.5185/amlett.2012.9423.

Nahar P, Bora U. Microwave-mediated rapid immobilization of enzymes onto an activated surface through covalent bonding. Analytical Biochemistry, 2004, 328 (1): 81–83

Nanjing Zhongyiyao University, The Dictionary of Traditional Chinese Medicines (Shanghai Science and Technology Press, Shanghai, 2006.

Narayanan KB, Sakthivel N. Biological synthesis of metal nanoparticles by microbes. Advances in Colloid and Interface Science. 2010; 156: 1–13.

Narayanan KB, Sakthivel N. Coriander leaf mediated biosynthesis of gold nanoparticles. Mater Lett. 2008; 62: 4588–4590.

Narayanan KB, Sakthivel N. Green synthesis of biogenic metal nanoparticles by terrestrial and aquatic phototrophic and heterotrophic eukaryotes and biocompatible agents. Advances in Colloid and Interface Science. 2011; 169(2): 59–79.

Narayanan KB, Sakthivel N. Phytosynthesis of gold nanoparticles using leaf extract of Coleus amboinicus Lour. Mater Charact. 2010; 61:1232–1238.

Nazimudeen SK, Ramaswamy S, Kameswaran L. Effect of Andrographis paniculata on snake venom induced death and its mechanism. Indian Journal of Pharmaceutical Sciences. 1978; 40 (4): 132–133.

Nestler JE, Jakubowicz DJ, Reamer P. Ovulatory and metabolic effects of d-chiro-inositol in the polycystic ovary syndrome. The New England Journal of Medicine. 1999; 340(17): 1314–1320.

Nilesh P, Luigi B, Giuseppe P, Sanjay R. Influence of shear in the crystallization of polyethylene in the presence of SWCNTs. Carbon. 2010; 48(14):4116–4128.

Niranjan R, Nivedita R, Ritu I, Chandrasekaran S. Phenolic antibacterials from *Piper betle* in the prevention of halitosis. J Ethnopharmacol. 2002; 83: 149–152.

Nirmala G, Pandian K. One pot synthesis of polymer protected gold nanoparticles and nanoprisms in glycerol A. Colloids and Surfaces A: Physicochem Eng Aspects. 2006; 290:138–142.

Nishat A, Faheem A, Shalendra K, Anwar MS, Lu J, Bon HK, Lee CG. Microwave assisted synthesis of gold nanoparticles and their antibacterial activity against Escherichia Coli. Current Applied Physics. 2011; 11:S360–S363.

Noruzi M, Zare D, Khoshnevisan K, Davoodi D. Rapid green synthesis of gold nanoparticles using Rosa hybrida petal extract at room temperature. Spectrochim Acta A. 2011; 79:1461–1465.

Nune SK, Chanda N, Shukla R, et al. Green nanotechnology from tea: phytochemicals in tea as building blocks for production of biocompatible gold nanoparticles. Journal of Materials Chemistry. 2009; 19(19): 2912–2920.

Okitsu K, Mizukoshi Y, Bandow H, Maeda Y, Yamamoto T, Nagata Y. Formation of noble metal particles by ultrasonic irradiation. Ultrason Sonochem. 1996; 3:S249–S251.

Okitsu K, Yue A, Tanabe S, Matsumoto H, Yobiko Y. Sonochemical synthesis of gold nanoparticles on chitosan. Mater Lett. 2008; 61: 3429–3431.

O'Neal DP, Hirsch LR, Halas NJ, Payne JD, West JL. Photothermal tumor ablation in mice using near infrared-absorbing nanoparticles. Cancer Letters. 2004; 209(2):171–176.

Palgave RG, Parkin IP. Surfactant directed chemical vapour deposition of gold nanoparticles with narrow size distributions. Gold Bull. 2008; 41:66–69.

Pankhurst QA, Connolly J, Jones SK, Dobson J. Applications of magnetic nanoparticles in biomedicine. Journal of Physics D: Applied Physics. 2003; 36(13):R167–R181.

Panyam J, Labhasetwar V. Biodegradable nanoparticles for drug and gene delivery to cells and tissue. Advanced Drug Delivery Reviews. 2003; 55(3):329–347.

Parak RB. Cell Motility and Metastatic Potential Studies Based on QuantumDot Imaging of Phagokinetic Tracks. Advanced Materials. 2002; 14(12):882–885.

Parak WJ, Gerion D, Pellegrino T, Zanchet D, Micheel C, Williams SC, Boudreau R, Gros MAL, Larabell CA, Alivisatos AP. Biological applications of colloidal nanocrystals. Nanotechnology. 2003; 14(7):R15–R27.

Parish RV, Cotrill SM. Medicinal gold compounds. Gold Bull. 1987; 20: 3–12.

Patel K, Kapoor S, Dave DP, Mukherjee T. Synthesis of nanosized silver colloids by microwave dielectric heating. Journal of Chemical Sciences. 2005; 117(1): 53–60.

Patel K, Kapoor S, Dave DP, Mukherjee T. Synthesis of nanosized silver colloids by microwave dielectric heating. Journal of Chemical Sciences. 2005; 117(1): 53–60.

Pérez-Arantegui J, Molera JT, Larrea A, Pradell T, Vendrell-Saz M. Luster Pottery from the Thirteenth Century to the Sixteenth Century: A Nanostructured Thin Metallic Film. J Am Ceram Soc. 2001; 84: 442–446.

Philip D, Unni C, Aromal SA, Vidhu VK. Murraya Koenigii leaf-assisted rapid green synthesis of silver and gold nanoparticles. Spectrochim Acta A. 2011b; 78:899–904.

Philip D, Unni C. Extracellular biosynthesis of gold and silver nanoparticles using Krishna tulsi (Ocimum sanctum) leaf. Physica E. 2011a; 43:1318–1322.

Philip D. Biosynthesis of Au, Ag and Au–Ag nanoparticles using edible mushroom extract. Spectrochim Acta. 2009; 73: 374–381.

Philip D. Green synthesis of gold and silver nanoparticles using Hibiscus rosa sinensis. Physica E. 2009; 42:1417–1424.

Philip D. Rapid green synthesis of spherical gold nanoparticles using Mangifera indica leaf. Spectrochim Acta A. 2010; 77:807–810.

Pongpech P, Prasertsilpe VJ. The study of antimicrobial activity of *Piper betle* cream and gel against some fungi, yeast and bacteria. GPO. 1993; 19: 8–22.

Prabhu MS, Patel K, Saraawathi G, Srinivasan K. Effect of orally administered betel leaf (*Piper betle* leaf Linn.) on digestive enzymes of pancreas and intestinal mucosa and on bile production in rats. Indian J Exp Biol. 1995; 33: 752–756.

Pradeep K, Prashant S, Kamlesh K, Subho M, Ramesh C. A green approach for the synthesis of gold nanotriangles using aqueous leaf extract of Callistemon viminalis. Mater Lett. 2011; 65: 595–7.

Preeti D, Mausumi M. Prunus domestica Fruit Extract-Mediated Synthesis of Gold Nanoparticles and Its Catalytic Activity for 4-Nitrophenol Reduction. Ind Eng Chem Res. 2012; 51(40): 13014–13020.

Puri A, Saxena R, Saxena RP, et al. Immunostimulant agents from Andrographis paniculata. Journal of Natural Products. 1993; 56 (7): 995–999.

Quetin-Leclercq J, Elias R., Balansard G, Bassleer R, Angenot L. Cytotoxic Activity of Some Triterpenoid Saponins. Planta Med. 1992; 58: 279–281.

Raghunandan D, Basavaraja S, Mahesh B. Biosynthesis of stable polyshaped gold nanoparticles from microwave-exposed aqueous extracellular anti-malignant guava (Psidium guajava) leaf extract. Nanobiotechnology. 2009; 5(1–4): 34–41.

Raj CR, Okajima T, Ohsaka T. Gold nanoparticle arrays for the voltammetric sensing of dopamine. Journal of Electroanalytical Chemistry. 2003; 543(2):127–133.

Raju D, Mehta UJ, Hazra S. Synthesis of gold nanoparticles by various leaf fractions of Semecarpus anacardium L tree. Trees. 2011; 25:145–151.

Raju M, Varakumar S, Lakshminarayana R, Krishnakantha TP, Baskaran V. Carotenoid composition and vitamin A activity of medicine important green leafy vegetables. Food Chem. 2007; 101: 1598–1605.

Ramezani N, Ehsanfar Z, Shamsa F, Amin G, Shahverdi HR, Esfahani HRM, et al. Screening of Medicinal Plant Methanol Extracts for the Synthesis of Gold Nanoparticles by Their Reducing Potential. Z Naturforsch. 2008; 63b:903–908.

Raveendran P, Fu J, Wallen SL. Completely"green" synthesis and stabilization of metal nanoparticles, Journal of the American Chemical Society. 2003; 125 (46): 13940–13941.

Razak FA, Othman RY, Haji ZHA. Evaluation of antihistaminic activity of *Piper betel* leaf in guinea pig. J Oral Sci. 2006; 48: 71–75.

Reich DH, Tanase M, Hultgren A, Bauer LA, Chen CS, Meyer GJ. Biological applications of multifunctional magnetic nanowires (invited). Journal of Applied Physics. 2003; 93(10):7275–7280.

Rodriguez E, Peralta-Videa JR, Sanchez-Salcido B, Parsons JG, Romero J, Gardea-Torresdey JL. Improving gold phyto extraction in desert willow (*chilopsis linearis*) using thiourea: a spectreoscopic investigation. Environ Chem. 2007; 4(2):98–108.

Roy I, Ohulchanskyy TY, Pudavar HE, Bergey EJ, Oseroff AR, Morgan J, Dougherty TJ, Prasad PN. Ceramic-BasedNanoparticles Entrapping Water-Insoluble Photosensitizing AnticancerDrugs: A Novel Drug-Carrier System for Photodynamic Therapy. J Am Chem Soc. 2003; 125(26):7860–7865.

Rudge S, Peterson C, Vessely C, Koda J, Stevens S, Catterall L. Adsorption and desorption of chemotherapeutic drugs from a magnetically targeted carrier (MTC). J Control Release. 2001; 74:335–340.

Sahoo R, Sahoo S, Sahoo S, et al. Synthesis and characterization of polycaprolactone–gelatin nanocomposites for control release anticancer drug paclitaxel. European Journal of Scientific Research. 2011; 48(3): 527–537.

Sahu A, Goswami P, Bora U. Microwavemediated rapid synthesis of chitosan. Journal of Materials Science. 2009; 20(1): 171–175.

Salata O. Applications of nanoparticles in biology and medicine. J Nanobiotechnol. 2004; 2:3.

Salata OV. Applications of nanoparticles in biology and medicine. Journal of Nanobiotechnology. 2004; 2:3–6.

Salem AK, Searson PC, Leong KW. Multifunctional nanorods for gene delivery. Nature Mater. 2003; 2:668–671.

Sanghi R, Verma P. Biomimetic synthesis and characterisation of protein capped silver nanoparticles. Bioresour Technol. 2009; 100:501–504.

Santhanam G, Nagarjan S. Development and validation of UV spectroscopic methods for the quick estimation of *Piper betle* leaf (PBL) extract. Fitoterapia. 1990; 61: 458–459.

Sato M, Webster TJ. Nanobiotechnology: implications for the future ofnanotechnology in orthopedic applications. Expert Rev Med Devices. 2004; 1(1):105–114.

Schlögl R, Hamid SBA. Nanocatalysis: Mature Science Revisited or Something Really New?. Angew Chem Int Ed. 2004; 43:1628–1637.

Schultz DA. Plasmon resonant particles for biological detection. Curr Opin Biotechnol. 2003; 14:13–22.

Selvakannan PR, Mandal S, Pasricha R, Adyanthaya SD, Sastry M. One-step synthesis of hydrophobized gold nanoparticles of controllable size by the reduction of aqueous chloroaurate ions by hexadecylaniline at the liquid–liquid interface. Chem Comm. 2002; 13: 1334–1335.

Selvakannan PR, Mandal S, Renu P, Murali S. Hydrophobic organically dispersible gold nanoparticles of variable shape produced by the spontaneous reduction of aqueous chloroaurate ions by hexadecylaniline molecules. Journal of Colloid and Interface Science. 2004; 279:124–131.

Shah Mohammadi M, Ahmed I, Marelli B, et al. Modulation of polycaprolactone composite properties through incorporation of mixed phosphate glass formulations. Acta Biomaterialia. 2010; 6 (8): 3157–3168.

Shaligram NS, Bule M, Bhambure R, Singhal RS, Singh SK, Szakacs G, et al. Biosynthesis of silver nanoparticles using aqueous extract from the compactin producing fungal strain. Proc Biochem. 2009; 44:939–943.

Shankar SS, Ahmad A, Pasricha R, Sastry M. Bioreduction of chloroaurate ions by geranium leaves and its endophytic fungus yields gold nanoparticles of different shapes. J Mat Chem. 2003; 13:1822–1826.

Shankar SS, Rai A, Ahmad A, et al. Rapid synthesis of Au, Ag, and bimetallic Au core–Ag shell nanoparticles using Neem (Azadirachta indica) leaf broth. Journal of Colloid and Interface Science. 2004a; 275(2): 496–502.

Shankar SS, Rai A, Ahmad A, Sastry M. Biological synthesis of triangular nanoprisms. Nat. mat, 2004a (3), 482–489.

Shankar SS, Rai A, Ahmad A, Sastry M. Rapid synthesis of Au, Ag, and bimetallic Au core–Ag shell nanoparticles using Neem (Azadirachta indica) leaf broth. J Colloid Interface Sci. 2004c; 275:496–502.

Shankar SS, Rai A, Ankamwar B, Singh A, Ahmad A, Sastry M. Biological synthesis of triangular gold nanoprisms. Nat Mater. 2004b; 3: 482–488.

Sharma NC, Sahi SV, Nath S, Parsons JG, Gardea-Torresdey JL, Pal. Synthesis of Plant-Mediated Gold Nanoparticles and Catalytic Role of Biomatrix-Embedded Nanomaterials. T. Environ Sci Technol, 2007, 41:5137–5142.

Shashi PD, Manu L, Mika S. Tansy fruit mediated greener synthesis of silver and gold nanoparticles. Process Biochemistry. 2010; 45: 1065–1071.

Shaw CF. Gold-based therapeutic agents. Chem. Rev. 1999, 99, 2589–2600.

Sheeja K, Kuttan G. Effect of Andrographis paniculata as an adjuvant in combined chemo-radio and whole body hyperthermia treatment — a preliminary study. Immunopharmacology and Immunotoxicology. 2008; 30(1): 181–194.

Shenton W, Douglas T, Young M, Stubbs G, Mann S. Inorganic–Organic Nanotube Composites from Template Mineralization of Tobacco Mosaic Virus. AdvMatter. 1999; 11:253–256.

Sheny DS, Mathew J, Philip D. Phytosynthesis of Au, Ag and Au–Ag bimetallic nanoparticles using aqueous extract and dried leaf of Anacardium occidentale. Spectrochim Acta A. 2011; 79:254–262.

Shi D, Jiang G, Wen X. In vitro bioactive behavior of hydroxylapatite- coated porous Al2O3. J Biomed Mater Res. 2000; 53:457–66.

Shimizu T, Teranishi T, Hasegawa S, Miyake M. Size Evolution of Alkanethiol- Protected Gold Nanoparticles by Heat Treatment in the Solid State. J Phys Chem B. 2003; 107:2719–2724.

Singaravelu G, Arockiamary JS, Kumar VG, Govindaraju K. A novel extracellular synthesis of monodisperse gold nanoparticles using marine alga Sargassum wightii Greville. Colloids Surf B Biointerfaces. 2007; 57:97–101.

Singh N, Singh RK, Bhunia A K, Stroshine RL. Efficacy of chlorine dioxide, ozone, and thyme essential oil or a sequential washing in killing Escherichia coli O157:H7 on lettuce and baby carrots. Lebensm. Wiss. Technol. 2002; 35: 720–729.

Singh AK, Talat M, Singh DP, Srivastava ON. Biosynthesis of gold and silver nanoparticles by natural precursor clove and their functionalization with amine group. J Nanopart Res. 2010; 12:1667–1675.

Singha PK, Roy S, Dey S. Antimicrobial activity of Andrographis paniculata. Fitoterapia. 2003; 74(7–8): 692–694.

Siripong P, Kongkathip B, Preechanukool K. Cytotoxic diterpenoid constituents from Andrographis paniculata Nees. leaves. Journal of the Science Society of Thailand. 1992; 18(4): 187–194.

Smitha SL, Philip D, Gopchandran KG. Green synthesis of gold nanoparticles using Cinnamomum zeylanicum leaf broth. Spectrochim Acta A. 2009; 74:735–739.

Song JY, Jang HK, Kim BS. Biological synthesis of gold nanoparticles using Magnolia kobus and Diopyros kaki leaf extracts. Proc Biochem. 2009; 44:1133–1138.

Song JY, Jang HK, Kim BS. Rapid biological synthesis of silver nanoparticles using plant leaf extracts. Bioproc Biosystems Eng. 2009; 32: 79–84.

Song JY, Kim BS. Rapid biological synthesis of silver nanoparticles using plant leaf extracts. Bioprocess and Biosystems Engineering. 2009; 32(1): 79–84.

Su L, Mao L. Gold nanoparticle/alkanedithiol conductive films selfassembled onto gold electrode: Electrochemistry and electroanalytical application for voltammetric determination of trace amount of catechol. Talanta. 2006; 70(1):68–74.

Sun Y, Xia Y. Shape-controlled synthesis of gold and silver nanoparticles. Science. 2002; 298: 2176–2179.

Sushmita S, Jyoti PS, Alak KB. A novel green synthesis of colloidal silver nanoparticles (SNP) using Dillenia indica fruit extract. Colloids and Surfaces B: Biointerfaces. 2013; 102:83–85.

Susie E, Mostafa A, El-Sayed. Why gold nanoparticles are more precious than pretty gold: Noble metal surface plasmon resonance and its enhancement of the radiative and nonradiative properties of nanocrystals of different shapes. Chem Soc Rev. 2006; 35:209–217.

Suslick KS. Sonochemistry. Science. 1990; 247(4949): 1439– 1445.

Syu W, Don M, Lee G, Sun C. Cytotoxic and Novel Compounds from Solanum indicum. J Nat Prod. 2001; 64: 1232—1233.

T. Marshall, Agterveld DV, Jason G,. Accumulation of Gold Nanoparticles in Brassic Juncea. Int J Phytoremediation 2007; 9:197–206.

Takagi K, Park EH, Kato H. Anti-inflammatory Activities of Hederagenin and Crude Saponin Isolated from Sapindus mukorossi Gaertn. Chem Pharm Bull. 1980; 28: 1183–1188.

Taleb A, Petit C, Pileni MP. Optical properties of self-assembled 2D and 3D superlattices of silver nanoparticles. J Phys Chem B. 1998; 102: 2214–2240.

Talwar GP, Dar SA, Rai MK, Reddy KV, Mitra D, Kulkarni SV, Doncel GF, Buck CB, Schiller JT, Muralidhar S, Bala M, Agrawal SS, Bansal K, Verma JK. A Novel Polyherbal Microbicide with Inhibitory Effect on Bacterial, Fungal and Viral Genital Pathogens. Int J Antimicrob Agent. 2008; 32: 180–185.

Tang JL, Cheng SF, Hsu WT, Chiang TY, Chau LK. Fiber-optic biochemical sensing with a colloidal gold-modified long period fiber grating. Sensors and Actuators B: Chemical. 2006; 119(1):105–109.

Tappayuthpijarn P, Dejatiwongse Q, Pongpech P, Leelaporn A. Antibacterial activity of extracts of *Piper betle* leaf. Thai J Pharmacol. 1982; 4: 205–212.

Terry N, Zayed A. Phytoremediation of selenium. In: Frankenberger JrWT, Engberg RA, editors. Environmental chemistry of selenium. New York: Dekker. 1998; 633–55.

Thiebaut JM, Roussy G, Medjram MS, Garin F, Seyfried L, Maire G. Durable changes of the catalytic properties of alumina-supported platinum induced by microwave irradiation. Catalysis Letters. 1993; 21(1-2): 133–138.

Thisoda P, Rangkadilok N, Pholphana N. Inhibitory effect of Andrographis paniculata extract and its active diterpenoids on platelet aggregation. European Journal of Pharmacology. 2006; 553(1–3): 39–45.

Tiekink ERT. Gold compounds in medicine: Potential anti-tumour agents. Gold Bull. 2003; 36: 117–124.

Tolles WM. Nanoscience and nanotechnology in Europe. Nanotechnology 1996; 7: 59.

Tominaga M, Shimazoe T, Nagashima M, Taniguchi I. Electrocatalytic oxidation of glucose at gold nanoparticle-modified carbon electrodes in alkaline and neutral solutions. Electrochemistry Communications. 2005; 7(2):189–193.

Tomotake H, Shimaoka I, Kayashita J. Stronger suppression of plasma cholesterol and enhancement of the fecal excretion of steroids by a buckwheat protein product than by a soy protein isolate in rats fed on a cholesterol-free diet. Bioscience, Biotechnology, and Biochemistry, 2001, 65(6): 1412–1414.

Toshio S, Hiroto E, KanjiroT, Hideki S, Masahiko. Surfactant and reducer-free synthesis of gold nanoparticles in aqueous solutions. Colloids and Surfaces A: Physiochem Eng Aspects. 2009; 347:18–26.

Uboldi C, Bonacchi D, Lorenzi G, Iris H, Pohl CM, Baldi G, et al. Gold nanoparticles induce cytotoxicity in the alveolar type-II cell lines A549 and NCIH44. Part Fibre Toxicol. 2009; 6(18): 1–12.

Uboldi C, Bonacchi D, Lorenzi G, Iris H, Pohl CM, Baldi G, Unger RE, James KC. Gold nanoparticles induce cytotoxicity in the alveolar type-II cell lines A549 and NCIH44. Particle and Fibre Toxicology. 2009; 6(18): 1–12.

Usuki A, Kawasumi M, Kojima Y, Okada A, Kurauchi T, Kamigaito O. Swelling behavior of montmorillonite cation exchanged for • -amino acids by ∈-caprolactam. Journal of Materials Research. 1993a; 8(5):1174–1178.

Usuki A, Kojima Y, Kawasumi M, Okada A, Fukushima Y, Kurauchi T, Kamigaito O. Synthesis of nylon 6-clay hybrid. Journal of Materials Research. 1993b; 8(5):1179–1184.

Valden M, Lai X, Goodman DW. Onset of Catalytic Activity of Gold Clusters on Titania with the Appearance of Nonmetallic Properties. Science. 1998; 281:1647–1650.

Vigneshwaran N, Kathe AA, Varadarajan PV, Nachane RP, Balasubramanya RH. Biomimetics of silver nanoparticles by white rot fungus Phaenerochaete chrysosporium. Coll Surf B: Interf. 2006; 53:55–59.

Vilchis-Nestor AR, Sanchez-Mendieta V, Camacho-Lopez MA, Gomez-Espinosa RM, Camacho-Lopez MA, Arenas-Alatorre JA. Solventless synthesis and optical properties of Au and Ag nanoparticles using Camellia sinensis extract. Mater Lett. 2008; 62:3103–3105.

Vivek DB, Jane JB, Jesse WE, Shivendra VS, Chad BW, Rajalingum D. Single-Step Biofriendly Synthesis of Surface Modifiable Near-Spherical Gold Nanoparticles for Applications in Biological Detection and Catalysis. Langmiur. 2011; 27:5549–5554.

Wada Y, Kuramoto H, Anand J. Microwave-assisted size control of CdS nanocrystallites. Journal of Materials Chemistry. 2001; 11(7): 1936–1940.

Wada Y, Kuramoto H, Sakata T. Preparation of nanosized nickel metal particles by microwave irradiation. Chemistry Letters. 1999; 7: 607–608.

Wang CY, Zhou Y, Chen ZY, Lu Q Y, Mo X. PVA-templated assembly of Pd nanorod and Pd fractal pattern. J Nanopart Res. 1999; 1: 479–83.

Wang J, Wang F, Zou X, Xu Z, Dong S. Surface plasmon resonance and electrochemistry for detection of small molecules using catalyzed deposition of metal ions on gold substrate. Electrochemistry Communications. 2007; 9(2):343–347.

Wang L, Bai J, Huang P, Wang H, Zhang L, Zhao Y. Self-assembly of gold nanoparticles for the voltammetric sensing of epinephrine. Electrochemistry Communications. 2006; 8(6):1035–1040.

Wang SY, Jiang SP, White TJ, Guo J, Wang X. Electrocatalytic Activity and Interconnectivity of Pt Nanoparticles on Multiwalled Carbon Nanotubes for Fuel Cells. J Phys Chem C. 2009; 113:18935–18945.

Wang Y, He X, Wang K, Zhang X, Tan W. Barbated Skullcup herb extract-mediated biosynthesis of gold nanoparticles and its primary application in electrochemistry. Colloids Surf B Biointerfaces. 2009; 73:75–79.

Wang ZJ, Zhang QX, Kuehner D, Xu XY, Ivaska A, Niu L. The synthesis of ionic-liquid-functionalized multiwalled carbon nanotubes decorated with highly dispersed Au nanoparticles and their use in oxygen reduction by electrocatalysis. Carbon. 2008; 46:1687–1692.

Wen L, Lin Z, Gu P, Zhou J, Yao B, Chen G, et al. Extracellular biosynthesis of monodispersed gold nanoparticles by a SAM capping route. J Nanopart Res. 2009; 11:279–288.

Wheeler DL, Montfort MJ, McLoughlin SW. Differential healing response of bone adjacent to porous implants coated with hydroxyapatite and 45S5 bioactive glass. J Biomed Mater Res A. 2001; 55:603–12.

Willems van den Wildenberg. Roadmap Report on Nanoparticles. Barcelona, Spain: W&W Espana sl; 2005.

Xiao Y, Pavlov V, Levine S, Niazov T, Markovitch GWillner I. Catalytic growth of Au nanoparticles by NAD(P)H cofactors: optical sensors for NAD(P)+-dependent biocatalyzed transformations. Angewandte Chemie. 2004; 43(34): 4519–4522.

Xie J, Lee JY, Wang DYC. Synthesis of Single-Crystalline Gold Nanoplates in Aqueous Solutions through Biomineralization by Serum Albumin Protein. J Phys Chem C. 2007; 111:10226–10232.

Xunjun Y, Shougang C, Aiguo W. Green chemistry synthesis of gold nanoparticles using lactic acid as a reducing agent. Micro & Nano Letters. 2010; 5:270–273.

Xynos ID, Hukkanen MVJ, Buttery LDK, Hench LL, Polak JM. Bioglass 45S5 stimulates osteoblast turnover and enhances bone formation in vitro: implications and applications for bone tissue engineering. Calcif Tissue Int. 2000; 67:321–9.

Yang L, Wu DF, Luo KW, et al. Andrographolide enhances 5- fluorouracil-induced apoptosis via caspase-8-dependent mitochondrial pathway involving p53 participation in hepatocellular carcinoma (SMMC-7721) cells. Cancer Letters. 2009; 276(2): 180–188.

Yang X, Li Q, Wang H, Huang J, Lin L, Wang W, et al. Green synthesis of palladium nanoparticles using broth of Cinnamomum camphora leaf. J Nanopart Res. 2010; 12:1589–1598.

Yin H, Yamamoto T, Wada Y, Yanagida S. Large-scale and size-controlled synthesis of silver nanoparticles under microwave irradiation. Materials Chemistry and Physics. 2004; 83(1): 66–70.

Young JWH, Ge L, Ng YF, Tan SN. The chemical composition and biological properties of coconut (*Cocos nucifera* L.) water. Molecules. 2009; 14: 5144–5164.

Zandiatashbar A, Picu CR, Koratkar N. Control of Epoxy Creep Using Graphene. Small. 2012; 8(11):1676–1682.

Zhang B, Kuang YJ, Pang HL, Liu B, Chen JH, Zhang XH. Synthesis of carbon nanotube supported Pt-Sn nanoparticles by replacement reaction and their electrocatalytic properties for ethanol oxidation. Indian J Chem A. 2009; 48:1345–1351.

Zhang JJ, Gu MM, Zheng TT, Zhu JJ. Synthesis of Gelatin-Stabilized Gold Nanoparticles and Assembly of Carboxylic Single-Walled Carbon Nanotubes/Au Composites for Cytosensing and Drug Uptake. Anal Chem. 2009; 81:6641–6648.

1. **Babu PJ**, Sharma P, Saranya S, Bora U. UV Light mediated synthesis of gold nanoparticles using ethonolic leaf extract of *Bacopa monnieri*. Materials Letters. 2012; 93: 431–434.
2. **Babu PJ,** Sharma P, Bora U. *Sapindus mukorossi* aqueous fruit extract as reducing, capping and dispersing agents in synthesis of gold nanoparticles. (Accepted for publication in Micro and Nano Letters, 2012).
3. **Babu PJ,** Saranya S, Sharma P, Tamuli R, Bora U. Sonocatalytic Synthesis of Gold Nanoparticles Using Ethnolic Extract of *Andrographis paniculata* and Functionalization with Gelatin-Polycaprolactone Composites. Front Mater Sci. 2012**;** 6(3): 236–249.
4. **Babu PJ**, Das RK, Gogoi N, Sharma P, Bora U. Microwave mediated rapid synthesis of gold nanoparticles using *Calotropis procera* latex and study of optical properties. ISRN Nanomaterials. 2012: 1–6.
5. **Babu PJ**, Sharma P, Saranya S, Tamuli R, Bora U. *Piper betle* Mediated Green Synthesis of Biocompatible Gold Nanoparticles. International Nano Letters. 2012; 2:18–28.
6. **Babu PJ,** Sharma P, Kalita MC, Bora U. Green Synthesis of Biocompatible Gold Nanoparticles Using *Fagopyrum esculentum* Leaf Extract. Front Mater Sci. 2011**;** 5(4): 379–387**.**
7. **Babu PJ,** Das RK, Kumar A, Bora U. Microwave Mediated Synthesis of Gold Nanoparticles Using Coconut Water. Int J Green Nanotechnol Biomed. 2011; 3:13–21.
8. **Babu PJ,** Sharma P, Borthakur BB, Das RK, Nahar P, Bora U. Synthesis of Gold Nanoparticles Using *Mentha arvensis* Leaf Extract. Int J Green Nanotechnol Phys and chem. **2010;** 2(2): 62–68.

Manuscripts in Communication

9. **Babu PJ,** Saranya S, Sharma P, Tamuli R, Bora U. Green Synthesis and Characterization of Biocompatible Gold Nanoparticles Using *Solanum indicum* Fruits (Minor Review under progress in Nanomaterials and Nanotechnology, 2012).

List of other publications

10. Das RK, Gogoi N, **Babu PJ**, Sharma P, Bora U. Synthesis of gold nanoparticles using *Amaranthus spinosus* leaf extract and study of their optical properties. AMPC. 2012**;** 2: 275–281.

11. Kasoju N, Ali SS, Sahu A, Das RK, **Babu PJ**, Bora U. Surface fictionalization of chitosan-PEO electrospun nanofibrous scaffold. Asian Chitin Journal. 2010; 6(1): 41-46.

List of presentations

1. **Babu PJ**, Bora U. APAS Young Scientist Convention 2011, held at Guntur, AP, during 27-28 Oct, 2011.
2. **Babu PJ**, Bora U. MRSI Young Scientist Colloquium 2012, held at Kolkata, WB, on 08 Aug 2012.

Workshops Attended

1. Introductory Workshop on Optical Microscopy, organized Biotech Hub, Center for the Environment, IITG, June 16 – 17 (2011) Guwahati, India.
2. Cancer Biology 2011: Basic Theoretical Aspects, organized by Biotech Hub, Cneter for the Environment, IITG, August 26-27 (2011) Guwahati, India.
3. Hands on Training on "Mammalian Cell Culture Techniques for toxicology Studies" organized by Dept. of Biotechnology, IITG, September 9-17 (2011) Guwahati, India.
4. "Basic Techniques in Bioinformatics" organized by Dept. of Biotechnology, IITG, October 12-14 (2011) Guwahati, India.
5. "GENOME ANNOTATION 2011" organized by Dept. of Biotechnology, IITG, October 15 (2011) Guwahati, India.
6. Quality Improvement Programmed in Advances in Drug Discovery, organized by Dept. of Biotechnology, IITG, June (2009) Guwahati, India.
7. "Intellectual Property and Innovation management in Knowledge Era" conducted by Dept. of Chemistry at IITG, Guwahati, India.

BIOGRAPHY

Punuri Jayasekhar Babu was born and brought up in Kondapi, and completed his Secondary School Certificate (10th Std.) in 2000 and Intermediate education (12th Std.) in 2002 from Jawahar Navodaya Vidyalaya (JNV), Ongole. He completed his Bachelor's degree in Biochemistry and Microbiology and chemistry as optional subjects in 2005, from AKVK College (NAAC A Grade), Ongole, affiliated to Acharya Nagarjuna University.He obtained his Master's degree in Biochemistry, in 2007, from SDHR PG College (NAAC A Grade), Rayachoty, Kadapa, A.P, affiliated to Sri Venkateswara University. He bagged first class first rank in his B. Sc and M. Sc.

He qualified GATE (2008) and joined in Bioengineering Research laboratory (BRL) (Formally known as Biomaterial and Tissue Engineering Laboratory), IIT Guwahati in July 2008 for his doctoral studies under the supervision of Dr. Utpal Bora and Dr. RanjanTamuli. His Ph. D.focused on the screening of reducing and stabilizing properties of plant material for gold nanoparticles synthesis and their functionalization for drug delivery. He has published about 10 papers at the time of compilation of his thesis and a few more are in communication and the work is published in peer-reviewed international journals. He has awarded institutional fellowship from IIT Guwahati. He is an invited reviewer for International Journal of Advanced Nano Science, Nano Technology and Nano Engineering (IJANNN) and International Nano Letters (INN). He is currently a life member of professional societies such as BRSI (Regd. No: T-5100) and an annual member of MRSI (Regd. No: AMB 246). He is elected as Member of Management Council, BRSI for the period of 2013-2015.